

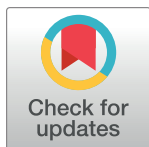
RESEARCH ARTICLE

# Cholinergic-like neurons carrying PSEN1 E280A mutation from familial Alzheimer's disease reveal intraneuronal sAPP $\beta$ fragments accumulation, hyperphosphorylation of TAU, oxidative stress, apoptosis and Ca<sup>2+</sup> dysregulation: Therapeutic implications

Viviana Soto-Mercado, Miguel Mendivil-Perez, Carlos Velez-Pardo, Francisco Lopera, Marlene Jimenez-Del-Rio \*

Neuroscience Research Group, Medical Research Institute, Faculty of Medicine, University of Antioquia (UdeA), SIU Medellin, Medellin, Colombia

\* [marlene.jimenez@udea.edu.co](mailto:marlene.jimenez@udea.edu.co)



## OPEN ACCESS

**Citation:** Soto-Mercado V, Mendivil-Perez M, Velez-Pardo C, Lopera F, Jimenez-Del-Rio M (2020) Cholinergic-like neurons carrying PSEN1 E280A mutation from familial Alzheimer's disease reveal intraneuronal sAPP $\beta$  fragments accumulation, hyperphosphorylation of TAU, oxidative stress, apoptosis and Ca<sup>2+</sup> dysregulation: Therapeutic implications. PLoS ONE 15(5): e0221669. <https://doi.org/10.1371/journal.pone.0221669>

**Editor:** Firas H Kobeissy, University of Florida, UNITED STATES

**Received:** August 8, 2019

**Accepted:** May 6, 2020

**Published:** May 21, 2020

**Peer Review History:** PLOS recognizes the benefits of transparency in the peer review process; therefore, we enable the publication of all of the content of peer review and author responses alongside final, published articles. The editorial history of this article is available here: <https://doi.org/10.1371/journal.pone.0221669>

**Copyright:** © 2020 Soto-Mercado et al. This is an open access article distributed under the terms of the [Creative Commons Attribution License](https://creativecommons.org/licenses/by/4.0/), which permits unrestricted use, distribution, and reproduction in any medium, provided the original author and source are credited.

## Abstract

Alzheimer's disease (AD) is a neurodegenerative disorder characterized by progressive memory loss and cognitive disturbance as a consequence of the loss of cholinergic neurons in the brain, neuritic plaques and hyperphosphorylation of TAU protein. Although the underlying mechanisms leading to these events are unclear, mutations in presenilin 1 (PSEN1), e.g., E280A (PSEN1 E280A), are causative factors for autosomal dominant early-onset familial AD (FAD). Despite advances in the understanding of the pathophysiology of AD, there are no efficient therapies to date. Limitations in culturing brain-derived live neurons might explain the limited effectiveness of AD research. Here, we show that mesenchymal stromal (stem) cells (MSCs) can be used to model FAD, providing novel opportunities to study cellular mechanisms and to establish therapeutic strategies. Indeed, we cultured MSCs with the FAD mutation PSEN1 E280A and wild-type (WT) PSEN1 from umbilical cords and characterized the transdifferentiation of these cells into cholinergic-like neurons (ChLNs). PSEN1 E280A ChLNs but not WT PSEN1 ChLNs exhibited increased intracellular soluble amyloid precursor protein (sAPP $\beta$ ) fragments and extracellular A $\beta$ 42 peptide and TAU phosphorylation (at residues Ser202/Thr205), recapitulating the molecular pathogenesis of FAD caused by mutant PSEN1. Furthermore, PSEN1 E280A ChLNs presented oxidative stress (OS) as evidenced by the oxidation of DJ-1Cys<sup>106</sup>-SH into DJ-1Cys<sup>106</sup>-SO<sub>3</sub> and the detection of DCF-positive cells and apoptosis markers such as activated pro-apoptosis proteins p53, c-JUN, PUMA and CASPASE-3 and the concomitant loss of the mitochondrial membrane potential and DNA fragmentation. Additionally, mutant ChLNs displayed Ca<sup>2+</sup> flux dysregulation and deficient acetylcholinesterase (AChE) activity compared to control ChLNs. Interestingly, the inhibitor JNK SP600125 almost completely blocked TAU phosphorylation. Our findings demonstrate that FAD MSC-derived cholinergic neurons with the

**Data Availability Statement:** All relevant data are within the manuscript and its Supporting Information files.

**Funding:** This study was funded by MinCiencias grant # 1115-807-62912, contract #749-2018 to MJ-Del-Rio, CV-P and MM-P. VS-M is a doctoral student of the Basic Biomedical Sciences Academic Corporation program at the Universidad de Antioquia (UdeA), and is funded by the 2019 Bicentennial Doctoral Excellence Scholarship, MinCiencias-Colombia.

**Competing interests:** The authors have declared that no competing interests exist.

PSEN1 E280A mutation provide important clues for the identification of targetable pathological molecules.

## Introduction

Alzheimer's disease (AD) is a chronic neurodegenerative condition characterized by loss of memory, reasoning and decision-making functions [1] due to the severe loss of cholinergic neurons from the nucleus basalis magnocellularis of Meynert and cholinergic projections to the cortex and hippocampus [2]. The neuropathological profile of AD is associated with the extracellular accumulation of insoluble forms of amyloid- $\beta$  (A $\beta$ ) in plaques and intracellular aggregation of the microtubule protein TAU in neurofibrillary tangles [3]. A $\beta$  is derived by the proteolytic cleavage of amyloid  $\beta$  precursor protein (APP). The full length APP is first cleaved by  $\beta$ -secretase (BACE1) freeing a soluble proteolytic fragment, recognized as soluble APP $\beta$  (sAPP $\beta$ ). The remaining C-terminal membrane bound APP fragment, CTF $\beta$  or C99 fragment, undergoes additional cleavages by  $\gamma$ -secretase to generate a series of peptides prone to aggregation [4]. Interestingly, both hAPP and A $\beta$  species have been shown to aggregate intracellularly [5–7]. Most mutations in the presenilin 1 (*PSEN1*) gene, which codes for the catalytic component of  $\gamma$ -secretase [8], result in the overproduction of A $\beta$ , specifically, the 42-amino acid A $\beta$  isoform (A $\beta$ <sub>1–42</sub>, hereafter A $\beta$ <sub>42</sub>) [9], and occur most frequently in familial AD (FAD; <http://www.molgen.ua.ac.be/ADMutations/>). Glu280Ala (p. E280A, c.839A > C, exon 8) in *PSEN1* is a well-characterized FAD mutation found in a large kindred localized in Antioquia, Colombia [10–13] that shows typical phenotypes of AD with complete penetrance [14]. Similar to the majority of dominant-negative *PSEN1* mutations [15, 16], PSEN1 E280A produces increased A $\beta$ <sub>42</sub> deposition [17], hippocampal neuron loss [18], and A $\beta$ /TAU accumulation in young adults [19, 20].

Despite advances in the understanding of the physiopathology of AD [21], there are no efficient therapies to date. Although limitations in culturing brain-derived live neurons might slow AD research, the rapid advances in cellular genetic reprogramming, in particular the induction of somatic cells (e.g., fibroblast) into stem cells (e.g., human induced pluripotent stem cells, hiPSCs), has led to the modeling of FAD PSEN1 mutations *in vitro* [22–25]. Obtaining iPSCs from patients bearing *PSEN1* mutations is appealing; however, the isolation and purification procedures are technically challenging, expensive, time consuming and labor intensive. Alternatively, the human mesenchymal stromal (stem) cells derived from Wharton's jelly tissue (WJ-MSCs) are multipotent cells that can differentiate and/or transdifferentiate into mesodermal and ectodermal lineage cells [26–29]. Because MSCs might be equivalent to human embryonic stem cells (hESCs) and hiPSCs [30, 31]; these cells have become an interesting and promising tool for modeling FAD PSEN1 E280A *in vitro*.

The aim of the present study was to establish an *in vitro* cellular model that reveals the major pathologic features of the FAD PSEN1 E280A mutation, thereby enabling investigation of the pathomechanisms of early onset FAD. Therefore, A $\beta$ <sub>42</sub> accumulation, A $\beta$ <sub>42</sub> production, TAU phosphorylation, oxidative stress (OS), cell death, and neuronal dysfunction were investigated in cholinergic-like neurons (ChLNs) derived from wild-type (control) and PSEN1 E280A MSCs. We demonstrate for the first time that FAD PSEN1 E280A pathology can be recapitulated in MSC-derived ChLNs. These findings in ChLNs show great promise for modeling human FAD *in vitro* and identifying therapeutic targets for AD treatment.

## Materials and methods

The collection and use of umbilical cords from newborns was approved by Ethics Committee of the Hospital San Vicente Fundacion Research act # 13–2015 Colombia, and was provided following natural childbirth with written consent. Donors had a familial background of AD. The mother's medical history was negative for human pathogens, such as human immunodeficiency virus 1/2, hepatitis B and C virus, and syphilis. The cord (~7 cm long) was immersed in low-glucose DMEM (Sigma) supplemented with 100 U Penicillin/streptomycin (Sigma) and 5 µg/ml Plasmocin (Invivogen) and immediately transported to the laboratory.

## Isolation and expansion of hWJ-MSCs

The human umbilical cords were obtained from ten healthy, natural childbirths (Tissue Bank Code (TBC) # WJMSC-11, -12, -13, -14, -15, -16, -17, -18, -19, -20) and aseptically stored at 4 °C PBS containing 1% penicillin and streptomycin. The cords were rinsed several times to drain blood from vessels, cut into 2–3-cm-long segments and rinsed again. Umbilical arteries and veins were removed, and the remaining tissue was transferred to a sterile container and chopped into small fragments in PBS. The explants were digested with an enzyme mixture containing 0.25% trypsin, 0.1% Dispase and 0.5% collagenase II for 2 h at 37 °C under constant agitation. Then, the digestion products were centrifuged at 447 x g for 40 min, and the pellet was cultured in T75 cell culture flasks (Corning) in hWJ-MSC regular culture medium (low-glucose DMEM supplemented with 20% fetal bovine serum (FBS, Sigma), 100 U penicillin/streptomycin and 5 µg/ml Plasmocin). Once confluence had been reached, adherent cells (passage 0) were detached with 0.25% trypsin and passaged at 13,000 cells/ cm<sup>2</sup> in a T75 flask. Cells from passages 2 or 4 were harvested during the first expansion period for further characterization and cryopreservation.

## Identification of the PSEN1 E280A mutation in WJMSCs

The PSEN1 E280A mutation was detected by PCR using mismatch primers and digestion of the products with *BsmI* [32]. Digested products were separated on a 3% agarose gel. According to different mobility electrophoretic patterns, samples were classified as wild-type (WT) or mutant PSEN1 E280A when compared to PSEN1 E280A carrier (positive case NeuroBank (NB) code #18233) or wild type PSEN1 genotype (NB code#18574). The TBC# WJMSC-12 (female) sample was identified for PSEN1 E280A mutation. For comparative purposes, we pre-selected female WT PSEN1 samples (TBC# WJMSC-11, -15, -17), and TBC# WJMSC-11 WT PSEN1 was randomly selected for further experiments.

**APOE genotyping analysis.** Genotyping of the APOE polymorphism (n = 10) was performed using polymerase chain reaction amplification of a 244-bp fragment followed by digestion with *HhaI* as described by [33].

**Karyotyping.** Karyotype analysis was performed by the Medical Genetics Unit of the Faculty of Medicine–UdeA, using standard cytogenetic protocols. At 60–70% confluence, WJMSC-11 WT and WJMSC-12 PSEN1 E280A cells were incubated with 0.1 mg/ml Colcemid (Sigma) for 90 min at 37 °C. Then, the cells were detached with 0.25% trypsin and centrifuged at 591 x g for 20 min. The medium was removed, and the hypotonic solution (0.075 M KCl, 0.017 M Na-citrate) was added and incubated for 20 min at 37 °C. After a new centrifugation, cells were fixed with freshly prepared Carnoy's solution. Metaphase spreads were analyzed after staining with quinacrine (Sigma) for karyotyping. Analysis was performed on three different primary cultures counting 20 metaphases for each sample.

### Colony-forming units assay

The colony formation assay is an *in vitro* cell survival assay based on the ability of a single cell to grow into a colony [34]. WJMSC-11 WT and WJMSC-12 PSEN1 E280A cells were seeded at a density of 200 cells/ well on 6-well plates followed by the addition of 3 mL of regular culture medium. The cultures were left to grow in a humidified atmosphere with 5% CO<sub>2</sub> at 37 °C for 15 days. The culture medium was changed twice a week. After 15 days of cultivation, both WT and mutant PSEN-1 cells were stained with 0.5% crystal violet and counted using the cell counter plugin from ImageJ program. The experiment was conducted three times.

### Immuno-phenotypic characterization

Standard flow cytometry techniques were used to determine the cell surface epitope profile (CD9, CD73, CD90, CD34 and CD45) of both WT and mutant PSEN1 MSCs. Briefly, hWJ-MSCs were incubated with saturating concentrations (1:500) of mouse monoclonal antibodies conjugated to human CD9-peridinin chlorophyll protein (PerCP)-cy5.5, CD73-phycoerythrin (PE), CD90 PE-cy5.5, CD34 PE, and CD45- fluorescein isothiocyanate (FITC). All antibodies were purchased from BD Biosciences (San Diego, CA). Cells were incubated for 1 h at 4 °C. Prior to antibody labeling, the cells were preincubated with 5% fetal bovine sera (FBS) for 10 min to block nonspecific binding. Cell suspensions were washed and resuspended in PBS for analysis on an LSRFortessa (BD Biosciences). Ten thousand events were acquired, and the acquisition analysis was performed using FlowJo 7.6.2. Positive staining was defined as the fluorescence emission that exceeded levels obtained by more than 99% of cells from the population stained with the corresponding negative controls. The isotype (negative) control used in this study was IgG1 PE-Cy5.5, IgG1-PE and IgG1- FITC (BD Biosciences).

### Cell differentiation

**Adipogenic differentiation.** Adipogenic differentiation was performed according to [35] with minor modifications. Briefly, WT and mutant MSCs at passages 4–7 were plated at a density 20,000 cells/cm<sup>2</sup> in a 12-well plate in regular culture medium. At 90–100% confluence, the culture medium was replaced by adipogenic induction medium, including high-glucose DMEM, 10% FBS, 0.5 mM 3-isobutyl-1-methylxanthine (Sigma, cat # I5879), 100 μM indomethacin (Sigma, cat # I7378), 0.1 μM dexamethasone and 10 μg/ mL insulin. After 28 days, cells were fixed with 4% formaldehyde (FA) and immediately stained with the standard Oil-Red-O protocol. Control cells were kept in regular culture medium.

**Osteogenic differentiation.** Osteogenic differentiation was performed according to [35] with minor modifications. Briefly, WT and mutant cells at passages 4–7 were plated at a density of 10,000 cells/ cm<sup>2</sup> in 12-well plates in regular culture medium. After 72 h, the culture medium was replaced by osteogenic differentiation medium containing high-glucose DMEM (Sigma), 10% FBS, 1 μM dexamethasone (Alfa Aesar, cat # A17590), 250 μM sodium ascorbate (Sigma, cat # A4034), and 10 mM β-glycerophosphate (Alfa Aesar, cat # L03425). The medium was changed every 3–4 days. Control cells were kept in regular culture medium. After 28 days of induction, cells were fixed in 4% FA and stained with standard Von Kossa Staining.

**Chondrogenic differentiation.** Chondrogenic differentiation was performed according to ref. [36] with minor modifications. Briefly, 2.5×10<sup>5</sup> WT and mutant cells were left aggregated in microwell plates and then provided with chondrogenic medium containing high-glucose DMEM, 10% FBS, 10 μg/ L TGF-β3, 0.1 μmol/ L dexamethasone, 50 μmol/ L vitamin C, and 6.25 mg/L insulin. The medium was changed every 3–4 days. Control cells were kept in regular culture medium. After 28 days of induction, cells were fixed in 4% formaldehyde, stained with toluidine blue for 2 min at room temperature and viewed by light microscopy.



**Cholinergic-Like Neuron (ChLN) differentiation.** ChLN differentiation was performed according to ref. [29]. WT and mutant MSCs were seeded at  $1\text{--}1.5 \times 10^4$  cells/  $\text{cm}^2$  in laminin-treated culture plates for 24 h in regular culture medium (RCm). Then, the medium was removed, and cells were incubated in minimal culture medium (hereafter MCm) containing low-glucose DMEM and 1% FBS or in cholinergic differentiation medium (*Cholinergic-N-Run medium*, hereafter Ch-N-Rm) containing DMEM/F-12 media 1:1 Nutrient Mixture (Gibco cat# 10565018), 10 ng/ mL basic fibroblast growth factor (bFGF) recombinant human protein (Gibco Cat# 13256029), 50  $\mu\text{g}/\text{mL}$  sodium heparin (Hep, Sigma-Aldrich cat# H3393), 0.5  $\mu\text{M}$  all-trans retinoic acid, 50 ng/ml sonic hedgehog peptide (SHH, Sigma cat# SRP3156) and 1% FBS at 37 °C for 7 days. After this process of transdifferentiation, the cells were labeled as WT PSEN1 or PSEN1 E280A ChLNs. Since Ch-N-Rm contains several factors that might interfere with the experiment interpretation and measurements, WT PSEN1 and PSEN1 E280A ChLNs (obtained after 7 days in Ch-N-Rm) were left in regular culture medium (RCm) for 0, 2 or 4 additional days, hereafter 0, 2, or 4 days of post transdifferentiation.

### Immunofluorescence analysis

For the analysis of neural-, Alzheimer's disease-, oxidative stress- and cell death-related markers, the cells treated under different conditions were fixed with cold ethanol (-20 °C) for 20 min, followed by Triton X-100 (0.1%) permeabilization and 10% bovine serum albumin (BSA) blockage. Cells were incubated overnight with primary neural antibodies against glial fibrillary acidic protein (GFAP 1:200, cat# sc6170, Santa Cruz), microtubule-associated protein 2 (MAP2, 1:250, cat MA1-25044, Invitrogen),  $\beta$ -tubulin III (1:250, cat# G712 A, Promega) and choline-acetyltransferase (ChAT, 1:50, cat# AB144 P, Millipore); primary antibodies against APP<sub>751</sub> and/or protein amyloid  $\beta_{1-42}$  (1:500; clone 6E10 cat# 803014, Biolegend), total TAU (1:500; t-Tau; cat# T6402, Sigma), and phospho-TAU (p-Tau, 1:500, Ser202/Thr205, cat# MN1020 (AT8), Thermo Fisher Scientific); and primary antibodies against oxidized DJ-1 (1:500; ox(Cys106)DJ1; spanning residue C<sup>106</sup> of human PARK7/DJ1; oxidized to produce cysteine sulfonic (SO<sub>3</sub>) acid; cat # MABN1773, Millipore). To assess cell death, we used primary antibodies against p53-upregulated modulator of apoptosis (1:500; PUMA, cat# ab-9643, Abcam), p53 (1:500; cat# MA5-12453, Millipore), phospho-c-Jun (1:250; c-Jun (S63/73) cat# sc-16312, Santa Cruz), and caspase-3 (1:250; cat # AB3623, Millipore). After exhaustive rinsing, we incubated the cells with secondary fluorescent antibodies (DyLight 488 and 594 horse anti-rabbit, -goat and -mouse, cat DI 1094, DI 3088, and DI 2488, respectively) at 1:500. The nuclei were stained with 1  $\mu\text{M}$  Hoechst 33342 (Life Technologies), and images were acquired on a Floyd Cells Imaging Station microscope.

### Western blot analysis

Cells were incubated as described above, detached with 0.25% trypsin and lysed in 50 mM Tris-HCl, pH 8.0, with 150 mM sodium chloride, 1.0% Igepal CA-630 (NP-40), and 0.1% sodium dodecyl sulfate and a protease inhibitor cocktail (Sigma-Aldrich). All lysates were quantified using the bicinchoninic acid assay (Thermo Scientific cat # 23225). Extracted samples (30  $\mu\text{g}$  of proteins) were heated at 95 °C for 5 min in 2 x SDS and 20x reducing agent (except for protein oxDJ-1) and loaded into 12% Bis/Tris gels at 120 V for 90 min, and the bands were transferred onto nitrocellulose membranes (Hybond-ECL, Amersham Biosciences) at 270 mA for 90 min using an electrophoretic transfer system (BIO-RAD) according to ref. [37] with minor modifications. The membranes were incubated overnight at 4 °C with anti-GFAP, MAP2,  $\beta$ -tubulin III, ChAT, amyloid  $\beta_{1-42}$ , total TAU, phospho-TAU, ox(Cys<sup>106</sup>) DJ1, PUMA, p53, p-c-Jun, and caspase-3 primary antibodies (1:5000). The anti-actin antibody

(1:1000, cat #MAB1501, Millipore) was used as an expression control. Secondary infrared antibodies (goat anti-rabbit IRDye<sup>®</sup> 680RD, cat #926–68071; donkey anti-goat IRDye<sup>®</sup> 680RD, cat # 926–68074; and goat anti mouse IRDye<sup>®</sup> 800CW, cat #926–32270; LI-COR Biosciences) at 1:1000 were used for western blotting analysis, and data were acquired using Odyssey software. To directly control the conformation-dependent differences among A $\beta$  assemblies, we prepared a homogenous synthetic unaggregated (i.e., monomers) and large oligomeric A $\beta$ <sub>42</sub> assemblies according to ref. [38]. Briefly, after solubilization of the peptide (Sigma Cat #A9810) in DMSO, the “unaggregated” peptide was obtained by dissolving the DMSO-solubilized peptide in water and used immediately (0 days). To obtain the “large oligomers”, 10 mM Tris was added to DMSO-solubilized peptide solution and incubated it for 15 days at 4 °C. The determination of the aggregation state of A $\beta$ <sub>42</sub> was performed by Western analysis of SDS-PAGE as described above. The assessment was repeated three times in independent experiments.

### Mass spectrometry analysis

Gel region between 60 and 125 kDa was excised from the experimental lane, cut into 1 x 1 mm cubes, incubated consequently with 10 mM dithiothreitol and 55 mM iodoacetamid in 100 mM ammonium bicarbonate, and dehydrated with acetonitrile. Then, the proteins were in-gel digested overnight at 37 °C with LysC protease (Promega, Mannheim). The resulting peptide mixture was extracted twice with exchange of 5% formic acid and 100% acetonitrile, the extracts pulled together and dried down. The peptides were re-suspended in 25  $\mu$ l of 5% formic acid and 5  $\mu$ l were taken for LC-MS/MS analysis. The analysis was performed on a nano-UPLC Ultimate 3000 interfaced on-line to a Q-Exactive HF Hybrid Quadrupole-Orbitrap mass spectrometer (both Thermo Fischer Scientific, Bremen). The UPLC system was equipped with Acclam PepMap<sup>™</sup> 100 75  $\mu$ m x 2 cm trapping column and 75  $\mu$ m x 15 cm separating column packed with 3  $\mu$ m diameter C18 particles (Thermo Fischer Scientific, Bremen). Peptides were separated using 180 min linear gradient (solvent A– 0.1% formic acid in water, solvent B– 0.1% formic acid in neat acetonitrile). Spectra were acquired in DDA mode using top 20 method. Spectra were then converted into (.mgf) format and searched human sequences in the UniProt database (January 2020) using MASCOT software (version 2.2.04) and against human Amyloid-beta precursor protein (ACC No P05067) without enzyme specificity. Mass tolerance was set on 5 ppm and 0.025 Da for precursor and fragment ions respectively; variable modification–Cysteine carbamidomethyl and propionamide, methionine oxidation, protein N-terminal acetyl. The result of the database search was evaluated by Scaffold software (v.4.7.5, Proteome Software, Portland) and the spectra matched Amyloid-beta precursor protein also manually inspected. To investigate the presence of A $\beta$ <sub>42</sub>, the spectra were acquitted in DDA targeted mode using masses of C- and N-terminal peptides which are unique for 671–713 fragment, and then processed by SkyLine software.

### Analysis of cells

**Evaluation of intracellular hydrogen peroxide (H<sub>2</sub>O<sub>2</sub>) by fluorescence microscopy.** To determine the levels of intracellular H<sub>2</sub>O<sub>2</sub>, we used 2',7'-dichlorofluorescein diacetate (5  $\mu$ M, DCFH<sub>2</sub>-DA; Invitrogen). hWJ-MSCs or ChLNs were left in RCm for 0, 2 and 4 days. Then, the cells (5 x 10<sup>3</sup>) were incubated with the DCFH<sub>2</sub>-DA reagent for 30 min at 37 °C in the dark. Cells were then washed, and DCF fluorescence intensity was determined by analysis of fluorescence microscopy images. The assessment was repeated three times in independent experiments. The nuclei were stained with 0.5  $\mu$ M Hoechst 33342 (2.5  $\mu$ M) staining compound. The assessment was repeated three times in independent experiments blind to experimenter.

**Evaluation of intracellular hydrogen peroxide ( $H_2O_2$ ) by flow cytometry.**  $H_2O_2$  was determined with 2',7'-dichlorofluorescein diacetate (1  $\mu$ M, DCFH<sub>2</sub>-DA). ChLNs were left in regular medium (RCm) for 0, 2 and 4 days. Then, the cells ( $1 \times 10^5$ ) were incubated with DCFH<sub>2</sub>-DA reagent for 30 min at 37 °C in the dark. Cells were then washed, and DCF fluorescence was determined using an LSRFortessa (BD Biosciences). The assessment was repeated 3 times in independent experiments. Quantitative data and figures were obtained using FlowJo 7.6.2 Data Analysis Software. The assessment was repeated three times in independent experiments blind to experimenter and flow cytometer analyst.

**Analysis of mitochondrial membrane potential ( $\Delta\Psi$ m) by fluorescence microscopy.** The hWJ-MSCs or ChLNs were left in regular culture medium (RCm) for 0, 2 and 4 days. Then, the cells ( $5 \times 10^3$ ) were incubated with the passively diffusing and active mitochondria-accumulating dye deep-red MitoTracker compound (20 nM, final concentration) for 20 min at RT in the dark (Invitrogen, cat # M22426). Cells were then washed twice with PBS. MitoTracker fluorescence intensity was determined by analysis of fluorescence microscopy images. The assessment was repeated three times in independent experiments. The nuclei were stained with 0.5  $\mu$ M Hoechst 33342 (2.5  $\mu$ M) staining compound. The assessment was repeated three times in independent experiments blind to experimenter and flow cytometer analyst.

**Analysis of mitochondrial membrane potential ( $\Delta\Psi$ m) by flow cytometry.** ChLNs were left in regular medium for 0, 2 and 4 days. Then, the cells ( $1 \times 10^5$ ) were incubated for 30 min at RT in the dark with MitoTracker (20 nM, final concentration). The cells were analyzed using an LSRFortessa (BD Biosciences). The experiment was performed three times in independent experiments, and 10,000 events were acquired for analysis. Quantitative data and figures were obtained using FlowJo 7.6.2 Data Analysis Software. The assessment was repeated three times in independent experiments blind to experimenter and flow cytometer analyst.

**Determination of DNA fragmentation by flow cytometry.** DNA fragmentation was determined using a hypotonic solution of PI. Cells entering the cellular cycle phase sub-G<sub>0</sub> were identified as those undergoing apoptosis. ChLNs were left in regular medium for 0, 2 and 4 days. Then, the cells ( $1 \times 10^5$ ) were detached, washed twice with PBS (pH 7.2) and stored in 95% ethanol overnight at -20 °C. The cells were washed and incubated in 400  $\mu$ L solution containing propidium iodide (PI; 50  $\mu$ g/ml), RNase A (100  $\mu$ g/ mL), EDTA (50 mM), and Triton X-100 (0.2%) for 60 min at 37 °C. The cell suspension was analyzed for PI fluorescence using an Epics XL flow cytometer (Beckman Coulter). DNA fragmentation was assessed 3 times in independent experiments. Quantitative data and figures from the sub-G<sub>0</sub>/G<sub>1</sub> population were obtained using FlowJo 7.6.2 Data Analysis Software. The assessment was repeated three times in independent experiments blind to experimenter and flow cytometer analyst.

**Acetylcholinesterase activity measurement.** We determined the acetylcholinesterase (AChE) activity using the AChE Assay Kit (Abcam, Cat# ab138871) according to the manufacturer's protocol. Briefly, ChLNs at days 0, 2 and 4 of post differentiation were detached with 0.25% trypsin and mechanically lysed by freezing/sonication. Lysates were centrifuged at 18,894 x g for 15 min, and supernatants were used for protein quantification by the BCA method (see above) and the detection of AChE activity. AChE degrades the neurotransmitter acetylcholine (ACh) into choline and acetic acid. We used the DTNB (5,5'-dithiobis(2-nitrobenzoic acid)) reagent to quantify the thiocholine produced from the hydrolysis of acetylthiocholine by AChE. The absorption intensity of the DTNB adduct was used to measure the amount of thiocholine formed, which was proportional to AChE activity. We read the absorbance in a microplate reader at ~410 nm. The data obtained were compared to the standard curve values, and the AChE amounts (mU) were normalized to protein values (mU/ mg protein). The assessment was repeated three times in independent experiments blind to experimenter.

**Measurement of A $\beta$ <sub>1–42</sub> peptide in culture medium.** The level of A $\beta$ <sub>1–42</sub> peptide was measured according to a previous report [39] with minor modifications. Briefly, WT and PSEN1 E280A ChLNs were left in regular medium for 0, 2 and 4 days. Then, 100  $\mu$ l of conditioned medium was collected, and the levels of secreted A $\beta$ <sub>1–42</sub> peptides were determined by a solid-phase sandwich ELISA (Invitrogen, Cat# KHB3544) following the manufacturer's instructions. The assessment was repeated three times in independent experiments blind to experimenter.

**Intracellular calcium imaging.** Intracellular calcium (Ca<sup>2+</sup>) concentration changes evoked by cholinergic stimulation were assessed according to refs. [40, 41] with minor modifications. For the measurement, the fluorescent dye Fluo-3 (Fluo-3 AM; Thermo Fisher Scientific, cat: F1242) was employed. The dye was dissolved in DMSO (1 mM) to form a stock solution. Before the experiments, the stock solution was diluted in neuronal buffer solution (NBS buffer: 137 mM NaCl, 5 mM KCl, 2.5 mM CaCl<sub>2</sub>, 1 mM MgCl<sub>2</sub>, pH 7.3, and 22 mM glucose). The working concentration of the dye was 2  $\mu$ M. The WT and PSEN1 E280A ChLNs were incubated for 30 min at 37 °C with the dye-containing NBS and then washed five times. Intracellular Ca<sup>2+</sup> transients were evoked by acetylcholine (1 mM final concentration) at 0, 2 and 4 days post differentiation. The measurements were carried out using the 100x objective of the microscope. Several regions of interest (ROIs) were defined in the visual field of the camera. One of the ROIs was cell-free, and the fluorescence intensity measured here was considered background fluorescence (F<sub>bg</sub>). The time dependence of the fluorescence emission was acquired, and the fluorescence intensities (hence the Ca<sup>2+</sup> levels) were represented by pseudo-colors. To calculate the changes of the average Ca<sup>2+</sup>-related fluorescence intensities, the F<sub>bg</sub> value was determined from the cell-free ROI, and then the resting fluorescence intensities (F<sub>rest</sub>) of the cell-containing ROIs were obtained as the average of the points recorded during a period of 10 s prior to the addition of acetylcholine. The peaks of the fluorescence transients were found by calculating the average of four consecutive points and identifying those points that gave the highest average value (F<sub>max</sub>). The amplitudes of the Ca<sup>2+</sup>-related fluorescence transients were expressed relative to the resting fluorescence ( $\Delta F/F$ ) and were calculated by the following formula:  $\Delta F/F = (F_{\text{max}} - F_{\text{rest}})/(F_{\text{rest}} - F_{\text{bg}})$ . For the calculation of the fluorescence intensities, ImageJ was used. The terms fluorescence intensity was used as an indirect indicator of intracellular Ca<sup>2+</sup> concentration. The assessment was repeated three times in independent experiments blind to experimenter.

**JNK inhibition experiment.** The ChLNs were left in regular medium for 0, 2 and 4 days alone or co-incubated with the anthrapyrazolone JNK inhibitor SP600125 (1  $\mu$ M final concentration). This compound competes with ATP to inhibit the phosphorylation of c-JUN. After this time, cells were evaluated for p-TAU and t-TAU protein expression by immunofluorescence, as described above. The assessment was repeated three times in independent experiments blind to experimenter.

## Photomicrography and image analysis

Light microscopy photographs were taken using a Zeiss Axiostart 50 Fluorescence Microscope equipped with a Canon PowerShot G5 digital camera (Zeiss Wöhlk-Contact-Linsen, Gmb Schöckirchen, Germany), and fluorescence microscopy photographs were taken using a Zeiss Axiostart 50 Fluorescence Microscope equipped with a Zeiss AxioCam Cm1 and (Zeiss Wöhlk-Contact-Linsfluoreen, Gmb Schöckirchen, Germany) and Floyd Cells Imaging Station microscope. Fluorescence images were analyzed by ImageJ software (<http://imagej.nih.gov/ij/>). The figures were transformed into 8-bit images, and the background was subtracted. The cellular measurement regions of interest (ROIs) were drawn around the nucleus (for the

case of transcription factors and apoptosis effectors) or over all cells (for cytoplasmic probes), and the fluorescence intensity was subsequently determined by applying the same threshold for cells in the control and treatment conditions. Mean fluorescence intensity (MFI) was obtained by normalizing total fluorescence to the number of nuclei.

### Data analysis

In this experimental design, a vial of MSCs was thawed, cultured and the cell suspension was pipetted at a standardized cellular density of  $2.6 \times 10^4$  cells/cm<sup>2</sup> into different wells of a 24-well plate. Cells (i.e., the biological and observational unit [42]) were randomized to wells by simple randomization (sampling without replacement method), and then wells (i.e., the experimental units) were randomized to treatments by similar method. Experiments were conducted in triplicate wells. The data from individual replicate wells were averaged to yield a value of  $n = 1$  for that experiment and this was repeated on three occasions blind to experimenter and/or flow cytometer analyst for a final value of  $n = 3$  [42]. Based on the assumptions that the experimental unit (i.e. the well) data comply with independence of observations, the dependent variable is normally distributed in each treatment group (Shapiro-Wilk test), and there is homogeneity of variances (Levene's test), the statistical significance was determined by a One-way analysis of variance (ANOVA) followed by Tukey's post hoc comparison calculated with GraphPad Prism 5.0 software. Differences between groups were only deemed significant when a p-value of  $< 0.05$  (\*),  $< 0.001$  (\*\*) and  $< 0.001$  (\*\*\*). All data are illustrated as the mean  $\pm$  S.D.

## Results

### PSEN1 E280A and wild-type WJ-MSCs show similar phenotype, immunophenotype, lineage differentiation and transdifferentiation

We first evaluated whether the PSEN1 E280A mutation affects the capacity of MSCs to generate mesodermal and ectodermal lineages through differentiation and transdifferentiation, respectively. Therefore, WJ-MSCs were isolated from ten umbilical cords of volunteers according to standard procedures [43], and PCR-RFLP electrophoretic profile analysis identified one umbilical cord sample out of ten as a carrier of the mutation *PSEN1* c.839A > C, p.E280A (PSEN1 E280A MSCs, S1 Fig). Then, PSEN1 E280A MSCs and wild-type WJ-MSCs (WT PSEN1 MSCs) were further cultured and characterized for morphological, karyotype, immuno-phenotypic features and differentiation capabilities. As shown in Fig 1, WT PSEN1 and PSEN1 E280A MSCs displayed the typical colony-forming units (Fig 1A and 1B), adherent growth, and fibroblast-like cellular morphology (Fig 1C and 1D). Karyotype analysis showed no chromosomal alterations (Fig 1E and 1F), and APOE genotyping analysis showed that PSEN1 E280A cells had the APOE\*3/4 genotype and WT PSEN1 cells had the APOE\*3/3 genotype (S2 Fig). Flow cytometry analysis showed that both wild-type and mutant MSCs were positive (>95% of positive cells) for mesenchymal associated markers CD73, CD90 and CD9 (Fig 1G and 1H) but negative (<5% of positive cells) for hematopoietic cell surface antigens CD34/ CD45. WT and PSEN1 E280A MSCs cultured in adipogenic, osteogenic, or chondrogenic induction medium differentiated into adipocytes (Fig 1J and 1P), osteoblasts (Fig 1L and 1R), and chondrocytes (Fig 1N and 1T), respectively, while MSCs cultured in regular culture medium were undifferentiated (Fig 1I, 1O, 1K, 1Q, 1M and 1S).

Additionally, MSCs were transdifferentiated into cholinergic-like neurons (ChLNs) from WJ-MSCs using a new method [29]. As shown in Fig 2, WT PSEN1 and PSEN1 E280A WJ-MSCs cultured in minimal culture medium (MCm) for 7 days expressed basal levels of protein MAP2 (Fig 2A and 2B) and  $\beta$  Tub III (Fig 2A and 2C) and undetectable levels of



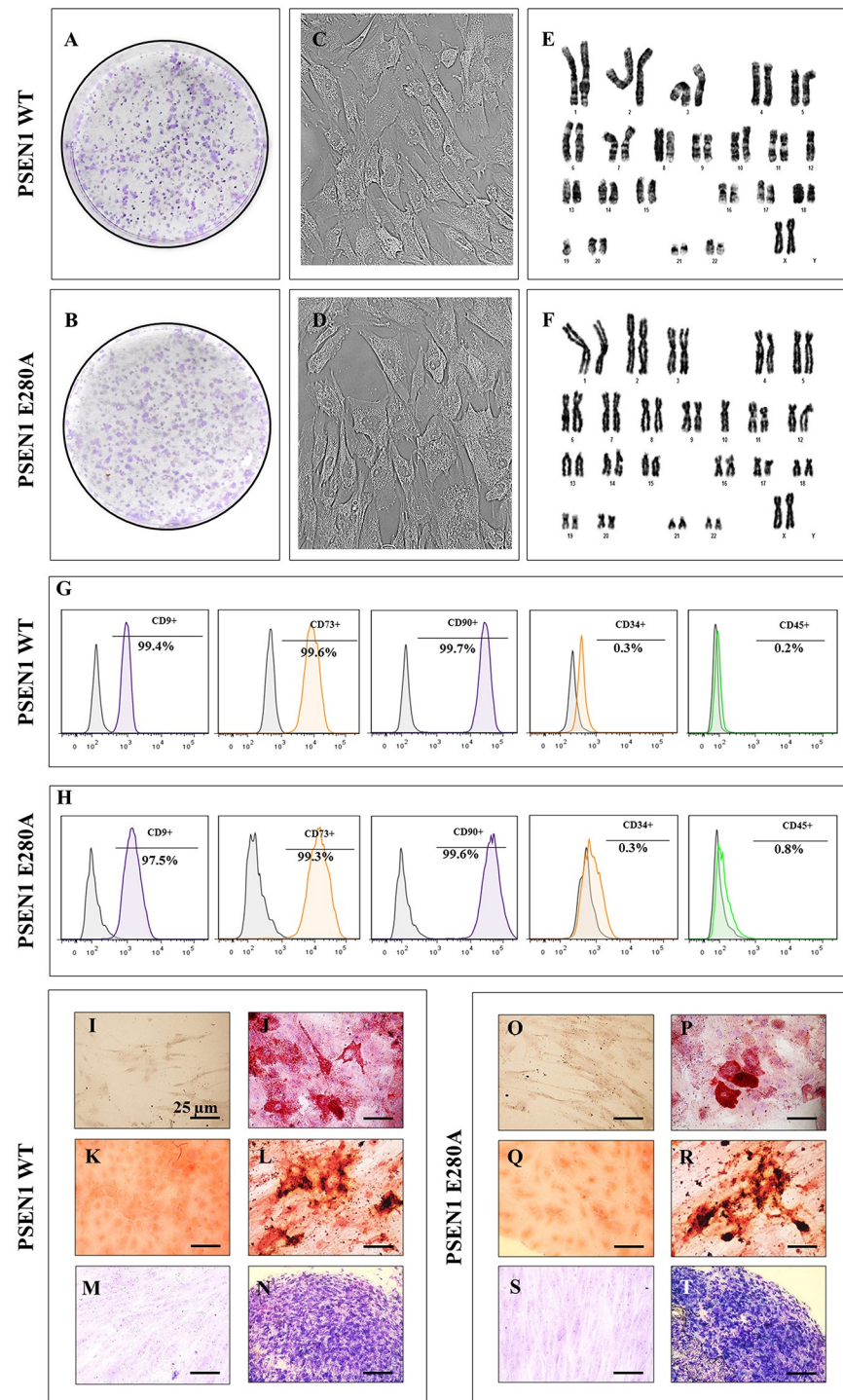


**Fig 1. Characterization of WT PSEN1 and PSEN1 E280A WJ-MSCs.** (A-B) Representative images showing the colony-forming units and (C-D) adherent growth and fibroblast-like morphology typical of WJ-MSCs. (E-F) Karyotype analysis performed at passage 2 showing chromosomal normality (46XX). (G-H) Flow cytometry analyses showing the percentage of double-positive CD9/ CD73/ CD90/ CD34 and CD45 WJ-MSCs. (I, O) Oil-Red-O negatively stained undifferentiated WJ-MSCs grown on regular culture medium. (J, P) Oil-Red-O positively stained adipocytes differentiated from WJ-MSCs showing intracellular red lipidic vacuoles. (K, Q) Von Kossa negatively stained undifferentiated WJ-MSCs grown on regular culture medium. (L, R) Von Kossa positively stained osteoblasts differentiated from WJ-MSCs showing silver intracellular precipitates. (M, S) Toluidine blue negatively stained undifferentiated WJ-MSCs grown on regular culture medium. (N, T) Toluidine blue positively stained chondrocytes differentiated from WJ-MSCs showing extracellular glycoprotein matrix. Image magnification, 400x. The images represent 1 out of 3 independent experiments.

<https://doi.org/10.1371/journal.pone.0221669.g001>

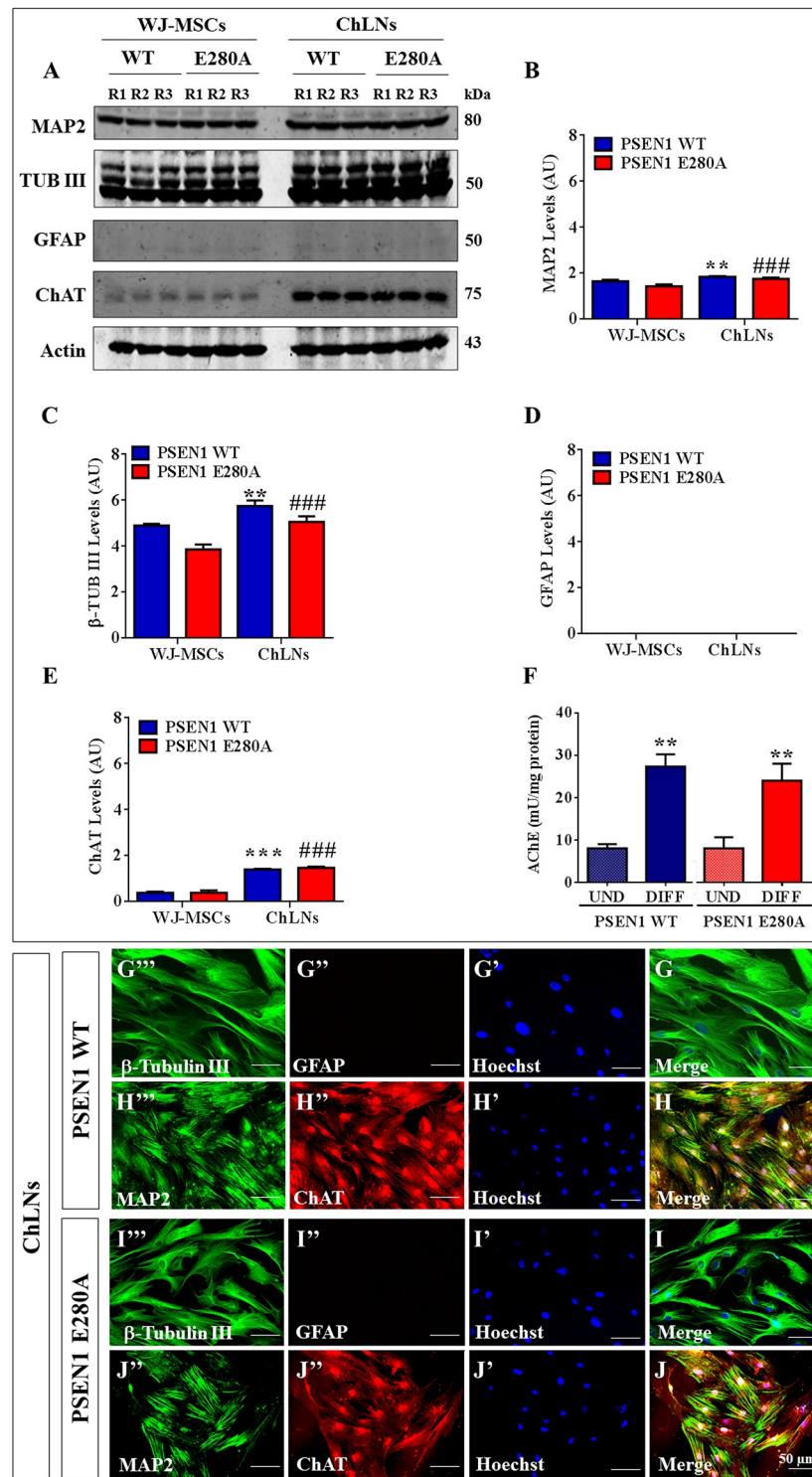


**Fig 2. Cholinergic-like neurons differentiate from WT PSEN1 and PSEN1 E280A WJ-MSCs.** WT PSEN1 and PSEN1 E280A WJ-MSCs were cultured in cholinergic differentiation medium as described in the *Materials and Methods* section for 7 days. After this time, the proteins in the extracts were blotted with primary antibodies against MAP2,  $\beta$ -tubulin III, GFAP, ChAT and actin proteins. The intensities of the western blot bands shown in (A) were measured (B, C, D, E) by an infrared imaging system (Odyssey, LI-COR), and the intensity was normalized to that of actin. (F) Measurements of acetylcholinesterase activity in WT PSEN1 and PSEN1 E280A ChLNs after 7 days of transdifferentiation. (G-J) Cells were double stained as indicated in the figure with primary antibodies against  $\beta$ -

tubulin III (green; G<sup>'''</sup> and I<sup>'''</sup>) and GFAP (red; G<sup>''</sup> and I<sup>''</sup>) or MAP2 (green; H<sup>'''</sup> and J<sup>'''</sup>) and ChAT (red; H<sup>''</sup> and J<sup>''</sup>). The nuclei were stained with Hoechst 33342 (blue; G<sup>'</sup>-J<sup>'</sup>). Data are expressed as the mean  $\pm$  SD; \* $p < 0.05$ ; \*\* $p < 0.01$ ; \*\*\* $p < 0.001$ . The blots and figures represent 1 out of 3 independent experiments. Image magnification, 200x.

<https://doi.org/10.1371/journal.pone.0221669.g002>

GFAP (Fig 2A and 2D) and ChAT (Fig 2A and 2E). As expected, when the cells were exposed to cholinergic-N-Run medium (Ch-N-Rm) for 7 days [29], the levels of protein MAP2 (Fig 2A and 2B),  $\beta$  Tub III (Fig 2A and 2C) and ChAT (Fig 2A and 2E) were significantly higher than those in cells exposed to MCm. Noticeably, ChLNs remained negative for the specific glial cell lineage marker GFAP (Fig 2A and 2D). These observations were confirmed by immunofluorescence (Fig 2G–2J). Because the enzyme AChE catalyzes the breakdown of the neurotransmitter acetylcholine (ACh, [44]), we evaluated whether ChLNs expressed a catalytically functional AChE enzyme. As shown in Fig 2F, the AChE enzyme presented basal activity in WJ-MSCs under MCm culture conditions ( $\sim 8 \pm 1.2$  mU/mg protein), while the AChE enzyme activity was significantly higher (at least a 3-fold increase) in both control and mutant ChLNs ( $\sim 26 \pm 1.6$  mU/mg protein). Remarkably, there was no significant difference in AChE enzymatic activity ( $p < 0.05$ ) between WT and PSEN1 E280A ChLNs (at day 0 of post differentiation).

### WT and PSEN1 E280A WJ-MSCs show similar levels of intracellular APP / A $\beta_{42}$ , oxidized DJ-1, mitochondrial membrane potential ( $\Delta\Psi_m$ ) and Reactive Oxygen Species (ROS)

Next, we evaluated whether the PSEN1 E280A mutation induced overproduction of APP/A $\beta_{42}$  and OS, and alterations in  $\Delta\Psi_m$  and ROS production in MSCs. After 7 days of culture in MCm, MSCs were left in RCm for 0, 2 and 4 additional days. Western blot measurements and immunofluorescence analysis revealed that both WT and PSEN1 E280A MSCs displayed undetectable levels of intracellular APP / A $\beta_{42}$  and oxidized DJ-1 at days 0, 2 and 4 (S3A–S3J Fig). Moreover, both WT and PSEN1 E280A MSCs displayed normal  $\Delta\Psi_m$  (S4A Fig), undetectable levels of ROS (S4B Fig) and no changes in DNA content (S4C Fig) at days 0, 2 and 4 in RCm according to flow cytometry (S4A–S4C Fig) and DCF/ MitoTracker fluorescence (S4D–S4K Fig).

### PSEN1 E280A Cholinergic-Like Neurons (ChLNs) show high levels of intracellular sAPP $\beta$ f, oxidized DJ-1, reactive oxygen species (ROS), loss of mitochondrial membrane potential ( $\Delta\Psi_m$ ) and DNA fragmentation, but none of those markers are detected in WT PSEN1 ChLNs

The above observations prompted us to evaluate the same cell parameters in ChLNs. We initially verify that the antibody clone 6E10 recognizes A $\beta$  monomers as well as large aggregates of A $\beta_{42}$  and APP. Effectively, the antibody recognized the “unaggregated” (monomers), and large aggregates forms of synthetic A $\beta_{42}$  peptide (Fig 3A). The WT PSEN1 and PSEN1 E280A ChLNs (obtained after 7 days in Ch-N-Rm) were left in regular culture medium (RCm) for 0, 2 and 4 additional days post transdifferentiation (hereafter labelled as 0, 2, or 4). Western blot also revealed that WT PSEN1 ChLNs displayed undetectable levels of intracellular APP/ A $\beta_{42}$  aggregates (Fig 3A and 3B) and oxidized DJ-1 (Fig 3A and 3C), whereas flow cytometry showed no loss of  $\Delta\Psi_m$  (Fig 4A–4C) and no ROS generation (Fig 4D–4F) at any time tested. However, PSEN1 E280A ChLNs exhibited significantly higher levels of intracellular APP/ A $\beta_{42}$  aggregates (Fig 3A and 3B) and oxidized DJ-1 (Fig 3A and 3C) and lower  $\Delta\Psi_m$  than WT PSEN1 ChLNs at days 2 and 4 (Fig 4B and 4C). These observations were confirmed by



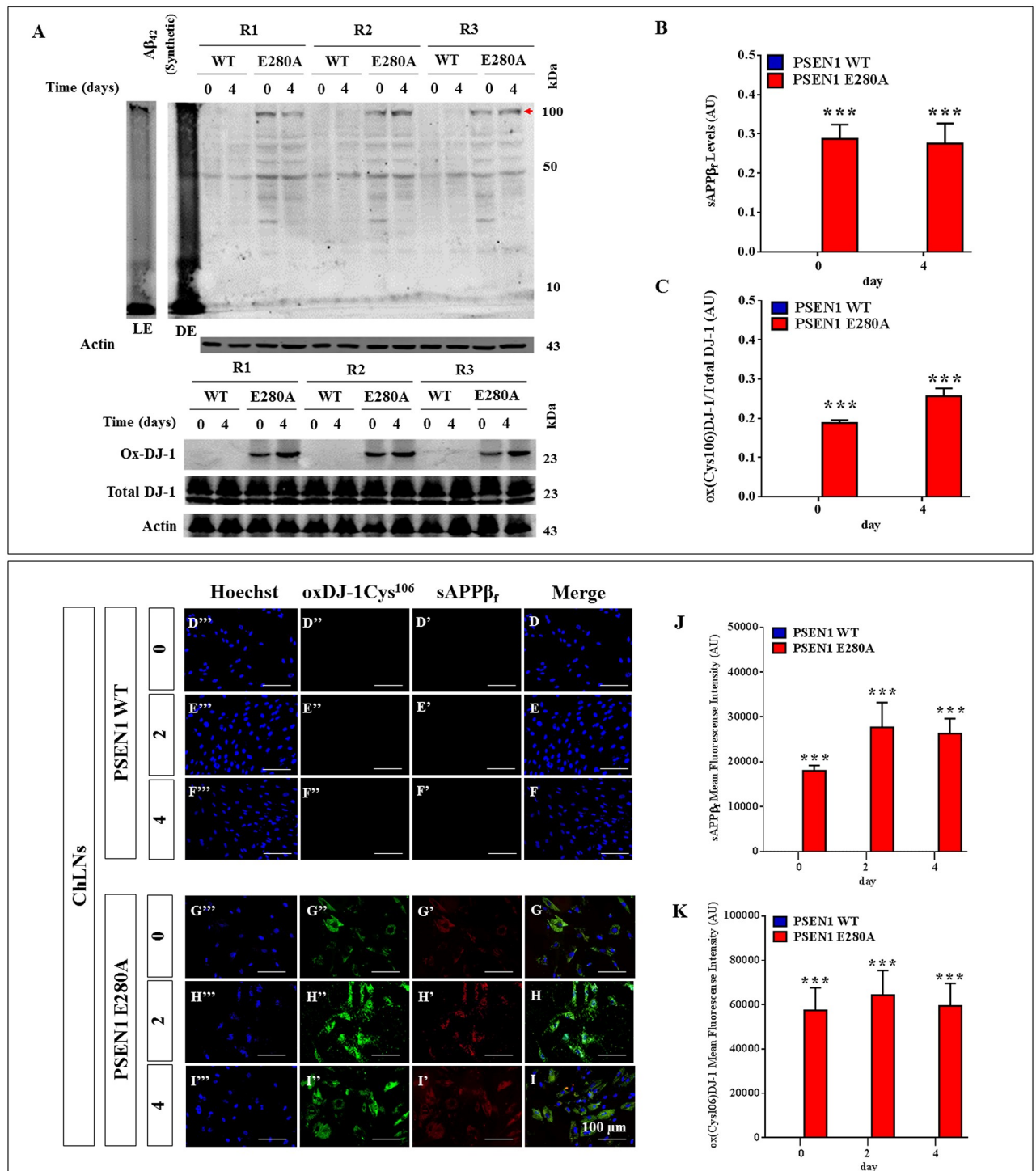


**Fig 3. PSEN1 E280A Cholinergic-Like Neurons (ChLNs) show high levels of intracellular sAPP $\beta$ f and oxidized DJ-1.** Synthetic unaggregated (i.e., monomers) and large oligomeric  $A\beta_{42}$  assemblies were prepared as described in *Material and Methods* section according to Ref. [38]. The ChLNs were obtained as follows. After 7 days of transdifferentiation, WT PSEN1 and PSEN1 E280A ChLNs were left in regular culture medium (RCM) for 0 and 4 days, as indicated in the figure. After this time, the proteins in the extracts were blotted with primary antibodies against  $A\beta_{42}$ , oxDJ-1Cys<sup>106</sup> and actin proteins. The intensities of the western blot bands shown in (A) were measured (B, C) by an infrared imaging system (Odyssey, LI-COR), and the intensity was normalized to that of actin. Additionally, cells were double stained as indicated in the figure (D-I) with primary antibodies against APP<sub>751</sub>/ $A\beta_{42}$  (red; D'-I') and oxDJ-1Cys<sup>106</sup> (green; D''-I''). The nuclei were stained with Hoechst 33342 (blue; D'''-I'''). (J) Quantification of  $A\beta_{42}$  fluorescence intensity. (K) Quantification of oxDJ-1Cys<sup>106</sup> fluorescence intensity. Data are expressed as the mean  $\pm$  SD; \* $p < 0.05$ ; \*\* $p < 0.01$ ; \*\*\* $p < 0.001$ . The blots and figures represent 3 independent experiments (Repeat 1, R2, and R3). The arrowhead represents APP and/or  $A\beta_{42}$  aggregates. Image magnification, 200x; inset magnification, 800x. LE = light exposure; DE = dark exposure.

<https://doi.org/10.1371/journal.pone.0221669.g003>

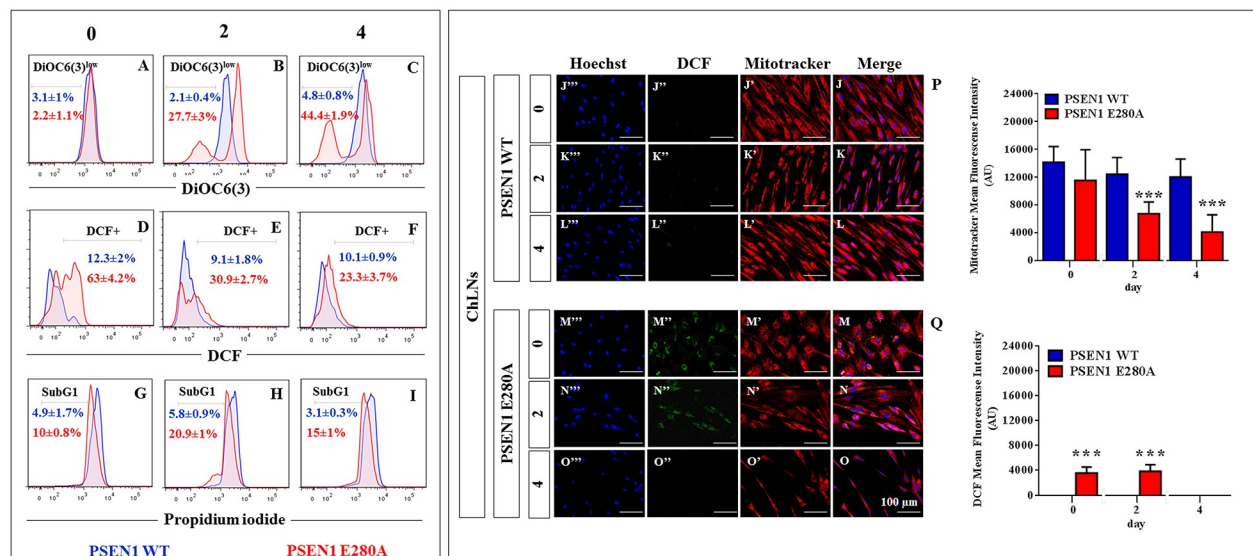


**Fig 4. PSEN1 E280A Cholinergic-Like Neurons (ChLNs) show loss of mitochondrial membrane potential ( $\Delta\Psi_m$ ), high levels of intracellular reactive oxygen species (ROS), and fragmentation of DNA.** After 7 days of transdifferentiation, WT PSEN1 and PSEN1 E280A ChLNs were left in regular culture medium (RCm) for 0, 2 and 4 days, as indicated in the figure. Representative histograms showing DiOC<sub>6</sub>(3)<sup>low</sup> (A–C), DCF+ (D–F) and SubG<sub>1</sub> (G–I) populations from WT PSEN1 (blue) and PSEN1 E280A (red) ChLNs. Representative MitoTracker (J'–O'), DCF (J''–O''), Hoechst (J'''–O''') and merge (J–O) pictures of WT PSEN1 and PSEN1 E280A ChLNs. (P) Quantification of MitoTracker fluorescence intensity. (Q) Quantification of DCF fluorescence intensity. Data are expressed as the mean  $\pm$  SD; \* $p < 0.05$ ; \*\* $p < 0.01$ ; \*\*\* $p < 0.001$ . The histograms and figures represent 1 out of 3 independent experiments. Image magnification, 200x.

<https://doi.org/10.1371/journal.pone.0221669.g004>

immunofluorescence microscopy (Figs 3D–3K and 4J'–4O'). To confirm the identity of the intracellular APP/  $A\beta_{42}$  aggregates displayed in the Western blot (Fig 3A, arrowhead), we used LC-MS/MS technique. The LC-MS/MS analysis identified two peptides <sup>364</sup>LPTTAASP-DAVDK<sup>377</sup> (S5A Fig) and <sup>430</sup>AVIQHFQEK<sup>438</sup> (S5B Fig) that showed high homology with APP fragments (e.g., APP714, APP733, APP751, APP752, S5C Fig), hereafter sAPP $\beta$ . No  $A\beta_{42}$  fragment was identified in the interrogated gel region. Interestingly, PSEN1 E280A ChLNs showed high levels of ROS production as early as day 0, that is, at day 7 of transdifferentiation (Fig 4D, 4M'' and 4Q) and at day 2 post transdifferentiation (Fig 4E, 4N'' and 4Q), but ROS were severely reduced at day 4 (Fig 4F, 4O'' and 4Q). Furthermore, both WT and PSEN1 E280A ChLNs exhibited a typical quiescent cell cycle (i.e., phase G<sub>0</sub>, Fig 4G–4I) and showed similar numbers of cells in the SubG<sub>0</sub> population at day 0 (Fig 4G); nonetheless, the SubG<sub>0</sub> population was significantly elevated in PSEN1 E280A ChLNs at day 2 (~15% compared to that in WT cells; Fig 4H) and day 4 (~12% compared to WT cells; Fig 4I) according to propidium iodide (PI) fluorescence analysis.

### PSEN1 E280A ChLNs display activation of p53, PUMA, c-JUN and CASPASE-3

Next, we wanted to investigate whether the intracellular sAPP $\beta$  induced cell death signaling in PSEN1 ChLNs. Therefore, we used the transcription factors p53 and c-JUN, pro-apoptotic BH3-only protein PUMA, and protease CASPASE-3 as cell death markers to examine the pro-death activity of sAPP $\beta$  in ChLNs over time. As shown in Fig 5, while WT PSEN1 ChLNs showed no detectable levels of apoptogenic proteins at any time tested (Fig 5A–5E), the PSEN1 E280A ChLNs displayed significant detection of c-JUN (at day 0, 2 and 4, Fig 5A and 5B), p53 (at day 2 and 4, Fig 5A and 5C), PUMA (at day 4, Fig 5A and 5D) and CASP-3 (at day 4,



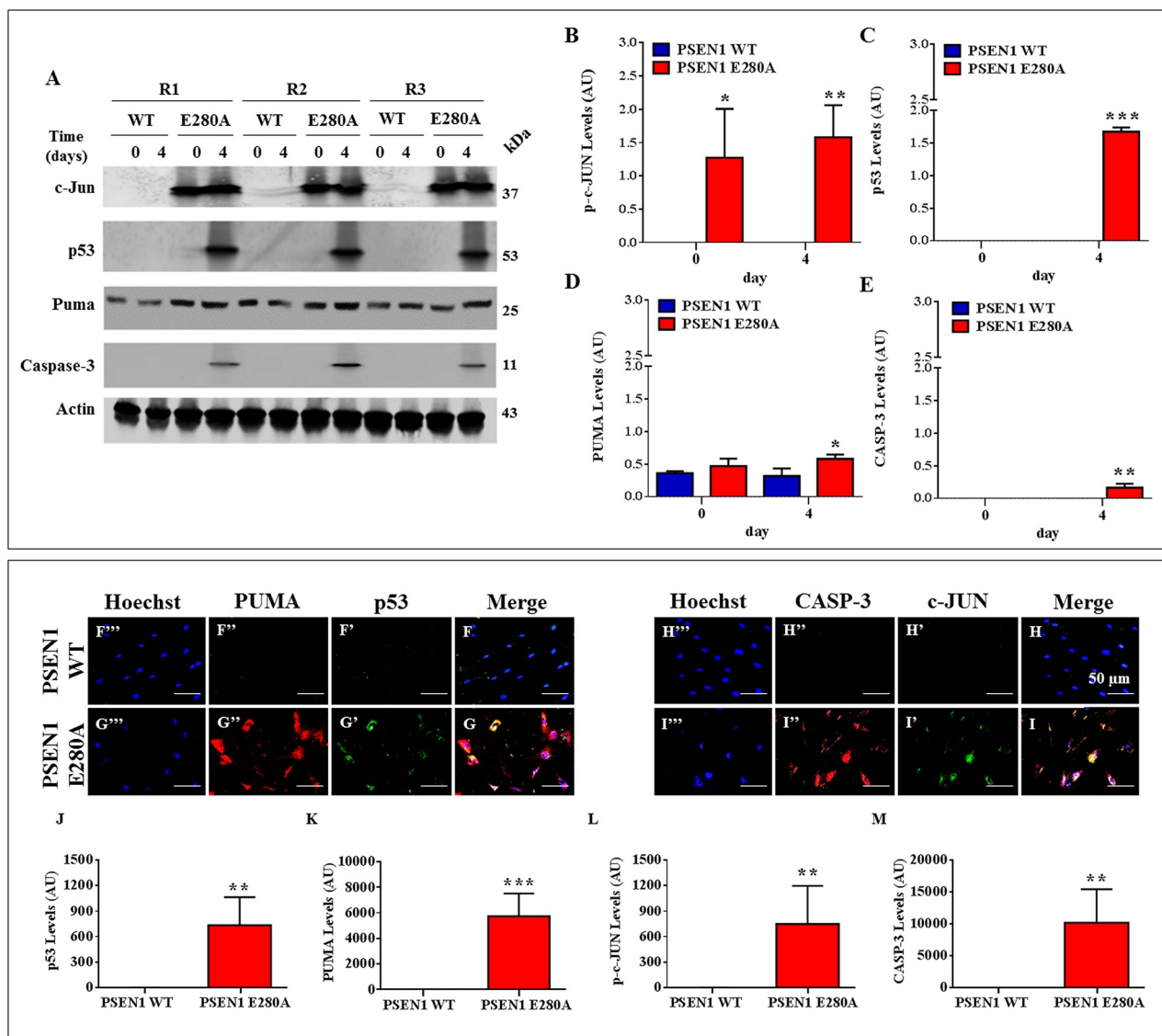


**Fig 5. PSEN1 E280A ChLNs display activation of p53, PUMA, c-JUN and CASPASE-3.** After 7 days of transdifferentiation, WT PSEN1 and PSEN1 E280A ChLNs were left in regular culture medium (RCm) for 0, 2 and 4 additional days, as indicated in the figure. After this time, the proteins in the extracts were blotted with primary antibodies against phosphorylated c-JUN (c-JUN), p53, PUMA, CASPASE-3 (CASP-3) and actin proteins. The intensities of the western blot bands shown in (A) were measured (B, C, D and E) by an infrared imaging system (Odyssey, LI-COR), and the intensity was normalized to that of actin. Additionally, after 4 days, ChLNs were double stained as indicated in the figure (F-I) with primary antibodies against p53 (green; F' and G'), PUMA (red; F'' and G''), c-JUN (green; H' and I') and CASP-3 (red; H'' and I''). The nuclei were stained with Hoechst 33342 (blue; F'''-I'''). (J-M) Quantification of p53 (J), PUMA (K), c-JUN (L) and CASP-3 (M) fluorescence intensity. Data are expressed as the mean  $\pm$  SD; \* $p < 0.05$ ; \*\* $p < 0.01$ ; \*\*\* $p < 0.001$ . The blots and figures represent 1 out of 3 independent experiments. Image magnification, 200x.

<https://doi.org/10.1371/journal.pone.0221669.g005>

Fig 5A and 5E). These observations were confirmed by immunofluorescence analysis at day 4 (Fig 5F–5M).

### PSEN1 E280A ChLNs show reduced functional response to Acetylcholine (ACh), low acetylcholinesterase activity, and generation of high levels of extracellular A $\beta$ <sub>42</sub> peptide

We further investigated whether WT and PSEN1 E280A ChLNs responded to ACh stimuli as an evaluation of cholinergic neuronal Ca<sup>2+</sup> responsiveness and functionality [29]. To this aim,

we simultaneously measured the secreted levels of  $A\beta_{42}$  and evaluated the response of ChLNs to ACh. ELISA revealed that both WT PSEN1 and PSEN1 E280A ChLNs secreted similarly low levels of extracellular  $A\beta_{42}$  at days 0 and 2, but at day 4, PSEN1 E280A ChLNs showed significantly higher extracellular levels of  $A\beta_{42}$  compared to PSEN1 WT ChLNs ( $\sim 3.2$ -fold, Fig 6A). For functional analysis, both control and mutant PSEN1 ChLN cultures were puffed with ACh (1 mM final concentration) into a bath solution. As expected, ACh induced a transient elevation of intracellular  $Ca^{2+}$  in WT PSEN1 ChLNs at day 0 (Fig 6B and 6D), 2 (Fig 6E and 6G) and 4 post-transdifferentiation (Fig 6H and 6J). The average fluorescence change ( $\Delta F/F$ ) was  $6.4 \pm 0.6$ ,  $6.4 \pm 0.7$  and  $5.9 \pm 1.4$ -fold, respectively, with a mean duration of  $40 \pm 10$  s ( $n = 20$  ChLN cells imaged,  $N = 3$  dishes) according to cytoplasmic  $Ca^{2+}$  responses to Fluo-3-mediated imaging. Interestingly, PSEN1 E280A ChLNs showed higher intracellular  $Ca^{2+}$  in response to ACh treatment at day 0 (Fig 6C and 6D) and 2 (Fig 6F and 6G) than WT PSEN1 ChLNs (Fig 6D and 6G). The average fluorescence change ( $\Delta F/F$ ) was  $4.6 \pm 1.2$  and  $5.1 \pm 1.1$ -fold, respectively, with a mean duration of  $40 \pm 10$  s ( $n = 20$  ChLN cells imaged,  $N = 3$  dishes). Nevertheless, we found a significant difference in the  $\Delta F/F$  response ( $\Delta F/F = 1.1 \pm 0.75$ ,  $p < 0.001$ ) in PSEN1 E280A ChLNs exposed to ACh at 4 days post differentiation (Fig 6I and 6J) compared to that in WT ChLNs (Fig 6H and 6J).

The above findings compelled us to evaluate whether ChLNs expressed a catalytically functional acetylcholinesterase (AChE) enzyme at similar times post of transdifferentiation. As shown in Fig 6K, the AChE enzyme showed similar catalytic activity at days 2 and 4 in both WT PSEN1 and PSEN1 E280A ChLNs. However, the AChE enzyme activity in PSEN1 E280A ChLNs was significantly lower (at least 5-fold) than that in WT PSEN1 ChLNs at day 4.

### PSEN1 E280A ChLNs induce phosphorylation of TAU protein

Several experimental data support  $A\beta$ -induced TAU pathology (e.g., ref. [45]), however no data is available to determine whether sAPP $\beta$ f can induce protein TAU phosphorylation. We thus evaluated whether PSEN1 E280A ChLNs display abnormal levels of phosphorylated TAU protein at residues Ser<sup>202</sup> and Thr<sup>205</sup>, two well-known hyperphosphorylated epitopes involved in AD pathology [46]. To this end, wild-type and mutant ChLNs were left in regular culture medium (RCm) for 0, 2 and 4 days. Then, the ratio of phosphorylated TAU (p-TAU)/total TAU (t-TAU) was determined by western blot and immunofluorescence imaging analyses. As shown in Fig 7, while WT PSEN1 ChLNs showed no phosphorylation of TAU protein according to western blot (Fig 7A and 7B) and immunofluorescence microscopy (Fig 7C'–7E' and 7I), PSEN1 E280A ChLNs presented an increase in the p-TAU/ t-TAU ratio at 4 days post transdifferentiation (Fig 7A, 7B, 7F'–7H' and 7I). JNK has been suggested to phosphorylate TAU at the Ser202/Thr205 epitopes [47]. Therefore, we determined whether JNK was implicated in TAU phosphorylation in ChLNs. To this end, PSEN1 E280A ChLNs were incubated with the JNK inhibitor SP600125 for 0, 2 and 4 days. Notably, the p-TAU/ t-TAU ratio remained unaltered at 0 (Fig 7J, 7K, 7O' and 7R), 2 (Fig 7J, 7K, 7P' and 7R) and 4 days post differentiation (Fig 7J, 7K, 7Q' and 7R).

### Discussion

Currently, the neuropathology of AD includes extracellular deposits of  $A\beta$  in plaques, intracellular neurofibrillary tangles comprising hyperphosphorylated TAU, synaptic dysfunction, and neuronal death. In an effort to explain such observations, several theories have been proposed [48]; however, the amyloid cascade hypothesis has prevailed for more than 25 years [49]. The  $A\beta$  hypothesis postulates that an imbalance in the production of extracellular  $A\beta_{42}$  plaques by mutations in at least three genes (e.g., *APP*, *PSEN1*; *PSEN2*) is an early initiating factor in AD.

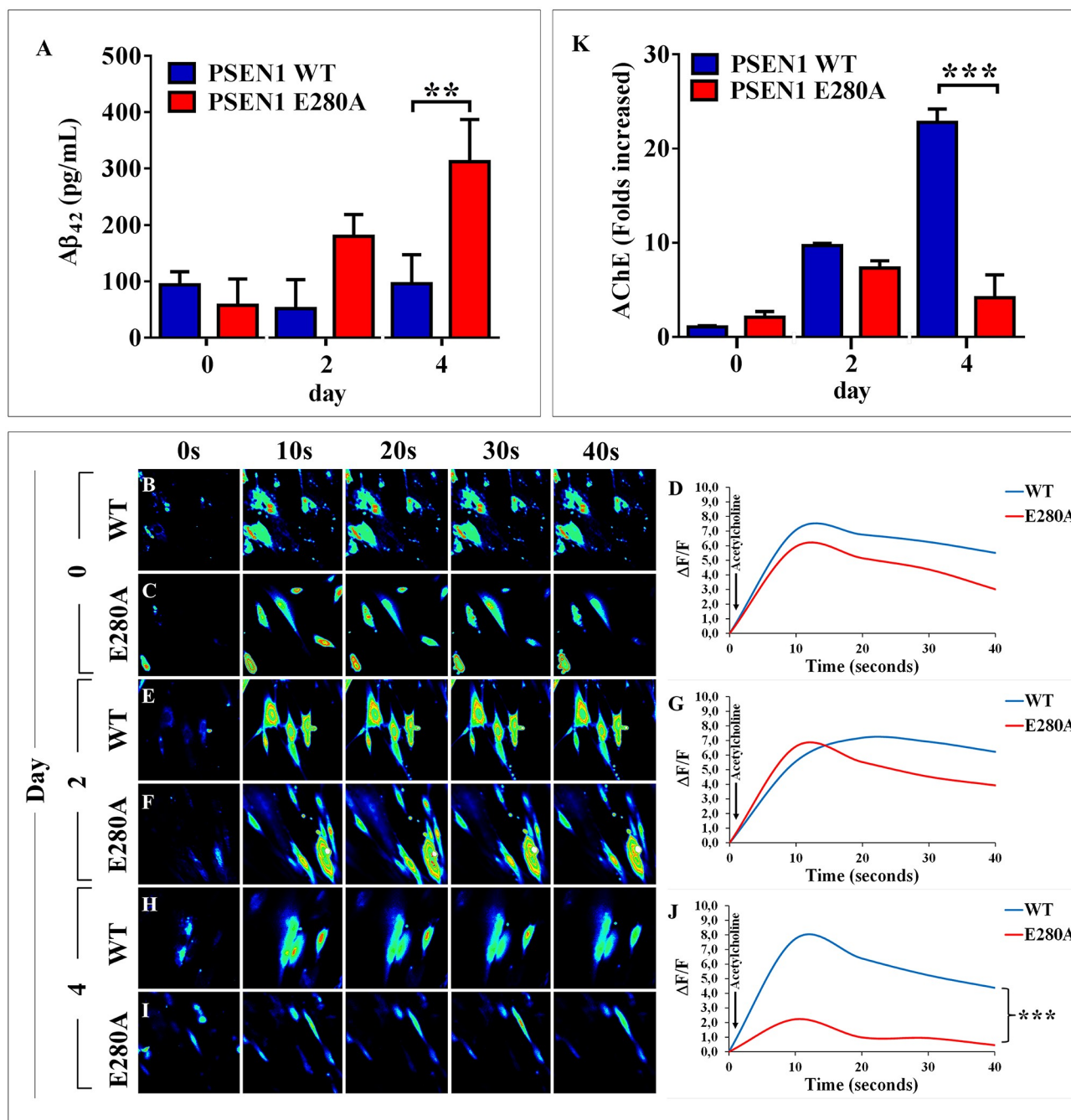


**Fig 6. PSEN1 E280A ChLNs show a reduced functional response to Acetylcholine (ACh), low acetylcholinesterase activity and high levels of extracellular Aβ<sub>42</sub> peptide.** After 7 days of transdifferentiation, WT PSEN1 and PSEN1 E280A ChLNs were left in regular culture medium for 0, 2 and 4 days, as indicated in the figure. (A) ELISA quantification of extracellular Aβ<sub>42</sub> peptide in supernatants. Time-lapse images (0, 10, 20, 30, 40 s) of Ca<sup>2+</sup> fluorescence in WT PSEN1 and PSEN1 E280A ChLNs after 0 (B–C), 2 (E–F) and 4 days (H–I) in response to ACh treatment. ACh was puffed into the culture at 10 s (arrow). Then, the Ca<sup>2+</sup> fluorescence of the cells was monitored at the indicated times. Color contrast indicates fluorescence intensity: dark blue < light blue < green < yellow < red. (D, G, J) Normalized mean fluorescence signal (ΔF/F) over time from the cells indicating temporal cytoplasmic Ca<sup>2+</sup> elevation in response to ACh treatment. (K) Measurement of acetylcholinesterase activity at 0, 2 and 4 days post transdifferentiation. Data are presented as the means ± SD. \**p* < 0.05; \*\**p* < 0.01; \*\*\**p* < 0.001. The histograms and figures represent 1 out of 3 independent experiments. Image magnification, 400x.

<https://doi.org/10.1371/journal.pone.0221669.g006>

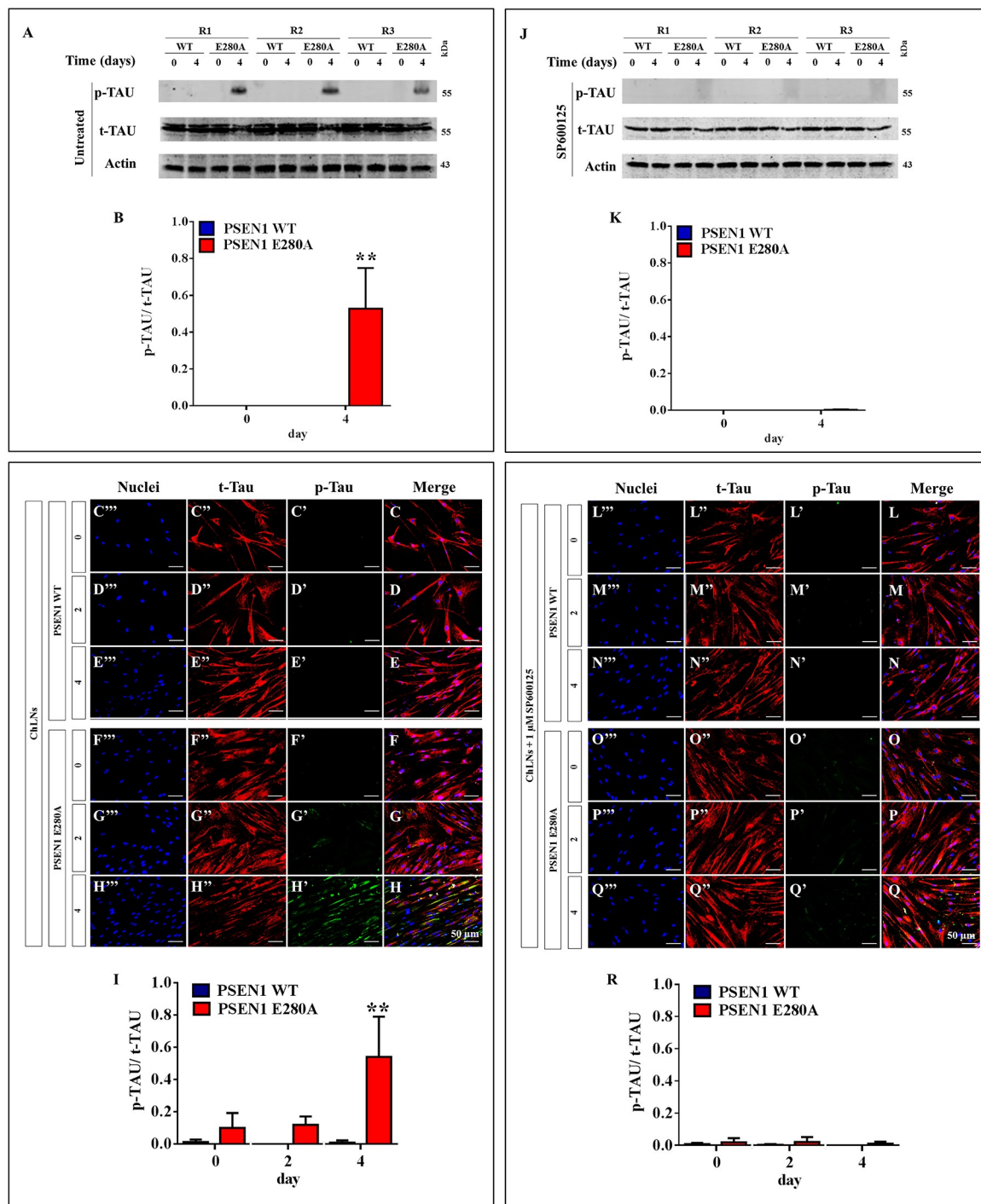


**Fig 7. PSEN1 E280A ChLNs induce phosphorylation of TAU protein.** After 7 days of transdifferentiation, WT PSEN1 and PSEN1 E280A ChLNs were left untreated (A-I) or treated with 1  $\mu$ M JNK inhibitor SP600125 (J-R) in regular culture medium for 0, 2 and 4 days as indicated in the figure. After this time, the proteins in the extracts were blotted with primary antibodies against phosphorylated TAU (p-TAU), total TAU (t-TAU) and actin proteins. The intensities of the western blot bands shown in (A or J) were measured (B or K) by an infrared imaging system (Odyssey, LI-COR), and the p-TAU/t-TAU ratio was normalized to that of actin. Additionally, ChLNs were double stained as indicated in the figure (C-H or L-Q) with primary antibodies against p-TAU (green; C'-H' or L'-Q') and t-TAU (red; C''-H'' or L''-Q''). The nuclei were stained with Hoechst 33342 (blue; C'''-H''' or L'''-Q'''). (I and R) Quantification of the p-TAU/t-TAU fluorescence ratio. Data are expressed as the mean  $\pm$  SD; \* $p < 0.05$ ; \*\* $p < 0.01$ ; \*\*\* $p < 0.001$ . The blots and figures represent 1 out of 3 independent experiments. Image magnification, 200x.

<https://doi.org/10.1371/journal.pone.0221669.g007>



However, experimental therapies targeting A $\beta$  have thus far been unsuccessful [50]. Several factors have probably contributed to the failures in AD drug development, including unsuitable preclinical research models that do not fully recapitulate the human disease; consequently, druggable targets remain missing [51]. Furthermore, the mechanism(s) by which hAPP/ A $\beta$ <sub>42</sub> might induce toxicity is not yet fully established. Because UC-MSCs possess plasticity properties enabling them to transdifferentiate into non-mesenchymal lineages, they provide a unique opportunity to study the effect of *PSEN1* mutations in neuronal cells. Most importantly, MSC-derived neurons are natural, non-genetically modified cells of the FAD *PSEN1* mutation. Here, we used UC-MSCs bearing the mutation *PSEN1* E280A for the first time and found that the mutation alters none of the typical MSC characteristics, such as colony-forming capacity, fibroblast-like morphology, immunophenotype and/or ability to differentiate or transdifferentiate into ChLNs. Furthermore, we did not detect any APP/ A $\beta$ <sub>42</sub> produced by the cells or any other cellular alterations (e.g., ROS production, mitochondria depolarization, and oxidation of stress sensor DJ-1) in mutant MSCs. These observations suggest that the *PSEN1* E280A mutation might not affect the physiology of the multipotent MS cells at this stage of development.

In this study, we report for the first time that ChLNs derived from hMSCs carrying the *PSEN1* E280A mutation recapitulate typical pathologic features of AD at 4 days post transdifferentiation, i.e., eleven days of culture (7 days in Ch-N-Rm and 4 days in RCm) including increased secretion of A $\beta$ <sub>42</sub>, intracellular accumulation of sAPP $\beta$ f, and TAU phosphorylation. Furthermore, *PSEN1* E280A ChLNs not only show OS and apoptosis markers but also display Ca<sup>2+</sup> flux dysregulation and altered acetylcholinesterase activity. Our data provide evidence that intracellular sAPP $\beta$ f specifically induces neurotoxicity through a temporal and sequential order of molecular events in *PSEN1* E280A ChLNs. In agreement with commercial laboratory Western blot data (<https://www.biolegend.com/en-us/products/anti-beta-amyloid-1-16-antibody-10998>), the antibody 6E10 recognized monomers (4 kDa), and aggregated (~100 kDa) synthetic A $\beta$ <sub>42</sub>, and high molecular weight APP/ A $\beta$ <sub>42</sub> (~100 kDa) in *PSEN1* E280A ChLNs. Interestingly, no A $\beta$ <sub>42</sub> monomers were detected in mutant ChLNs. These observations suggested aggregation of APP. In agreement with this assumption, mass spectrometry (MS) analysis identified several APP fragments (e.g., APP714, APP733, APP751, APP752, collectively named sAPP $\beta$ f) but no A $\beta$ <sub>42</sub> fragment was present at the gel region of HMW proteins (60–120 kDa). Outstandingly, the sAPP fragments can be generated not only by the  $\beta$ -secretase but also by the  $\delta$ -secretase,  $\eta$ -secretase or Meprin  $\beta$  [4]. Taken together these observations suggest that sAPP fragments rather than A $\beta$ <sub>42</sub> are accumulating early in the *PSEN1* E280A cholinergic neurons. Accordingly, we found intracellular sAPP $\beta$ f accumulation in ChLNs after 7 days of transdifferentiation (day 0), at which time fully developed ChLNs were obtained [29]. Whether intracellular APP fragments build up because full length APP processing is altered and consequently some APP fragments remain intracellular leading to cell death require further investigation. However, recent data support this view. Indeed, it has been shown that hAPP overexpression causes A $\beta$ -independent neuronal death in olfactory sensory neurons via intrinsic apoptosis pathway [5, 6]. In contrast, others have found that the *PSEN1* L166P and G384A mutations cause relocalization of  $\gamma$ -secretase, which significantly promotes the generation of intracellular long A $\beta$ <sub>42</sub> [52]. Although it is not yet known whether the *PSEN1* E280A mutation induces relocalization of  $\gamma$ -secretase, similar to *PSEN1* mutations, our data suggest that the *PSEN1* E280A mutation strongly enhances intraneuronal sAPP $\beta$ f aggregates in ChLNs. These results support the view that intracellular accumulation of sAPP $\beta$ f is the earliest event in the development of the neuropathological changes of AD [53]. Since the *PSEN1* E280A mutation might represent a typical trans-dominant negative mutation on  $\gamma$ -secretase [15, 16], we do not discard the possibility that APP-derived intracellular A $\beta$ <sub>42</sub> aggregates might



be a late event in the process of neurodegeneration [7, 54, 55]. Interestingly, we simultaneously found a significant increase in DCF fluorescent-positive cells, DJ-1 Cys<sup>106</sup>-sulfonate (DJ-1 Cys<sup>106</sup>SO<sub>3</sub>), which is the most sensitive thiol group towards H<sub>2</sub>O<sub>2</sub> reactivity [56], and activation of transcription factor c-JUN in PSEN1 E280A ChLNs. These observations suggest that sAPPβf (aggregates) > H<sub>2</sub>O<sub>2</sub> > oxDJ-1 Cys<sup>106</sup>-SO<sub>3</sub> and c-JUN are the earliest events detectable in PSEN1 E280A ChLNs. These findings imply that hAPP and/or sAPPβf (high molecular weight aggregates) can trigger events related to oxidative stress and cell death [5, 6]. How then does intracellular sAPPβf generate H<sub>2</sub>O<sub>2</sub>? Several lines of evidence for the intracellular toxicity of APP have been suggested, including inhibition of mitochondrial import channels (e.g., TOM40 and TIM23), impairment of mitochondrial transport (e.g., Cytochrome c oxidase), and disruption the electron transfer [57]. Whatever the mechanism, we demonstrated for the first time that sAPPβf endogenously produces H<sub>2</sub>O<sub>2</sub> in PSEN1 E280A ChLNs. Because H<sub>2</sub>O<sub>2</sub> can function as a second messenger [58], it might also activate other redox proteins, such as apoptosis-signal regulating kinase 1 (ASK-1, [59], which in turn directly or indirectly activate other signaling pathways, e.g., JNK/c-JUN [60]. We found that sAPPβf induced phosphorylation of c-JUN [61], p53 and PUMA in PSEN1 E280A ChLNs. Notably, c-JUN- and p53-dependent apoptosis is triggered by transactivation of the pro-apoptotic gene PUMA [62–64]. Remarkably, JNK can also stabilize and activate p53 [65]. Taken together, these results suggest that sAPPβf > H<sub>2</sub>O<sub>2</sub> activates a cascade of events leading to the JNK > c-JUN, p53 > PUMA pathway. Although PUMA has been shown to cooperate with direct activator proteins (e.g., BAX) to promote mitochondrial outer membrane permeabilization (MOMP) and apoptosis [66], the exact mechanism by which MOMP occurs is not fully understood [67]. Interestingly, PSEN1 E280A ChLNs showed loss of ΔΨ<sub>m</sub> concomitant with overexpression of CASPASE-3 and fragmentation of nuclei at day 4 post transdifferentiation. These observations suggest that mitochondria play an important role in intracellular sAPPβf-induced apoptosis in mutant ChLNs. However, whether ΔΨ<sub>m</sub> dysfunction is a consequence of a direct effect of intracellular sAPPβf on the organelle or whether the damage is the result of the impact of PUMA on mitochondria is an unresolved issue. Our findings suggest that both sAPPβf / PUMA might separately or jointly damage ΔΨ<sub>m</sub>. Taken together, these data indicate that sAPPβf induce a cascade of events in PSEN1 E280A ChLNs through the H<sub>2</sub>O<sub>2</sub> signaling pathway involving CASP-3, as an end executor protein, and DNA fragmentation of nuclei, all indicative of apoptosis. Taken together, these data comply with the idea that intraneuronal accumulation of the APP fragments (sAPPβf) are the first step of a lethal cascade in FAD neurons.

Neuronal calcium (Ca<sup>2+</sup>) dyshomeostasis has been proposed to play a crucial role in AD disease progression [68]. However, the mechanisms of Ca<sup>2+</sup> dysregulation are not clear. In contrast to Demuro and Parker [69], who found that intracellular Aβ<sub>42</sub> oligomers disrupted cellular Ca<sup>2+</sup> regulation, we observed no Ca<sup>2+</sup> dysregulation in PSEN1 E280A ChLNs evaluated at 0, 2, and 4 days post transdifferentiation. This discrepancy can be explained by differences in experimental methodology. Whereas those authors elucidated the actions of intracellular Aβ<sub>42</sub> by imaging Ca<sup>2+</sup> responses to injections of Aβ<sub>42</sub> oligomers into *Xenopus* oocytes, we directly imaged Ca<sup>2+</sup> responses to endogenously generated intracellular APP in mutant ChLNs. Under the present experimental conditions, we concluded that intracellular sAPPβf did not affect Ca<sup>2+</sup> flux in PSEN1 E280A ChLNs. However, increasing evidence has shown that extracellular Aβ specifically interacts with nAChRs, resulting in Ca<sup>2+</sup> dysregulation [70]. We found that the PSEN1 E280A ChLN response to ACh was significantly reduced by day 4 post transdifferentiation. Notably, Aβ has been shown to directly affect α7 nicotinic ACh receptor (α7 nAChR) function by acting as an agonist (~100 nM) and a negative modulator (at high concentrations) [71]. Consistent with this view, we confirmed that PSEN1 E280A ChLNs secreted aberrant amounts of Aβ<sub>42</sub> (e.g., ~2500-f.i.) compared to WT PSEN1 ChLNs. These

observations confirm that overproduction of extracellular A $\beta$ 42 is a paramount feature of the majority of PSEN1 mutations *in vitro* and *in vivo* [9], including the E280A mutation [25]. Despite these observations, further investigation is required to determine whether  $\alpha$ 7 nAChRs specifically are affected by A $\beta$ 42 in PSEN1 E280A ChLNs. In contrast to others (e.g., [72]), our observations do not support the common view that extracellular A $\beta$  is capable of increasing neuronal Ca<sup>2+</sup> flux through A $\beta$ 42-forming pores. However, we do not discard the possibility that given a longer incubation time, A $\beta$ 42 could affect Ca<sup>2+</sup> flux via A $\beta$ 42-forming pores in PSEN1 E280A ChLNs. Taken together, and our data suggest that extracellular A $\beta$ 42 might bind to nAChRs in PSEN1 E280A ChLNs, affecting neuronal Ca<sup>2+</sup> flux.

The accumulation of hyperphosphorylated TAU in neurons leads to neurofibrillary degeneration in AD [73]. Mounting evidence suggests that TAU pathogenesis is promoted by A $\beta$ 42 [74,75]. We found that PSEN1 E280A ChLNs showed hyperphosphorylation of TAU protein. In fact, PSEN1 E280A ChLNs exhibited a significantly higher p-TAU/ t-TAU ratio than WT PSEN1 ChLNs at 4 days post transdifferentiation. Because absence of A $\beta$ 42, these observations imply that sAPP $\beta$  rather than A $\beta$ 42 signaling precedes TAU phosphorylation [75, 76] in PSEN1 E280A ChLNs. These findings suggest that sAPP $\beta$  accumulation might affect TAU pathology. However, the molecular link between sAPP $\beta$  and TAU is still not yet completely defined. In agreement with others [77], our data suggest that JNK is a strong candidate TAU kinase involved in the hyperphosphorylation of TAU in PSEN1 E280A ChLNs. This assumption is supported by two observations. First, JNK phosphorylates TAU at Ser<sup>202</sup>/ Thr<sup>205</sup> [47], two phosphorylation epitopes identified in the present study. Second, PSEN1 E280A ChLNs exposed to the JNK inhibitor SP600125 significantly reduced TAU phosphorylation. Given that JNK plays a pivotal role in both OS-induced apoptosis and TAU phosphorylation, these findings identify JNK as a potential therapeutic target [78]. Although we do not discard the possibility that other kinases might be implicated in TAU pathology (e.g., LRRK2, GSK-3, Cdk5), our findings suggest that JNK plays a key role in TAU hyperphosphorylation in PSEN1 E280A ChLNs. Our results suggest that PSEN1 E280A-induced neural alterations may precede A $\beta$ 42 deposition and that those alterations represent longstanding effects of intracellular sAPP $\beta$  toxicity and possibly even developmental changes. The molecular alterations might start when neurons develop into neuron-specific cholinergic-type cells or may even exist at birth. These findings may explain why functional and structural brain changes manifest in children (9–17 years old) and young individuals (18–26 years old) who are carriers of the PSEN1 E280A mutation [79, 80]. Furthermore, these observations suggest that intracellular sAPP $\beta$  toxicity is an early and slowly progressive process that might damage neuronal cells in a TAU-dependent and independent fashion (OS,  $\Delta\Psi_m$  shutdown, apoptosis and intraneuronal Ca<sup>2+</sup> dysregulation) more than two decades before the stage of dementia [10, 81].

## Conclusion

We demonstrate that intracellular accumulation of sAPP $\beta$ , generation of H<sub>2</sub>O<sub>2</sub>, oxidation of the DJ-1 protein (DJ-1 Cys<sup>106</sup>-SO<sub>3</sub>), and activation of the pro-apoptosis protein c-JUN were the earliest cellular changes in PSEN1 E280A ChLNs (obtained after 7 days in Ch-N-Rm (i.e., day 0 in RCm), Fig 8 step 1, s2, s3, s4/s5). These changes were followed by the activation of pro-apoptosis proteins p53 (s6) and PUMA (s7), loss of mitochondria membrane potential ( $\Delta\Psi_m$ , s8), activation of CASP-3 (s9), fragmentation of nuclei (s10), and complete expression of markers of apoptosis (at day 4 post transdifferentiation in RCm). These biochemical abnormalities were found concomitant with irregular secretion of A $\beta$ 42 (day 4, s11), Ca<sup>2+</sup> flux dysregulation (s12), diminished secretion of AChE (s13), and hyperphosphorylation of TAU protein (day 4, s14). Therefore, our data support the view that FAD PSEN1 E280A cholinergic

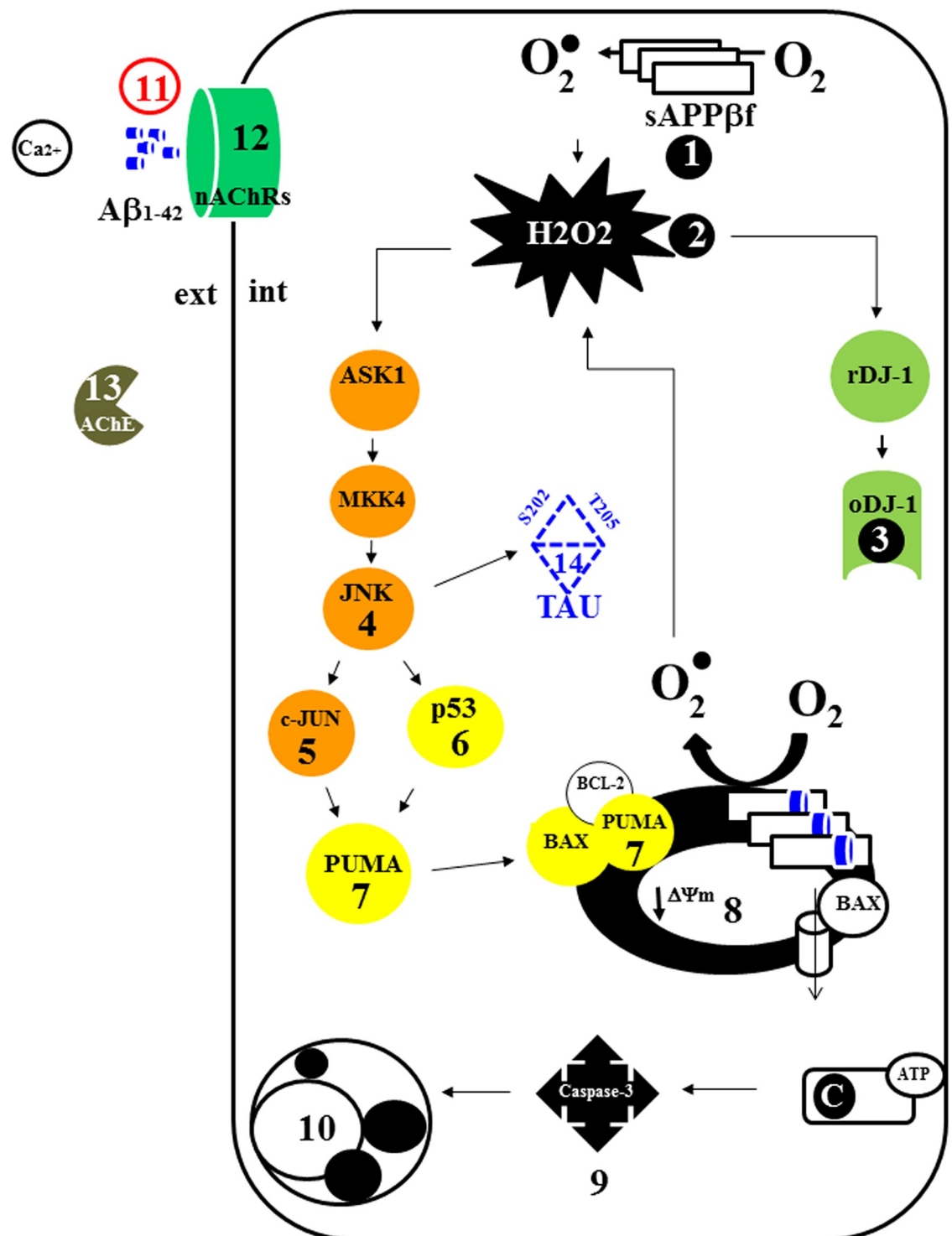


**Fig 8.** Schematic effects of the sAPPβf and Aβ<sub>42</sub> peptide in mutant PSEN1 E280A ChLNs.

<https://doi.org/10.1371/journal.pone.0221669.g008>

neuronal pathology is instigated by early intracellular accumulation of sAPPβf [55, 82]. These findings raise the question of whether strategies to remove extracellular Aβ<sub>42</sub> such as immunotherapy [83] should be complemented with treatments to remove intracellular sAPPβf [84] and OS (i.e., H<sub>2</sub>O<sub>2</sub>) to avoid apoptosis and TAU pathology and treatment with nAChR

agonists to increase neuronal functionality. The present findings naturally (i.e., not genetically manipulated) recapitulated for the first time the neuropathological features of FAD PSEN1 E280A. We anticipate that the present *in vitro* model will inspire new and innovative therapies for early onset PSEN1 E280A patients. Despite the fact that the mutation PSEN1 E280A is 100% penetrant in those individuals bearing such mutation, and given that our findings are based on ChLNs obtained from a single PSEN1 E280A MSCs, the conclusions from such analyses require verification through additional studies with larger sample size.

## Supporting information

### S1 Fig. Identification of PSEN1 genotype in WT PSEN1 and PSEN1 E280A in WJ-MSCs.

The PSEN1 E280A mutation was detected as described in *Materials and Methods* section. According to different mobility electrophoretic patterns, samples were classified as wild-type (WT) or mutant PSEN1 E280A when compared to PSEN1 E280A carrier (positive case NB code#18233) or wild type PSEN1 genotype (NB code#18574). **Abbreviations:** TBC# = tissue bank code number; F = female, M = male; (+) = positive; (-) = negative; numbers on the left are molecular size markers expressed in bp.

(TIF)

### S2 Fig. Apolipoprotein E (APOE) genotype in WT PSEN1 and PSEN1 E280A (n = 1) WJ-MSCs.

Electrophoretic separation of *HhaI* fragments after gene amplification of DNA from WT PSEN1 and PSEN1 E280A WJ-MSCs. The DNA band pattern was determined according to ref. [29]. Numbers on the left are molecular size markers expressed in bp. **Abbreviations:** TBC# = tissue bank code number; F = female, M = male.

(TIF)

**S3 Fig. WT PSEN1 and PSEN1 E280A WJ-MSCs show similar levels of intracellular APP/A $\beta_{42}$  and oxidized DJ-1.** WT PSEN1 and PSEN1 E280A WJ-MSCs were cultured in MCm for 7 days, and then cultured for 4 additional days in regular culture medium (RCm). Then, the proteins in the extracts and control extracts were blotted with primary antibodies against A $\beta_{42}$ , oxDJ-1Cys<sup>106</sup> and actin proteins. The intensities of the western blot bands shown in (A) were measured (B, C) by an infrared imaging system (Odyssey, LI-COR), and the intensity was normalized to that of actin. Control lysates were included to validate the results. Additionally, after 0, 2 and 4 days, WJ-MSCs were double stained as indicated in the figure (D-I) with primary antibodies against A $\beta_{42}$  (red; D'-I') and oxDJ-1Cys<sup>106</sup> (green; D''-I''). The nuclei were stained with Hoechst 33342 (blue; D'''-I'''). (J) Quantification of A $\beta_{42}$  fluorescence intensity. (K) Quantification of oxDJ-1Cys<sup>106</sup> fluorescence as MFI. Data are expressed as the mean  $\pm$  SD; \* $p < 0.05$ ; \*\* $p < 0.01$ ; \*\*\* $p < 0.001$ . The blots and figures represent 1 out of 3 independent experiments. Image magnification, 200x.

(TIF)

**S4 Fig. WT PSEN1 and PSEN1 E280A WJ-MSCs show similar levels of mitochondrial membrane potential ( $\Delta\Psi_m$ ), intracellular reactive oxygen species (ROS) and DNA fragmentation.** Representative histograms showing DiOC<sub>6</sub>(3)<sup>low</sup> (A), DCF+ (B) and SubG<sub>1</sub> (C) populations from WT PSEN1 (blue) and PSEN1 E280A (Red) WJ-MSCs after 7 days in MCm plus 4 days in RCm. Representative MitoTracker (D'-I'), DCF (D''-I''), Hoechst (D'''-I''') and merged (D-I) pictures of WT PSEN1 and PSEN1 E280A WJ-MSCs after 0, 2 and 4 days in RCm. (J) Quantification of MitoTracker fluorescence intensity. (K) Quantification of DCF fluorescence intensity. Data are expressed as the mean  $\pm$  SD; \* $p < 0.05$ ; \*\* $p < 0.01$ ; \*\*\* $p < 0.001$ . The histograms and figures represent 1 out of 3 independent experiments. Image

magnification, 200x.  
(TIF)

**S5 Fig.** Mascot Search Results of (A) MS/MS fragmentation of LPTTAASTPDVADK, and (B) MS/MS fragmentation of AVIQHFQEK. (C) List of proteins identified in the PAGE gel region of high molecular weight between 60 and 125 kDa.  
(PDF)

**S1 File.**  
(ZIP)

**S1 Data.**  
(XLSX)

## Acknowledgments

We greatly acknowledge KA Herrera-Galeano (Nurse), F Piedrahita (Nurse), L Lopez (Psychologist) and AA Espinosa-Rojas (MD) for technical support for obtaining human umbilical cord tissue at Hospital San Juan de Dios, Yarumal, Colombia. We specially acknowledge the newborns' parents for human umbilical cord tissue. We thank Dr. A Shevchenko (Head of Mass Spectrometry, Max Plank Institute of Molecular Cell Biology and Genetics, Dresden-Germany) for LC-MS/MS analysis.

## Author Contributions

**Conceptualization:** Carlos Velez-Pardo, Marlene Jimenez-Del-Rio.

**Data curation:** Viviana Soto-Mercado, Miguel Mendivil-Perez, Carlos Velez-Pardo, Marlene Jimenez-Del-Rio.

**Formal analysis:** Viviana Soto-Mercado, Miguel Mendivil-Perez, Carlos Velez-Pardo.

**Funding acquisition:** Francisco Lopera, Marlene Jimenez-Del-Rio.

**Investigation:** Viviana Soto-Mercado, Miguel Mendivil-Perez.

**Methodology:** Viviana Soto-Mercado, Miguel Mendivil-Perez.

**Project administration:** Marlene Jimenez-Del-Rio.

**Resources:** Francisco Lopera, Marlene Jimenez-Del-Rio.

**Supervision:** Carlos Velez-Pardo, Francisco Lopera.

**Writing – original draft:** Carlos Velez-Pardo, Marlene Jimenez-Del-Rio.

**Writing – review & editing:** Viviana Soto-Mercado, Miguel Mendivil-Perez, Carlos Velez-Pardo, Francisco Lopera, Marlene Jimenez-Del-Rio.

## References

1. Lane CA, Hardy J, Schott JM. Alzheimer's disease. *Eur J Neurol*. 2018; 25(1):59–70. Epub 2017/09/06. <https://doi.org/10.1111/ene.13439> PMID: 28872215.
2. Douchamps V, Mathis C. A second wind for the cholinergic system in Alzheimer's therapy. *Behav Pharmacol*. 2017; 28(2 and 3-Spec Issue):112–23. Epub 2017/02/28. <https://doi.org/10.1097/FBP.0000000000000300> PMID: 28240674.
3. Perl DP. Neuropathology of Alzheimer's disease. *Mt Sinai J Med*. 2010; 77(1):32–42. Epub 2010/01/27. <https://doi.org/10.1002/msj.20157> PMID: 20101720.



4. Andrew RJ, Kellett KA, Thinakaran G, Hooper NM. A Greek Tragedy: The Growing Complexity of Alzheimer Amyloid Precursor Protein Proteolysis. *J Biol Chem*. 2016; 291(37):19235–44. Epub 2016/07/31. <https://doi.org/10.1074/jbc.R116.746032> PMID: 27474742.
5. Cheng N, Jiao S, Gumaste A, Bai L, Belluscio L. APP Overexpression Causes Abeta-Independent Neuronal Death through Intrinsic Apoptosis Pathway. *eNeuro*. 2016; 3(4). Epub 2016/08/16. <https://doi.org/10.1523/eneuro.0150-16.2016> PMID: 27517085.
6. Cheng N, Cai H, Belluscio L. In vivo olfactory model of APP-induced neurodegeneration reveals a reversible cell-autonomous function. *J Neurosci*. 2011; 31(39):13699–704. Epub 2011/10/01. <https://doi.org/10.1523/JNEUROSCI.1714-11.2011> PMID: 21957232.
7. Takahashi RH, Nagao T, Gouras GK. Plaque formation and the intraneuronal accumulation of beta-amyloid in Alzheimer's disease. *Pathol Int*. 2017; 67(4):185–93. Epub 2017/03/07. <https://doi.org/10.1111/pin.12520> PMID: 28261941.
8. Steiner H, Fukumori A, Tagami S, Okochi M. Making the final cut: pathogenic amyloid- $\beta$  peptide generation by  $\gamma$ -secretase. *Cell Stress*. 2018; 2(11):292–310. <https://doi.org/10.15698/cst2018.11.162> PMID: 31225454
9. Sun L, Zhou R, Yang G, Shi Y. Analysis of 138 pathogenic mutations in presenilin-1 on the in vitro production of Abeta42 and Abeta40 peptides by gamma-secretase. *Proc Natl Acad Sci U S A*. 2017; 114(4):E476–e85. Epub 2016/12/09. <https://doi.org/10.1073/pnas.1618657114> PMID: 27930341.
10. Acosta-Baena N, Sepulveda-Falla D, Lopera-Gómez CM, Jaramillo-Elorza MC, Moreno S, Aguirre-Acevedo DC, et al. Pre-dementia clinical stages in presenilin 1 E280A familial early-onset Alzheimer's disease: a retrospective cohort study. *Lancet Neurol*. 2011; 10(3):213–20. [https://doi.org/10.1016/S1474-4422\(10\)70323-9](https://doi.org/10.1016/S1474-4422(10)70323-9) PMID: 21296022.
11. Lopera F, Ardilla A, Martinez A, Madrigal L, Arango-Viana JC, Lemere CA, et al. Clinical features of early-onset Alzheimer disease in a large kindred with an E280A presenilin-1 mutation. *Jama*. 1997; 277(10):793–9. Epub 1997/03/12. PMID: 9052708.
12. Sepulveda-Falla D, Glatzel M, Lopera F. Phenotypic profile of early-onset familial Alzheimer's disease caused by presenilin-1 E280A mutation. *J Alzheimers Dis*. 2012; 32(1):1–12. <https://doi.org/10.3233/JAD-2012-120907> PMID: 22766738.
13. Fuller JT, Cronin-Golomb A, Gatchel JR, Norton DJ, Guzman-Velez E, Jacobs HIL, et al. Biological and Cognitive Markers of Presenilin1 E280A Autosomal Dominant Alzheimer's Disease: A Comprehensive Review of the Colombian Kindred. *J Prev Alzheimers Dis*. 2019; 6(2):112–20. Epub 2019/02/14. <https://doi.org/10.14283/jpad.2019.6> PMID: 30756118.
14. Lalli MA, Cox HC, Arcila ML, Cadavid L, Moreno S, Garcia G, et al. Origin of the PSEN1 E280A mutation causing early-onset Alzheimer's disease. *Alzheimers Dement*. 2014; 10(5 Suppl):S277–S83.e10. Epub 2013/11/19. <https://doi.org/10.1016/j.jalz.2013.09.005> PMID: 24239249.
15. Heilig EA, Gutti U, Tai T, Shen J, Kelleher RJ 3rd. Trans-dominant negative effects of pathogenic PSEN1 mutations on gamma-secretase activity and Abeta production. *J Neurosci*. 2013; 33(28):11606–17. Epub 2013/07/12. <https://doi.org/10.1523/JNEUROSCI.0954-13.2013> PMID: 23843529.
16. Zhou R, Yang G, Shi Y. Dominant negative effect of the loss-of-function gamma-secretase mutants on the wild-type enzyme through heterooligomerization. *Proc Natl Acad Sci U S A*. 2017; 114(48):12731–6. Epub 2017/10/29. <https://doi.org/10.1073/pnas.1713605114> PMID: 29078389.
17. Lemere CA, Lopera F, Kosik KS, Lendon CL, Ossa J, Saido TC, et al. The E280A presenilin 1 Alzheimer mutation produces increased A beta 42 deposition and severe cerebellar pathology. *Nat Med*. 1996; 2(10):1146–50. <https://doi.org/10.1038/nm1096-1146> PMID: 8837617.
18. Velez-Pardo C, Arellano JI, Cardona-Gomez P, Jimenez Del Rio M, Lopera F, De Felipe J. CA1 hippocampal neuronal loss in familial Alzheimer's disease presenilin-1 E280A mutation is related to epilepsy. *Epilepsia*. 2004; 45(7):751–6. Epub 2004/07/03. <https://doi.org/10.1111/j.0013-9580.2004.55403.x> PMID: 15230697.
19. Fleisher AS, Chen K, Quiroz YT, Jakimovich LJ, Gomez MG, Langois CM, et al. Florbetapir PET analysis of amyloid- $\beta$  deposition in the presenilin 1 E280A autosomal dominant Alzheimer's disease kindred: a cross-sectional study. *Lancet Neurol*. 2012; 11(12):1057–65. [https://doi.org/10.1016/S1474-4422\(12\)70227-2](https://doi.org/10.1016/S1474-4422(12)70227-2) PMID: 23137949.
20. Quiroz YT, Sperling RA, Norton DJ, Baena A, Arboleda-Velasquez JF, Cosio D, et al. Association Between Amyloid and Tau Accumulation in Young Adults With Autosomal Dominant Alzheimer Disease. *JAMA Neurol*. 2018; 75(5):548–56. Epub 2018/02/13. <https://doi.org/10.1001/jamaneurol.2017.4907> PMID: 29435558.
21. Kumar K, Kumar A, Keegan RM, Deshmukh R. Recent advances in the neurobiology and neuropharmacology of Alzheimer's disease. *Biomed Pharmacother*. 2018; 98:297–307. Epub 2017/12/24. <https://doi.org/10.1016/j.biopha.2017.12.053> PMID: 29274586.

22. Oksanen M, Petersen AJ, Naumenko N, Puttonen K, Lehtonen S, Gubert Olive M, et al. PSEN1 Mutant iPSC-Derived Model Reveals Severe Astrocyte Pathology in Alzheimer's Disease. *Stem Cell Reports*. 2017; 9(6):1885–97. Epub 2017/11/21. <https://doi.org/10.1016/j.stemcr.2017.10.016> PMID: 29153989.
23. Ochalek A, Mihalik B, Avci HX, Chandrasekaran A, Teglas A, Bock I, et al. Neurons derived from sporadic Alzheimer's disease iPSCs reveal elevated TAU hyperphosphorylation, increased amyloid levels, and GSK3B activation. *Alzheimers Res Ther*. 2017; 9(1):90. Epub 2017/12/02. <https://doi.org/10.1186/s13195-017-0317-z> PMID: 29191219.
24. Yang J, Zhao H, Ma Y, Shi G, Song J, Tang Y, et al. Early pathogenic event of Alzheimer's disease documented in iPSCs from patients with PSEN1 mutations. *Oncotarget*. 2017; 8(5):7900–13. Epub 2016/12/08. <https://doi.org/10.18632/oncotarget.13776> PMID: 27926491.
25. Mendivil-Perez M, Velez-Pardo C, Kosik KS, Lopera F, Jimenez-Del-Rio M. iPSCs-derived nerve-like cells from familial Alzheimer's disease PSEN 1 E280A reveal increased amyloid-beta levels and loss of the Y chromosome. *Neurosci Lett*. 2019; 703:111–8. Epub 2019/03/25. <https://doi.org/10.1016/j.neulet.2019.03.032> PMID: 30904577.
26. Cheng H, Ghetu N, Wallace C, Wei F, Liao S. The Impact of Mesenchymal Stem Cell Source on Proliferation, Differentiation, Immunomodulation and Therapeutic Efficacy. *J Stem Cell Res Ther*. 2014; 4(10):1–8. <https://doi.org/10.4172/2157-7633.1000237>
27. Zhang HT, Fan J, Cai YQ, Zhao SJ, Xue S, Lin JH, et al. Human Wharton's jelly cells can be induced to differentiate into growth factor-secreting oligodendrocyte progenitor-like cells. *Differentiation*. 2010; 79(1):15–20. Epub 2009/10/06. <https://doi.org/10.1016/j.diff.2009.09.002> PMID: 19800163.
28. Bonilla-Porras AR, Velez-Pardo C, Jimenez-Del-Rio M. Fast transdifferentiation of human Wharton's jelly mesenchymal stem cells into neurospheres and nerve-like cells. *J Neurosci Methods*. 2017; 282:52–60. Epub 2017/03/14. <https://doi.org/10.1016/j.jneumeth.2017.03.005> PMID: 28286110.
29. Mendivil-Perez M, Velez-Pardo C, Jimenez-Del-Rio M. Direct transdifferentiation of human Wharton's jelly mesenchymal stromal cells into cholinergic-like neurons. *J Neurosci Methods*. 2019; 312:126–38. Epub 2018/11/26. <https://doi.org/10.1016/j.jneumeth.2018.11.019> PMID: 30472070.
30. Choi J, Lee S, Mallard W, Clement K, Tagliazucchi GM, Lim H, et al. A comparison of genetically matched cell lines reveals the equivalence of human iPSCs and ESCs. *Nat Biotechnol*. 2015; 33(11):1173–81. Epub 2015/10/27. <https://doi.org/10.1038/nbt.3388> PMID: 26501951.
31. Song L, Tsai AC, Yuan X, Bejoy J, Sart S, Ma T, et al. Neural Differentiation of Spheroids Derived from Human Induced Pluripotent Stem Cells-Mesenchymal Stem Cells Coculture. *Tissue Eng Part A*. 2018; 24(11–12):915–29. Epub 2017/11/22. <https://doi.org/10.1089/ten.tea.2017.0403> PMID: 29160172.
32. The structure of the presenilin 1 (S182) gene and identification of six novel mutations in early onset AD families. *Nat Genet*. 1995; 11(2):219–22. Epub 1995/10/01. <https://doi.org/10.1038/ng1095-219> PMID: 7550356.
33. Hixson JE, Vernier DT. Restriction isotyping of human apolipoprotein E by gene amplification and cleavage with HhaI. *J Lipid Res*. 1990; 31(3):545–8. Epub 1990/03/01. PMID: 2341813.
34. Franken NA, Rodermond HM, Stap J, Haveman J, van Bree C. Clonogenic assay of cells in vitro. *Nat Protoc*. 2006; 1(5):2315–9. Epub 2007/04/05. <https://doi.org/10.1038/nprot.2006.339> PMID: 17406473.
35. Huang S, Feng C, Wu Y, Yang S, Ma K, Wu X, et al. Dissimilar characteristics of umbilical cord mesenchymal stem cells from donors of different ages. *Cell Tissue Bank*. 2013; 14(4):707–13. Epub 2013/03/12. <https://doi.org/10.1007/s10561-013-9364-2> PMID: 23475054.
36. Xie X, Du X, Li K, Chen Y, Guan Y, Zhao X, et al. Construction of engineered corpus cavernosum with primary mesenchymal stem cells in vitro. *Sci Rep*. 2017; 7(1):18053. Epub 2017/12/24. <https://doi.org/10.1038/s41598-017-18129-9> PMID: 29273785.
37. Sandoval KE, Farr SA, Banks WA, Crider AM, Morley JE, Witt KA. Somatostatin receptor subtype-4 agonist NNC 26–9100 mitigates the effect of soluble Abeta(42) oligomers via a metalloproteinase-dependent mechanism. *Brain Res*. 2013; 1520:145–56. Epub 2013/05/15. <https://doi.org/10.1016/j.brainres.2013.05.006> PMID: 23669069.
38. Stine WB, Jungbauer L, Yu C, LaDu MJ. Preparing Synthetic Aβ in Different Aggregation States. *Methods Mol Biol*. 2011; 670:13–32. [https://doi.org/10.1007/978-1-60761-744-0\\_2](https://doi.org/10.1007/978-1-60761-744-0_2) PMID: 20967580.
39. Armijo E, Gonzalez C, Shahnawaz M, Flores A, Davis B, Soto C. Increased susceptibility to Abeta toxicity in neuronal cultures derived from familial Alzheimer's disease (PSEN1-A246E) induced pluripotent stem cells. *Neurosci Lett*. 2017; 639:74–81. Epub 2016/12/31. <https://doi.org/10.1016/j.neulet.2016.12.060> PMID: 28034781.
40. Pap P, Koszeghy A, Szucs G, Rusznak Z. Cytoplasmic Ca(2+) concentration changes evoked by cholinergic stimulation in primary astrocyte cultures prepared from the rat cochlear nucleus. *Hear Res*. 2009; 255(1–2):73–83. Epub 2009/06/06. <https://doi.org/10.1016/j.heares.2009.05.006> PMID: 19497356.

41. Sekiguchi-Tonosaki M, Obata M, Haruki A, Himi T, Kosaka J. Acetylcholine induces Ca<sup>2+</sup> signaling in chicken retinal pigmented epithelial cells during dedifferentiation. *Am J Physiol Cell Physiol*. 2009; 296(5):C1195–206. Epub 2009/02/27. <https://doi.org/10.1152/ajpcell.00423.2008> PMID: 19244481.
42. Lazic SE, Clarke-Williams CJ, Munafo MR. What exactly is 'N' in cell culture and animal experiments? *PLoS Biol*. 2018; 16(4):e2005282. Epub 2018/04/05. <https://doi.org/10.1371/journal.pbio.2005282> PMID: 29617358.
43. Mendivil-Perez M, Velez-Pardo C, Jimenez-Del-Rio M. Neuroprotective Effect of the LRRK2 Kinase Inhibitor PF-06447475 in Human Nerve-Like Differentiated Cells Exposed to Oxidative Stress Stimuli: Implications for Parkinson's Disease. *Neurochem Res*. 2016; 41(10):2675–92. Epub 2016/07/11. <https://doi.org/10.1007/s11064-016-1982-1> PMID: 27394417.
44. Taylor P, Camp S, Radić Z. Acetylcholinesterase. In: Squire LR, editor. *Encyclopedia of Neuroscience*. Oxford: Academic Press; 2009. p. 5–7.
45. Stancu IC, Vasconcelos B, Terwel D, Dewachter I. Models of beta-amyloid induced Tau-pathology: the long and "folded" road to understand the mechanism. *Mol Neurodegener*. 2014; 9:51. Epub 2014/11/20. <https://doi.org/10.1186/1750-1326-9-51> PMID: 25407337.
46. Zhou Y, Shi J, Chu D, Hu W, Guan Z, Gong CX, et al. Relevance of Phosphorylation and Truncation of Tau to the Etiopathogenesis of Alzheimer's Disease. *Front Aging Neurosci*. 2018; 10:27. Epub 2018/02/24. <https://doi.org/10.3389/fnagi.2018.00027> PMID: 29472853.
47. Simic G, Babic Leko M, Wray S, Harrington C, Delalle I, Jovanov-Milosevic N, et al. Tau Protein Hyperphosphorylation and Aggregation in Alzheimer's Disease and Other Tauopathies, and Possible Neuroprotective Strategies. *Biomolecules*. 2016; 6(1):6. Epub 2016/01/12. <https://doi.org/10.3390/biom6010006> PMID: 26751493.
48. Du X, Wang X, Geng M. Alzheimer's disease hypothesis and related therapies. *Transl Neurodegener*. 2018; 7:2. Epub 2018/02/10. <https://doi.org/10.1186/s40035-018-0107-y> PMID: 29423193.
49. Hardy J. The discovery of Alzheimer-causing mutations in the APP gene and the formulation of the "amyloid cascade hypothesis". *Febs j*. 2017; 284(7):1040–4. Epub 2017/01/06. <https://doi.org/10.1111/febs.14004> PMID: 28054745.
50. Doig AJ, Del Castillo-Frias MP, Berthoumieu O, Tarus B, Nasica-Labouze J, Sterpone F, et al. Why Is Research on Amyloid-beta Failing to Give New Drugs for Alzheimer's Disease? *ACS Chem Neurosci*. 2017; 8(7):1435–7. Epub 2017/06/07. <https://doi.org/10.1021/acscchemneuro.7b00188> PMID: 28586203.
51. Khachaturian AS, Hayden KM, Mielke MM, Tang Y, Lutz MW, Gustafson DR, et al. Future prospects and challenges for Alzheimer's disease drug development in the era of the NIA-AA Research Framework. *Alzheimers Dement*. 2018; 14(4):532–4. Epub 2018/04/15. <https://doi.org/10.1016/j.jalz.2018.03.003> PMID: 29653605.
52. Sannerud R, Esselens C, Ejsmont P, Mattera R, Rochin L, Tharkeshwar AK, et al. Restricted Location of PSEN2/gamma-Secretase Determines Substrate Specificity and Generates an Intracellular Abeta Pool. *Cell*. 2016; 166(1):193–208. Epub 2016/06/14. <https://doi.org/10.1016/j.cell.2016.05.020> PMID: 27293189.
53. Lauritzen I, Pardossi-Piquard R, Bourgeois A, Becot A, Checler F. Does Intraneuronal Accumulation of Carboxyl-terminal Fragments of the Amyloid Precursor Protein Trigger Early Neurotoxicity in Alzheimer's Disease? *Curr Alzheimer Res*. 2019; 16(5):453–7. Epub 2019/03/26. <https://doi.org/10.2174/1567205016666190325092841> PMID: 30907322.
54. Wirths O, Multhaup G, Bayer TA. A modified beta-amyloid hypothesis: intraneuronal accumulation of the beta-amyloid peptide—the first step of a fatal cascade. *J Neurochem*. 2004; 91(3):513–20. Epub 2004/10/16. <https://doi.org/10.1111/j.1471-4159.2004.02737.x> PMID: 15485483.
55. LaFerla FM, Green KN, Oddo S. Intracellular amyloid-beta in Alzheimer's disease. *Nat Rev Neurosci*. 2007; 8(7):499–509. Epub 2007/06/07. <https://doi.org/10.1038/nrn2168> PMID: 17551515.
56. Kinumi T, Kimata J, Taira T, Ariga H, Niki E. Cysteine-106 of DJ-1 is the most sensitive cysteine residue to hydrogen peroxide-mediated oxidation in vivo in human umbilical vein endothelial cells. *Biochem Biophys Res Commun*. 2004; 317(3):722–8. <https://doi.org/10.1016/j.bbrc.2004.03.110> PMID: 15081400.
57. Spuch C, Ortolano S, Navarro C. New insights in the amyloid-Beta interaction with mitochondria. *J Aging Res*. 2012; 2012:324968. <https://doi.org/10.1155/2012/324968> PMID: 22523685.
58. Di Marzo N, Chisci E, Giovannoni R. The Role of Hydrogen Peroxide in Redox-Dependent Signaling: Homeostatic and Pathological Responses in Mammalian Cells. *Cells*. 2018; 7(10). Epub 2018/10/06. <https://doi.org/10.3390/cells7100156> PMID: 30287799.
59. Saitoh M, Nishitoh H, Fujii M, Takeda K, Tobiume K, Sawada Y, et al. Mammalian thioredoxin is a direct inhibitor of apoptosis signal-regulating kinase (ASK) 1. *EMBO J*. 1998; 17(9):2596–606. <https://doi.org/10.1093/emboj/17.9.2596> PMID: 9564042.

60. Reddy CE, Albanito L, De Marco P, Aiello D, Maggiolini M, Napoli A, et al. Multisite phosphorylation of c-Jun at threonine 91/93/95 triggers the onset of c-Jun pro-apoptotic activity in cerebellar granule neurons. *Cell Death Dis.* 2013; 4:e852. Epub 2013/10/12. <https://doi.org/10.1038/cddis.2013.381> PMID: 24113186.
61. Morishima Y, Gotoh Y, Zieg J, Barrett T, Takano H, Flavell R, et al. Beta-amyloid induces neuronal apoptosis via a mechanism that involves the c-Jun N-terminal kinase pathway and the induction of Fas ligand. *J Neurosci.* 2001; 21(19):7551–60. Epub 2001/09/22. <https://doi.org/10.1523/JNEUROSCI.21-19-07551.2001> PMID: 11567045.
62. Lu H, Hou G, Zhang Y, Dai Y, Zhao H. c-Jun transactivates Puma gene expression to promote osteoarthritis. *Mol Med Rep.* 2014; 9(5):1606–12. Epub 2014/02/26. <https://doi.org/10.3892/mmr.2014.1981> PMID: 24566851.
63. Yu J, Zhang L, Hwang PM, Kinzler KW, Vogelstein B. PUMA induces the rapid apoptosis of colorectal cancer cells. *Mol Cell.* 2001; 7(3):673–82. Epub 2001/07/21. [https://doi.org/10.1016/s1097-2765\(01\)00213-1](https://doi.org/10.1016/s1097-2765(01)00213-1) PMID: 11463391.
64. Nakano K, Vousden KH. PUMA, a novel proapoptotic gene, is induced by p53. *Mol Cell.* 2001; 7(3):683–94. Epub 2001/07/21. [https://doi.org/10.1016/s1097-2765\(01\)00214-3](https://doi.org/10.1016/s1097-2765(01)00214-3) PMID: 11463392.
65. Fuchs SY, Adler V, Pincus MR, Ronai Z. MEKK1/JNK signaling stabilizes and activates p53. *Proc Natl Acad Sci U S A.* 1998; 95(18):10541–6. PMID: 9724739.
66. Hikiş P, Kilianska ZM. PUMA, a critical mediator of cell death—one decade on from its discovery. *Cell Mol Biol Lett.* 2012; 17(4):646–69. Epub 2012/09/25. <https://doi.org/10.2478/s11658-012-0032-5> PMID: 23001513.
67. Pena-Blanco A, Garcia-Saez AJ. Bax, Bak and beyond—mitochondrial performance in apoptosis. *Febs j.* 2018; 285(3):416–31. Epub 2017/07/30. <https://doi.org/10.1111/febs.14186> PMID: 28755482.
68. Briggs CA, Chakroborty S, Stutzmann GE. Emerging pathways driving early synaptic pathology in Alzheimer's disease. *Biochem Biophys Res Commun.* 2017; 483(4):988–97. Epub 2016/09/24. <https://doi.org/10.1016/j.bbrc.2016.09.088> PMID: 27659710.
69. Demuro A, Parker I. Cytotoxicity of intracellular abeta42 amyloid oligomers involves Ca<sup>2+</sup> release from the endoplasmic reticulum by stimulated production of inositol trisphosphate. *J Neurosci.* 2013; 33(9):3824–33. Epub 2013/03/01. <https://doi.org/10.1523/JNEUROSCI.4367-12.2013> PMID: 23447594.
70. Ju Y, Asahi T, Sawamura N. Arctic mutant Abeta40 aggregates on alpha7 nicotinic acetylcholine receptors and inhibits their functions. *J Neurochem.* 2014; 131(5):667–74. Epub 2014/07/26. <https://doi.org/10.1111/jnc.12837> PMID: 25059095.
71. Lasala M, Fabiani C, Corradi J, Antolini S, Bouzat C. Molecular Modulation of Human alpha7 Nicotinic Receptor by Amyloid-beta Peptides. *Front Cell Neurosci.* 2019; 13:37. Epub 2019/02/26. <https://doi.org/10.3389/fncel.2019.00037> PMID: 30800059.
72. Kandel N, Zheng T, Huo Q, Tatulian SA. Membrane Binding and Pore Formation by a Cytotoxic Fragment of Amyloid beta Peptide. *J Phys Chem B.* 2017; 121(45):10293–305. Epub 2017/10/19. <https://doi.org/10.1021/acs.jpcc.7b07002> PMID: 29039658.
73. Avila J. Our Working Point of View of Tau Protein. *J Alzheimers Dis.* 2018; 62(3):1277–85. Epub 2017/10/19. <https://doi.org/10.3233/JAD-170600> PMID: 29036830.
74. Zheng WH, Bastianetto S, Mennicken F, Ma W, Kar S. Amyloid beta peptide induces tau phosphorylation and loss of cholinergic neurons in rat primary septal cultures. *Neuroscience.* 2002; 115(1):201–11. Epub 2002/10/29. [https://doi.org/10.1016/s0306-4522\(02\)00404-9](https://doi.org/10.1016/s0306-4522(02)00404-9) PMID: 12401334.
75. Hu X, Li X, Zhao M, Gottesdiener A, Luo W, Paul S. Tau pathogenesis is promoted by Abeta1-42 but not Abeta1-40. *Mol Neurodegener.* 2014; 9:52. Epub 2014/11/25. <https://doi.org/10.1186/1750-1326-9-52> PMID: 25417177.
76. Welikovitsh LA, Do Carmo S, Magloczky Z, Szocsics P, Loke J, Freund T, et al. Evidence of intraneuronal Abeta accumulation preceding tau pathology in the entorhinal cortex. *Acta Neuropathol.* 2018; 136(6):901–17. Epub 2018/10/27. <https://doi.org/10.1007/s00401-018-1922-z> PMID: 30362029.
77. Ma QL, Yang F, Rosario ER, Ubeda OJ, Beech W, Gant DJ, et al. Beta-amyloid oligomers induce phosphorylation of tau and inactivation of insulin receptor substrate via c-Jun N-terminal kinase signaling: suppression by omega-3 fatty acids and curcumin. *J Neurosci.* 2009; 29(28):9078–89. Epub 2009/07/17. <https://doi.org/10.1523/JNEUROSCI.1071-09.2009> PMID: 19605645.
78. Yarza R, Vela S, Solas M, Ramirez MJ. c-Jun N-terminal Kinase (JNK) Signaling as a Therapeutic Target for Alzheimer's Disease. *Front Pharmacol.* 2015; 6:321. Epub 2016/01/23. <https://doi.org/10.3389/fphar.2015.00321> PMID: 26793112.
79. Reiman EM, Quiroz YT, Fleisher AS, Chen K, Velez-Pardo C, Jimenez-Del-Rio M, et al. Brain imaging and fluid biomarker analysis in young adults at genetic risk for autosomal dominant Alzheimer's disease

- in the presenilin 1 E280A kindred: a case-control study. *Lancet Neurol.* 2012; 11(12):1048–56. Epub 2012/11/10. [https://doi.org/10.1016/S1474-4422\(12\)70228-4](https://doi.org/10.1016/S1474-4422(12)70228-4) PMID: 23137948.
80. Quiroz YT, Schultz AP, Chen K, Protas HD, Brickhouse M, Fleisher AS, et al. Brain Imaging and Blood Biomarker Abnormalities in Children With Autosomal Dominant Alzheimer Disease: A Cross-Sectional Study. *JAMA Neurol.* 2015; 72(8):912–9. Epub 2015/06/30. <https://doi.org/10.1001/jamaneurol.2015.1099> PMID: 26121081.
  81. Jack CR Jr., Knopman DS, Jagust WJ, Petersen RC, Weiner MW, Aisen PS, et al. Tracking pathophysiological processes in Alzheimer's disease: an updated hypothetical model of dynamic biomarkers. *Lancet Neurol.* 2013; 12(2):207–16. Epub 2013/01/22. [https://doi.org/10.1016/S1474-4422\(12\)70291-0](https://doi.org/10.1016/S1474-4422(12)70291-0) PMID: 23332364.
  82. Cline EN, Bicca MA, Viola KL, Klein WL. The Amyloid-beta Oligomer Hypothesis: Beginning of the Third Decade. *J Alzheimers Dis.* 2018; 64(s1):S567–s610. Epub 2018/05/31. <https://doi.org/10.3233/JAD-179941> PMID: 29843241.
  83. Cehlar O, Skrabana R, Revajova V, Novak M. Structural aspects of Alzheimer's disease immunotherapy targeted against amyloid-beta peptide. *Bratisl Lek Listy.* 2018; 119(4):201–4. Epub 2018/04/18.
  84. Chun YS, Kwon OH, Oh HG, Cho YY, Yang HO, Chung S. Justicidin A Reduces beta-Amyloid via Inhibiting Endocytosis of beta-Amyloid Precursor Protein. *Biomol Ther (Seoul).* 2019; 27(3):276–82. Epub 2018/10/20. <https://doi.org/10.4062/biomolther.2018.112> PMID: 30332887.



# Multi-Target Effects of the Cannabinoid CP55940 on Familial Alzheimer's Disease PSEN1 E280A Cholinergic-Like Neurons: Role of CB<sub>1</sub> Receptor

Viviana Soto-Mercado, Miguel Mendivil-Perez, Marlene Jimenez-Del-Rio\* and Carlos Velez-Pardo\*  
*Neuroscience Research Group, Medical Research Institute, Faculty of Medicine, University of Antioquia (UdeA), SIU Medellin, Colombia*

Accepted 12 October 2020  
Pre-press 23 November 2020

## Abstract.

**Background:** Alzheimer's disease (AD) is characterized by structural damage, death, and functional disruption of cholinergic neurons (ChNs) as a result of intracellular amyloid- $\beta$  (A $\beta$ ) aggregation, extracellular neuritic plaques, and hyperphosphorylation of protein tau (p-Tau) overtime.

**Objective:** To evaluate the effect of the synthetic cannabinoid CP55940 (CP) on PSEN1 E280A cholinergic-like nerve cells (PSEN1 ChLNs)—a natural model of familial AD.

**Methods:** Wild type (WT) and PSEN1 ChLNs were exposed to CP (1  $\mu$ M) only or in the presence of the CB<sub>1</sub> and CB<sub>2</sub> receptors (CB<sub>1</sub>Rs, CB<sub>2</sub>Rs) inverse agonist SR141716 (1  $\mu$ M) and SR144528 (1  $\mu$ M) respectively, for 24 h. Untreated or treated neurons were assessed for biochemical and functional analysis.

**Results:** CP in the presence of both inverse agonists (hereafter SR) almost completely inhibits the aggregation of intracellular sA $\beta$ PP $\beta$ f and p-Tau, increases  $\Delta\Psi_m$ , decreases oxidation of DJ-1Cys<sup>106</sup>-SH residue, and blocks the activation of c-Jun, p53, PUMA, and caspase-3 independently of CB<sub>1</sub>Rs signaling in mutant ChLNs. CP also inhibits the generation of reactive oxygen species partially dependent on CB<sub>1</sub>Rs. Although CP reduced extracellular A $\beta$ <sub>42</sub>, it was unable to reverse the Ca<sup>2+</sup> influx dysregulation as a response to acetylcholine stimuli in mutant ChLNs. Exposure to anti-A $\beta$  antibody 6E10 (1:300) in the absence or presence of SR plus CP completely recovered transient [Ca<sup>2+</sup>]<sub>i</sub> signal as a response to acetylcholine in mutant ChLNs.

**Conclusion:** Taken together our findings suggest that the combination of cannabinoids, CB<sub>1</sub>Rs inverse agonists, and anti-A $\beta$  antibodies might be a promising therapeutic approach for the treatment of familial AD.

**Keywords:** Apoptosis, cannabinoids, cholinergic neurons, CP55940, E280A mutation, familial Alzheimer disease, neuronal dysfunction, oxidative stress, PSEN1, sA $\beta$ PP $\beta$ f, tau

## INTRODUCTION

Alzheimer's disease (AD) is a multifactorial neurodegenerative condition [1] characterized by severe loss of cholinergic neurons from the nucleus basalis magnocellularis of Meynert and cholinergic projections to the cortex and hippocampus [2]. The neuronal destruction is associated with the extracellular accumulation of insoluble forms of amyloid- $\beta$  (A $\beta$ ) in plaques, mostly fragment A $\beta$ <sub>1–42</sub> (hereafter

\*Correspondence to: Carlos Velez-Pardo and Marlene Jimenez-Del-Rio, Neuroscience Research Group, Medical Research Institute, Faculty of Medicine, University of Antioquia (UdeA), Calle 70 No. 52-21, and Calle 62 # 52-59, Building 1, Room 412; SIU Medellin, Colombia. E-mail: calberto.velez@udea.edu.co., ORCID #0000-0002-0557-0411 (Velez-Pardo); E-mail: marlene.jimenez@udea.edu.co., ORCID #0000-0003-3477-2386 (Jimenez-Del-Rio)

A $\beta$ <sub>42</sub>), intracellular aggregation of the microtubule protein tau in neurofibrillary tangles, neuronal cell death, and synaptic dysfunction [3]. The A $\beta$ <sub>42</sub> peptide is derived from the amyloid- $\beta$  protein precursor (A $\beta$ PP) via sequential cleavage by the beta-site amyloid precursor protein cleaving enzyme 1 (BACE1) and by the gamma-site aspartyl protease  $\gamma$ -secretase [4]. This last protein is composed of four subunits, namely presenilins (PSEN1 and PSEN2), presenilin enhancer 2 (PEN2), anterior pharynx-defective 1 (APH-1), and nicastrin. While PEN2, APH-1, and nicastrin stabilize the complex, PSEN1 and PSEN2 function as the catalytic core of the protease [5]. Over two hundred autosomal dominant mutations in the presenilin 1 (*PSEN1*) gene result in the overproduction of extracellular (e)A $\beta$ <sub>42</sub> [6] and occur most frequently in familial AD (FAD; <https://www.alzforum.org/mutations/psen-1>). Among PSEN1 mutations, the Glu280Ala (p. E280A, c.839A>C, exon 8) in *PSEN1* causes FAD with complete penetrance in a large kindred localized in Antioquia, Colombia [7–10]. As the majority of dominant-negative *PSEN1* mutations [11], PSEN1 E280A produces increased A $\beta$ <sub>42</sub> deposition [12], hippocampal neuron loss [13], and A $\beta$ /tau accumulation in young adults [14, 15]. Recently, we have recapitulated the molecular pathogenesis of FAD caused by PSEN1 E280A in umbilical cord mesenchymal stem cells-derived cholinergic-like neurons (ChLNs [16]). It has demonstrated that PSEN1 E280A ChLNs effectively exhibited not only an increased eA $\beta$ <sub>42</sub> but also an early increased of intracellular sA $\beta$ PP $\beta$  fragments (but not A $\beta$ <sub>42</sub> peptide) and tau phosphorylation. Moreover, PSEN1 E280A ChLNs exhibited oxidized DJ-1 (at Cys<sup>106</sup>SO<sub>3</sub>) indicative of oxidative stress (OS), and concomitant loss of the mitochondrial membrane potential ( $\Delta\Psi_m$ ), activation of apoptogenic proteins, and DNA fragmentation, markers of apoptosis—a type of regulated cell death. Additionally, mutant ChLNs displayed Ca<sup>2+</sup> flux dysregulation when challenged to acetylcholine (ACh) and deficient acetylcholinesterase (AChE) activity compared to wild type (WT) ChLNs most probably due to eA $\beta$ <sub>42</sub> peptide. Taken together these observations suggest that PSEN1 E280A ChLNs display the typical neuropathological markers of AD; therefore, mutant ChLNs provide a unique FAD model for screening of candidate molecule(s)/drug(s).

Due to the lack of effective therapies to date for AD, the need for new drugs has become increasingly urgent. Phytocannabinoids, a group of biologically

active compounds isolated from the plant *Cannabis sativa* [17], have been postulated to possess therapeutic potential for clinical purposes in AD [18]. *Cannabis* contains at least 120 kinds of cannabinoids mainly classified as  $\Delta^9$ -trans-tetrahydrocannabinol (THC), cannabidiol (CBD), CBG (Cannabigerol), and CBN (Cannabinol), among others [19]. Biologically, cannabinoids, endocannabinoids (e.g., anandamide, 2-arachidonoylglycerol), and synthetic cannabimimetic compounds (e.g., CP55940) bind cannabinoid type 1 and 2 receptors (CB<sub>1</sub>R/ CB<sub>2</sub>R), two G-protein-coupled receptors (GPCR) [20, 21]. Interestingly, it has been shown *in vitro* that 9 out of 11 cannabinoids studied, including THC, were able to protect cells (e.g., MC65—a human neuron-like cell line, HT22 mouse hippocampal nerve cell line, primary cortical neurons from 18-day-old rat embryos, BV2—a microglial cell line) in four distinct phenotypic neurodegeneration screening assays including proteotoxicity, loss of trophic support, OS, energy loss, and inflammation [22]. Outstandingly, cannabinoids were able to remove intraneuronal A $\beta$ , reduce oxidative damage, and protect from the loss of energy or trophic support in neurons in which CB<sub>1</sub> and CB<sub>2</sub> receptors were lacking (e.g., MC65 and HT22 cells). Furthermore, CB<sub>1</sub> agonists (e.g., CP55940) were also effective neuroprotective agents against A $\beta$  toxicity in MC65 neurons [22]. These data suggest that cannabinoids might be antioxidant and anti-amylogenic compounds through receptor-independent mechanisms in a cell- and species-specific manner [22–28]. Despite these observations, no data are available to establish whether cannabinoids might reverse the neuropathological markers, i.e., intracellular sA $\beta$ PP $\beta$  aggregation, hyperphosphorylation of tau protein, and DJ-1 oxidation in PSEN1 E280A ChLNs. Furthermore, it is not yet known whether cannabinoids might be able to block neuronal apoptosis, eA $\beta$ <sub>42</sub>, and/or prevent Ca<sup>2+</sup> dysregulation in those mutant cholinergic neurons.

To get insight into these issues, we have selected the commercially available CP55940 ((-)-cis-3-[2-Hydroxy-4-(1,1-dimethylheptyl)phenyl]-trans-4-(3-hydroxypropyl)cyclohexanol, hereafter CP), a CB<sub>1</sub> and CB<sub>2</sub> potent bicyclic analog of THC [29], to evaluate its effect on wild-type and PSEN1 E280A ChLNs concerning the intracellular sA $\beta$ PP $\beta$  accumulation, tau phosphorylation, OS, cell death, and Ca<sup>2+</sup> neuronal dysfunction in ChLNs. We demonstrate for the first time that CP can protect FAD PSEN1 E280A ChLNs against neuronal structural

damage and OS-induced cell death signaling and that it can reverse the cholinergic dysfunction in the presence of eA $\beta$ <sub>42</sub> blocking agents (e.g., anti-A $\beta$ <sub>42</sub> antibody 6E10). These findings might favor the use of cannabinoids as potential lead compound candidates as a combined therapy for FAD.

## MATERIALS AND METHODS

### *Cholinergic-like neuron (ChLN) differentiation*

ChLN differentiation was performed according to [30]. The WT (TBC# WJMSC-11) and PSEN1 E280A (TBC# WJMSC-12) [16] MSCs were seeded at  $1\text{--}1.5 \times 10^4$  cells/cm<sup>2</sup> in laminin-treated culture plates for 24 h in regular culture medium (RCm). Then, the medium was removed, and cells were incubated in cholinergic differentiation medium (*Cholinergic-N-Run medium*, hereafter *Ch-N-Rm*) containing DMEM/F-12 media 1:1 Nutrient Mixture (Gibco cat# 10565018), 10 ng/mL basic fibroblast growth factor (bFGF) recombinant human protein (Gibco Cat# 13256029), 50  $\mu$ g/mL sodium heparin (Hep, Sigma-Aldrich cat# H3393), 0.5  $\mu$ M all-trans retinoic acid, 50 ng/mL sonic hedgehog peptide (SHH, Sigma cat# SRP3156) and 1% FBS at 37°C for 7 days. After this process of transdifferentiation, the cells were labeled as WT PSEN1 or PSEN1 E280A ChLNs. Since *Ch-N-Rm* contains several factors that might interfere with the experiment interpretation and measurements, WT PSEN1 and PSEN1 E280A ChLNs (obtained after 7 days in *Ch-N-Rm*) were left in regular culture medium (RCm) for 4 additional days of post transdifferentiation.

### *Immunofluorescence analysis*

For the analysis of markers of AD, oxidative stress, and cell death, the cells treated under different conditions were fixed with 4% paraformaldehyde for 20 min, followed by Triton X-100 (0.1%) permeabilization and 10% bovine serum albumin (BSA) blockage. Cells were incubated overnight with primary antibodies against APP<sub>751</sub> and/or protein amyloid  $\beta$ <sub>1-42</sub> (1:500; clone 6E10 cat# 803014, Biolegend), total tau (1:500; t-Tau; cat# T6402, Sigma), and phospho-tau (p-Tau, 1:500, Ser202/Thr205, cat# MN1020 (AT8), Thermo Fisher Scientific); and primary antibodies against oxidized DJ-1 (1:500; ox(Cys106)DJ-1; spanning residue C<sup>106</sup> of human PARK7/DJ1; oxidized to produce cysteine sulfonic (SO<sub>3</sub>) acid; cat # ab169520, Abcam). To assess cell death, we used primary antibodies

against p53-upregulated modulator of apoptosis (1:500; PUMA, cat# ab-9643, Abcam), p53 (1:500; cat# MA5-12453, Millipore), phospho-c-Jun (1:250; c-Jun (S63/73) cat# sc-16312, Santa Cruz), and caspase-3 (1:250; cat # AB3623, Millipore). After exhaustive rinsing, we incubated the cells with secondary fluorescent antibodies (DyLight 488 and 594 horse anti-rabbit, -goat and -mouse, cat DI 1094, DI 3088, and DI 2488, respectively) at 1:500. The nuclei were stained with 1  $\mu$ M Hoechst 33342 (Life Technologies), and images were acquired on a Floyd Cells Imaging Station microscope.

### *Western blot analysis*

Cells were incubated as described above, detached with 0.25% trypsin and lysed in 50 mM Tris-HCl, pH 8.0, with 150 mM sodium chloride, 1.0% Igepal CA-630 (NP-40), and 0.1% sodium dodecyl sulfate and a protease inhibitor cocktail (Sigma-Aldrich). All lysates were quantified using the bicinchoninic acid assay (Thermo Scientific cat # 23225). Extracted samples (30  $\mu$ g of proteins) were heated at 95°C for 5 min in 2  $\times$  SDS and 20 $\times$  reducing agent (except for protein oxDJ-1) and loaded on to 12% gels at 120 V for 90 min, and the bands were transferred onto nitrocellulose membranes (Hybond-ECL, Amersham Biosciences) at 270 mA for 90 min using an electrophoretic transfer system (BIO-RAD) according to Bio-Rad protocol ([http://www.bio-rad.com/webroot/web/pdf/lsr/literature/Bulletin\\_6376](http://www.bio-rad.com/webroot/web/pdf/lsr/literature/Bulletin_6376)). The membranes were incubated overnight at 4°C with anti-APP<sub>751</sub>, total tau, phospho-Tau, ox(Cys<sup>106</sup>) DJ1, PUMA, p53, p-c-Jun, and caspase-3 primary antibodies (1:5000). The anti-actin antibody (1:1000, cat #MAB1501, Millipore) was used as an expression control. Secondary infrared antibodies (goat anti-rabbit IRDye® 680 RD, cat #926-68071; donkey anti-goat IRDye® 680 RD, cat # 926-68074; and goat anti-mouse IRDye® 800 CW, cat #926-32270; LI-COR Biosciences) at 1:1000 were used for western blotting analysis, and data were acquired using Odyssey software. The determination of the aggregation state of APP<sub>751</sub> (i.e., sA $\beta$ PP $\beta$ ) was performed by western analysis of SDS-PAGE as described above. The assessment was repeated three times in independent experiments.

### *Analysis of cells*

#### *Assay protocol*

The methodology for both WT and PSEN1 E280A ChLNs cell culture assays was the same. Initial

CP55940 screening was performed at least twice in triplicate between 10 nM and 1  $\mu$ M. Subsequently, CP55940 (1  $\mu$ M) was established as an optimal concentration for further experiments. ChLNs were divided in four groups: 1) untreated; 2) treated with SR141716 (CB<sub>1</sub> receptor inverse agonist) and SR144528 (CB<sub>2</sub> receptor inverse agonist) at 1  $\mu$ M final concentration each (hereafter SR); 3) CP55940 (or CP); 4) RS + CP55940 (also named as SR + CP cocktail). To block eA $\beta$ <sub>42</sub> [31], WT and mutant ChLNs were incubated four days with anti-A $\beta$ <sub>42</sub> antibody 6E10 (1:300 in *RCm*) after differentiation in the presence or absence of CP or CP + RS.

#### *Evaluation of intracellular hydrogen peroxide (H<sub>2</sub>O<sub>2</sub>) by fluorescence microscopy*

To determine the levels of intracellular H<sub>2</sub>O<sub>2</sub>, we used 2',7'-dichlorofluorescein diacetate (5  $\mu$ M, DCFH<sub>2</sub>-DA; Invitrogen). ChLNs were left in *RCm* for 4 days. Then, the cells ( $5 \times 10^3$ ) were incubated with the DCFH<sub>2</sub>-DA reagent for 30 min at 37°C in the dark. Cells were then washed, and DCF fluorescence intensity was determined by analysis of fluorescence microscopy images. The assessment was repeated three times in independent experiments. The nuclei were stained with 0.5  $\mu$ M Hoechst 33342 staining compound. The assessment was repeated three times in independent experiments blind to the experimenter.

#### *Analysis of mitochondrial membrane potential ( $\Delta\Psi_m$ ) by fluorescence microscopy*

The ChLNs were left in regular culture medium (*RCm*) for 4 days. Then, the cells ( $5 \times 10^3$ ) were incubated with the passively diffusing and active mitochondria-accumulating dye deep red MitoTracker compound (20 nM, final concentration) for 20 min at room temperature in the dark (Invitrogen, cat # M22426). Cells were then washed twice with PBS. MitoTracker fluorescence intensity was determined by analysis of fluorescence microscopy images. The assessment was repeated three times in independent experiments. The nuclei were stained with 0.5  $\mu$ M Hoechst 33342 staining compound. The assessment was repeated three times in independent experiments blind to the experimenter and flow cytometer analyst.

#### *Measurement of A $\beta$ <sub>42</sub> peptide in culture medium*

The level of A $\beta$ <sub>1-42</sub> peptide was measured according to a previous report [32] with minor modifications. Briefly, WT and PSEN1 E280A ChLNs were left in *RCm* for 4 days. Then, 100  $\mu$ l of con-

ditioned medium was collected, and the levels of secreted A $\beta$ <sub>42</sub> peptides were determined by a solid-phase sandwich ELISA (Invitrogen, Cat# KHB3544) following the manufacturer's instructions. The assessment was repeated 4 times in independent experiments blind to the experimenter.

#### *Intracellular calcium imaging*

Intracellular calcium (Ca<sup>2+</sup>) concentration changes evoked by cholinergic stimulation were assessed according to [33, 34] with minor modifications. For the measurement, the fluorescent dye Fluo-3 (Fluo-3 AM; Thermo Fisher Scientific, cat: F1242) was employed. The dye was dissolved in DMSO (1 mM) to form a stock solution. Before the experiments, the stock solution was diluted in neuronal buffer solution (NBS buffer: 137 mM NaCl, 5 mM KCl, 2.5 mM CaCl<sub>2</sub>, 1 mM MgCl<sub>2</sub>, pH 7.3, and 22 mM glucose). The working concentration of the dye was 2  $\mu$ M. The WT and PSEN1 E280A ChLNs were incubated for 30 min at 37°C with the dye-containing NBS and then washed five times. Intracellular Ca<sup>2+</sup> transients were evoked by acetylcholine (1 mM final concentration) at 4 days post differentiation. The measurements were carried out using the 20 $\times$  objective of the microscope. Several regions of interest (ROIs) were defined in the visual field of the camera. One of the ROIs was cell-free, and the fluorescence intensity measured here was considered background fluorescence ( $F_{bg}$ ). The time dependence of the fluorescence emission was acquired, and the fluorescence intensities (hence the Ca<sup>2+</sup> levels) were represented by pseudo colors. To calculate the changes of the average Ca<sup>2+</sup>-related fluorescence intensities, the  $F_{bg}$  value was determined from the cell-free ROI, and then the resting fluorescence intensities ( $F_{rest}$ ) of the cell-containing ROIs were obtained as the average of the points recorded during a consecutive period of 10 s before the addition of acetylcholine. The peaks of the fluorescence transients were found by calculating the average of six consecutive points and identifying those points that gave the highest average value ( $F_{max}$ ). The amplitudes of the Ca<sup>2+</sup>-related fluorescence transients were expressed relative to the resting fluorescence ( $\Delta F/F$ ) and were calculated by the following formula:  $\Delta F/F = (F_{max} - F_{rest}) / (F_{rest} - F_{bg})$ . For the calculation of the fluorescence intensities, ImageJ was used. The terms fluorescence intensity was used as an indirect indicator of intracellular Ca<sup>2+</sup> concentration. The assessment was repeated three times in independent experiments blind to the experimenter.



### Photomicrography and image analysis

Light microscopy photographs were taken using a Zeiss Axiostart 50 Fluorescence Microscope equipped with a Canon PowerShot G5 digital camera (Zeiss Wöhlk-Contact-Linsen, Gmb Schöckirchen, Germany), and fluorescence microscopy photographs were taken using a Zeiss Axiostart 50 Fluorescence Microscope equipped with a Zeiss AxioCam Cm1 and (Zeiss Wöhlk-Contact-Linsfluoreen, Gmb Schöckirchen, Germany) and Floyd Cells Imaging Station microscope. Fluorescence images were analyzed by ImageJ software (<http://imagej.nih.gov/ij/>). The figures were transformed into 8-bit images, and the background was subtracted. The cellular measurement ROIs were drawn around the nucleus (for the case of transcription factors and apoptosis effectors) or overall cells (for cytoplasmic probes), and the fluorescence intensity was subsequently determined by applying the same the threshold for cells in the control and treatment conditions. Mean fluorescence intensity (MFI) was obtained by normalizing total fluorescence to the number of nuclei.

### Data analysis

In this experimental design, a vial of MSCs was thawed, cultured and the cell suspension was pipetted at a standardized cellular density of  $2.6 \times 10^4$  cells/cm<sup>2</sup> into different wells of a 24-well plate. Cells (i.e., the biological and observational unit [35]) were randomized to wells by simple randomization (sampling without replacement method), and then wells (i.e., the experimental units) were randomized to treatments by a similar method. Experiments were conducted in triplicate wells. The data from individual replicate wells were averaged to yield a value of  $n = 1$  for that experiment and this was repeated on three occasions blind to the experimenter and/or flow cytometer analyst for a final value of  $n = 3$  [35]. Based on the assumption that the experimental unit (i.e., the well) data comply with the independence of observations, the dependent variable is normally distributed in each treatment group (Shapiro-Wilk test), and variances are homogeneous (Levene's test), the statistical significance was determined by one-way analysis of variance (ANOVA) followed by Tukey's *post hoc* comparison calculated with GraphPad Prism 5.0 software. Differences between groups were only deemed significant when a  $p$ -value of  $<0.05$  (\*),  $<0.001$  (\*\*) and  $<0.001$  (\*\*\*). All data are illustrated as the mean  $\pm$  S.D.

## RESULTS

### *CP55940 restores the mitochondrial membrane potential ( $\Delta\Psi_m$ ) and blunts generation of ROS in PSEN1 E280A ChLNs in an independent concentration fashion*

Previously, it has been shown that PSEN 1 E280A ChLNs present aggregation of sA $\beta$ PP $\beta$ f, endogenously generated OS, and loss of  $\Delta\Psi_m$  as the earliest neuropathological markers in mutant ChLNs [16]. Therefore, we initially determined whether CP could recover  $\Delta\Psi_m$  and scavenge ROS in those cells. To this aim, cholinergic cells were exposed to increasing concentrations of CP. As shown in Fig. 1A'-E', CP did not affect  $\Delta\Psi_m$  in wild type ChLNs (Fig. 1A-E, K). However, it significantly increased the  $\Delta\Psi_m$  in PSEN1 E280A ChLNs in a concentration-independent fashion (Fig. 1F'-J'). Accordingly, we found 500 nM –1000 nM ( $= 1 \mu\text{M}$ ), but not low concentrations (10, 100 nM), as the maximal optimal concentrations to raise  $\Delta\Psi_m$  in mutant cells (Fig. 1F-J, K). Figure 1 shows mutant ChLNs (Fig. 1F'') but no WT ChLNs (Fig. 1A'') endogenously produce ROS. CP blunted ROS yield in mutant ChLNs (Fig. 1G''-J'') compared to WT ChLNs (Fig. 1B''-E'') in an independent concentration fashion. Since CP (1  $\mu\text{M}$ ) recovered  $\Delta\Psi_m$  to control levels and completely diminished ROS in mutant ChLNs (Fig. 1K, L), we selected this concentration for further experiments.

### *CP55940 restores $\Delta\Psi_m$ in a CB<sub>1</sub> receptor-independent manner but diminishes ROS production partially dependent on CB<sub>1</sub> receptors in PSEN1 E280A ChLNs*

We wanted to establish whether the neuroprotective effect on mitochondria and antioxidant activity of CP was due to interaction with CB<sub>1</sub>Rs. Although these receptors are expressed in cholinergic neurons [36] and CP is a CB<sub>1</sub> and CB<sub>2</sub> receptor agonist, we used both potent and highly specific CB<sub>1</sub> and CB<sub>2</sub> receptor inverse agonist SR141716 and SR144528 (hereafter SR at 1  $\mu\text{M}$  each) only or with CP agonist (i.e., SR + CP cocktail) to avoid ambiguous observations. Figure 2 shows that while SR only neither affects  $\Delta\Psi_m$  in wild type ChLNs (i.e., high  $\Delta\Psi_m$  Fig. 2C) nor in mutant ChLNs (i.e., low  $\Delta\Psi_m$  Fig. 2D) when compared to untreated neurons

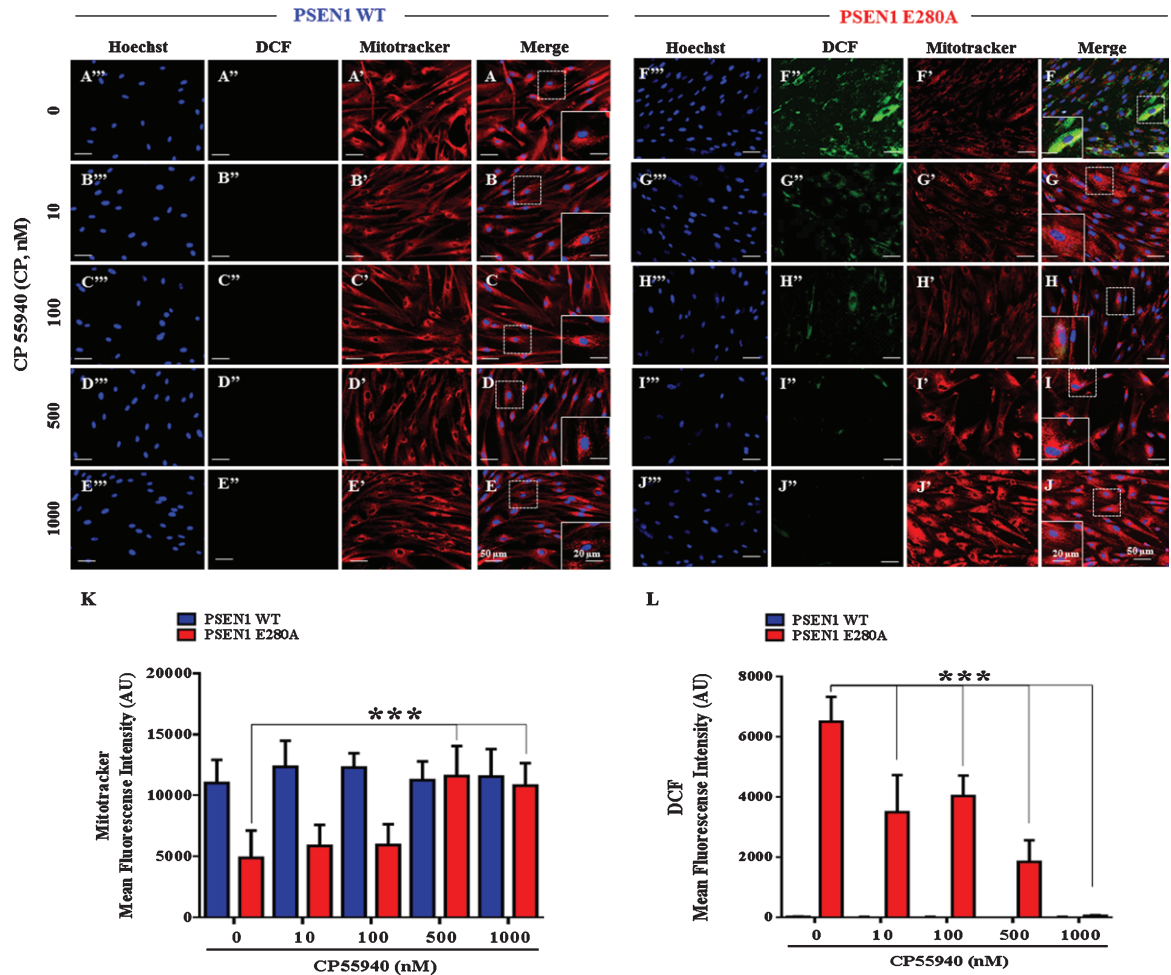


Fig. 1. CP55940 restores the mitochondrial membrane potential ( $\Delta\Psi_m$ ) and reduces the levels of intracellular reactive oxygen species independent of its concentration in PSEN1 E280A ChLNs. After 7 days of transdifferentiation, WT PSEN1 and PSEN1 E280A ChLNs were left untreated or treated with CP at increasing concentrations (0, 10, 100, 500, and 1000 nM) in regular culture medium (RCm) for 4 days. Representative MitoTracker (A'-J'), DCF (A''-J''), Hoechst (A'''-J'''), and merge (A-J) pictures of WT PSEN1 and PSEN1 E280A ChLNs treated as described. K) Quantification of MitoTracker fluorescence intensity. L) Quantification of DCF fluorescence intensity. Data are expressed as the mean  $\pm$  SD; \* $p < 0.05$ ; \*\* $p < 0.01$ ; \*\*\* $p < 0.001$ . The histograms and figures represent 1 out of 3 independent experiments. Image magnification, 200 $\times$ . Inset magnification, 800 $\times$ .

(Fig. 2A, B), CP (Fig. 2F) or CP+SR (Fig. 2H) significantly increased the  $\Delta\Psi_m$  in mutant ChLNs (Fig. 2I). Neither CP nor the cocktail altered  $\Delta\Psi_m$  in WT ChLNs (Fig. 2E, G, I). However, analysis of ROS disappearance in ChLNs shows that while CP only almost completely scavenged ROS in mutant ChLNs (Fig. 2J), the SR+CP cocktail diminished ROS by almost half of the value of untreated or treated with SR only in PSEN1 E280A ChLNs (Fig. 2J). WT ChLNs produced no detectable ROS in any experimental condition (Fig. 2J). Of note, SR only treatment showed no effect in  $\Delta\Psi_m$  and ROS conditions in both WT (Fig. 2I) and mutant ChLNs (Fig. 2J).

### CP55940 reduces intracellular sA $\beta$ PP $\beta$ f aggregation in a CB<sub>1</sub>Rs-independent fashion but it reduces oxidized DJ-1 partially dependent of CB<sub>1</sub>Rs in PSEN1 E280A ChLNs

Next, we assessed whether CP could inhibit intracellular aggregation of sA $\beta$ PP $\beta$ f and avoid oxidation of the stress sensor protein DJ-1. To this aim, WT and mutant ChLNs were left untreated or exposed to CP in the absence or presence of SR. Western blot analysis revealed that CP only or with SR reduced the aggregation of sA $\beta$ PP $\beta$ f in a CB<sub>1</sub>Rs-independent manner (Fig. 3A, B) but blunted the oxidation of

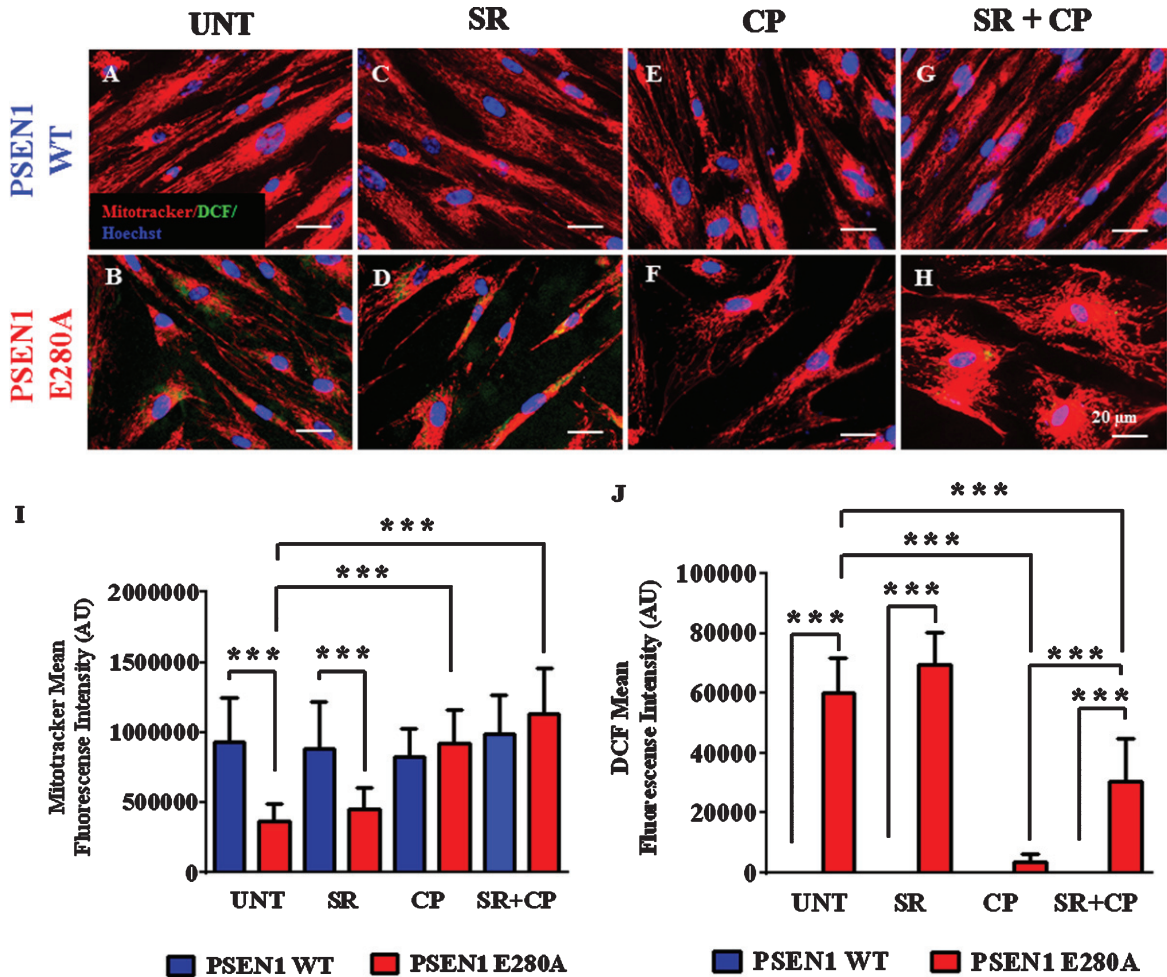


Fig. 2. CP55940 augments the  $\Psi_m$  independent of CB<sub>1</sub>R but reduced the levels of intracellular reactive oxygen species partially dependent on those receptors in PSEN1 E280A ChLNs. After 7 days of transdifferentiation, WT PSEN1 and PSEN1 E280A ChLNs were left untreated or treated with SR, CP, or SR + CP in RCm for 4 days. A-H) Representative MitoTracker/DCF/Hoechst merge pictures of WT PSEN1 and PSEN1 E280A ChLNs treated as described. I) Quantification of MitoTracker fluorescence intensity. J) Quantification of DCF fluorescence intensity. Data are expressed as the mean  $\pm$  SD; \* $p$  < 0.05; \*\* $p$  < 0.01; \*\*\* $p$  < 0.001. The histograms and figures represent 1 out of 3 independent experiments. Image magnification, 400 $\times$ .

DJ-1 partially dependent of CB<sub>1</sub>Rs (Fig. 3A, C). As expected, WT ChLNs remained unaltered to CP and to the cocktail exposure. Neither sA $\beta$ PP $\beta$ f nor oxidized DJ-1 were detected in those neurons (Fig. 3A–C). These results were confirmed by fluorescent microscopy (Fig. 3D–M).

#### CP55940 blocks apoptosis in a CB<sub>1</sub>Rs-independent manner in PSEN1 E280A ChLNs

Cell death by apoptosis is a prominent feature in mutant ChLNs [16]. We used, therefore, the activation of the transcription factors p53 and c-Jun,

pro-apoptotic BH3-only protein PUMA, and protease caspase-3 as apoptosis markers to examine the effect of CP and/or SR plus CP on those neuronal cells. Effectively, we confirmed that ChLNs displayed high levels of protein c-Jun (Fig. 4A, B), p53 (Fig. 4A, C), PUMA (Fig. 4A, D), and caspase-3 (Fig. 4A, E) in mutant but not in WT ChLNs (Fig. 4A–E). No significant difference was found between untreated and SR treatment for all the apoptosis markers in both types of cells. However, CP only or CP + SR significantly reduced c-Jun (Fig. 4A, B), p53 (Fig. 4A, C), PUMA (Fig. 4A, D), and caspase-3 (Fig. 4A, E) in PSEN1 E280A neurons when compared to untreated cells or WT ChLNs. Interestingly, mutant neurons exposed to

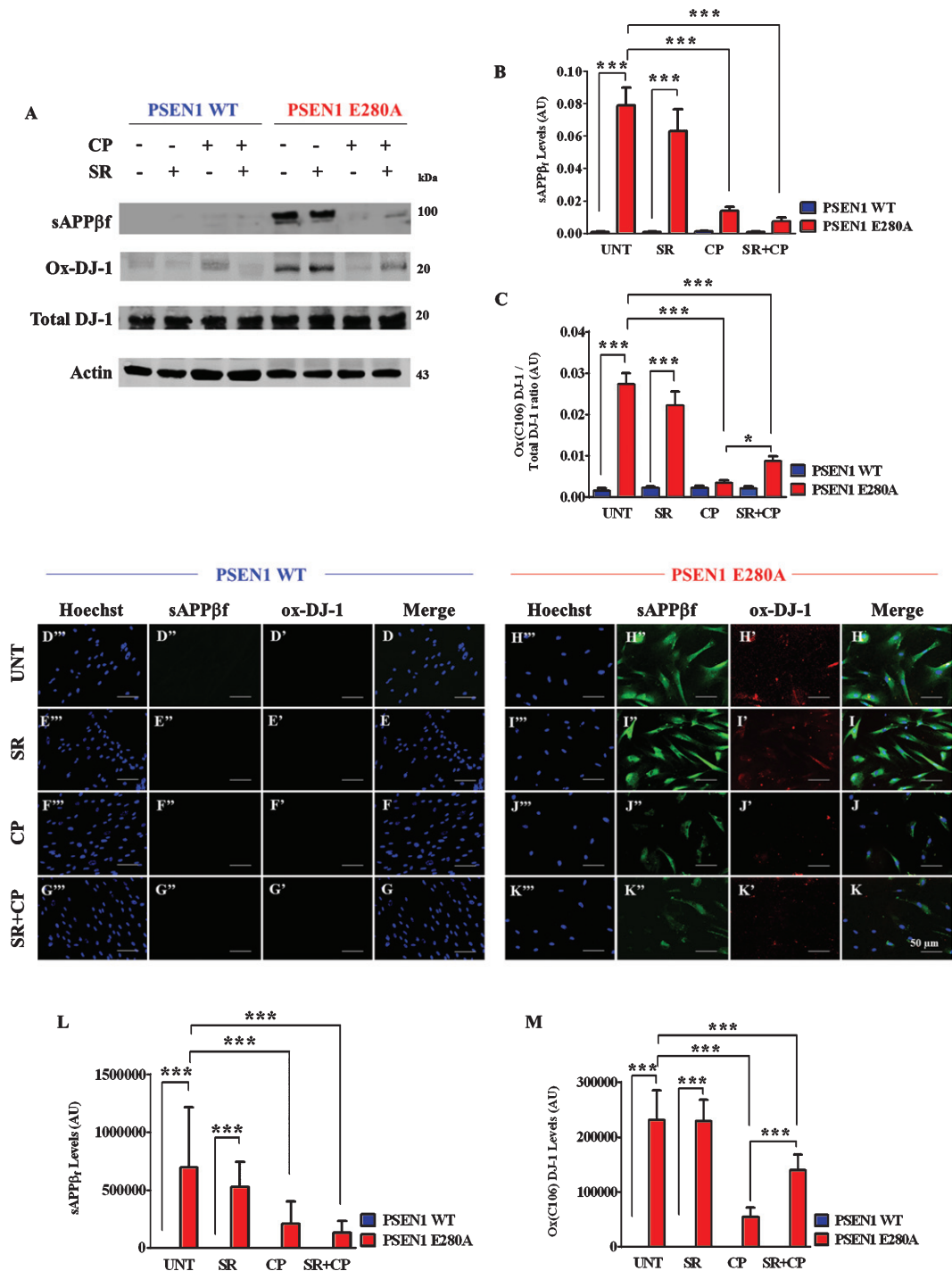


Fig. 3. CP55940 reduced intracellular sAPP $\beta$ f and oxidized DJ-1 independent of CB $_1$ Rs in PSEN1 E280A ChLNs. After 7 days of transdifferentiation, WT PSEN1 and PSEN1 E280A ChLNs were left untreated or treated with SR, CP, or SR + CP in RCm for 4 days. Further, the proteins in the extracts were blotted with primary antibodies against A $\beta$ <sub>42</sub>, oxDJ-1Cys<sup>106</sup>, and actin proteins. The intensities of the western blot bands shown in (A) were measured (B, C) by an infrared imaging system (Odyssey, LI-COR), and the intensity was normalized to that of actin. Additionally, cells were double-stained as indicated in the figure (D-K) with primary antibodies against oxDJ-1Cys<sup>106</sup> (red; D'-K') and APP<sub>751</sub>/A $\beta$ <sub>42</sub> (green; D''-K''). The nuclei were stained with Hoechst 33342 (blue; D'''-K'''). L) Quantification of A $\beta$ <sub>42</sub> fluorescence intensity. M) Quantification of oxDJ-1Cys<sup>106</sup> fluorescence intensity. Data are expressed as the mean  $\pm$  SD; \*p < 0.05; \*\*p < 0.01; \*\*\*p < 0.001. The blots and figures represent 1 out of 3 independent experiments. Image magnification, 200 $\times$ .

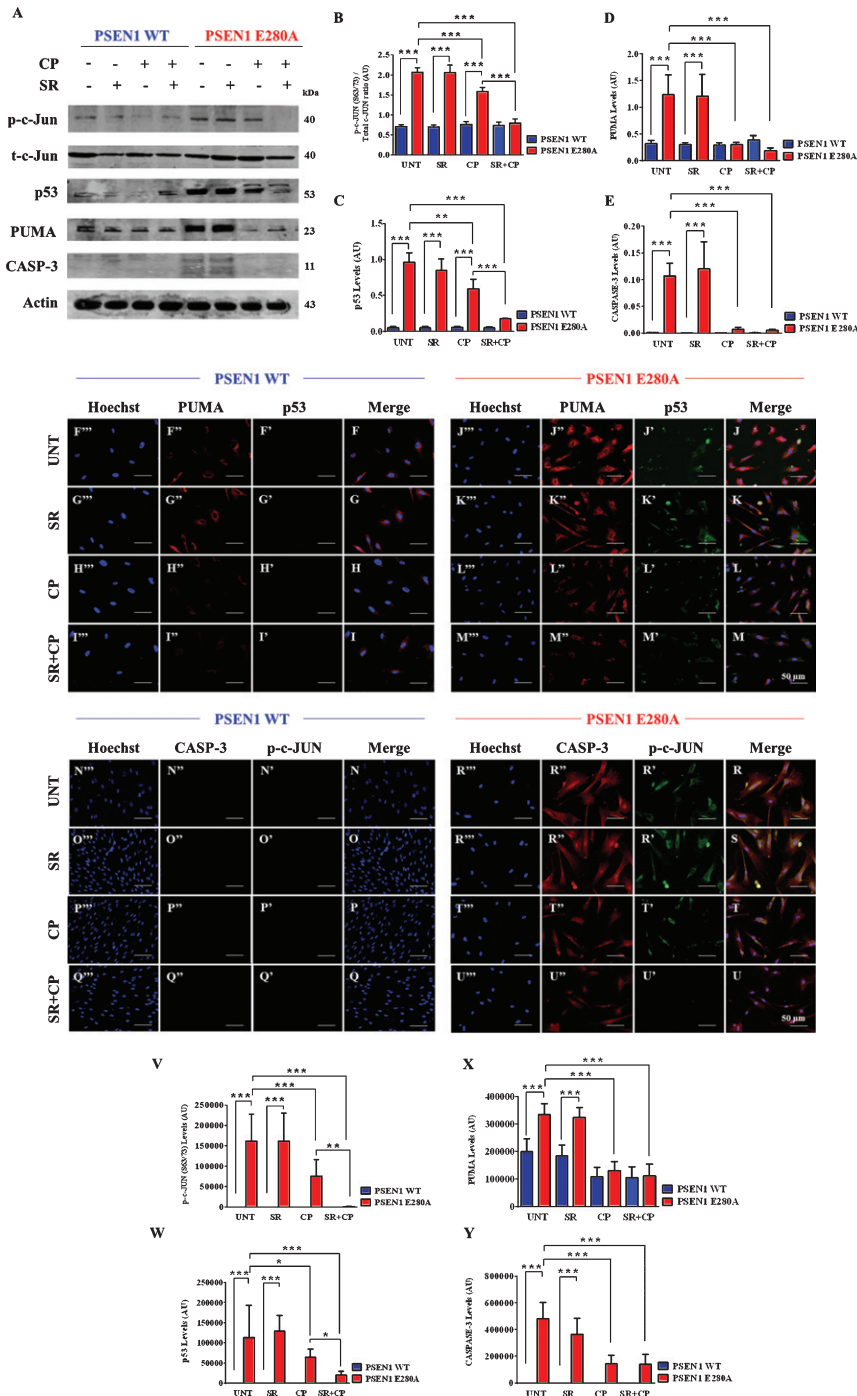


Fig. 4. CP55940 reduced the activation of p53, PUMA, c-Jun, and caspase-3 independent of CB<sub>1</sub>R<sub>s</sub> signaling in PSEN1 E280A ChLNs. After 7 days of transdifferentiation, WT PSEN1 and PSEN1 E280A ChLNs were left Untreated or treated with SR, CP, or SR + CP in regular culture medium for 4 days. After this time, the proteins in the extracts were blotted with primary antibodies against phosphorylated c-Jun (p-c-JUN)/total c-Jun, p53, PUMA, caspase-3 (CASP-3) and actin proteins. The intensities of the western blot bands shown in (A) were measured (B-E) by an infrared imaging system (Odyssey, LI-COR), and the intensity was normalized to that of actin. Additionally, cells were double-stained as indicated in the figure (F-U) with primary antibodies against p53 (green; F'-M'), PUMA (red; F''-M''), c-JUN (green; N'-U'), and CASP-3 (red; N''-U''). The nuclei were stained with Hoechst 33342 (blue; F'''-U'''). V-X) Quantification of c-JUN (V), p53 (W), PUMA (X), and CASP-3 (Y) fluorescence intensity. Data are expressed as the mean  $\pm$  SD; \* $p$  < 0.05; \*\* $p$  < 0.01; \*\*\* $p$  < 0.001. The blots and figures represent 1 out of 3 independent experiments. Image magnification, 200 $\times$ .



CP + SR displayed almost basal levels of all proteins comparable to WT ChLNs. These observations were confirmed by fluorescent microscopy (Fig. 4F–Y).

*CP55940 inhibits tau phosphorylation in a CB<sub>1</sub>Rs-independent fashion PSEN1 E280A ChLNs*

It has been established that intracellular sAβPPβf induce phosphorylation of tau [16]. We then investigated whether CP could inhibit tau phosphorylation in PSEN1 E280A ChLNs. As shown in Fig. 5, while the level of tau phosphorylation was detected to a similar extend in WT ChLNs under any experimental conditions (Fig. 5A, B), CP or CP + SR cocktail dramatically reduced phosphorylation of protein tau when compared to untreated or SR only treatment in mutant ChLNs (Fig. 5A, B). No statistically differences were observed between CP and CP + SR treatments in mutant ChLNs (Fig. 5B). These observations were confirmed by fluorescent microscopy (Fig. 5C–K).

*CP55940 reduces the levels of eAβ<sub>42</sub> protein fragment independent of CB<sub>1</sub>Rs in PSEN1 E280A ChLNs*

Based on the observation that CP inhibited the intracellular aggregation of sAβPPβf (see Fig. 3), we assessed whether CP could have the same effect on eAβ<sub>42</sub> [16]. Effectively, CP and CP + SR but not SR only significantly diminished the amounts of eAβ<sub>42</sub> compared to untreated neurons in mutant ChLNs according to the ELISA technique (Fig. 6). No statistically differences were observed between CP and CP + SR treatments in mutant ChLNs (Fig. 6). The amount of eAβ<sub>42</sub> was not affected by any of the treatments in WT ChLNs (Fig. 6).

*CP55940 does not recover Ca<sup>2+</sup> dysregulation in PSEN1 E280A ChLNs*

The above observations prompted us to test whether CP could ameliorate the physiological response of mutant ChLNs to ACh neurotransmitter stimuli. As expected, ACh induced a transient elevation of intracellular Ca<sup>2+</sup> in WT ChLNs (control, the average maximum fluorescence change ( $\Delta F/F$ ) was  $3.95 \pm 0.19$  at 10 s ( $n=20$  ChLN cells imaged,  $N=3$  dishes were used as a standard condition in this and following experiments) according to cytoplasmic Ca<sup>2+</sup> responses to Fluo-3-mediated

imaging (Fig. 7A, E). We found no statistical differences between SR (Fig. 7B, E;  $\Delta F/F = 5.05 \pm 0.35$ ), SR + CP (Fig. 7D, E;  $\Delta F/F = 4.31 \pm 0.26$ ) and untreated conditions (Fig. 7E). In contrast, CP only and ACh significantly depressed intracellular Ca<sup>2+</sup> (by  $-68\%$ ) in WT ChLNs (Fig. 7C, E,  $\Delta F/F = 2.35 \pm 0.12$ ). When mutant neurons were exposed to ACh only (Fig. 7F, J,  $\Delta F/F = 0.02 \pm 0.00$ ) and CP (Fig. 7H, J,  $\Delta F/F = 0.06 \pm 0.00$ ), mutant cells were irresponsive to both stimuli (Fig. 7J). Interestingly, while SR only slightly increased intracellular Ca<sup>2+</sup> (Fig. 7G, J,  $\Delta F/F = 0.63 \pm 0.07$ ), the CP + SR cocktail and ACh increased inflow Ca<sup>2+</sup> (Fig. 7H, J,  $\Delta F/F = 3.32 \pm 0.23$ ) in PSEN1 E280A ChLNs to similar extend as [Ca<sup>2+</sup>]<sub>i</sub> in WT ChLNs (Fig. 7E, J).

*Anti-Aβ<sub>42</sub> antibodies completely recuperate Ca<sup>2+</sup> influx in PSEN1 E280A ChLNs*

Since PSEN1 E280A ChLNs response to ACh decline in a time-dependent fashion [16], and since SR alone treatment was innocuous for WT and E280A ChLNs, we evaluated whether early inhibition of eAβ<sub>42</sub> by anti-Aβ antibodies could ameliorate the mutant ChLNs response to ACh under CP and CP + SR treatments. As shown in Fig. 8, incubation of WT with anti-Aβ antibody 6E10 only (Fig. 8A, D;  $\Delta F/F = 4.27 \pm 0.21$ ) or in the presence of CP (Fig. 8B, D;  $\Delta F/F = 3.11 \pm 0.25$ ) or CP + SR (Fig. 8C, D;  $\Delta F/F = 4.01 \pm 0.20$ ) showed similar transient intracellular Ca<sup>2+</sup>. We found no statistical differences between those treatments (Fig. 8D). Remarkably, ACh and the anti-Aβ antibody 6E10 completely recovered Ca<sup>2+</sup> influx in mutant ChLNs (Fig. 8E, H;  $\Delta F/F = 3.37 \pm 0.20$ ). The anti-Aβ antibody 6E10 and CP (Fig. 8F, H;  $\Delta F/F = 5.78 \pm 0.87$ ) and antibody + CP + SR (Fig. 8G, H;  $\Delta F/F = 5.93 \pm 0.29$ ) dramatically induced a transient elevation of intracellular Ca<sup>2+</sup> in mutant ChLNs (Fig. 8H).

## DISCUSSION

In the present investigation, we demonstrate that CP inhibits the aggregation of (i)sAβPPβf, and p-Tau, increases  $\Delta\Psi_m$ , inhibits the generation of ROS and oxidation of DJ-1Cys<sup>106</sup>-SH to DJ-1Cys<sup>106</sup>-SO<sub>3</sub>, blocks the activation of the transcription factor p53 and c-Jun, pro-apoptotic protein PUMA, and protease caspase-3—all markers of cell death by apoptosis, and reduce eAβ<sub>42</sub> in a CB<sub>1</sub>R-dependent and-independent fashion in PSEN1 E280A ChLNs, used as a neuronal cell model of FAD [16]. Although

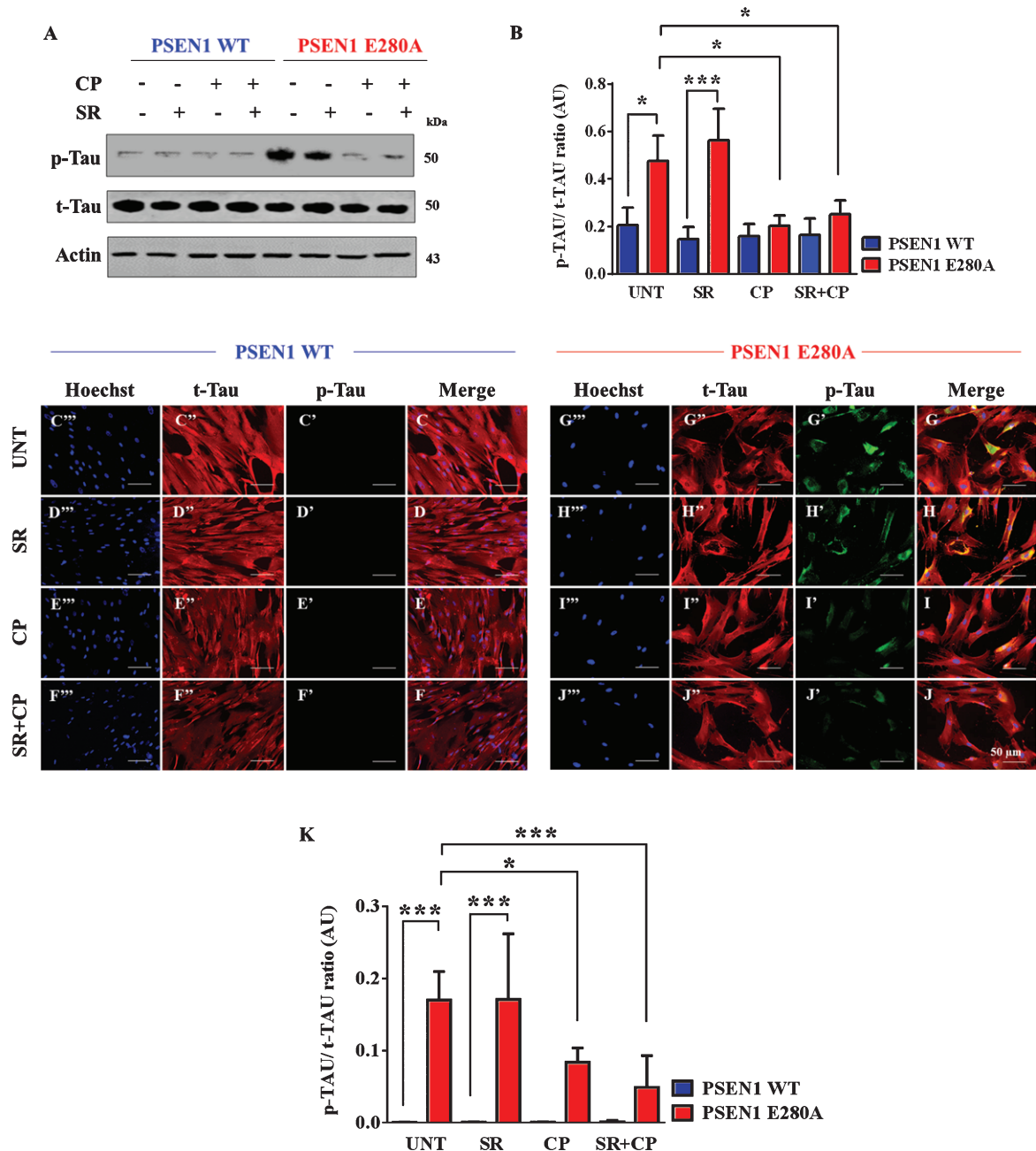


Fig. 5. CP55940 reduced the phosphorylation of tau protein independent of CB<sub>1</sub>R in PSEN1 E280A ChLNs. After 7 days of transdifferentiation, WT PSEN1 and PSEN1 E280A ChLNs were left untreated or treated with SR, CP, or SR + CP in regular culture medium for 4 days. After this time, the proteins in the extracts were blotted with primary antibodies against phosphorylated tau (p-Tau), total tau (t-Tau), and actin proteins. The intensities of the western blot bands shown in (A) were measured (B) by an infrared imaging system (Odyssey, LI-COR), and the p-Tau/t-Tau ratio was normalized to that of actin. Additionally, cells were double-stained as indicated in the figure (C-J) with primary antibodies against p-Tau (green; C'-J') and t-Tau (red; C''-J''). The nuclei were stained with Hoechst 33342 (blue; C'''-J'''). K) Quantification of the p-Tau/t-Tau fluorescence ratio. Data are expressed as the mean  $\pm$  SD; \* $p$  < 0.05; \*\* $p$  < 0.01; \*\*\* $p$  < 0.001. The blots and figures represent 1 out of 3 independent experiments. Image magnification, 200 $\times$ .

CP was unable to reverse the Ca<sup>2+</sup> influx dysregulation as a response to ACh stimuli, it is demonstrated that CP affects several cellular molecular targets.

Several observations support these assumptions. First, in agreement with previous work [27], we found that CP reduced OS by directly scavenging ROS

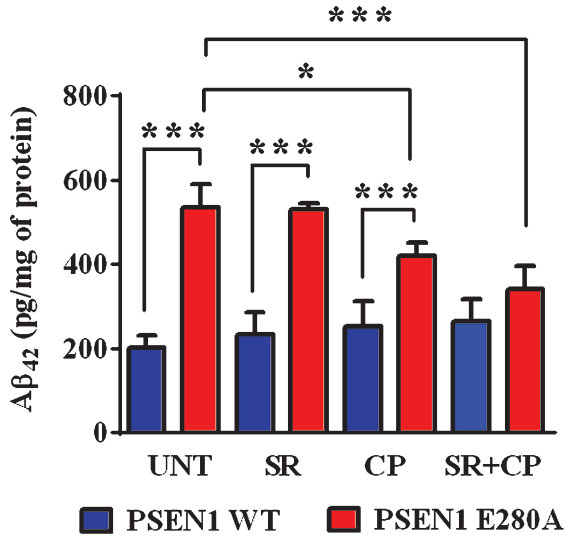


Fig. 6. CP55940 reduced the levels of extracellular Aβ<sub>42</sub> peptide in PSEN1 E280A ChLNs by a CB<sub>1</sub>R-independent mechanism. After 7 days of transdifferentiation, WT PSEN1 and PSEN1 E280A ChLNs were left untreated or treated with SR, CP, or SR + CP in RCm for 4 days. ELISA quantification of extracellular Aβ<sub>42</sub> peptide in supernatants. Data are presented as means ± SD. \**p* < 0.05; \*\**p* < 0.01; \*\*\**p* < 0.001. The histograms and figures represent 1 out of 4 independent experiments.

(e.g., H<sub>2</sub>O<sub>2</sub>) [22–28] and partially diminished ROS through CB<sub>1</sub>Rs signaling. These observations may indicate that CP operates in a dual-way: as an antioxidant and as a CB<sub>1</sub>Rs ligand. Second, CP dramatically increases the ΔΨ<sub>m</sub> in PSEN1 E280A ChLNs. Several data indicate that CP and other cannabinoids (e.g., THC, arachidonyl-2-chloroethylamide) can protect mitochondria against OS stimuli by inhibition of mitochondria permeability transition pore (mPTP) opening [37] or through activation of mitochondrial (mt)CB<sub>1</sub>Rs [38, 39]. Even though, mtCB<sub>1</sub>Rs activation have been linked to an intra-mitochondrial signaling cascade involving lessening of the activity of the electron transport system, oxygen consumption, and ATP production [40], our data favor the view that inhibition of mPTP opening by CP might be responsible for neuroprotective action on mutant ChLNs [37]. Indeed, it has been shown that the CB<sub>2</sub> agonist JWH-015 attenuated mitochondrial damage against OS stimuli by scavenging anion superoxide radical (O<sub>2</sub><sup>•−</sup>) and H<sub>2</sub>O<sub>2</sub>, maintaining ΔΨ<sub>m</sub> and avoiding Ca<sup>2+</sup>-induced mitochondrial swelling [37]. Additionally, CP may indirectly protect mitochondria by blocking the interaction of sAβPPβ and mitochondrial respiratory complexes [41, 42] or

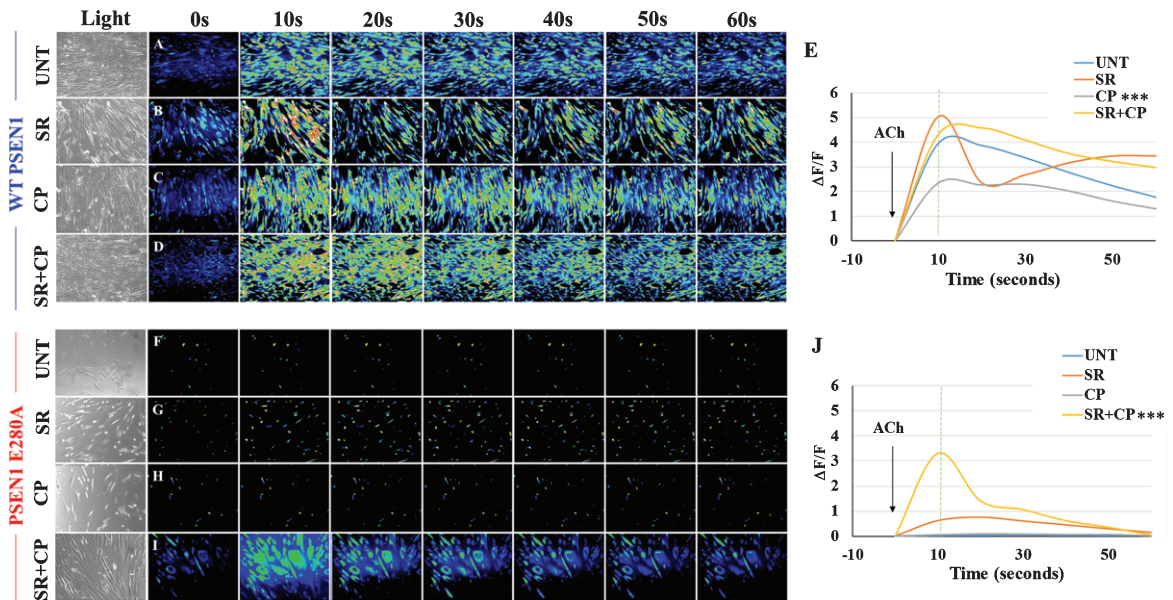


Fig. 7. CP55940 does not recover Ca<sup>2+</sup> dysregulation in PSEN1 E280A ChLNs. After 7 days of transdifferentiation, WT PSEN1 and PSEN1 E280A ChLNs were left untreated or treated with SR, CP, or SR + CP in regular culture medium for 4 days. A–D, F–I) Time-lapse images (0, 10, 20, 30, 40, 50, and 60 s) of Ca<sup>2+</sup> fluorescence in WT PSEN1 and PSEN1 E280A ChLNs on day 4 in response to ACh treatment. ACh was puffed into the culture at 0 s (arrow). Then, the Ca<sup>2+</sup> fluorescence of the cells was monitored at the indicated times. Color contrast indicates fluorescence intensity: dark blue < light blue < green < yellow < red. E, J) Normalized mean fluorescence signal (ΔF/F) over time from the cells indicating temporal cytoplasmic Ca<sup>2+</sup> elevation in response to ACh treatment. Data are presented as the mean ± SD. \**p* < 0.05; \*\**p* < 0.01; \*\*\**p* < 0.001 compared to UNT. The histograms and figures represent 1 out of 3 independent experiments. Image magnification, 200×.

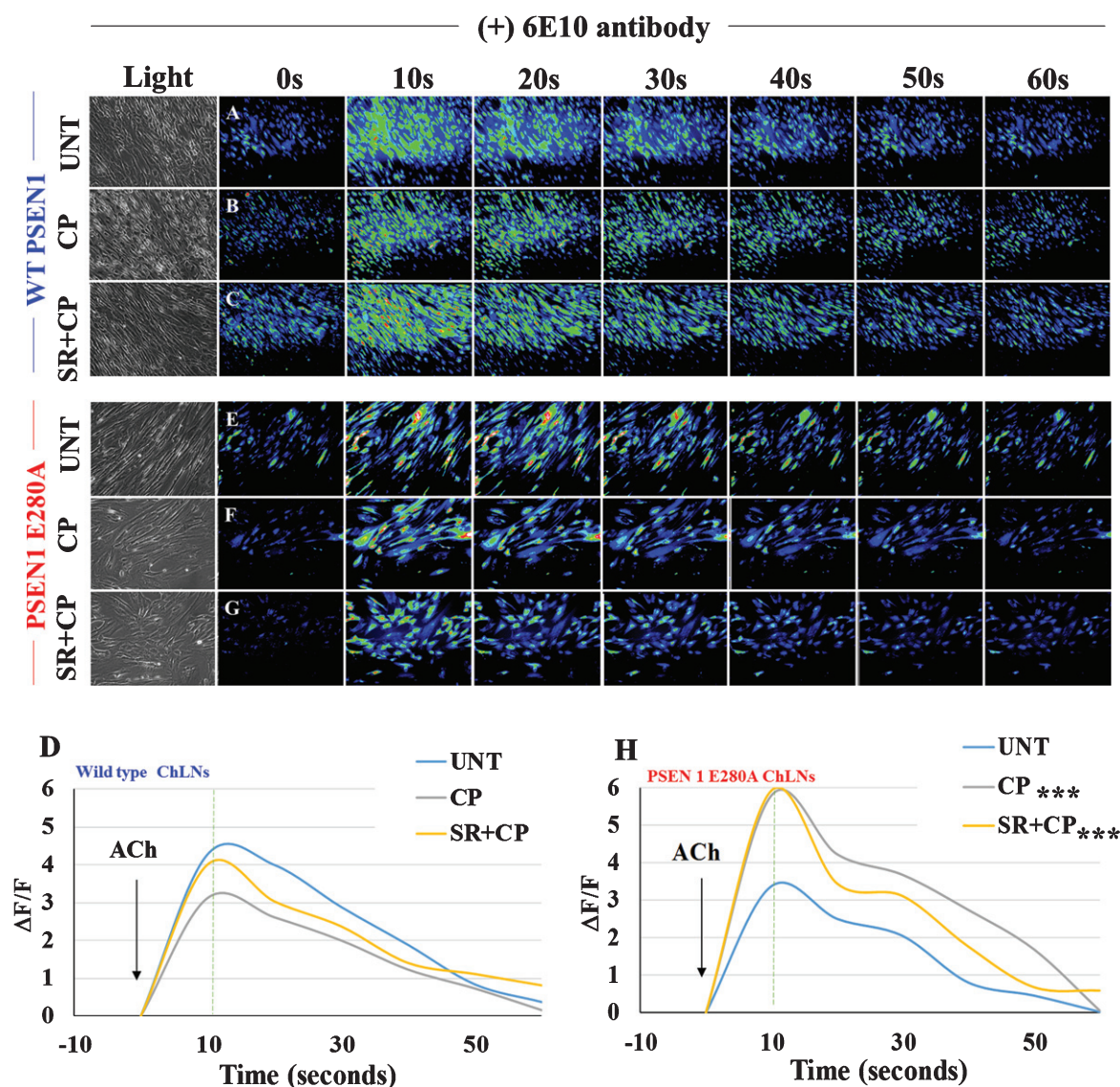


Fig. 8. CP55940 plus SR and anti- $A\beta_{42}$  antibody 6E10 completely recover  $Ca^{2+}$  influx in PSEN1 E280A ChLNs. After 7 days of transdifferentiation, WT PSEN1 and PSEN1 E280A ChLNs were incubated with 6E10 antibody as described in Materials and Methods section. Simultaneously cells were left untreated or treated with CP or SR + CP in RCm for 4 days. A-C, E-G) Time-lapse images (0, 10, 20, 30, 40, 50, and 60 s) of  $Ca^{2+}$  fluorescence in WT PSEN1 and PSEN1 E280A ChLNs at day4 in the presence of 6E10 antibody as a response to ACh treatment. ACh was puffed into the culture at 0 s (arrow). Then, the  $Ca^{2+}$  fluorescence of the cells was monitored at the indicated times. Color contrast indicates fluorescence intensity: dark blue < light blue < green < yellow < red. D, H) Normalized mean fluorescence signal ( $\Delta F/F$ ) over time from the cells indicating temporal cytoplasmic  $Ca^{2+}$  elevation in response to ACh treatment. Data are presented as means  $\pm$  SD. \* $p < 0.05$ ; \*\* $p < 0.01$ ; \*\*\* $p < 0.001$  compared to UNT. The histograms and figures represent 1 out of 3 independent experiments. Image magnification, 200 $\times$ .

by inhibition of mitochondria-targeted pro-apoptotic proteins (e.g., PUMA, this work). Taken together our findings suggest that CP reverses the loss of  $\Delta\Psi_m$  and mitochondria damage independently of plasma membrane  $CB_1$  receptors or (mt) $CB_1$ Rs. Third, it is known that cannabinoids (e.g., THC) stimulate the removal of intracellular  $A\beta$  through a dependent [43] or

independent  $CB_1$ Rs mechanism [22]. Here, we report for the first time that CP inhibits the aggregation of (i)sA $\beta$ PP $\beta$ f in PSEN1 E280A ChLNs independently of  $CB_1$  receptor signaling. Since  $A\beta_{42}$  is still detected extracellularly in mutant neurons treated with CP, it might imply that this cannabinoid does not interfere with the  $A\beta$ PP metabolism. Finally, CP significantly



diminished oxidation of protein DJ-1, as evidence of OS. Because DJ-1Cys<sup>106</sup>SH residue is specifically sensible to H<sub>2</sub>O<sub>2</sub> oxidation [44], it is likely that CP might directly interact with ROS or induces its suppression via CB<sub>1</sub>Rs activation. Taken together our results comply with the view that early aggregation of (i)sAβPPβf and generation of H<sub>2</sub>O<sub>2</sub> can be blocked by the direct action of cannabinoid CP and by partial activation of CB<sub>1</sub>Rs, respectively.

Recent data have shown that (i)sAβPPβf (H<sub>2</sub>O<sub>2</sub>) induce activation of JNK/c-Jun and p53, which in turn activate PUMA and caspase-3 [16]. Interestingly, we found that CP blocks activation of transcription factors c-Jun, p53, PUMA, and caspase-3 independently of CB<sub>1</sub>Rs stimulation. These observations suggest that CP exerted a direct role in protecting PSEN1 E280A ChLNs against endogenously OS-induced cell death signaling. Since downregulation of c-Jun and p53 may reduce transcription of PUMA [45–47], CP may restrain mitochondria from leaking pro-apoptogenic proteins such as caspase-9, and ensuing activation of caspase-3. These actions avoid neuronal dismantling and increase the survival of mutant ChLNs.

Previously, it has been shown that (i)sAβPPβf induces p-Tau through JNK kinase in PSEN1 E280A ChLNs [16]. In this work, we demonstrate that CP almost completely inhibits the phosphorylation of protein tau independently of CB<sub>1</sub>Rs. One possible explanation is that CP can suppress H<sub>2</sub>O<sub>2</sub> generation, which serves as a messenger molecule that triggers activation of JNK [48, 49], and phosphorylation of tau [50]. It is therefore not surprising that p-Tau was untraceable in PSEN1 E280A ChLNs. However, we do not discard the possibility that CP blocks p-Tau by alternative CB<sub>1</sub>Rs-independent mechanisms in ChLNs [51].

Mounting evidence has demonstrated that eAβ is neurotoxic before the appearance of plaques [16, 52, 53]. Interestingly, CP reduced the amounts of eAβ<sub>42</sub> in a CB<sub>1</sub>Rs-independent manner. This observation suggests that CP directly modulates intracellular and extracellular AβPP-derived protein fragments. However, the action of CP on eAβ<sub>42</sub> did not impact on the response of mutant ChLNs to ACh stimuli. Here, we confirm that ACh receptors (AChRs) are physiologically altered in PSEN1 E280A ChLNs [16] most probably through Aβ-induced inhibition of nicotinic (n)AChRs [54, 55], which normally revealed a rapid elevation of intracellular Ca<sup>2+</sup> [56–58] as shown in WT ChLNs. Indeed, AChRs were irresponsive to ACh stimuli, thereby nullifying the transient rise

of intracellular Ca<sup>2+</sup> in mutant ChLNs (i.e., –99% reduction in [Ca<sup>2+</sup>]<sub>i</sub>) compared to wild type ChLNs. On the other hand, CP decreased [Ca<sup>2+</sup>]<sub>i</sub> by –68% in WT ChLNs. These observations suggest that CP either directly inhibited the function of AChRs [59, 60] and/ or inhibited the inflow of Ca<sup>2+</sup> via activation of CB<sub>1</sub>Rs on calcium channels (e.g., T, N- and P/Q-type [20]). Since the response of PSEN1 E280A ChLNs to ACh is already compromised, CP was not able to modify the influx of Ca<sup>2+</sup> when challenged with the neurotransmitter. Interestingly, SR only or with CP increased [Ca<sup>2+</sup>]<sub>i</sub> in PSEN1 E280A ChLNs compared to untreated mutant ChLNs. This positive improvement of Ca<sup>2+</sup> inflow was comparable to WT ChLNs (see CP + SR effect on neurons). These observations can be explained by the fact that SR can either stimulate Ca<sup>2+</sup> influx through Ca<sup>2+</sup> channels (e.g., Ca<sub>v</sub>2: N-, P/Q channels [61]) or block the negative interaction of CP with nAChRs in WT ChLNs when exposed to ACh (this work). Our findings suggest that CB<sub>1</sub>Rs are marginally active in PSEN1 E280A ChLNs. Interestingly; anti-Aβ<sub>42</sub> antibody completely recovered transient intracellular Ca<sup>2+</sup> signal in mutant ChLNs. The Ca<sup>2+</sup> signal was further increased when neurons were co-cultured with CP only or SR plus CP. These last observations reinforce the view that Aβ<sub>42</sub> and SR interfere with CP and AChRs. Similar to PSEN1 E280A ChLNs, anti-body anti-Aβ<sub>42</sub> increased transient intracellular Ca<sup>2+</sup> signals in WT ChLNs. These observations imply that eAβ<sub>42</sub> secreted in low amounts by WT ChLNs or abnormally secreted in high amounts by mutant ChLNs is an AChRs regulator in ChLNs. Taken together these observations suggest that a combination of CP with anti-Aβ<sub>42</sub> would be therapeutically beneficial to FAD patients.

## Conclusion

In an attempt to modify the neuropathological expression of ChLNs bearing the mutation PSEN1 E280A (e.g., intracellular aggregation of sAβPPβf, tau phosphorylation, OS, apoptosis, and Ca<sup>2+</sup> influx dysfunction) (Fig. 9A), we found that cannabinoid CP is a multi-target molecule that promotes the recovery FAD cholinergic neurons by increasing ΔΨ<sub>m</sub>, impedes phosphorylation of protein tau, and blocks OS-induced apoptosis signaling (Fig. 9B). However, CP was unable to modify the neuronal functionality as evidenced by an inability of ACh to increase Ca<sup>2+</sup> influx in PSEN1 E280A ChLNs. Since the nature of



the neuronal cholinergic dysfunctionality stems from the blocking of nAChRs by A $\beta_{42}$  [54, 55], drugs that interfere with the interaction of A $\beta$  and the AChRs might ameliorate the ligand-gated ion Ca $^{2+}$  channel interactions (e.g., [62]). In this respect, we show that anti-A $\beta_{42}$  antibody 6E10 plus CP or anti-A $\beta_{42}$  and SR + CP change mutant ChLNs response to ACh

by increasing Ca $^{2+}$  influx to similar [Ca $^{2+}$ ] $_i$  in WT ChLNs (Fig. 9C, D). It is therefore proposed that combinations of cannabinoids, anti-A $\beta_{42}$  antibodies (e.g., crenezumab [63, 64]), and CB $_1$  inverse agonists might be a promising multi-target drugs for therapy [65] in the early treatment of FAD PSEN 1 E280A ChLNs neurodegeneration.

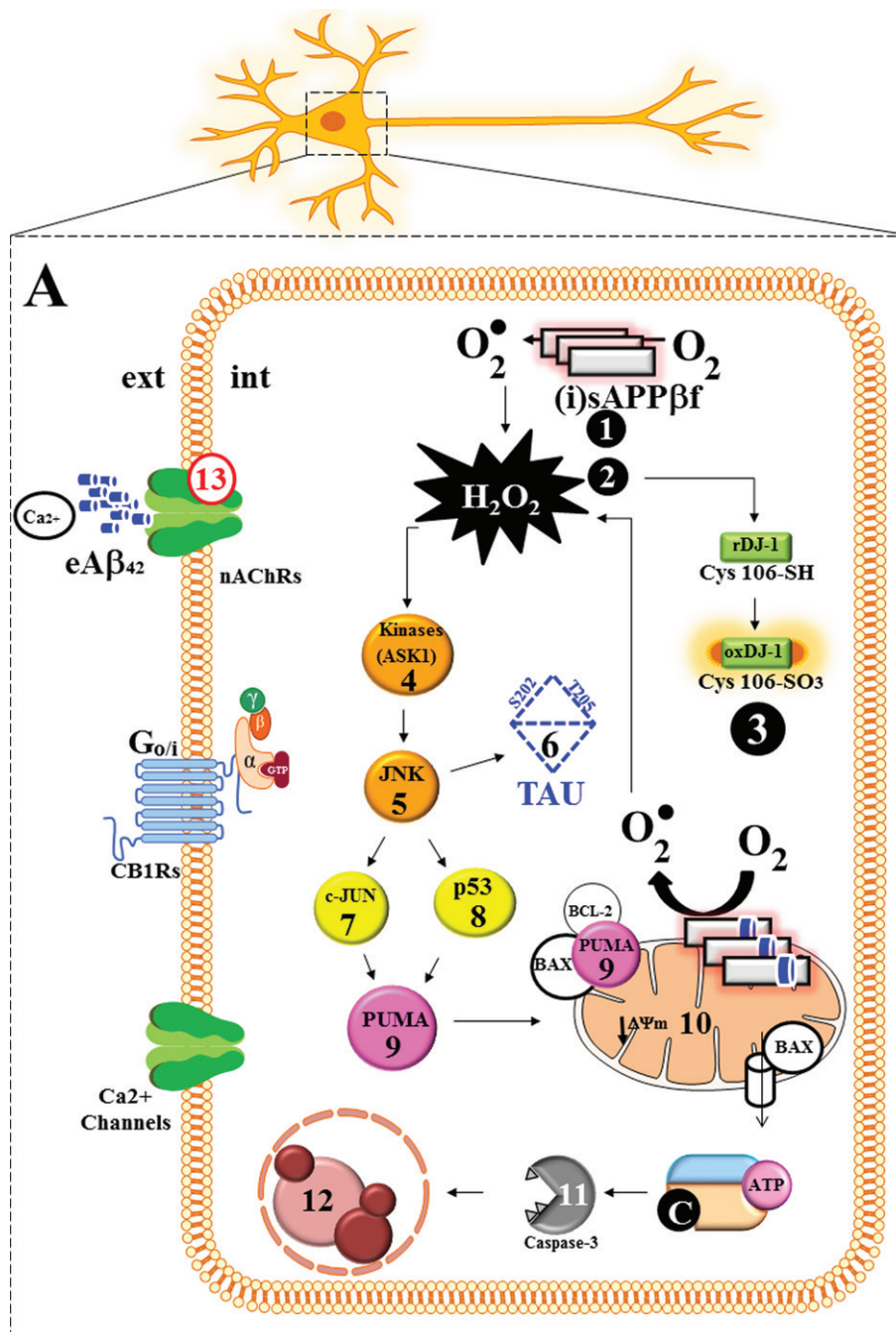


Fig. 9. (Continued)

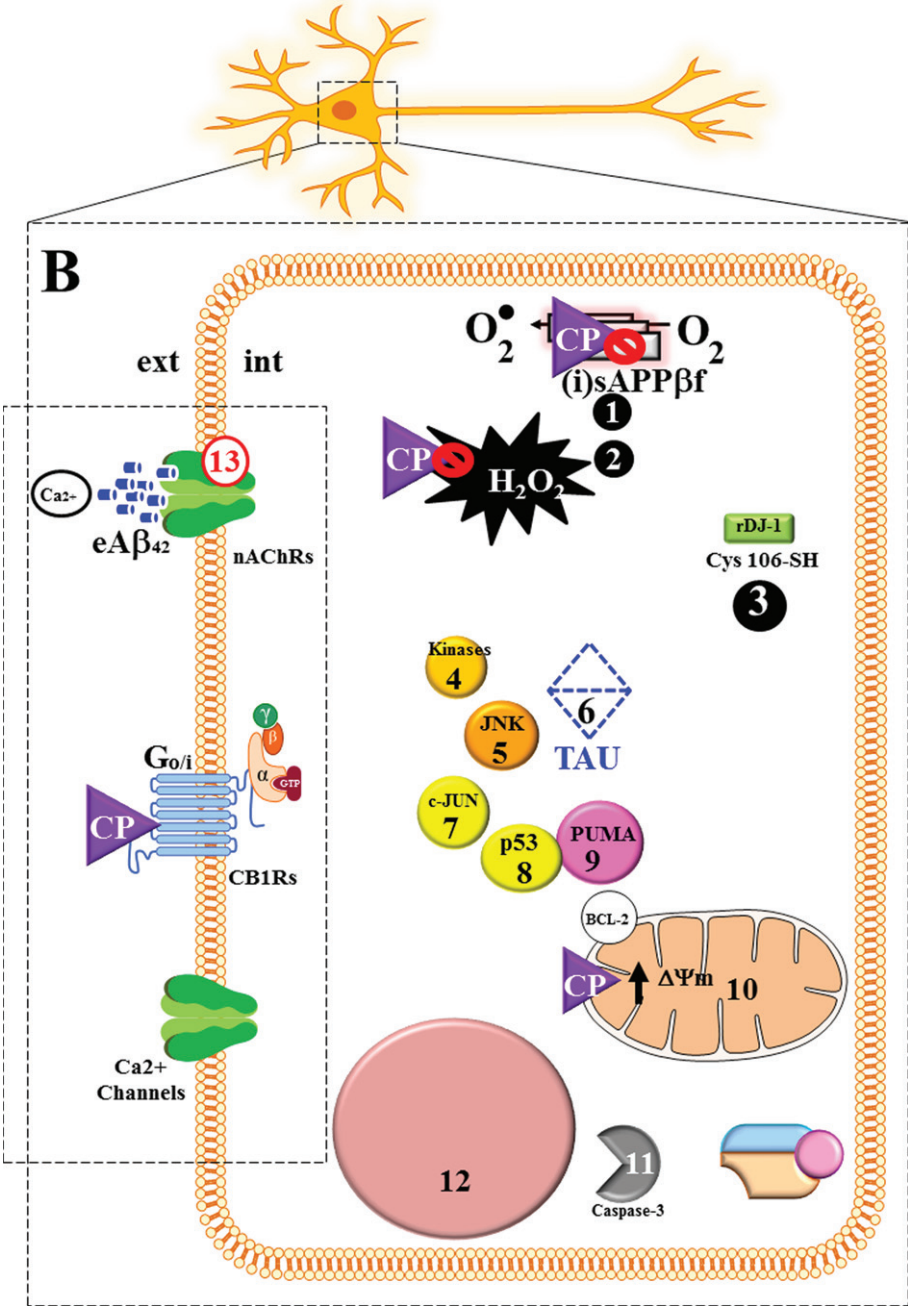


Fig. 9. (Continued)

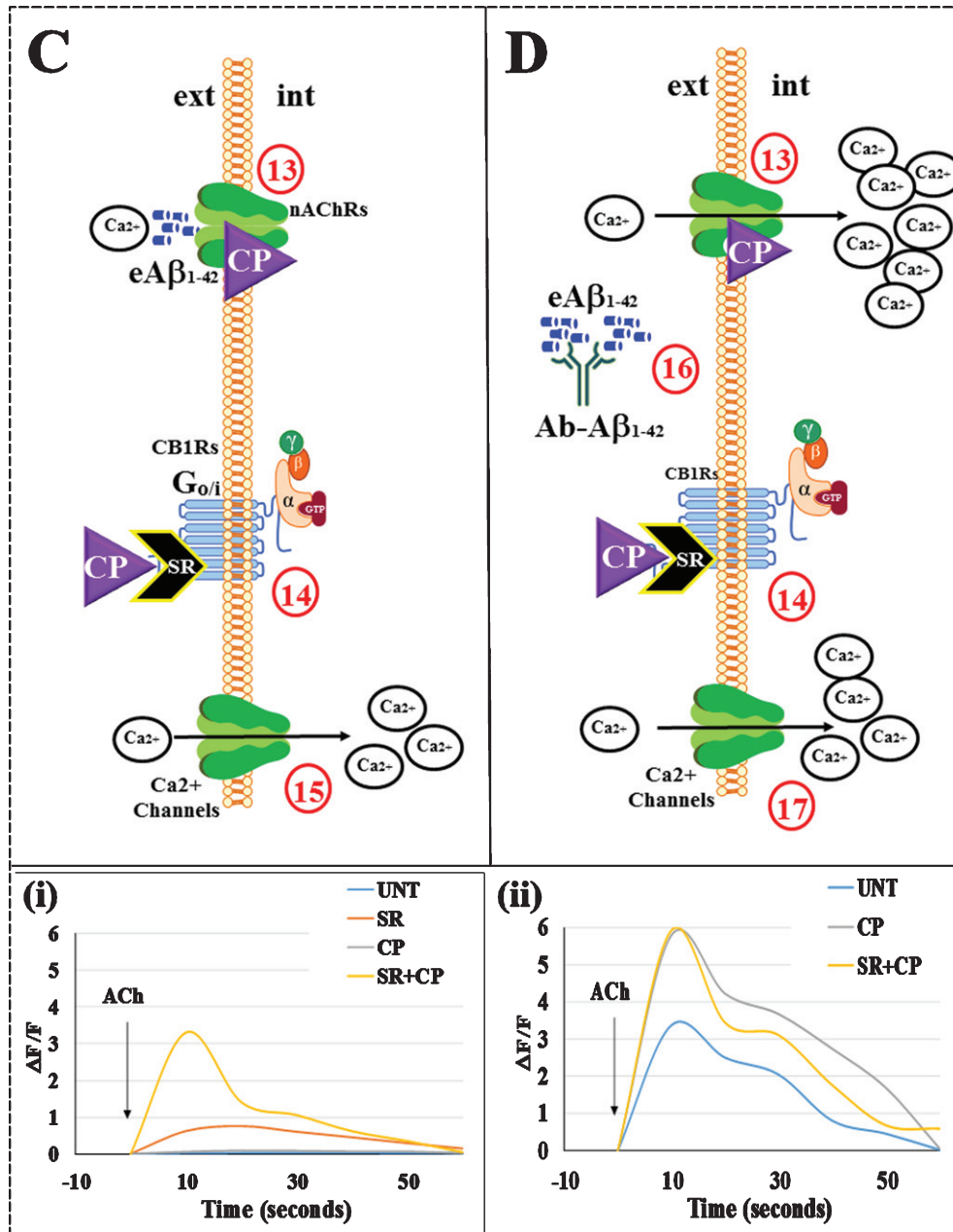


Fig. 9. Schematic representation of the protective effect of CP55940 on PSEN 1 E280A ChLNs. A) Intracellularly accumulation of sA $\beta$ PP $\beta$ f (step 1) generates H<sub>2</sub>O<sub>2</sub> (s2), which in turn oxidized the OS sensor protein DJ-1 at Cys<sup>-106</sup>-SH residue into DJ-1Cys<sup>106</sup>-SO<sub>3</sub> (s3) and activates a domino-like pro-death signaling mechanism by triggering kinases (s4, e.g., ASK1) and JNK kinase (s5). This last kinase phosphorylates protein tau (s6) and activates the transcription factors c-Jun (s7) and p53 (s8). Both transcription factors transcribe the BH-3-only protein PUMA (s9), which together with other pro-apoptosis proteins (e.g., BAX), it induces depolarization of mitochondria, opening of the mitochondrial transition pore, and loss of mitochondrial membrane potential ( $\Delta\Psi_m$ , s10). Damage of mitochondria potential provokes the release of pro-apoptogenic protein cytochrome C, ensuing activation of caspase-3 (s11). In turn, this protease activates the endonuclease DFF40 by cleaving the nuclease's inhibitor DFF45. Finally, DFF40 causes the nuclear chromatin fragmentation, typical of apoptosis (s12). Additionally, ChLNs do not respond to ACh stimuli, i.e., intracellular transient  $Ca^{2+}$  increase is missing due to extracellular interaction between A $\beta_{42}$  (eA $\beta_{42}$ ) and nicotinic (n)ACh receptors (s13). The sA $\beta$ PP $\beta$ f-induced process (s1-s13) leads ChL neurons to structural alterations (e.g., aggregation/ hyperphosphorylation of protein tau), cell death (apoptosis) and intracellular  $Ca^{2+}$  dysfunction. B) Upon exposure to CP55940 (CP), ChLNs show normal features such as no oxidized protein DJ-1 (s3), unaltered  $\Delta\Psi_m$  (s10), and intact nuclei

morphology (s12). Moreover, CP inhibits aggregation of sA $\beta$ PP $\beta$ f (s1), and blocks generation of H<sub>2</sub>O<sub>2</sub> (s2) most probably by quenching anion superoxide radicals (O<sub>2</sub><sup>•-</sup>). As a consequence, no further activation of kinases (s4, s5), phosphorylation of protein tau (s6), and c-Jun (s7), and activation of p53 (s8), PUMA (s9), and caspase-3 (s11) occurs in PSEN1 E280A ChLNs just leaving mitochondria and nuclei unchanged from sA $\beta$ PP $\beta$ f-induced damage. C) Since nAChRs are blocked by eA $\beta$ <sub>42</sub> (s13), CP was unable to modify the response of mutant ChLNs to ACh (inset graph i). Interestingly, the CB<sub>1</sub> and CB<sub>2</sub> receptor inverse agonists SR141716 plus SR144528 (= SR) only or in the presence of CP induce a significant increase in intracellular Ca<sup>2+</sup> (s14) most probably through activation of Ca<sup>2+</sup> channels (s15 and inset graph i). D) When mutant ChLNs were exposed to CP, SR, and anti-A $\beta$ <sub>42</sub> antibody 6E10 (s16), the mixture induced a dramatic increase in the transient intracellular Ca<sup>2+</sup> flow (s13, s17 and inset graph ii).

## ACKNOWLEDGMENTS

This study was funded by MinCiencias grant # 1115-844-67062, contract #830-2019 to CV-P, MJ-Del-Rio, and MM-P. VS-M is a doctoral student of the Basic Biomedical Sciences Academic Corporation program at the Universidad de Antioquia (UdeA) funded by the “2019 Bicentennial Doctoral Excellence Scholarship”, MinCiencias-Colombia.

Authors' disclosures available online (<https://www.j-alz.com/manuscript-disclosures/20-1045r2>).

## REFERENCES

- [1] Long JM, Holtzman DM (2019) Alzheimer disease: An update on pathobiology and treatment strategies. *Cell* **179**, 312-339.
- [2] Hampel H, Mesulam MM, Cuellar AC, Farlow MR, Giacobini E, Grossberg GT, Khachaturian AS, Vergallo A, Cavedo E, Snyder PJ, Khachaturian ZS (2018) The cholinergic system in the pathophysiology and treatment of Alzheimer's disease. *Brain* **141**, 1917-1933.
- [3] DeTure MA, Dickson DW (2019) The neuropathological diagnosis of Alzheimer's disease. *Mol Neurodegener* **14**, 32.
- [4] Yuksel M, Tacal O (2019) Trafficking and proteolytic processing of amyloid precursor protein and secretases in Alzheimer's disease development: An up-to-date review. *Eur J Pharmacol* **856**, 172415.
- [5] Kabir MT, Uddin MS, Setu JR, Ashraf GM, Bin-Jumah MN, Abdel-Daim MM (2020) Exploring the role of PSEN mutations in the pathogenesis of Alzheimer's disease. *Neurotox Res* **38**, 833-849.
- [6] Sun L, Zhou R, Yang G, Shi Y (2017) Analysis of 138 pathogenic mutations in presenilin-1 on the *in vitro* production of A $\beta$ 42 and A $\beta$ 40 peptides by gamma-secretase. *Proc Natl Acad Sci U S A* **114**, E476-E485.
- [7] Lopera F, Ardilla A, Martinez A, Madrigal L, Arango-Viana JC, Lemere CA, Arango-Lasprilla JC, Hincapié L, Arcos-Burgos M, Ossa JE, Behrens IM, Norton J, Lendon C, Goate AM, Ruiz-Linares A, Rosselli M, Kosik KS (1997) Clinical features of early-onset Alzheimer disease in a large kindred with an E280A presenilin-1 mutation. *JAMA* **277**, 793-799.
- [8] Sepulveda-Falla D, Glatzel M, Lopera F (2012) Phenotypic profile of early-onset familial Alzheimer's disease caused by presenilin-1 E280A mutation. *J Alzheimers Dis* **32**, 1-12.
- [9] Fuller JT, Cronin-Golomb A, Gatchel JR, Norton DJ, Guzman-Velez E, Jacobs HIL, Hanseeuw B, Pardilla-Delgado E, Artola A, Baena A, Bocanegra Y, Kosik KS, Chen K, Tariot PN, Johnson K, Sperling RA, Reiman EM, Lopera F, Quiroz YT (2019) Biological and cognitive markers of presenilin1 E280A autosomal dominant Alzheimer's disease: A comprehensive review of the Colombian kindred. *J Prev Alzheimers Dis* **6**, 112-120.
- [10] Lalli MA, Cox HC, Arcila ML, Cadavid L, Moreno S, Garcia G, Madrigal L, Reiman EM, Arcos-Burgos M, Bedoya G, Brunkow ME, Glusman G, Roach JC, Hood L, Kosik KS, Lopera F (2014) Origin of the PSEN1 E280A mutation causing early-onset Alzheimer's disease. *Alzheimers Dement* **10**, S277-S283.e210.
- [11] Zhou R, Yang G, Shi Y (2017) Dominant negative effect of the loss-of-function gamma-secretase mutants on the wild-type enzyme through heterooligomerization. *Proc Natl Acad Sci U S A* **114**, 12731-12736.
- [12] Lemere CA, Lopera F, Kosik KS, Lendon CL, Ossa J, Saido TC, Yamaguchi H, Ruiz A, Martinez A, Madrigal L, Hincapié L, Arango JC, Anthony DC, Koo EH, Goate AM, Selkoe DJ (1996) The E280A presenilin 1 Alzheimer mutation produces increased A $\beta$  42 deposition and severe cerebellar pathology. *Nat Med* **2**, 1146-1150.
- [13] Velez-Pardo C, Arellano JI, Cardona-Gomez P, Jimenez Del Rio M, Lopera F, De Felipe J (2004) CA1 hippocampal neuronal loss in familial Alzheimer's disease presenilin-1 E280A mutation is related to epilepsy. *Epilepsia* **45**, 751-756.
- [14] Fleisher AS, Chen K, Quiroz YT, Jakimovich LJ, Gomez MG, Langois CM, Langbaum JB, Ayutyanont N, Roontiva A, Thiyyagura P, Lee W, Mo H, Lopez L, Moreno S, Acosta-Baena N, Giraldo M, Garcia G, Reiman RA, Huentelman MJ, Kosik KS, Tariot PN, Lopera F, Reiman EM (2012) Florbetapir PET analysis of amyloid- $\beta$  deposition in the presenilin 1 E280A autosomal dominant Alzheimer's disease kindred: A cross-sectional study. *Lancet Neurol* **11**, 1057-1065.
- [15] Quiroz YT, Sperling RA, Norton DJ, Baena A, Arboleda-Velasquez JF, Cosio D, Schultz A, Lapoint M, Guzman-Velez E, Miller JB, Kim LA, Chen K, Tariot PN, Lopera F, Reiman EM, Johnson KA (2018) Association between amyloid and tau accumulation in young adults with autosomal dominant Alzheimer disease. *JAMA Neurol* **75**, 548-556.
- [16] Soto-Mercado V, Mendivil-Perez M, Velez-Pardo C, Lopera F, Jimenez-Del-Rio M (2020) Cholinergic-like neurons carrying PSEN1 E280A mutation from familial Alzheimer's disease reveal intraneuronal sAPP $\beta$  fragments accumulation, hyperphosphorylation of tau, oxidative stress, apoptosis and Ca<sup>2+</sup>-dysregulation: Therapeutic implications. *PLoS One* **15**, e0221669.
- [17] Bonini SA, Premoli M, Tambaro S, Kumar A, Maccarinelli G, Memo M, Mastinu A (2018) Cannabis sativa: A comprehensive ethnopharmacological review of a medicinal plant with a long history. *J Ethnopharmacol* **227**, 300-315.
- [18] Cassano T, Villani R, Pace L, Carbone A, Bukke VN, Orkisz S, Avolio C, Serviddio G (2020) From Cannabis sativa to cannabidiol: Promising therapeutic candidate for the

- treatment of neurodegenerative diseases. *Front Pharmacol* **11**, 124.
- [19] ElSohly MA, Radwan MM, Gul W, Chandra S, Galal A (2017) Phytochemistry of Cannabis sativa L. *Prog Chem Org Nat Prod* **103**, 1-36.
- [20] Marcu J, Schechter J (2016) Molecular pharmacology of CB1 and CB2 cannabinoid receptors. In *Neuropathology of Drug Addictions and Substance Misuse*, Preedy V, ed. Academic Press, pp. 713-721.
- [21] Shahbazi F, Grandi V, Banerjee A, Trant JF (2020) Cannabinoids and cannabinoid receptors: The story so far. *iScience* **23**, 101301.
- [22] Schubert D, Kepchia D, Liang Z, Dargusch R, Goldberg J, Maher P (2019) Efficacy of cannabinoids in a pre-clinical drug-screening platform for Alzheimer's disease. *Mol Neurobiol* **56**, 7719-7730.
- [23] Hampson AJ, Grimaldi M, Axelrod J, Wink D (1998) Cannabidiol and (-)Delta9-tetrahydrocannabinol are neuroprotective antioxidants. *Proc Natl Acad Sci U S A* **95**, 8268-8273.
- [24] Chen Y, Buck J (2000) Cannabinoids protect cells from oxidative cell death: A receptor-independent mechanism. *J Pharmacol Exp Ther* **293**, 807-812.
- [25] Marsicano G, Moosmann B, Hermann H, Lutz B, Behl C (2002) Neuroprotective properties of cannabinoids against oxidative stress: Role of the cannabinoid receptor CB1. *J Neurochem* **80**, 448-456.
- [26] Jimenez-Del-Rio M, Daza-Restrepo A, Velez-Pardo C (2008) The cannabinoid CP55,940 prolongs survival and improves locomotor activity in *Drosophila melanogaster* against paraquat: Implications in Parkinson's disease. *Neurosci Res* **61**, 404-411.
- [27] Velez-Pardo C, Del Rio MJ (2006) Avoidance of Abeta[25-35]/(H2O2)-induced apoptosis in lymphocytes by the cannabinoid agonists CP55,940 and JWH-015 via receptor-independent and PI3K-dependent mechanisms: Role of NF-kappaB and p53. *Med Chem* **2**, 471-479.
- [28] Harvey BS, Ohlsson KS, Mååg JL, Musgrave IF, Smid SD (2012) Contrasting protective effects of cannabinoids against oxidative stress and amyloid- $\beta$  evoked neurotoxicity *in vitro*. *Neurotoxicology* **33**, 138-146.
- [29] Pertwee R, Cannabinoid Receptor Ligands, <https://www.tocris.com/literature/scientific-reviews/cannabinoid-receptor-ligands>, Accessed Aug. 2020.
- [30] Mendivil-Perez M, Velez-Pardo C, Jimenez-Del-Rio M (2019) Direct transdifferentiation of human Wharton's jelly mesenchymal stromal cells into cholinergic-like neurons. *J Neurosci Methods* **312**, 126-138.
- [31] Gulisano W, Melone M, Ripoli C, Tropea MR, Li Puma DD, Giunta S, Cocco S, Marcotulli D, Origlia N, Palmeri A, Arancio O, Conti F, Grassi C, Puzzo D (2019) Neuromodulatory action of picomolar extracellular A $\beta$ 42 oligomers on presynaptic and postsynaptic mechanisms underlying synaptic function and memory. *J Neurosci* **39**, 5986-6000.
- [32] Armijo E, Gonzalez C, Shahnawaz M, Flores A, Davis B, Soto C (2017) Increased susceptibility to Abeta toxicity in neuronal cultures derived from familial Alzheimer's disease (PSEN1-A246E) induced pluripotent stem cells. *Neurosci Lett* **639**, 74-81.
- [33] Pap P, Koszeghy A, Szucs G, Rusznak Z (2009) Cytoplasmic Ca(2+) concentration changes evoked by cholinergic stimulation in primary astrocyte cultures prepared from the rat cochlear nucleus. *Hear Res* **255**, 73-83.
- [34] Sekiguchi-Tonosaki M, Obata M, Haruki A, Himi T, Kosaka J (2009) Acetylcholine induces Ca2+signaling in chicken retinal pigmented epithelial cells during dedifferentiation. *Am J Physiol Cell Physiol* **296**, C1195-1206.
- [35] Lazic SE, Clarke-Williams CJ, Munafò MR (2018) What exactly is 'N' in cell culture and animal experiments? *PLoS Biol* **16**, e2005282.
- [36] Nyíri G, Szabadits E, Cserép C, Mackie K, Shigemoto R, Freund TF (2005) GABAB and CB1 cannabinoid receptor expression identifies two types of septal cholinergic neurons. *Eur J Neurosci* **21**, 3034-3042.
- [37] Velez-Pardo C, Jimenez-Del-Rio M, Lores-Arnaiz S, Bustamante J (2010) Protective effects of the synthetic cannabinoids CP55,940 and JWH-015 on rat brain mitochondria upon paraquat exposure. *Neurochem Res* **35**, 1323-1332.
- [38] Benard G, Massa F, Puente N, Lourenco J, Bellocchio L, Soria-Gomez E, Matias I, Delamarre A, Metna-Laurent M, Cannich A, Hebert-Chatelain E, Mulle C, Ortega-Gutierrez S, Martin-Fontecha M, Klugmann M, Guggenhuber S, Lutz B, Gertsch J, Chaouloff F, Lopez-Rodriguez ML, Grandes P, Rossignol R, Marsicano G (2012) Mitochondrial CB1 receptors regulate neuronal energy metabolism. *Nat Neurosci* **15**, 558-564.
- [39] Ma L, Niu W, Yang S, Tian J, Luan H, Cao M, Xi W, Tu W, Jia J, Lv J (2018) Inhibition of mitochondrial permeability transition pore opening contributes to cannabinoid type 1 receptor agonist ACEA-induced neuroprotection. *Neuropharmacology* **135**, 211-222.
- [40] Melser S, Pagano Zottola AC, Serrat R, Puente N, Grandes P, Marsicano G, Hebert-Chatelain E (2017) Functional analysis of mitochondrial CB1 cannabinoid receptors (mtCB1) in the brain. *Methods Enzymol* **593**, 143-174.
- [41] Devi L, Prabhu BM, Galati DF, Avadhani NG, Anandatheerthavarada HK (2006) Accumulation of amyloid precursor protein in the mitochondrial import channels of human Alzheimer's disease brain is associated with mitochondrial dysfunction. *J Neurosci* **26**, 9057-9068.
- [42] Anandatheerthavarada HK, Biswas G, Robin MA, Avadhani NG (2003) Mitochondrial targeting and a novel transmembrane arrest of Alzheimer's amyloid precursor protein impairs mitochondrial function in neuronal cells. *J Cell Biol* **161**, 41-54.
- [43] Currais A, Quehenberger O, M Armando A, Daugherty D, Maher P, Schubert D (2016) Amyloid proteotoxicity initiates an inflammatory response blocked by cannabinoids. *NPJ Aging Mech Dis* **2**, 16012.
- [44] Kinumi T, Kimata J, Taira T, Ariga H, Niki E (2004) Cysteine-106 of DJ-1 is the most sensitive cysteine residue to hydrogen peroxide-mediated oxidation *in vivo* in human umbilical vein endothelial cells. *Biochem Biophys Res Commun* **317**, 722-728.
- [45] Nakano K, Vousden KH (2001) PUMA, a novel proapoptotic gene, is induced by p53. *Mol Cell* **7**, 683-694.
- [46] Yu J, Zhang L, Hwang PM, Kinzler KW, Vogelstein B (2001) PUMA induces the rapid apoptosis of colorectal cancer cells. *Mol Cell* **7**, 673-682.
- [47] Lu H, Hou G, Zhang Y, Dai Y, Zhao H (2014) c-Jun transactivates Puma gene expression to promote osteoarthritis. *Mol Med Rep* **9**, 1606-1612.
- [48] Saitoh M, Nishitoh H, Fujii M, Takeda K, Tobiume K, Sawada Y, Kawabata M, Miyazono K, Ichijo H (1998) Mammalian thioredoxin is a direct inhibitor of apoptosis signal-regulating kinase (ASK) 1. *EMBO J* **17**, 2596-2606.
- [49] Nishitoh H, Saitoh M, Mochida Y, Takeda K, Nakano H, Rothe M, Miyazono K, Ichijo H (1998) ASK1 is essential for JNK/SAPK activation by TRAF2. *Mol Cell* **2**, 389-395.



- [50] Yoshida H, Hastie CJ, McLauchlan H, Cohen P, Goedert M (2004) Phosphorylation of microtubule-associated protein tau by isoforms of c-Jun N-terminal kinase (JNK). *J Neurochem* **90**, 352-358.
- [51] Esposito G, De Filippis D, Carnuccio R, Izzo AA, Iuvone T (2006) The marijuana component cannabidiol inhibits beta-amyloid-induced tau protein hyperphosphorylation through Wnt/beta-catenin pathway rescue in PC12 cells. *J Mol Med (Berl)* **84**, 253-258.
- [52] Lei M, Xu H, Li Z, Wang Z, O'Malley TT, Zhang D, Walsh DM, Xu P, Selkoe DJ, Li S (2016) Soluble A $\beta$  oligomers impair hippocampal LTP by disrupting glutamatergic/GABAergic balance. *Neurobiol Dis* **85**, 111-121.
- [53] Cline EN, Bicca MA, Viola KL, Klein WL (2018) The amyloid-beta oligomer hypothesis: Beginning of the third decade. *J Alzheimers Dis* **64**, S567-S610.
- [54] Liu Q, Kawai H, Berg DK (2001) beta-Amyloid peptide blocks the response of alpha 7-containing nicotinic receptors on hippocampal neurons. *Proc Natl Acad Sci U S A* **98**, 4734-4739.
- [55] Pettit DL, Shao Z, Yakel JL (2001) beta-Amyloid(1-42) peptide directly modulates nicotinic receptors in the rat hippocampal slice. *J Neurosci* **21**, RC120.
- [56] Szabo GG, Lenkey N, Holderith N, Andrasi T, Nusser Z, Hajos N (2014) Presynaptic calcium channel inhibition underlies CB(1) cannabinoid receptor-mediated suppression of GABA release. *J Neurosci* **34**, 7958-7963.
- [57] Shen JX, Yakel JL (2009) Nicotinic acetylcholine receptor-mediated calcium signaling in the nervous system. *Acta Pharmacol Sin* **30**, 673-680.
- [58] Uteshev VV (2012)  $\alpha$ 7 nicotinic ACh receptors as a ligand-gated source of Ca(2+) ions: The search for a Ca(2+) optimum. *Adv Exp Med Biol* **740**, 603-638.
- [59] Oz M, Ravindran A, Diaz-Ruiz O, Zhang L, Morales M (2003) The endogenous cannabinoid anandamide inhibits alpha7 nicotinic acetylcholine receptor-mediated responses in *Xenopus* oocytes. *J Pharmacol Exp Ther* **306**, 1003-1010.
- [60] Butt C, Alptekin A, Shippenberg T, Oz M (2008) Endogenous cannabinoid anandamide inhibits nicotinic acetylcholine receptor function in mouse thalamic synaptosomes. *J Neurochem* **105**, 1235-1243.
- [61] Twitchell W, Brown S, Mackie K (1997) Cannabinoids inhibit N- and P/Q-type calcium channels in cultured rat hippocampal neurons. *J Neurophysiol* **78**, 43-50.
- [62] Wang HY, Stucky A, Liu J, Shen C, Trocme-Thibierge C, Morain P (2009) Dissociating beta-amyloid from alpha 7 nicotinic acetylcholine receptor by a novel therapeutic agent, S 24795, normalizes alpha 7 nicotinic acetylcholine and NMDA receptor function in Alzheimer's disease brain. *J Neurosci* **29**, 10961-10973.
- [63] Tariot PN, Lopera F, Langbaum JB, Thomas RG, Hendrix S, Schneider LS, Rios-Romenets S, Giraldo M, Acosta N, Tobon C, Ramos C, Espinosa A, Cho W, Ward M, Clayton D, Friesenhahn M, Mackey H, Honigberg L, Sanabria Bohorquez S, Chen K, Walsh T, Langlois C, Reiman EM (2018) The Alzheimer's Prevention Initiative Autosomal-Dominant Alzheimer's Disease Trial: A study of crenezumab versus placebo in preclinical PSEN1 E280A mutation carriers to evaluate efficacy and safety in the treatment of autosomal-dominant Alzheimer's disease, including a placebo-treated noncarrier cohort. *Alzheimers Dement (N Y)* **4**, 150-160.
- [64] Meilandt WJ, Maloney JA, Imperio J, Lalehzadeh G, Earr T, Crowell S, Bainbridge TW, Lu Y, Ernst JA, Fuji RN, Atwal JK (2019) Characterization of the selective *in vitro* and *in vivo* binding properties of crenezumab to oligomeric A $\beta$ . *Alzheimers Res Ther* **11**, 97.
- [65] Benek O, Korabecny J, Soukup O (2020) A perspective on multi-target drugs for Alzheimer's disease. *Trends Pharmacol Sci* **41**, 434-445.



# Latent Tri-lineage Potential of Human Menstrual Blood–Derived Mesenchymal Stromal Cells Revealed by Specific In Vitro Culture Conditions

Diana Quintero-Espinosa<sup>1</sup> · Viviana Soto-Mercado<sup>1</sup> · Catherine Quintero-Quinchia<sup>1</sup> · Miguel Mendivil-Perez<sup>1</sup> · Carlos Velez-Pardo<sup>1</sup> · Marlene Jimenez-Del-Rio<sup>1</sup>

Received: 2 March 2021 / Accepted: 3 June 2021

© The Author(s), under exclusive licence to Springer Science+Business Media, LLC, part of Springer Nature 2021

## Abstract

Human menstrual blood–derived mesenchymal stromal cells (MenSCs) have become not only an important source of stromal cells for cell therapy but also a cellular source for neurologic disorders in vitro modeling. By using culture protocols originally developed in our laboratory, we show that MenSCs can be converted into floating neurospheres (NSs) using the Fast-N-Spheres medium for 24–72 h and can be transdifferentiated into functional dopaminergic-like (DALNs, ~26% TH + / DAT + flow cytometry) and cholinergic-like neurons (ChLNs, ~46% ChAT + / VACHT flow cytometry) which responded to dopamine- and acetylcholine-triggered neuronal Ca<sup>2+</sup> inward stimuli when cultured with the NeuroForsk and the Cholinergic-N-Run medium, respectively in a timely fashion (i.e., 4–7 days). Here, we also report a direct transdifferentiation method to induce MenSCs into functional astrocyte-like cells (ALCs) by incubation of MenSCs in commercial Gibco® Astrocyte medium in 7 days. The MSC-derived ALCs (~59% GFAP + / S100β +) were found to respond to glutamate-induced Ca<sup>2+</sup> inward stimuli. Altogether, these results show that MenSCs are a reliable source to obtain functional neurogenic cells to further investigate the neurobiology of neurologic disorders.

**Keywords** Menstrual blood · Stromal · Cholinergic · Dopaminergic · Astrocyte · Calcium · Neurogenic

## Introduction

Mesenchymal stromal cells (MSCs) are multipotent cells with self-renewal ability and differentiating potential [1, 2]. Because of these meaningful features, MSCs hold great promise for the treatment and modeling of neurological disorders such as Alzheimer's (AD) and Parkinson's diseases (PD), and for testing potential therapeutic approaches (e.g., [3, 4]). Since MSCs can be obtained from fetal (e.g., umbilical cord Wharton's jelly (UC-WJ), umbilical cord

blood, placenta) and adult sources (e.g., dental pulp, gingival tissue, adipocyte tissue, menstrual blood) with minimal technical limitations, minor ethical issues, and/or reduced tumorigenic risk, they have emerged as a useful strategy for regenerative medicine [5]. Accordingly, menstrual blood stromal cells (hereafter named as MenSCs) have become not only an important source of stromal cells for cell therapy (e.g., [6, 7]) but also a cellular source for neurologic disorders in vitro modeling. Indeed, it has been shown that MenSCs can be converted into clonogenic neurosphere-like cells (NSCs) in 10–20 days, which can be transdifferentiated into glial-like and neural-like cells in 12–16 days [8, 9]. However, no further data are available to determine whether MenSCs can transdifferentiate into other neuronal lineages such as dopaminergic, cholinergic, or astrocytic neuronal cells [10].

Recently, we have derived MSCs from UC-WJ to obtain neurospheres (NSs), i.e., free-floating spherical cell aggregates, also named as neural precursor cells, in 24 h, and NS-derived nerve-like cells (NLCs) in 4 days [11]. Moreover, MSCs have also been transdifferentiated into functional

Diana Quintero-Espinosa and Viviana Soto-Mercado contributed equally to this work

✉ Marlene Jimenez-Del-Rio  
marlene.jimenez@udea.edu.co

<sup>1</sup> Neuroscience Research Group, Medical Research Institute, Faculty of Medicine, University Research Center (URC), University of Antioquia (UdeA), Calle 70 no. 52-21, and Calle 62 no. 52-59, Building 1, Room 412, Medellín, Colombia

cholinergic-like neurons (ChLNs) in 7 days [12]. While UC-WJ-derived MSCs are available for only a minority of individuals who have their samples banked at birth, MenSCs can be isolated with minimal invasiveness and risk to the donor and can be obtained in sufficient numbers to enable expansion in culture. Therefore, MenMSC might represent a fast, safe, and efficient way of generating neural-like cells [4].

The present study aimed to investigate whether MenSCs can transdifferentiate into NSs and neuronal lineages with culture protocols originally developed in our laboratory including three culture media such as the Fast-N-Spheres [11], the NeuroForsk [11], and the Cholinergic-N-Run medium [12]. Similar to UC-WJ-MSCs, we show that MenSCs can be converted into floating NSs using the Fast-N-Spheres medium for 24–72 h and can be transdifferentiated into functional dopaminergic-like neurons (DALNs) and ChLNs which responded to dopamine- and acetylcholine-triggered neuronal  $\text{Ca}^{2+}$  inward stimuli when cultured with the NeuroForsk and the Cholinergic-N-Run medium, respectively, in 4–7 days of culture. We also report a direct transdifferentiation method to induce MenSCs into functional astrocyte-like cells (ALCs) by incubation of MenSCs in commercial Gibco® Astrocyte Medium in 7 days. Accordingly, MenSC-derived ALCs (~59% GFAP+/S100 $\beta$ +) were found to respond to glutamate-induced  $\text{Ca}^{2+}$  inward stimuli. Altogether these results show that MenSCs are a reliable source to obtain functional neurogenic cells to further investigate the neurobiology of AD and PD neurologic disorders.

## Material and Methods

### Isolation and Characterization of Mesenchymal Stromal Cells Derived from Human Menstrual Blood (MenSCs)

The menstrual blood samples were collected from three healthy females aged between 18 and 30 years. Donors provided a signed informed consent approved by the ethics committee of the Sede de Investigación Universitaria (SIU), University of Antioquia, Medellín, Colombia. Menstrual blood (MenB) was collected by cup collection (10–15 mL) during the first 3 days of menses. Briefly, menstrual blood samples were delivered into the laboratory and mixed with an equal volume of phosphate-buffered saline (PBS) containing 1 mM ethylenediamine tetra-acetic acid (EDTA), with 100 U/mL penicillin/streptomycin 0.25 mg/mL amphotericin B, and subject to cell lysis or standard Ficoll procedures within 24 h as previously described in ref. [13]. After centrifugation, the cells were suspended in a buffy coat ( $6.7 \times 10^6 \pm 3 \times 10^6$  cells,  $n = 3$ ), were transferred into a new tube, washed in PBS twice, re-suspended in growth medium (low-glucose

DMEM medium supplemented with 10% FBS (Gibco, USA), 100 U/mL penicillin/streptomycin, and 0.25 mg/mL amphotericin B), and seeded into 25-cm<sup>2</sup> plastic cell culture flasks at 37 °C with 5% humidified CO<sub>2</sub>. The medium was replaced every 3 days leaving behind the adherent cells that were growing as fibroblastic cells in clusters. When the cells reached 80–90% confluence (P0), the cells were detached by 0.25% trypsin/1 mM EDTA and sub-cultured to new flasks by the ratio of 1:3. The isolated MenSCs were evaluated for the following characteristics: colony formation capacity (i.e., colonies with a typical adherent growth, colony-forming unit fibroblast activity, and spindle-shaped and fibroblast-like morphology); positivity for the mesenchymal-associated surface markers CD90, CD9, and CD73 (99% positive); and karyotype with normal shape, number, and distribution. The differentiation capacity in an osteoblast, chondrocyte, and adipocyte lineage of MenSCs, as well as the presence of neuronal precursors and astrocyte markers (e.g., NFL,  $\beta$ -TUB III, GFAP, S100 $\beta$ , TH, ChAT), was assessed according to refs. [12, 14].

### Karyotyping

Karyotype analysis was performed by Genetica Lab, S.A.S., using standard cytogenetic protocols. Briefly, at 60–70% confluence, MenSCs cells were incubated with 0.1 mg/mL Colcemid (Sigma) for 90 min at 37 °C. Then, the cells were detached with 0.25% trypsin and centrifuged at  $591 \times g$  for 20 min. The medium was removed, and the hypotonic solution (0.075 M KCl, 0.017 M Na-citrate) was added and incubated for 20 min at 37 °C. After a new centrifugation, cells were fixed with freshly prepared Carnoy's solution. Metaphase spreads were analyzed after staining with quina-crine (Sigma) for karyotyping. Analysis was performed on three different primary cultures counting 20 metaphases for each sample.

### Cell Differentiation

#### Neurosphere (NS) Formation

MenSCs were seeded at a density of  $2.5 \times 10^4$  cells/cm<sup>2</sup> in a multi-well plate (Greiner-Bio-one, cat. no. 662102) using Fast-N-spheres medium (DMEN F-12 GIBCO® (cat. no. 11330-032), supplemented with 2% B27® GIBCO® (cat. no. 17504-044), 20 ng/mL basic fibroblast growth factor (bFGF, R&D Systems, Inc., MN), 20 ng/mL epidermal growth factor (EGF, Sigma cat. no. E9644), 1  $\mu$ g/mL heparin sodium salt®, and 100 U/mL penicillin/streptomycin) for 0, 1, and 3 days according to ref. [11].

### Astrocyte-Like Cell (ALC) Differentiation

For astrocyte differentiation,  $1 \times 10^4$  MenSCs/cm<sup>2</sup> were seeded in 25-cm<sup>2</sup> culture flasks in regular culture medium (RCm, DMEM low-glucose media (Sigma cat. no. D6046) supplemented with 10% FBS) until reach 40% of confluence. Then, the medium was replaced and cells were incubated either in DMEM low-glucose media supplemented with 2% FBS (minimal culture medium, thereafter MCm) or Astrocyte medium® (GIBCO®, cat. no. A1261301) for 0, 4, and 7 days.

### Dopaminergic-Like Neuron (DALN) Differentiation

The MenSCs were seeded at  $1 \times 10^4$  MenSCs/cm<sup>2</sup> in 25 cm<sup>2</sup> culture flasks for 24 h in a regular culture medium (DMEM low-glucose media supplemented with 10% FBS). Then, the medium was removed and cells were incubated either in MCm or dopaminergic differentiation medium (NeuroForsk medium, DMEM low-glucose media supplemented with 2% FBS Forskolin (Sigma cat. no. F6886) 1-μM final concentration) for 0, 4, and 7 days according to ref. [11].

### Cholinergic-Like Neuron (ChLN) Differentiation

The MenSCs were seeded at  $1.6\text{--}2 \times 10^4$  cells/cm<sup>2</sup> in 25-cm<sup>2</sup> culture flasks for 24 h in regular culture medium. Then, the medium was removed and cells were incubated either in MCm or cholinergic differentiation medium (Cholinergic-N-Run medium containing DMEM/F-12 media 1:1 Nutrient Mixture Gibco (cat. no. 10565018, 10 ng/mL), basic fibroblast growth factor (bFGF) recombinant human protein (Gibco cat. no. 13256029), 50 μg/mL sodium heparin (Sigma-Aldrich cat. no. H3393), 0.5 μM all-trans retinoic acid, 50 ng/mL sonic hedgehog peptide (SHH, Sigma cat. no. SRP3156), and 1% FBS) at 37 °C for 0, 4, and 7 days.

### Western Blotting (WB) Analysis

Cells treated with DALNs, ChLNs, NSs, and ALCs differentiation medium for 0, 4, and 7 days were detached with 0.25% trypsin and lysed in 50 mM Tris-HCl, pH 8.0, with 150 mM sodium chloride, 1.0% Igepal CA-630 (NP-40), and 0.1% sodium dodecyl sulfate and a protease inhibitor cocktail (Sigma-Aldrich). All lysates were (quantified using the bicinchoninic acid assay; Thermo Scientific cat. no. 23225) and 30 μg of proteins were loaded onto 12% electrophoresis gels and transferred onto nitrocellulose membranes (Hybond-ECL, Amersham Biosciences) at 270 mA for 90 min using an electrophoretic transfer system (BIO-RAD). The membranes were incubated overnight at 4 °C with monoclonal/polyclonal antibodies against sex-determining region Y-box 2 (SOX2 cat. no. PA1-094,

Thermo), anti-Nestin (Thermo, cat. no. MA1 5841), dopamine transporter (DAT cat. no. PA1-4656), tyrosine hydroxylase (TH, cat. no. AB152, Millipore), glial fibrillary acidic protein (GFAP, cat. no. sc6170, Santa Cruz), S100β (cat. no. 676604, Biolegend), β-tubulin III (β-TUB III cat. no. G712A, Promega), microtubule-associated protein 2 (MAP2, MA1-25044, Invitrogen), Neurofilament-L (NF-L, cat. no. 125044, Thermo), vesicular acetylcholine transporter (VACHT, cat. no. SAB4200559, Sigma-Aldrich), and choline acetyltransferase (ChAT, cat. no. AB144P, Millipore) primary antibodies (1:5000). Anti-actin antibody (cat. no. MAB1501, Millipore; 1:1000) was used as expression control. Secondary infrared antibodies (goat anti-rabbit IRDye® 680RD, cat. no. 926-68071; donkey anti-goat IRDye® 680RD, cat. no. 926-68074; and goat anti-mouse IRDye® 800CW, cat. no. 926-32270; LICORBiosciences) 1:1000 was used for Western blotting analysis and data were acquired by using Odyssey software.

### Immunofluorescence (IMF) Analysis

For immunofluorescence analysis of neural and astrocytes markers, cells treated with MCm, NeuroForsk, Gibco® Astrocyte Medium [15–17] or Ch-N-Rm medium for 0, 4, and 7 days and Neurospheres Fast medium for 0, 24, and 72 h were fixed with paraformaldehyde for 20 min, followed by Triton X-100 (0.1%) permeabilization and 5% bovine serum albumin (BSA) blockage. Cells were then incubated overnight with primary antibodies against DAT, TH, GFAP, S100β, β-TUB III, MAP2, NFL, VACHT, and ChAT proteins (1:500). After exhaustive rinsing, we incubated the cells with secondary fluorescent antibodies (DyLight 488 and 595 donkey anti-rabbit, -goat, and -mouse, Cat DI 2488 and DI 1094, respectively) 1:500. The nuclei were stained with Hoechst 33342 (1 μM, life technologies) and images were acquired on a Floyd Cells Imaging Station microscope. Imaging processing data for further statistical analysis were gathered by ImageJ software (<http://imagej.nih.gov/ij/>). The figures were transformed into 8-bit images and the background was subtracted. The cellular measurement regions of interest (ROI  $n = 7$  from three different experiments) were drawn around nuclear or over all cells (for cytoplasmic probes) and the fluorescence intensity was subsequently determined applying the same threshold. For mean fluorescence intensity (MFI) was obtained by normalizing total fluorescence to the number of nuclei.

### Flow Cytometry (FC) Analysis of Astrocytic, Dopaminergic, and Cholinergic Markers

Flow cytometry acquisition was used to determine the percentage of GFAP/S100β, DAT/TH, and ChAT/VACHT double-positive cells, according to previous reports [18–20].

Cells treated with MCm, NeuroForsk, astrocyte, or Ch–N–Rm medium at days 0, 4, and 7 were detached with 0.25% trypsin–EDTA 1 mM and fixed in suspension with paraformaldehyde (overnight). After washing, cells were simultaneously incubated with GFAP, S100 $\beta$ , DAT, TH, ChAT, and VChAT primary antibodies (1:500) at 4 °C overnight. Cell suspensions were washed and incubated with DyeLight 594 donkey anti-goat and DyeLight 488 donkey anti-rabbit antibodies (1:500). Finally, cells were washed and re-suspended in PBS for analysis on a Canto cytometer (Beckman Coulter). Ten thousand events were acquired and the acquisition analysis was performed using FlowJo 7.6.2 Data Analysis Software. Positive staining was defined as the fluorescence emission that exceeded levels of the population stained with the negative control (only secondary antibodies staining).

### Intracellular Calcium Imaging

The cytoplasmic  $\text{Ca}^{2+}$  concentration ( $[\text{Ca}^{2+}]_i$ ) was measured. Briefly, DALNs, ChLNs, and ALCs cultured in NeuroForsk, Ch–N–Rm, and Astrocyte medium respectively for 0, 4, and 7 days were transferred to a bath solution (NBS; in mM: 137 NaCl, 5 KCl 2.5  $\text{CaCl}_2$ , 1  $\text{MgCl}_2$ , 10 HEPES, pH 7.3, and 22 glucose) containing a  $\text{Ca}^{2+}$  sensitive indicator (2  $\mu\text{M}$  Fluo3-AM, an acetoxymethyl ester form of the fluorescent dye Fluo-3; Thermo Fisher Scientific Cat F1242) for 30 min at room temperature and then washed five times. The intracellular  $\text{Ca}^{2+}$  transients were evoked by dopamine-hydrochloride (DA, 1 mM final), acetylcholinesterase (ACh, 1 mM final), and glutamate (GLUT, 100  $\mu\text{L}$  final). The amplitudes of the  $\text{Ca}^{2+}$ -related fluorescence transients were expressed relative to the resting fluorescence ( $\Delta F/F$ ) and were calculated by the formula  $\Delta F/F = (F_{\text{max}} - F_{\text{rest}})/(F_{\text{rest}} - F_{\text{bg}})$  according to ref. [21]. The Image J program (<https://imagej.net/>) was used for the calculation of the fluorescence intensities as previously published in refs. [11, 12].

### Data Analysis

Statistical analyses were conducted using the Student t analysis or one-way ANOVA followed by Bonferroni post hoc comparison calculated with the GraphPad Prism 6 Scientific Software (GraphPad, Software, Inc. La Jolla, CA, U.S.A.). Statistical significance was accepted at  $*p < 0.05$ ,  $**p < 0.01$ , and  $***p < 0.001$ .

## Results

### Characterization of MenSCs

We first cultured and characterized the morphological, karyotype, immuno-phenotypic features, and differentiation

capabilities of MenSCs. Complying with the International Society for Cellular Therapy (ISCT) MSCs criteria [1, 2], MenSCs displayed the typical colony-forming units (Fig. 1A), adherent growth, and fibroblast-like cellular morphology (Fig. 1B). Karyotype analysis showed no chromosomal alterations (Fig. 1C). Flow cytometry analysis showed that MenSCs were positive ( $> 95\%$  of positive cells) for mesenchymal-associated markers CD73, CD90, and CD9 (Fig. 1D) but negative ( $< 5\%$  of positive cells) for hematopoietic cell surface antigens CD34/CD45. Likewise, MenSCs cultured in osteogenic, adipogenic, or chondrogenic induction medium differentiated into osteoblasts (Fig. 1F), adipocytes (Fig. 1H), and chondrocytes (Fig. 1J), respectively, while MenSCs cultured in regular culture medium were undifferentiated (Fig. 1E, G, I).

Next, we wanted to evaluate the presence of neural and astrocyte-associated molecules in MenSCs under in minimal culture medium (MCm). Analysis of protein expression by Western blotting showed a basal level of NFL (Fig. 2A, B),  $\beta$ -TUB III (Fig. 2A, C), GFAP (Fig. 2A, D), S100 $\beta$  (Fig. 2A, E), ChAT (Fig. 2A, F), and TH (Fig. 2A, G) proteins in MenSCs culture in MCm at days 0, 4, and 7. Similar observations were found in those cells on day 7 assessed by immunofluorescent microscopy (IFM, Fig. 2H–J).

### In Vitro Transdifferentiation of MenSCs into Dopaminergic-Like Neurons (DALNs) Involves the Upregulation of Specific Neural and Dopaminergic Proteins

To assess the ability of MenSCs to transdifferentiate into DALNs, MSCs were cultured with NeuroForsk medium for 4 or 7 days [14]. Figure 3 shows a statistically significant increase in the expression level of protein  $\beta$ -TUB III ( $\sim 0.5$  and  $\sim 0.6$  f.i., Fig. 3A, D), TH ( $\sim 1.0$  and  $\sim 1.4$  f.i., Fig. 3A, F), and DAT ( $\sim 2.0$  and  $\sim 1.0$  f.i., Fig. 3A, G) but protein expression dramatically decreased in GFAP ( $\sim 0.5$  and  $\sim 0.2$  f.d., Fig. 3A, E) as determined by WB assay and IFM analysis (e.g.,  $\beta$ -TUB III Fig. 3N', T, TH/DAT Fig. 3Q, V and W). Whereas the expression level of protein NFL (Fig. 3A, B, I'–K') and MAP2 (Fig. 3C, I'–K'') is unaffected by the NeuroForsk medium, the GFAP protein is significantly diminished (Fig. 3A, E, L'–N'). Remarkably, the expression level of protein VChAT increased ( $\sim 1.5$  and  $\sim 1.4$  f.i., Fig. 3A, H) on days 4 and 7.

To further confirm the dopaminergic lineage of MenSC-induced DALNs, we analyzed TH and DAT double staining. As shown in Fig. 4, flow cytometry (FC) analysis shows a statistically significant increase in the percentage of TH/DAT expressing cells at day 4 ( $\sim 14\%$ ) and 7 ( $\sim 26\%$ ) of cell-cultured in NeuroForsk medium compared to MenSCs at day 0 ( $\sim 8\%$ , Fig. 4A, B). We found no statistical difference



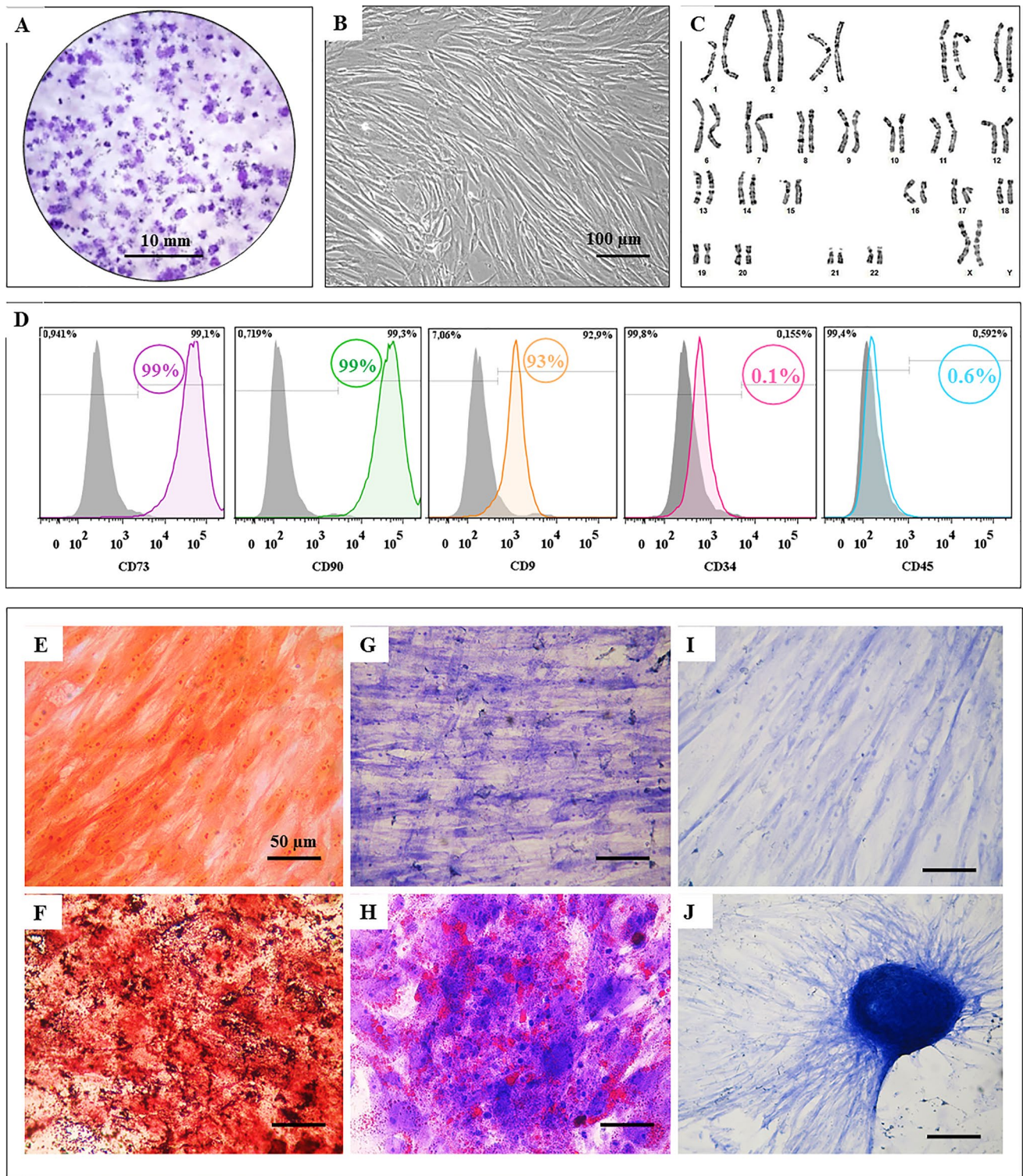


**Fig. 1** Characterization of MenSCs. **(A)** Representative images showing the colony-forming units; **(B)** adherent growth and fibroblast-like morphology typical of MenSCs. **(C)** karyotype analysis performed at passage 2 showing chromosomal normality (46XX). **(D)** Flow cytometry analyses showing the percentage of double-positive CD9/CD73/CD90/CD34 and CD45 MenSCs. **(E)** Von Kossa negatively stained undifferentiated MenSCs grown on a regular culture medium. **(F)** Von Kossa positively stained osteoblasts differentiated from MenSCs

showing silver intracellular precipitates. **(G)** Oil-Red-O negatively stained undifferentiated MenSCs grown on regular culture medium. **(H)** Oil-Red-O positively stained adipocytes differentiated from MenSCs showing intracellular red lipidic vacuoles. **(I)** Toluidine blue negatively stained undifferentiated MenSCs grown on regular culture medium. **(J)** Toluidine blue positively stained chondrocytes differentiated from MenSCs showing extracellular glycoprotein matrix. The images represent 1 out of 3 independent experiments

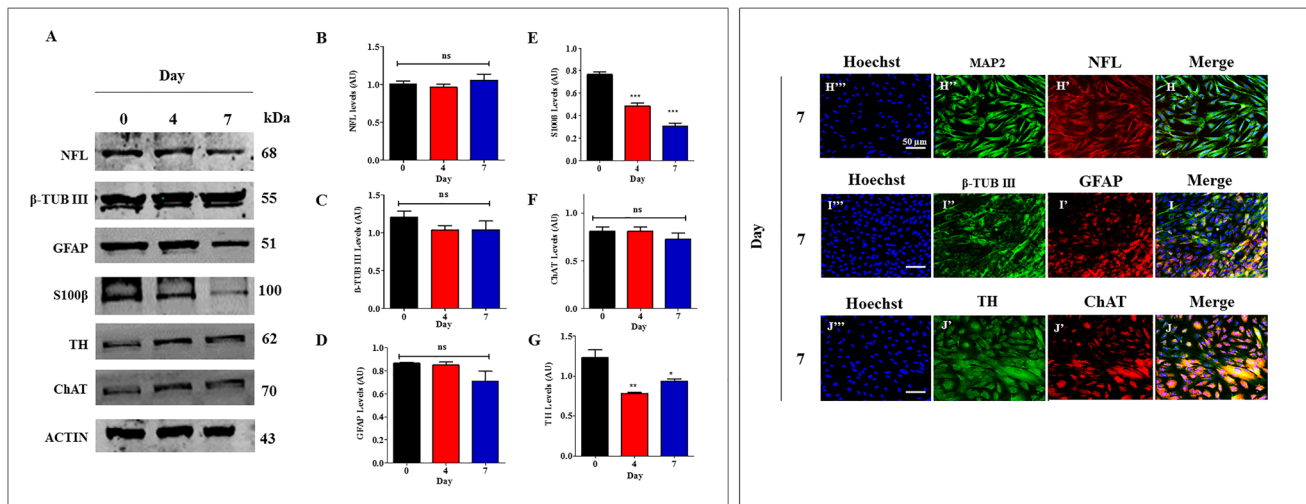


**Fig. 2** Western blot and immunofluorescence analysis of undifferentiated MenSCs. MenSCs were cultured in MCM as described in the [Materials and Methods](#) section for 0, 4, and 7 days. After this time, the proteins in the extracts were blotted with primary antibodies against NFL,  $\beta$ -TUB III, GFAP, S100 $\beta$ , TH, ChAT, and actin proteins. The intensities of the Western blot bands shown in **A** were measured (**B**, **C**, **D**, **E**, **F**, and **G**) by an infrared imaging system (Odyssey, LI-COR), and the intensity was normalized to that of actin. **H–J** At day 0, cells were double-stained as indicated in the

figure with primary antibodies against MAP2 (green; H'') and NFL (red; H');  $\beta$ -TUB III (green; I'') and GFAP (red; I'); or TH (green; J'') and ChAT (red; J'). The nuclei were stained with Hoechst 33,342 (blue; H'''–J'''). (R–W) Mean fluorescence intensity (MFI) quantification of images obtained by immunofluorescence analysis. The blots and figures represent 1 out of 3 independent experiments. One-way ANOVA, post hoc test Bonferroni. Data are presented as mean  $\pm$  SD (\* $p$  < 0.05; \*\* $p$  < 0.01; \*\*\* $p$  < 0.001)

( $p$  < 0.05) in the level of double expression of TH/DAT in DALNs at 4 and 7 days of culture.

### Dopamine Triggers Intracellular $\text{Ca}^{2+}$ Accumulation in MenSC-Derived DALNs

Based on the significant increase of dopaminergic cellular populations in MenSCs exposed to the NeuroForsk medium, we evaluated the functional response of DALNs under a dopamine stimulus. Therefore, the cytoplasmic  $\text{Ca}^{2+}$  accumulation in DALNs was evaluated with Fluo-3-mediated  $\text{Ca}^{2+}$  imaging. While DALNs were unaffected by dopamine at day 0, dopamine-induced a transient intracellular  $\text{Ca}^{2+}$  elevation at days 4 and 7 (Fig. 4C, D) under the same experimental conditions. Furthermore, the maximal fluorescence change ( $\Delta F/F$ ) at day 4 was  $0.75 \pm 0.05$ -fold after 10 s of dopamine exposure compared to cells at day 0 ( $p$  < 0.05), whereas the maximal  $\Delta F/F$  at day 7 was  $0.25 \pm 0.2$ -fold after 20 s of dopamine addition ( $p$  < 0.05) and it remains stable until the 50 s (Fig. 4D).

### In Vitro Transdifferentiation of MenSCs Into Cholinergic-Like Neurons (ChLNs) Involves the Upregulation of Specific Neural and Cholinergic Proteins

To determine whether MenSCs transdifferentiated into ChLNs, we determined the expression of several molecules

associated with neural differentiation in cells treated with Cholinergic-N-Run medium after 0, 4, and 7 days of incubation. Western blot analysis revealed that the MenSCs at day 0 expressed basal level of protein NFL (Fig. 5A, B), MAP2 (Fig. 5A, C),  $\beta$ -TUB III (Fig. 5A, D), GFAP (Fig. 5A, E), TH (Fig. 5A, F), ChAT (Fig. 5A, G), and VACHT (Fig. 5A, H). Interestingly, when the cells were exposed to Cholinergic-N-Run medium for 4 and 7 days, they significantly increased the levels of NFL ( $\sim 1.3$  and  $\sim 1.4$  f.i., Fig. 5B), ChAT ( $\sim 1.5$  and  $\sim 1.6$  f.i., Fig. 5G), and VACHT ( $\sim 2.2$  and  $\sim 2.5$  f.i., Fig. 5H), while they retained a basal and stable expression of protein MAP2 and  $\beta$ -TUB III (Fig. 5C, D). However, we found the expression level of protein GFAP ( $\sim 0.9$  and  $\sim 0.5$  f.r., Fig. 5E) and TH ( $\sim 0.7$  and  $\sim 0.7$  f.r., Fig. 5F) reduced after 4 and 7 days of incubation with the differentiation medium. Similar results were obtained by immunofluorescence analyses (Fig. 5I–W).

Since the choline acetyltransferase (ChAT) enzyme and vesicular acetylcholine transporter (VACHT) protein are specific cholinergic cell lineage markers [22, 23], we wanted to confirm whether the MenSCs transdifferentiated into ChLNs simultaneously expressed ChAT and VACHT. Accordingly, we establish the percentage of MenSCs derived ChLNs with Cholinergic-N-Run medium and we assessed the proportion (%) of ChAT/VACHT immunopositive neurons after the cholinergic induction. Flow cytometry analysis shows a statistically significant increase in the percentage of ChAT/VACHT expressing cells at day 4 ( $\sim 39\%$ ) and day 7 ( $\sim 46\%$ )



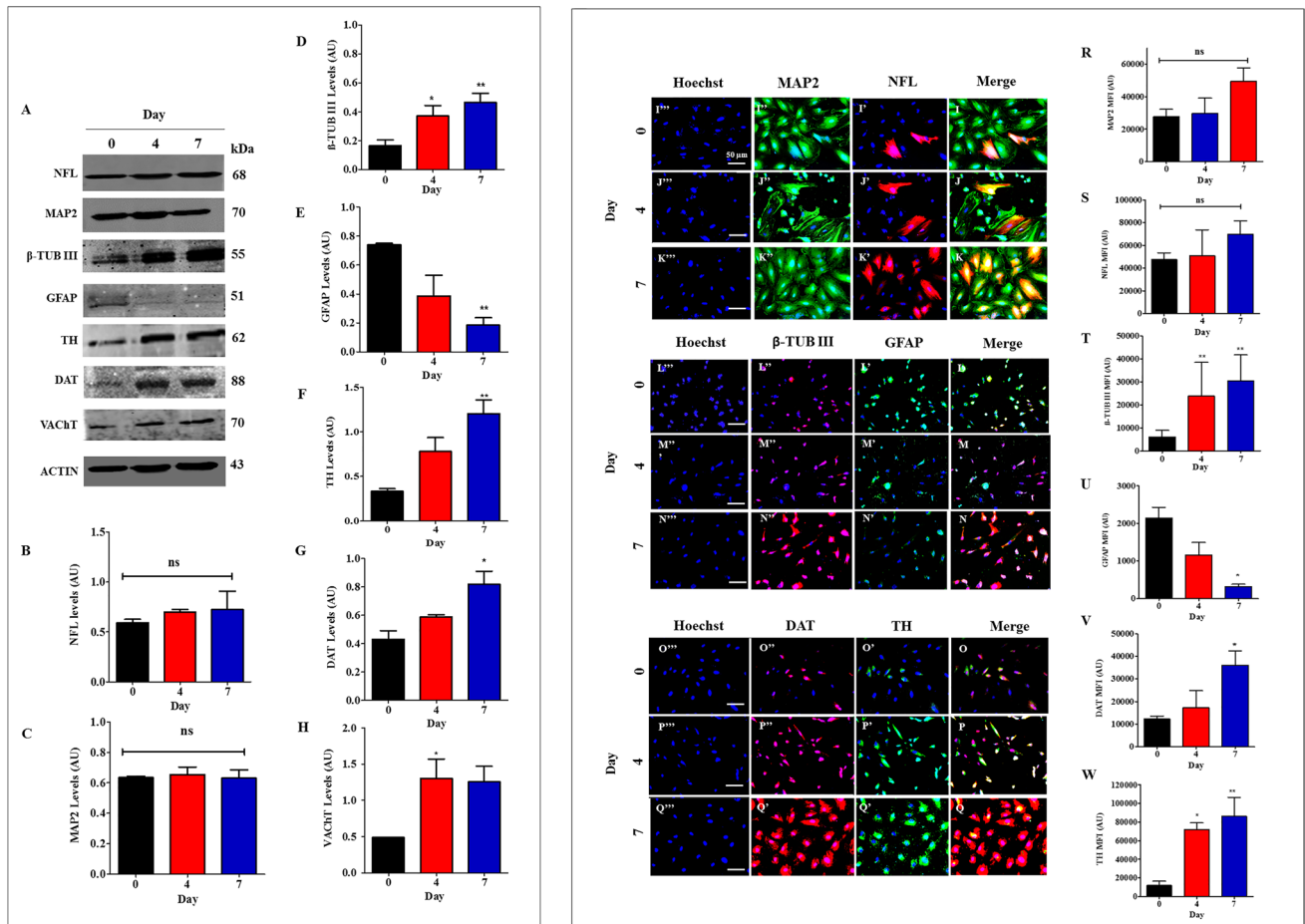


**Fig. 3** Western blot and immunofluorescence analysis of Dopaminergic-like differentiation of MenSCs. MenSCs were cultured in NeuroForsk medium as described in the [Materials and Methods](#) section for 0, 4, and 7 days. After this time, the proteins in the extracts were blotted with primary antibodies against NFL, MAP2,  $\beta$ -TUB III, GFAP, TH, DAT, VACHT, and actin proteins. The intensities of the Western blot bands shown in **A** were measured (**B**, **C**, **D**, **E**, **F**, **G**, and **H**) by an infrared imaging system (Odyssey, LI-COR), and the intensity was normalized to that of actin. (**I**–**Q**) Cells were double-stained as

indicated in the figure with primary antibodies against MAP2 (green; I''–K'') and NFL (red; I'–K');  $\beta$ -TUB III (green; L''–N'') and GFAP (red; L'–N'); or DAT (red; O''–Q'') and TH (green; O'–Q'). The nuclei were stained with Hoechst 33,342 (blue; I'''–Q'''). (R–W) Mean fluorescence intensity (MFI) quantification of images obtained by immunofluorescence analysis. The blots and figures represent 1 out of 3 independent experiments. One-way ANOVA, post hoc test Bonferroni. Data are presented as mean  $\pm$  SD (\* $p$  < 0.05; \*\* $p$  < 0.01; \*\*\* $p$  < 0.001)

of culture exposure compared to MenSCs at day 0 (~28%) (Fig. 6A, B). We found no statistical difference ( $p$  < 0.05) in the level of double expression of ChAT/VACHT in ChLNs at 4 and 7 days of culture.

### Acetylcholine Triggers Intracellular $\text{Ca}^{2+}$ Accumulation in MenSC-Derived ChLNs

The above findings encouraged us to evaluate the response of ChLNs cells to acetylcholine culture in Cholinergic-N-Run medium. Therefore, the cytoplasmic  $\text{Ca}^{2+}$  accumulation in ChLNs was evaluated with Fluo-3-mediated  $\text{Ca}^{2+}$  imaging. While ChLNs were unaffected by ACh at day 0 of Cholinergic-N-Run medium culture, ACh induced a transient intracellular  $\text{Ca}^{2+}$  elevation at day 4 and day 7

(Fig. 6C, D) under the same experimental conditions. Furthermore, the maximal fluorescence change ( $\Delta F/F$ ) at day 4 was  $6.14 \pm 1.5$ -fold and the maximal  $\Delta F/F$  at day 7 was  $5.57 \pm 1.2$ -fold after 10-s ACh exposure compared to cells at day 0 ( $p$  < 0.05, Fig. 6D).

### Transdifferentiation of MenSCs into Astrocyte-Like Cells (ALCs) Involves the Upregulation of Specific Glial Proteins

The transdifferentiation of MenSCs into astrocytes was evaluated after 0, 4, and 7 days of incubation with astrocyte medium®. As shown in Fig. 7, MenSC-derived ALCs express statistically significant increased expression level of S100 $\beta$  (e.g., ~1.2 f.i., Fig. 7A, C) and GFAP (~0.8 and ~0.6 f.i.,

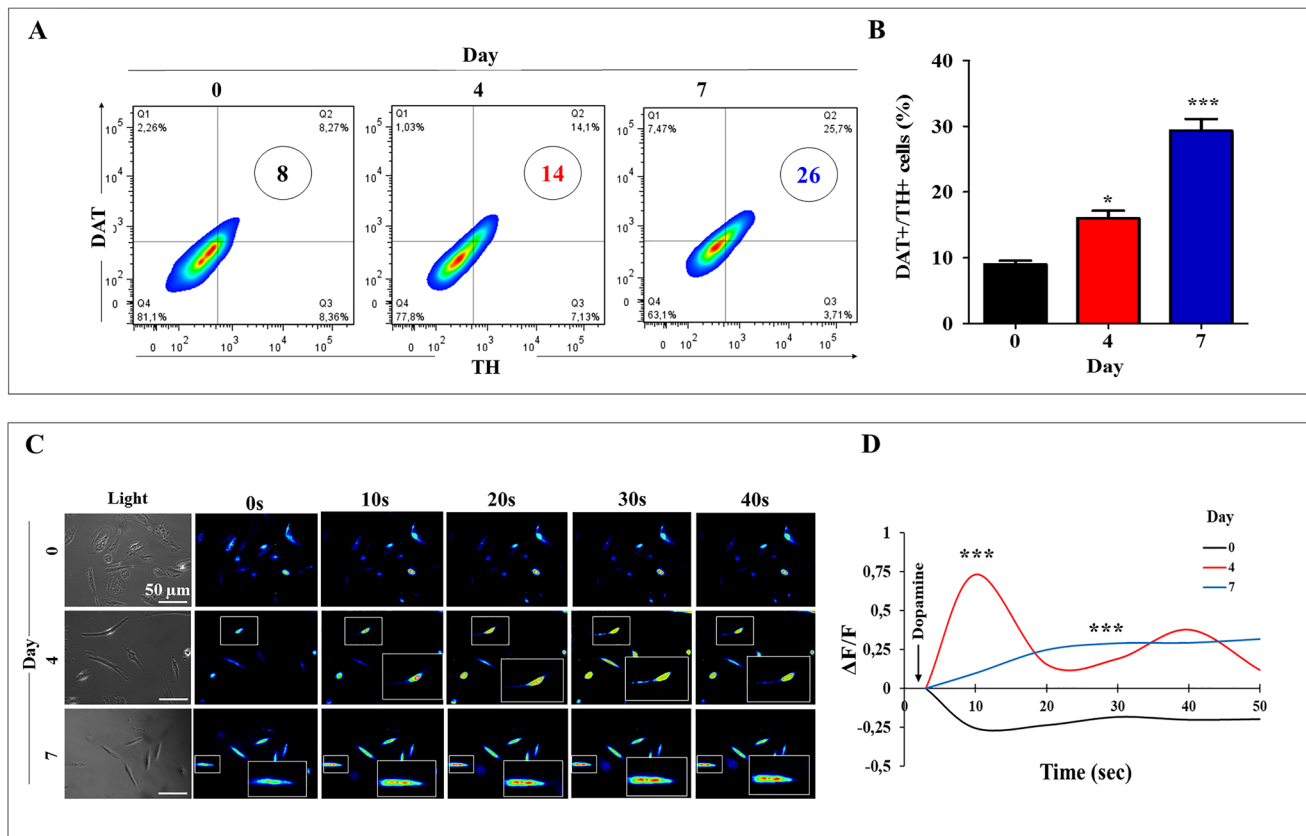


**Fig. 4** TH and DAT percentage expression and dopamine (DA) upregulation of cytoplasmic  $\text{Ca}^{2+}$  concentration in MenSCs differentiated into Dopaminergic-like cells. MenSCs were cultured in NeuroForsk medium as described in the **Materials and Methods** section for 0, 4, and 7 days. Representative density plot figures showing the DAT/TH double-positive population of NeuroForsk medium cultured MenSCs at days 0, 4, and 7 (**A**). (**B**) Percentage of DAT/TH double-positive cells. (**C**) Time-lapse images (0, 10, 20, 30, and 40 s) of  $\text{Ca}^{2+}$  fluorescence in differentiating MenSC at days 0, 4, and 7 ( $n=30$

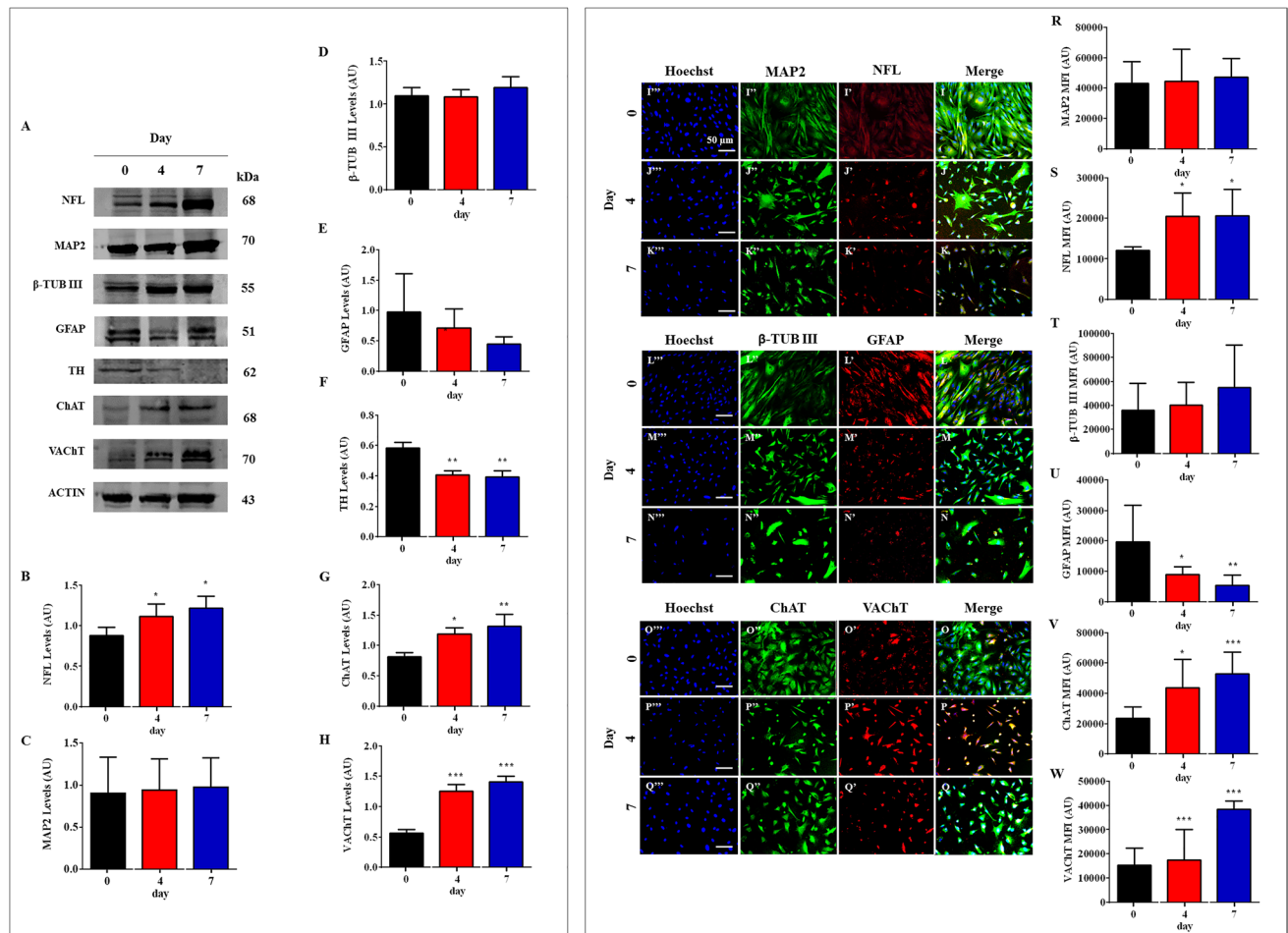
cells imaged,  $N=3$  dishes) as a response to DA treatment. DA was puffed into the culture at 0 s (arrow). Then, the  $\text{Ca}^{2+}$  fluorescence of cells was monitored at indicated times. Color contrast indicates fluorescence intensity: dark blue < light blue < green < yellow < red. (**D**) Normalized mean fluorescence signal ( $\Delta F/F$ ) over time, indicating temporal cytoplasmic  $\text{Ca}^{2+}$  elevation in response to DA treatment. One-way ANOVA, post hoc test Bonferroni. Data are presented as mean  $\pm$  SD (\* $p < 0.05$ ; \*\* $p < 0.01$ ; \*\*\* $p < 0.001$ )

Fig. 7A, D) proteins cultured for 4 and 7 days compared to levels of expression protein of cells cultured at day 0 (Fig. 7C, D). Western blotting analysis shows that MenSC-derived ALCs express almost basal level of protein NFL (Fig. 7A, E) and  $\beta$ -TUB III (Fig. 7A, F). Similar results were obtained by IMF analyses (Fig. 7G–P). Since GFAP is the gold standard marker to identify astrocytes and S100 $\beta$  indicates a mature stage of astrocytes, we evaluate those markers in the MenSC-derived ALC population. Accordingly, FC analysis shows a statistically significant increase in GFAP/S100 $\beta$  double-positive cells in ALCs at day 4 (~25%) and 7 (~59%) of culture compared to cells cultured at day 0 (Fig. 8A, B).

### Glutamate Triggers Intracellular $\text{Ca}^{2+}$ Accumulation in ALCs

Intracellular astrocyte calcium signaling is triggered by multiple factors, including glutamate at the synaptic

cleft, which stimulates G protein-coupled receptors on the membrane, leading to the production of IP3. IP3 activates IP3R2 receptors on the endoplasmic reticulum (ER), resulting in intracellular calcium release and subsequent exocytosis [24]. Therefore, the cytoplasmic  $\text{Ca}^{2+}$  accumulation in ALCs was evaluated with Fluo-3-mediated  $\text{Ca}^{2+}$  imaging. While ALCs were unaffected by glutamate at day 0 of Astrocyte medium culture, glutamate-induced a transient intracellular  $\text{Ca}^{2+}$  elevation at day 4 and day 7 (Fig. 8C, D) under the same experimental conditions. Furthermore, the maximal fluorescence change ( $\Delta F/F$ ) at day 4 was  $0.10 \pm 0.05$ -fold after 120 s of glutamate exposure compared to cells at day 0 ( $p < 0.05$ ), whereas the maximal  $\Delta F/F$  at day 7 was  $0.50 \pm 0.2$ -fold after 240 s of glutamine addition ( $p < 0.05$ ) and decline slowly.



**Fig. 5** Western blot and immunofluorescence analysis of Cholinergic-like differentiation of MenSCs. MenSCs were cultured in Ch-N-Rm as described in the [Materials and Methods](#) section for 0, 4, and 7 days. After this time, the proteins in the extracts were blotted with primary antibodies against NFL, MAP2,  $\beta$ -TUB III, GFAP, TH, ChAT, VACHT, and actin proteins. The intensities of the Western blot bands shown in (A) were measured (B, C, D, E, F, G, and H) by an infrared imaging system (Odyssey, LI-COR), and the intensity was normalized to that of actin. (I–Q) Cells were double-stained as

indicated in the figure with primary antibodies against MAP2 (green; I'–K'') and NFL (red; I'–K');  $\beta$ -TUB III (green; L'–N'') and GFAP (red; L'–N''); or ChAT (green; O'–Q'') and VACHT (red; O'–Q'). The nuclei are stained with Hoechst 33,342 (blue; I'''–Q'''). (R–W) Mean fluorescence intensity (MFI) quantification of images obtained by immunofluorescence analysis. The blots and figures represent 1 out of 3 independent experiments. One-way ANOVA, post hoc test Bonferroni. Data are presented as mean  $\pm$  SD (\* $p$  < 0.05; \*\* $p$  < 0.01; \*\*\* $p$  < 0.001)

### In Vitro Transdifferentiation of MenSCs into Neurospheres/Spheroids

To determine whether MenSCs transdifferentiate into NSs, we initially determined the morphology and the presence of molecules associated with NSs formation in cells treated with Fast-N-Spheres medium after 0, 1, and 3 days of incubation according to a previous report [11]. As shown in Fig. 9, MenSCs cultured with this specific display the typical morphology of NSs as early as 1 day and formed large NSs at 3 days when compared to 0 days of incubation. Interestingly, both the MenSCs (0 days) and the formed NSs (at 1 or 3 days) expressed high levels of

SOX2 and NESTIN proteins according to Western blot analysis (Fig. 9A–C). These results were confirmed by IMF analysis (Fig. 9D–K).

Next, we wanted to investigate whether large NSs expressed broad ( $\beta$ -TUB. III) and specific (TH; ChAT) neural and astrocytic proteins (GFAP). According to Western blot analysis, after 3 days of incubation with Fast-N-Spheres medium, NSs significantly increased the expression level of GFAP (Fig. 9L, M), TH (~1.2 f.i., Fig. 9L, N), ChAT (~1.2 f.i., Fig. 9L, O), and  $\beta$ -TUB III (~1.3 f.i., Fig. 9L, O) protein compared to cells at 0 days of incubation. These results were also confirmed by IMF analysis (Fig. 9Q–X).



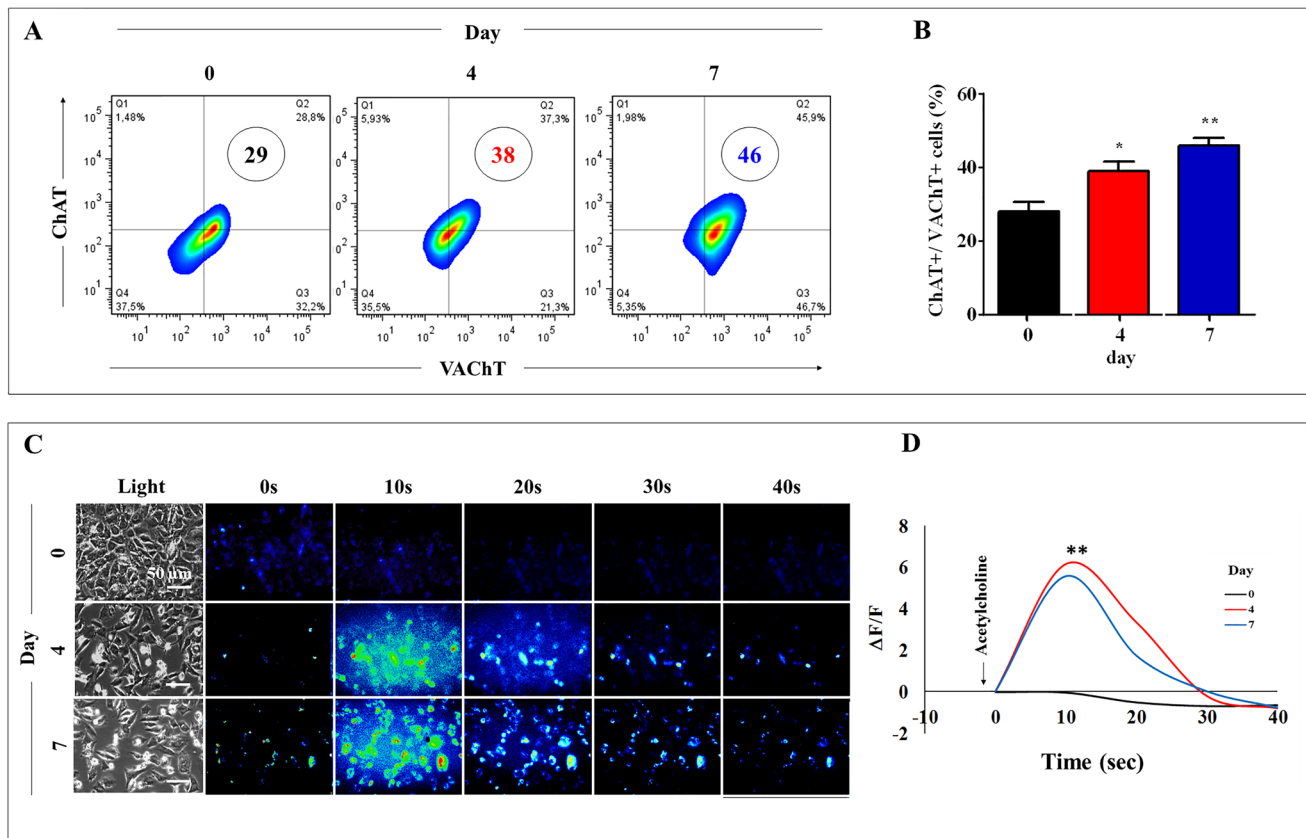


**Fig. 6** ChAT and VACHT percentage expression and acetylcholine (ACh) upregulation of cytoplasmic  $\text{Ca}^{2+}$  concentration in MenSCs differentiated into Cholinergic-like cells. MenSCs were cultured in Ch-N-Rm as described in the Materials and Methods section for 0, 4, and 7 days. Representative density plot figures showing the ChAT/VACHT double-positive population of Ch-N-Rm cultured MenSCs at day 0, 4, and 7 (A). (B) Percentage of ChAT/VACHT double-positive cells. (C) Time-lapse images (0, 10, 20, 30, and 40 s) of  $\text{Ca}^{2+}$  fluorescence in differentiating MenSC at days 0, 4, and 7 ( $n=30$  cells

imaged,  $N=3$  dishes) as a response to ACh treatment. ACh was puffed into the culture at 0 s (arrow). Then, the  $\text{Ca}^{2+}$  fluorescence of cells was monitored at indicated times. Color contrast indicates fluorescence intensity: dark blue < light blue < green < yellow < red. (D) Normalized mean fluorescence signal ( $\Delta F/F$ ) over time, indicating temporal cytoplasmic  $\text{Ca}^{2+}$  elevation in response to ACh treatment. One-way ANOVA, post hoc test Bonferroni. Data are presented as mean  $\pm$  SD (\* $p < 0.05$ ; \*\* $p < 0.01$ ; \*\*\* $p < 0.001$ )

## Discussion

The stromal cell-based disease model provides a platform for a better understanding of human neurodegenerative disease mechanisms (e.g., [25]) and the potential discovery of innovative therapeutics (e.g., [26]). As primary human neurons from living subjects are normally not accessible to researchers, there is a pressing need for an alternative source of authentic human neurons which allows modeling of neurodegeneration in vitro. Therefore, optimal cell culture conditions and timing are critical for experimental success. Recently, our laboratory has developed three original culture media known as NeuroForsk, Cholinergic-N-Run, and Fast-N-Spheres media to obtain dopaminergic-like (DALNs), cholinergic-like (ChLNs) neurons, and neurospheres (NSs) from UC-WJ-MSCs [11, 12]. By using those culture media, which seems more efficient compared to the already used

protocol in developing neural-like cells, we have successfully transdifferentiated MenSCs into functional DALNs, ChLNs, and NSs in 4–7 days of cell culture. Likewise, by using a commercial culture media (e.g., Astrocyte media®), we also obtained functional astrocyte-like cells (ALCs) in a similar time frame (i.e., 4–7 days). Also, MenSCs can differentiate into various mesoderm cell lineages, such as adipocyte (this work), chondrocytes [27], and osteocytes [28, 29] comparable to MSCs obtained from several tissue sources, including perinatal (e.g., WJ-MSCs [30, 31]), bone marrow, adipocyte, dental pulp, and human efflux (e.g., MenSCs [7, 10]), among others. Furthermore, naïve MenSCs (day 0) express basal protein levels of neuronal markers NFL,  $\beta$ -TUB III, TH, DAT, ChAT, VACHT, and MAP2. In contrast to Azedi et al., 2014 [9], we found that MenSCs express GFAP. Moreover, the expression of S100 $\beta$  protein confirms that MenSCs are primed to display glial-specific

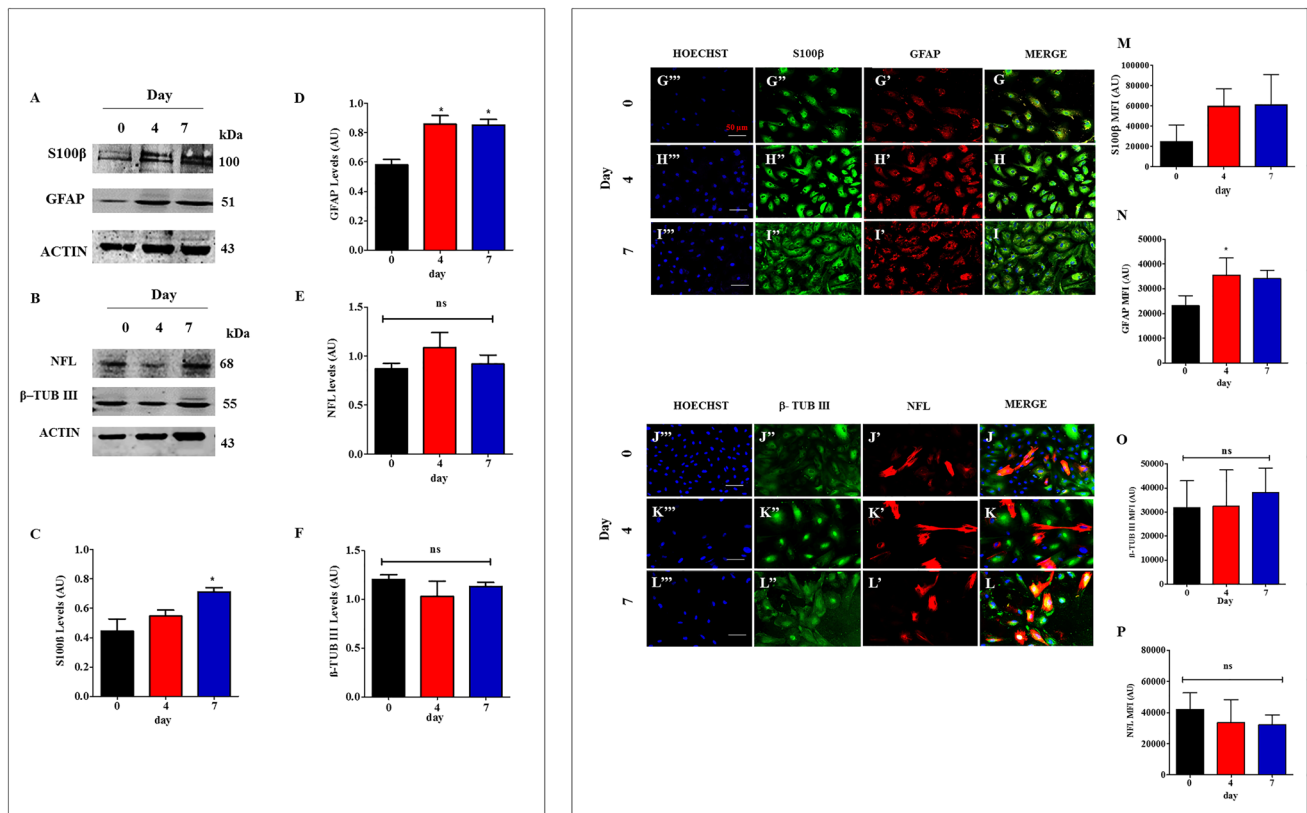


**Fig. 7** Western blot and immunofluorescence analysis of Astrocyte-like cells differentiation of MenSCs. MenSCs were cultured in Astrocyte medium as described in the [Materials and Methods](#) section for 0, 4, and 7 days. After this time, the proteins in the extracts were blotted with primary antibodies against GFAP, S100β, NFL, β-TUB III, GFAP, and actin proteins. The intensities of the Western blot bands shown in (A, B) were measured (C, D, E, and F) by an infrared imaging system (Odyssey, LI-COR), and the intensity was normalized

to that of actin. (G–L) Cells were double-stained as indicated in the figure with primary antibodies against S100 β (green; G'–I'') and GFAP (red; G'–I'); β-TUB III (green; J'–L'') and NFL (red; J'–L'). The nuclei were stained with Hoechst 33,342 (blue; G'''–L'''). (M–P) mean fluorescence intensity (MFI) quantification of images obtained by immunofluorescence analysis. One-way ANOVA, post hoc test Bonferroni. Data are presented as mean ± SD (\* $p < 0.05$ ; \*\* $p < 0.01$ ; \*\*\* $p < 0.001$ )

lineage markers. Differential experimental procedures might explain those divergent results. Taken together, these observations suggest that not only MenSCs differentiate in mesoderm lineages, but also express neuronal precursors typical of ectoderm lineages (i.e., neural lineage). These cellular features together with the fact that MenSCs have no ethical concerns, are easily recovering from women, are unexpensive and time-saving, and make MenSCs ideal for disease modeling.

We report for the first time that MenSCs can transdifferentiate into DALNs (~26%) cultured in NeuroForsk media for 7 days. Three observations support these findings. First, transdifferentiated DALNs expressed high levels of specific dopaminergic lineage markers TH—the enzyme necessary for the dopamine production from its precursor L-tyrosine—and DAT—a dopamine transporter plasma membrane glycoprotein, as well as expressed high levels of neuronal-specific protein markers NFL, MAP2, and β-TUB III. Both DAT and TH expression identifies bona fide dopaminergic neurons

[32]. Second, the percentage rates of protein expression of TH (~29% + cells), DAT (~33% + cells), and (~26% TH/DAT double-positive cells) found in DANs are comparable or even higher than previously reported from other sources such as those obtained in WJ-MSC cells after 7 days of differentiation with NeuroForsk only (~25% TH + [14]), or bone marrow-MSC (~26% TH +; ~16% DAT +), the dental pulp (~29% TH +; ~23% DAT +), and adipocyte-MSC (~29% TH +; ~23% DAT +) after 14 days of differentiation with Forskolin and FGF2 [33]. Finally, dopamine signaling evoked intracellular  $Ca^{2+}$  concentration changes in DALNs. Interestingly, the expression of TH (~17%) and DAT (~10%) proteins in naïve MenSCs reveal a strong potential of MSCs to generate DALNs. Moreover, although we found 8% TH/DAT double-positive cell markers at day 0, undifferentiated cells do not exhibit a functional phenotype in contrast to DALNs at days 4 and 7 (Fig. 4). This observation can be explained most probably by the absence of dopaminergic  $D_2$ -receptors in naïve MenSCs. However, mature

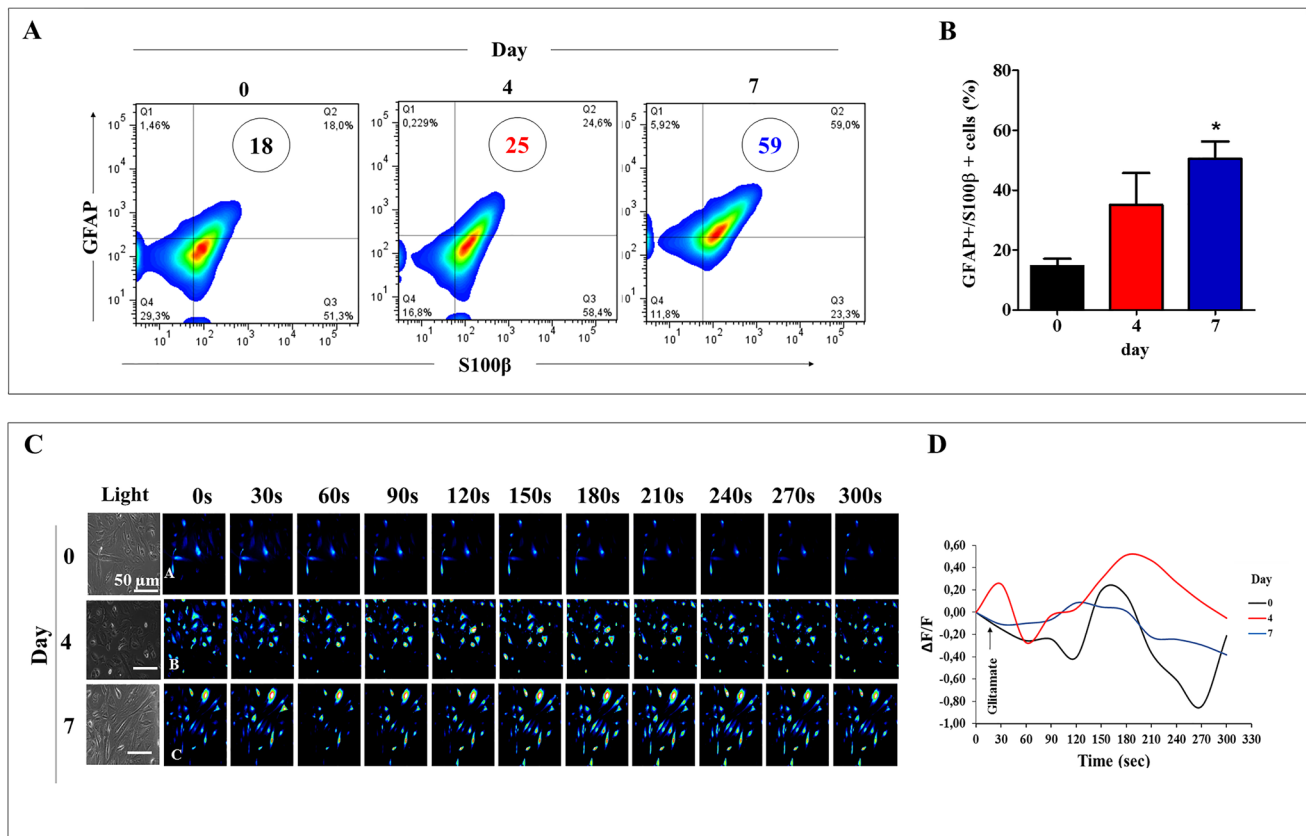


**Fig. 8** GFAP and S100β percentage expression glutamate upregulation of cytoplasmic Ca<sup>2+</sup> concentration in MenSCs differentiated into Astrocyte-like cells. MenSCs were cultured in Astrocyte medium as described in the [Materials and Methods](#) section for 0, 4, and 7 days. Representative density plot figures showing the GFAP/S100 β double-positive population of Astrocyte medium cultured MenSCs at day 0, 4, and 7 (A). (B) Percentage of GFAP/S100 β double-positive cells. (C) Time-lapse images (0, 30, 60, 90, 120, 150, 180, 210, 240, 270, and 300 s) of Ca<sup>2+</sup> fluorescence in differentiating MenSC at days 0,

4, and 7 ( $n=30$  cells imaged,  $N=3$  dishes) as a response to glutamate treatment. glutamate was puffed into the culture at 0 s (arrow). Then, Ca<sup>2+</sup> fluorescence of cells was monitored at indicated times. Color contrast indicates fluorescence intensity: dark blue < light blue < green < yellow < red. (D) Normalized mean fluorescence signal ( $\Delta F/F$ ) over time, indicating temporal cytoplasmic Ca<sup>2+</sup> elevation in response to glutamate treatment. One-way ANOVA, post hoc test Bonferroni. Data are presented as mean  $\pm$  SD (\* $p < 0.05$ ; \*\* $p < 0.01$ ; \*\*\* $p < 0.001$ )

dopaminergic neurons display an increase of dopaminergic receptors that are linked to synaptogenesis processes and Ca<sup>2+</sup> influx [34].

Here, we also report for the first time that MenSCs transdifferentiate into ChLNs in 4–7 days. Effectively, MenSC-derived ChLNs significantly express cholinergic markers ChAT—the enzyme that catalyzes the biosynthesis of ACh [35]—and VACHT—the ACh neurotransmitter transporter [22], two unique markers for cholinergic neurons according to WB, IMF, and FC analysis. In agreement with others, who have demonstrated that MSCs from dental pulp [36], adipose tissue [37], and UC-WJ [12] can transdifferentiate into ChNs/ChLNs, we show that MenSCs readily transdifferentiate into functional ChLNs. Similar to UC-WJ-MSC-derived ChLNs [12], the MenSC-derived ChLNs are responsive to ACh stimuli on days 4 and 7. Interestingly, although naïve MenSCs express both cholinergic ChAT/VACHT and ACh receptors [38], they are unresponsive to ACh at day 0.

These observations suggest that the presence/expression of cholinergic markers in undifferentiated MenSCs (i.e., ChAT/VACHT/AChRs) is not yet functional indicating a cellular immature state that necessitates an adequate micro-environmental stimulus, as provided by Cholinergic-N-Run media, to express functional (responsive) AChRs [39]. Interestingly, ChLNs maintained the expression of general neural lineage markers (e.g., NFL,  $\beta$ -TUB III) whereas other specific cell lineage markers diminished (e.g., GFAP, TH) at day 7 of transdifferentiating. Therefore, we conclude that MenSC-derived ChLNs are mature neural cells obtained timelessly.

In contrast to Mendivil-Perez and co-workers [12], who reported that MSCs from WJ-MSCs generated ~76% ChLNs according to double ChAT/VACHT analysis, we found that under similar experimental conditions, MenSCs derived from MenB produced ~46% ChLNs, a much less percentage yield when compared to WJ-MSC-derived ChLNs (i.e., ~40% reduction). These observations suggest that

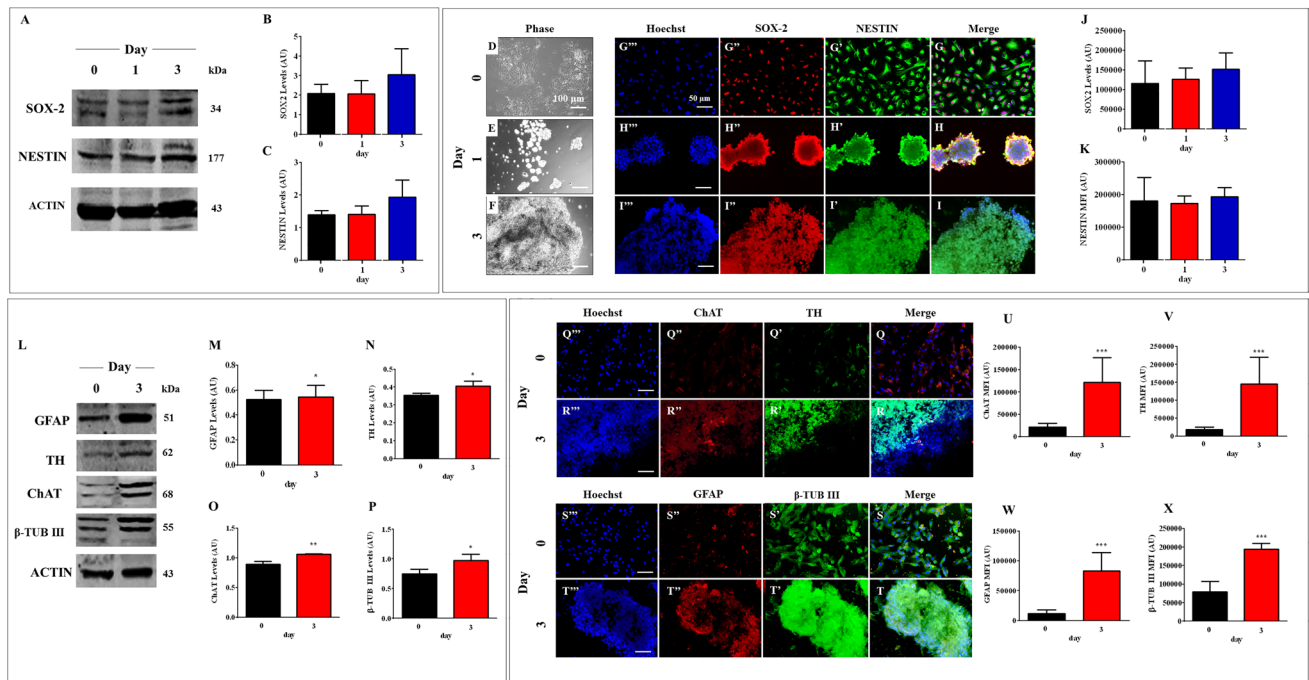


**Fig. 9** Western blot and immunofluorescence analysis of neurospheres/spheroids obtained from MenSCs. MenSCs were cultured in Fast-N-spheres medium as described in the **Materials and Methods** section for 0, 1, and 3 days. After this time, the proteins in the extracts were blotted with primary antibodies against SOX2, NESTIN, and actin proteins. The intensities of the Western blot bands shown in (A) were measured (B, C) by an infrared imaging system (Odyssey, LI-COR), and the intensity was normalized to that of actin. (D, E, and F) Phase-contrast light images of adherent or floating 3D spheres at day 0, 1, and 3. (G–I) Cells were double-stained as indicated in the figure with primary antibodies against SOX2 (red; G'–I'') and NESTIN (green; G'–I'). The nuclei were stained with Hoechst 33,342 (blue; G'–I''). (J–K) Mean fluorescence intensity (MFI) quantification of images obtained by immunofluorescence analysis.

Undifferentiated MenSCs (0 days) and 3D spheroid structures (3 days) were collected and the proteins in the extracts were blotted with primary antibodies against GFAP, TH, ChAT, β-TUB III, and actin proteins. The intensities of the Western blot bands shown in (L) were measured (M, N, O, and P) by an infrared imaging system (Odyssey, LI-COR), and the intensity was normalized to that of actin. (Q–T) Cells were double-stained as indicated in the figure with primary antibodies against ChAT (red; Q'–R'') and TH (green; Q'–R') or GFAP (red; S'–T'') and β-TUB III (green; S'–T'). The nuclei were stained with Hoechst 33,342 (blue; Q'–T''). (U–X) Mean fluorescence intensity (MFI) quantification of images obtained by immunofluorescence analysis. Student t test. Data are presented as mean ± SD (\* $p < 0.05$ ; \*\* $p < 0.01$ ; \*\*\* $p < 0.001$ )

MSCs from UC are more efficient to produce ChLNs than MenSCs derived from MenB. However, MenSC-derived ChLNs responded faster to ACh stimulus (maximal ( $\Delta F/F$ ) cytoplasmic ( $Ca^{2+}$ )<sub>i</sub> elevation at day 7 after 10 s) than WJ-MSC-derived ChLNs (maximal ( $\Delta F/F$ ) cytoplasmic ( $Ca^{2+}$ )<sub>i</sub> elevation at day 7 after 40 s). Despite these, both derived ChLNs responded almost 100% to ACh. Therefore, MenSCs are suitable for pharmacological studies.

Astrocytes are specialized glial cells of the central nervous system that play essential roles in the maintenance, metabolism, and immune response and assistance of neuronal cells in the brain [40–42]. Therefore, astrocytes are deeply implicated in the neuropathology of neurodegenerative disorders [43]. We confirm that MenSCs transdifferentiate into glial cells [9]. Specifically, we report for the first time that MenSC-derived astrocyte-like cells (ALCs) are obtained in 7 days of culture in Astrocyte medium®. As expected, ALCs expressed high expression levels of protein

GFAP—uniquely found in astrocytes [44] and S100β [45]—according to WB, FC, and IMF assays. Interestingly, the expression of β-TUB and NFL in ALCs were not affected by cultural conditions. Given that β-TUB is constitutively co-expressed with GFAP in midgestational human fetal astrocytes [46] and astrocyte in culture [47], it is not surprising that we detect β-TUB and NFL—two specific neuronal markers in ALCs. These observations suggest that the expression of β-TUB, NFL, and NESTIN [46] in ALCs is a common feature with neuronal cells.

Although the commercial Astrocyte medium® is regularly used to support the growth and maintenance of primary human astrocytes (<https://www.thermofisher.com/order/catalog/product/A1261301#A1261301>), we found that it can be used for the transdifferentiation of MenSCs into ALCs in 7 days of culture (59% GFAP<sup>+</sup>/S100β<sup>+</sup>). This is a fast, direct, economical, and time-saving protocol for the obtention of ALCs. Furthermore, ALCs tested at days 4 and 7 but not at



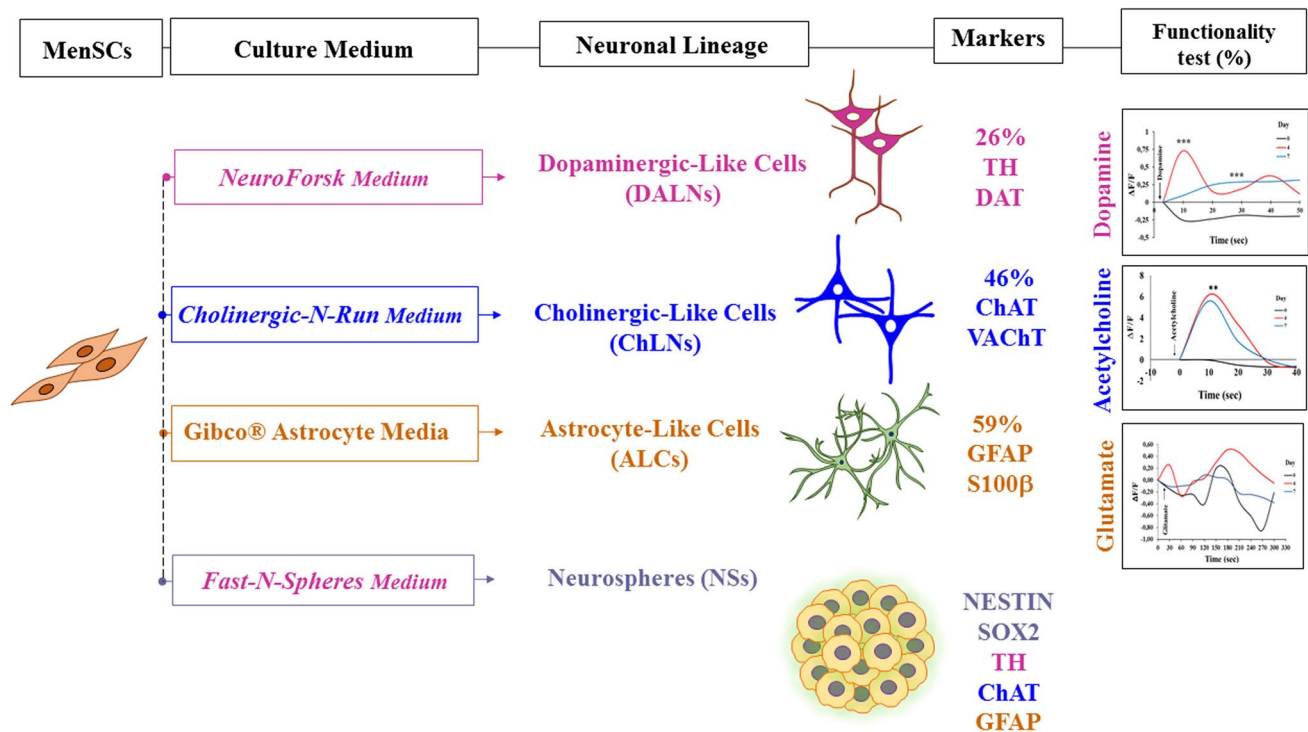


**Fig. 10** Human menstrual blood-derived mesenchymal stromal cells (MenSCs) readily transdifferentiate into functional dopaminergic-, cholinergic-, and astrocytic-like neuronal lineages and in neurospheres under specific in vitro culture conditions

day 0 were responsive to GLUT stimulus (Fig. 8). We conclude that ALCs represent functional glial cells.

Neurospheres (NSs) are 3D structures composed of free-floating conglomerates of neural progenitor cells (NPCs) derived from either isolated primary tissue (e.g., embryonic tissue) or from induced pluripotent stem cells (iPSCs) and grown for limited periods. Therefore, NSs provide an unmatched platform to evaluate the stem/stromal-cell-like behavior of neurogenic tissue and can be used in a variety of in vitro experiments to delineate the molecular and cellular characteristics of neuronal cells for in vivo transplantation in neurodegenerative disorders (e.g., [48]). We have reported a fast and easy method to obtain NSs from UC-MSCs in 24 h by using the Fast-N-Spheres medium [11]. Under similar experimental conditions, we have been able to transdifferentiate MenSCs into NSs phenotypically similar to MSC-derived NSs. However, while the MenSC-derived NSs were NESTIN- and SOX-2-positive—a key transcription factor in the regulation of pluripotency and neural differentiation [49]—the MSC-derived NSs were NESTIN-positive but SOX-2-negative [11]. These observations suggest that NSs derived from MenB conserved those specific markers similar to those observed in NSs from neurogenic niches in cerebral tissue [50]. Therefore, MenSC-derived NSs are a more reliable 3D cellular source for neurodevelopmental

studies. Moreover, in agreement with previous data [8], the MenSC-derived NSs cultured for 3 days significantly increased the expression of neuronal (e.g.,  $\beta$ -TUB III) as well astrocytic (e.g., GFAP) markers. We report for the first time that MenSC-derived NSs also express the specific neuronal lineage dopaminergic marker TH and cholinergic marker ChAT. Taken together, these results suggest that MenSC-derived NSs can highly regulate tri-neuronal lineage proteins typical of the dopaminergic, cholinergic, and glial neuronal cells, which might represent an excellent strategy not only to studying the tissular pathology of AD and PD but also to be used as starting material for the development of more complex structures such as organoids [51]. Therefore, as depicted in Fig. 10, MenSCs are a unique and reliable biological source for derivation of the most important neural cells such as dopaminergic, cholinergic, and astrocytic neuronal cells implicated in neurodegeneration (e.g., Alzheimer's and Parkinson's diseases).

**Acknowledgements** This work was supported by MinCiencias (grant. no. 1115-807-62912, contract no. 749-2018).

**Author Contribution** DQ-E, VS-M, CQ-Q, and MM-P performed MenSC-derived dopaminergic, cholinergic, astrocytic, and neurospheres in vitro experiments, respectively. All performed in vitro data analysis and wrote the first draft. MJdelR/CV-P conceived the in vitro



experiments, contributed with reagents, data analysis, wrote, reviewed, and edited the paper. All authors read and approved the final version of the paper.

**Funding** DQ-E and VS-M are doctoral students and CQ-Q is a master's student from the Neuroscience Study Program at the Basic Biomedical Sciences Academic Corporation, UdeA. MM-P is an associated researcher (contract no. 749–2018). DQ-E is founded by the Committee for Development and Research-CODI-UdeA (grant no. 2017–15829). VS-M is funded by the 2019 Bicentennial Doctoral Excellence Scholarship, MinCiencias-Colombia. CQ-Q is funded by the Young Research Award Program from MinCiencias (grant no. 111580762912).

**Availability of Data and Material** All datasets generated for this study are included in the manuscript.

## Declarations

**Ethics Approval** Menstrual specimen donors provided a signed informed consent approved by the ethics committee of the Sede de Investigación Universitaria (SIU), University of Antioquia, Medellín, Colombia (act 2020-10854).

**Consent to Participate** Not applicable.

**Consent for Publication** Not applicable.

**Conflict of Interest** The authors declare no competing interests.

## References

- Dominici M, Le Blanc K, Mueller I, Slaper-Cortenbach I, Marini FC, Krause DS, Deans RJ, Keating A et al (2006) Minimal criteria for defining multipotent mesenchymal stromal cells. The International Society for Cellular Therapy position statement. *Cytotherapy* 8(4):315–317
- Viswanathan S, Shi Y, Galipeau J, Krampera M, Leblanc K, Martin I, Nolte J, Phinney DG et al (2019) Mesenchymal stem versus stromal cells: International Society for Cell & Gene Therapy (ISCT®) Mesenchymal Stromal Cell committee position statement on nomenclature. *Cytotherapy* 21(10):1019–1024
- Staff NP, Jones DT, Singer W (2019) Mesenchymal stromal cell therapies for neurodegenerative diseases. *Mayo Clin Proc* 94(5):892–905
- Choudhary P, Gupta A, Singh S (2020) Therapeutic advancement in neuronal transdifferentiation of mesenchymal stromal cells for neurological disorders. *J Mol Neurosci* 71:889–90
- Shariati A, Nemati R, Sadeghipour Y, Yaghoubi Y, Baghbani R, Javidi K, Zamani M, Hassanzadeh A (2020) Mesenchymal stromal cells (MSCs) for neurodegenerative disease: a promising frontier. *Eur J Cell Biol* 99(6):151097
- Zhao Y, Chen X, Wu Y, Wang Y, Li Y, Xiang C (2018) Transplantation of human menstrual blood-derived mesenchymal stem cells alleviates Alzheimer's disease-like pathology in APP/PS1 transgenic mice. *Front Mol Neurosci* 11:140
- Chen L, Qu J, Cheng T, Chen X, Xiang C (2019) Menstrual blood-derived stem cells: toward therapeutic mechanisms, novel strategies, and future perspectives in the treatment of diseases. *Stem Cell Res Ther* 10(1):406
- Azedi F, Kazemnejad S, Zarnani AH, Soleimani M, Shojaei A, Arasteh S (2017) Comparative capability of menstrual blood versus bone marrow derived stem cells in neural differentiation. *Mol Biol Rep* 44(1):169–182
- Azedi F, Kazemnejad S, Zarnani AH, Behzadi G, Vasei M, Khanmohammadi M, Khanjani S, Edalatkhah H et al (2014) Differentiation potential of menstrual blood- versus bone marrow-stem cells into glial-like cells. *Cell Biol Int* 38(5):615–624
- Bozorgmehr M, Gurung S, Darzi S, Nikoo S, Kazemnejad S, Zarnani A-H, Gargett CE (2020) Endometrial and menstrual blood mesenchymal stem/stromal cells: biological properties and clinical application. *Front Cell Dev Biol* 8:497
- Bonilla-Porras AR, Velez-Pardo C, Jimenez-Del-Rio M (2017) Fast transdifferentiation of human Wharton's jelly mesenchymal stem cells into neurospheres and nerve-like cells. *J Neurosci Methods* 282:52–60
- Mendivil-Perez M, Velez-Pardo C, Jimenez-Del-Rio M (2019) Direct transdifferentiation of human Wharton's jelly mesenchymal stromal cells into cholinergic-like neurons. *J Neurosci Methods* 312:126–138
- Liu Y, Niu R, Yang F, Yan Y, Liang S, Sun Y, Shen P, Lin J (2018) Biological characteristics of human menstrual blood-derived endometrial stem cells. *J Cell Mol Med* 22(3):1627–1639
- Mendivil-Perez M, Velez-Pardo C, Jimenez-Del-Rio M (2016) Neuroprotective effect of the LRRK2 kinase inhibitor PF-06447475 in human nerve-like differentiated cells exposed to oxidative stress stimuli: implications for Parkinson's disease. *Neurochem Res* 41(10):2675–2692
- Liao Z-Q, Ye M, Yu P-G, Xiao C, Lin F-Y (2016) Glioma-associated oncogene homolog1 (Gli1)-Aquaporin1 pathway promotes glioma cell metastasis. *BMB Rep* 49(7):394–399
- Mytych J, Lewinska A, Zebrowski J, Wnuk M (2015) Gold nanoparticles promote oxidant-mediated activation of NF- $\kappa$ B and 53BP1 recruitment-based adaptive response in human astrocytes. *Biomed Res Int* 2015:304575
- Rao S, Morales AA, Pearse DD (2015) The comparative utility of viromer RED and lipofectamine for transient gene introduction into glial cells. *Biomed Res Int* 2015:458624
- Moghaddam SA, Yousefi B, Sanooghi D, Faghihi F, Roodbari NH, Bana N, Joghataei MT, Pooyan P et al (2017) Differentiation potential of human CD133 positive hematopoietic stem cells into motor neuron-like cells, in vitro. *J Chem Neuroanat* 86:35–40
- Tcw J, Wang M, Pimenova AA, Bowles KR, Hartley BJ, Lacin E, Machlovi SI, Abdelaal R et al (2017) An Efficient platform for astrocyte differentiation from human induced pluripotent stem cells. *Stem Cell Rep* 9(2):600–614
- Fathi A, Mirzaei M, Dolatyar B, Sharifitabar M, Bayat M, Shahbazi E, Lee J, Javan M et al (2018) Discovery of novel cell surface markers for purification of embryonic dopamine progenitors for transplantation in Parkinson's disease animal models. *Mol Cell Proteomics* 17(9):1670–1684
- Pap P, Kőszeghy Á, Szűcs G, Rusznák Z (2009) Cytoplasmic Ca(2+) concentration changes evoked by cholinergic stimulation in primary astrocyte cultures prepared from the rat cochlear nucleus. *Hear Res* 255(1–2):73–83
- Arvidsson U, Riedl M, Elde R, Meister B (1997) Vesicular acetylcholine transporter (VACHT) protein: a novel and unique marker for cholinergic neurons in the central and peripheral nervous systems. *J Comp Neurol* 378(4):454–467
- Oda Y (1999) Choline acetyltransferase: the structure, distribution and pathologic changes in the central nervous system. *Pathol Int* 49(11):921–937
- Jones JR, Kong L, Hanna MG, Hoffman B, Krencik R, Bradley R, Hagemann T, Choi J et al (2018) Mutations in GFAP disrupt the distribution and function of organelles in human astrocytes. *Cell Rep* 25(4):947–958.e4
- Soto-Mercado V, Mendivil-Perez M, Velez-Pardo C, Lopera F, Jimenez-Del-Rio M (2020) Cholinergic-like neurons carrying

- PSEN1 E280A mutation from familial Alzheimer's disease reveal intraneuronal sAPP $\beta$  fragments accumulation, hyperphosphorylation of TAU, oxidative stress, apoptosis and Ca<sup>2+</sup> dysregulation: therapeutic implications. *PLoS One* 15(5):e0221669
26. Soto-Mercado V, Mendivil-Perez M, Jimenez-Del-Rio M, Velez-Pardo C (2021) Multi-target effects of the cannabinoid CP55940 on familial Alzheimer's disease PSEN1 E280A cholinergic-like neurons: role of CB1 receptor. *J Alzheimers Dis* 82(s1):S359–S378
  27. Kazemnejad S, Akhondi M-M, Soleimani M, Zarnani AH, Khanmohammadi M, Darzi S, Alimoghadam K (2012) Characterization and chondrogenic differentiation of menstrual blood-derived stem cells on a nanofibrous scaffold. *Int J Artif Organs* 35(1):55–66
  28. Darzi S, Zarnani AH, Jeddi-Tehrani M, Entezami K, Mirzadegan E, Mehdi Akhondi M, Talebi S, Khanmohammadi M et al (2012) Osteogenic differentiation of stem cells derived from menstrual blood versus bone marrow in the presence of human platelet releasate. *Tissue Eng Part A* 18(15–16):1720–1728
  29. Karadas O, Yucel D, Kenar H, Kose GT, Hasirci V (2014) Collagen scaffolds with in situ-grown calcium phosphate for osteogenic differentiation of Wharton's jelly and menstrual blood stem cells. *J Tissue Eng Regen Med* 8(7):534–545
  30. Troyer DL, Weiss ML (2008) Wharton's jelly-derived cells are a primitive stromal cell population. *Stem Cells* 26(3):591–599
  31. Davies JE, Walker JT, Keating A (2017) Concise review: Wharton's jelly: the rich, but enigmatic, source of mesenchymal stromal cells. *Stem Cells Transl Med* 6(7):1620–1630
  32. Lammel S, Steinberg EE, Földy C, Wall NR, Beier K, Luo L, Malenka RC (2015) Diversity of transgenic mouse models for selective targeting of midbrain dopamine neurons. *Neuron* 85(2):429–438
  33. Singh M, Vaishnav PK, Dinda AK, Mohanty S (2020) Evaluation of priming efficiency of forskolin in tissue-specific human mesenchymal stem cells into dopaminergic neurons: an in vitro comparative study. *Cells* 9(9):2058
  34. Catoni C, Cali T, Brini M (2019) Calcium, dopamine and neuronal calcium sensor 1: their contribution to Parkinson's disease. *Front Mol Neurosci* 12:55
  35. Deutch A, Roth R (2014) Pharmacology and biochemistry of synaptic transmission: classical transmitters. In: Byrne RHJH, Waxham MN (eds) *From molecules to networks: an introduction to cellular and molecular network in neuroscience*, 3rd edn. Academic Press, Cambridge, Massachusetts, pp 207–237
  36. Kang Y-H, Shivakumar SB, Son Y-B, Bharti D, Jang S-J, Heo K-S, Park W-U, Byun J-H et al (2019) Comparative analysis of three different protocols for cholinergic neuron differentiation in vitro using mesenchymal stem cells from human dental pulp. *Anim Cells Syst (Seoul)* 23(4):275–287
  37. Marei HES, El-Gamal A, Althani A, Afifi N, Abd-Elmaksoud A, Farag A, Cenciarelli C, Thomas C et al (2018) Cholinergic and dopaminergic neuronal differentiation of human adipose tissue derived mesenchymal stem cells. *J Cell Physiol* 233(2):936–945
  38. Hoogduijn MJ, Cheng A, Genever PG (2009) Functional nicotinic and muscarinic receptors on mesenchymal stem cells. *Stem Cells Dev* 18(1):103–112
  39. Castell X, Cheviron N, Barnier J-V, Diebler M-F (2003) Exploring the regulation of the expression of ChAT and VACHT genes in NG108-15 cells: implication of PKA and PI3K signaling pathways. *Neurochem Res* 28(3–4):557–564
  40. Vasile F, Dossi E, Rouach N (2017) Human astrocytes: structure and functions in the healthy brain. *Brain Struct Funct* 222(5):2017–2029
  41. Liddel SA, Barres BA (2017) reactive astrocytes: production, function, and therapeutic potential. *Immunity* 46(6):957–967
  42. Dienel GA, Rothman DL (2020) Reevaluation of astrocyte-neuron energy metabolism with astrocyte volume fraction correction: impact on cellular glucose oxidation rates, glutamate-glutamine cycle energetics, glycogen levels and utilization rates vs. exercising muscle, and Na. *Neurochem Res* 45(11):2607–2630
  43. Acioglu C, Li L, Elkabes S (2021) Contribution of astrocytes to neuropathology of neurodegenerative diseases. *Brain Res* 1758:147291
  44. Yang Z, Wang KK (2015) Glial fibrillary acidic protein: from intermediate filament assembly and gliosis to neurobiomarker. *Trends Neurosci* 38(6):364–374
  45. Michetti F, D'Ambrosi N, Toesca A, Puglisi MA, Serrano A, Marchese E, Corvino V, Geloso MC (2019) The S100B story: from biomarker to active factor in neural injury. *J Neurochem* 148(2):168–187
  46. Dráberová E, Del Valle L, Gordon J, Marková V, Šmejkalová B, Bertrand L, de Chadarevian J-P, Agamanolis DP et al (2008) Class III beta-tubulin is constitutively coexpressed with glial fibrillary acidic protein and nestin in midgestational human fetal astrocytes: implications for phenotypic identity. *J Neuropathol Exp Neurol* 67(4):341–354
  47. Knight VB, Serrano EE (2017) Post-translational tubulin modifications in human astrocyte cultures. *Neurochem Res* 42(9):2566–2576
  48. Wang SS, Jia J, Wang Z (2018) Mesenchymal stem cell-derived extracellular vesicles suppresses iNOS expression and ameliorates neural impairment in Alzheimer's disease mice. *J Alzheimers Dis* 61(3):1005–1013
  49. Zhang S, Cui W (2014) Sox2, a key factor in the regulation of pluripotency and neural differentiation. *World J Stem Cells* 6(3):305–311
  50. Soares R, Ribeiro FF, Lourenço DM, Rodrigues RS, Moreira JB, Sebastião AM, Morais VA, Xapelli S (2020) Isolation and expansion of neurospheres from postnatal (P1–3) mouse neurogenic niches. *J Vis Exp* (159):e60822
  51. Watanabe F, Schoeffler A, Fair SR, Hester ME, Fedorko J, Imitola J (2021) Generation of neurosphere-derived organoid-like-aggregates (NEDAS) from neural stem cells. *Curr Protoc* 1(2):e15

**Publisher's Note** Springer Nature remains neutral with regard to jurisdictional claims in published maps and institutional affiliations.

## Article

# (–)-Epigallocatechin-3-Gallate Diminishes Intra- and Extracellular Amyloid-Induced Cytotoxic Effects on Cholinergic-like Neurons from Familial Alzheimer's Disease PSEN1 E280A

Viviana Soto-Mercado, Miguel Mendivil-Perez, Carlos Velez-Pardo  and Marlene Jimenez-Del-Rio \* 

Neuroscience Research Group, Medical Research Institute, Faculty of Medicine, University of Antioquia (UdeA), Calle 70 No. 52-21, and Calle 62 # 52-59, Building 1, Room 412, SIU, Medellín 050010, Colombia;

viviana.soto@udea.edu.co (V.S.-M.); miguel.mendivil@udea.edu.co (M.M.-P.); calberto.velez@udea.edu.co (C.V.-P.)

\* Correspondence: marlene.jimenez@udea.edu.co; Tel.: +57-604-219-6467



**Citation:** Soto-Mercado, V.; Mendivil-Perez, M.; Velez-Pardo, C.; Jimenez-Del-Rio, M.

(–)-Epigallocatechin-3-Gallate Diminishes Intra- and Extracellular Amyloid-Induced Cytotoxic Effects on Cholinergic-like Neurons from Familial Alzheimer's Disease PSEN1 E280A. *Biomolecules* **2021**, *11*, 1845. <https://doi.org/10.3390/biom11121845>

Academic Editors: Alessandra Morana, Giuseppe Squillaci and Ismene Serino

Received: 10 November 2021

Accepted: 26 November 2021

Published: 8 December 2021

**Publisher's Note:** MDPI stays neutral with regard to jurisdictional claims in published maps and institutional affiliations.



**Copyright:** © 2021 by the authors. Licensee MDPI, Basel, Switzerland. This article is an open access article distributed under the terms and conditions of the Creative Commons Attribution (CC BY) license (<https://creativecommons.org/licenses/by/4.0/>).

**Abstract:** Alzheimer's disease (AD) is a complex neurodegenerative disease characterized by functional disruption, death of cholinergic neurons (ChNs) because of intracellular and extracellular A $\beta$  aggregates, and hyperphosphorylation of protein TAU (p-TAU). To date, there are no efficient therapies against AD. Therefore, new therapies for its treatment are in need. The goal of this investigation was to evaluate the effect of the polyphenol epigallocatechin-3-gallate (EGCG) on cholinergic-like neurons (ChLNs) bearing the mutation E280A in PRESENILIN 1 (PSEN1 E280A). To this aim, wild-type (WT) and PSEN1 E280A ChLNs were exposed to EGCG (5–50  $\mu$ M) for 4 days. Untreated or treated neurons were assessed for biochemical and functional analysis. We found that EGCG (50  $\mu$ M) significantly inhibited the aggregation of (i)sAPP $\beta$ f, blocked p-TAU, increased  $\Delta\Psi_m$ , decreased oxidation of DJ-1 at residue Cys106-SH, and inhibited the activation of transcription factor c-JUN and P53, PUMA, and CASPASE-3 in mutant ChLNs compared to WT. Although EGCG did not reduce (e)A $\beta$ 42, the polyphenol reversed Ca<sup>2+</sup> influx dysregulation as a response to acetylcholine (ACh) stimuli in PSEN1 E280A ChLNs, inhibited the activation of transcription factor NF- $\kappa$ B, and reduced the secretion of pro-inflammatory IL-6 in wild-type astrocyte-like cells (ALCs) when exposed to mutant ChLNs culture supernatant. Taken together, our findings suggest that the EGCG might be a promising therapeutic approach for the treatment of FAD.

**Keywords:** cholinergic neurons; epigallocatechin-3-gallate; phytochemical; polyphenol; familial Alzheimer disease; PSEN1; E280A mutation; sAPP $\beta$ f; TAU; oxidative stress; apoptosis; neuronal dysfunction

## 1. Introduction

Alzheimer's disease (AD) is a multifaceted progressive neurodegenerative disorder [1] characterized by loss of memory and cognitive impairment caused by the deterioration of the cholinergic system, accumulation of insoluble intracellular (iA $\beta$ ) and extracellular forms of amyloid  $\beta$  (eA $\beta$ , mostly eA $\beta$ 42), intracellular aggregation of the microtubule protein TAU in neurofibrillary tangles, as well as neuronal cell death, synaptic dysfunction, and neuroinflammation [2–4]. The A $\beta$ 42 peptide originates from the sequential cleavage of the amyloid precursor protein (APP) by the beta-site amyloid precursor protein cleaving enzyme 1 (BACE1), and by the gamma-site aspartyl protease  $\gamma$ -secretase [5]. This last protein is a membrane-embedded protease complex composed of presenilins (PSEN1 and PSEN2), presenilin enhancer 2 (PEN2), anterior pharynx-defective 1 (APH-1), and nicastrin subunits, with presenilins as the catalytic component containing two transmembrane aspartates in the active site [6]. While there are no known mutations in *PEN2*, *APH-1*, and *NICASTRIN*, more than 300 variants have been reported in the *PSEN1* gene (<https://www.alzforum.org/mutations/psen-1>; accessed on 15 October 2021) resulting mostly in the overproduction of eA $\beta$ 42 [7]. Unfortunately, the Glu280Ala (p. E280A, c. 839A > C, exon 8) mutation in PSEN1 has been reported as causal of familial AD (FAD)

with complete penetrance in large kindred localized in Antioquia, Colombia [8–10]. Despite prevention efforts and treatment approaches [11,12], and advanced knowledge of the neuropathology of PSEN1 E280A (e.g., [13,14]), there are no efficient therapies to date. Therefore, new therapies for the treatment of FAD patients are in need.

Recently, we have recreated the molecular pathogenesis of FAD PSEN1 E280A mutation in vitro [15]. Umbilical cord mesenchymal stem cells-derived PSEN1 E280A Cholinergic-like neurons (PSEN1 E280A ChLNs) exhibit early intracellular accumulation of soluble APP $\beta$  fragments (iAPP $\beta$ f, but not A $\beta$ 42 peptide), oxidized DJ-1 (at residue Cys<sup>106</sup>SO<sub>3</sub>) indicative of oxidative stress (OS), and hyperphosphorylation of protein TAU [15]. Also, PSEN1 E280A ChLNs display loss of the mitochondrial membrane potential ( $\Delta\Psi$ m), activation of apoptogenic proteins, and DNA fragmentation, all markers of apoptosis—a type of regulated cell death. Moreover, mutant ChLNs secrete eA $\beta$ 42 and displayed Ca<sup>2+</sup> flux dysregulation when challenged to acetylcholine (ACh) compared to wild-type (WT) ChLNs [15]. Therefore, PSEN1 E280A ChLNs provide an excellent model for screening candidate molecule(s)/drug(s).

In response to the urgent need for available drugs for the treatment of AD [16], we used PSEN1 E280A ChLNs as a cellular system to evaluate potential natural (phytochemicals) or synthetic compounds to advance neuroprotective therapies (e.g., [17]). Lastly, natural products have been postulated to reduce the accumulation and toxic effects of A $\beta$  peptides via antioxidant activity, secretase- or structure-dependent pathways, metal chelation, and preventing A $\beta$  aggregation [18–20]. Specifically, the green tea polyphenol epigallocatechin-3-gallate (EGCG)—a subclass of flavan-3-ols has shown anti-amyloidogenic, antioxidant, anti-BACE1 secretase, metal chelation, neuroprotective and anti-inflammatory activity in vivo and in vitro [19–25], among other functions. Despite these observations, no data are available to establish whether EGCG can reverse the neuropathological markers in the aforementioned PSEN1 E280A ChLNs model [15]. Moreover, it is not yet known whether EGCG might be able to block aggregation of iAPP $\beta$ f, oxidation of DJ-1, phosphorylation of protein TAU, neuronal apoptosis, decrease toxic effect of eA $\beta$ 42, and/or prevent Ca<sup>2+</sup> dysregulation in those mutant cholinergic neurons.

Neuroinflammation plays an important role in AD [4] resulting from the hyperactivation of microglia and astrocytes that release pro-inflammatory cytokines due to the neurological insults caused by A $\beta$  plaques, leading to synaptic dysfunction and neuronal death [26]. Due to the importance of astrocytes in brain homeostasis and neuroinflammation, they have become the focus of active research in AD [27,28]. Recently, we have shown that functional astrocyte-like cells (ALCs, ~59% GFAP+/S100 $\beta$ + responsive to glutamate-induced Ca<sup>2+</sup> inward stimuli) can be derived from menstrual stromal cells (MenSCs) by direct transdifferentiation method using commercial Gibco® Astrocyte medium for 7 days [29]. Interestingly, it has been shown that A $\beta$ 42 can trigger reactive astrogliosis, releasing neuroinflammatory cytokines (e.g., IL-6) and via activation of transcription factor NF- $\kappa$ B [30]. However, it is not yet known whether EGCG diminishes the reactive astrogliosis induced by eA $\beta$ 42 in ALCs.

To get insight into these issues, we have selected the commercially available (–)-epigallocatechin-3-gallate (hereafter EGCG) to evaluate its effect on wild-type and PSEN1 E280A ChLNs concerning the iAPP $\beta$ f accumulation, TAU phosphorylation, OS, cell death, and Ca<sup>2+</sup> neuronal dysfunction in ChLNs. In addition, we also want to assess whether EGCG reduces wild-type reactive astrocytes induced by PSEN1 E280A ChLNs culture supernatant. We demonstrate for the first time that EGCG can reverse PSEN1 e280A cholinergic dysfunction not only by preventing structural and functional damage of neurons, and OS-induced cell death signaling induced by (i)APP $\beta$ f/eA $\beta$ 42 but also by acting as an anti-inflammatory agent. These findings might favor the use of EGCG as a potential lead compound candidate for FAD therapy.

## 2. Materials and Methods

### 2.1. Cholinergic-like Neuron (ChLN) Differentiation

ChLN differentiation was performed according to ref. [31]. The WT (TBC# WJMSC-11) and PSEN1 E280A (TBC# WJMSC-12) [15] MSCs were seeded at  $1\text{--}1.5 \times 10^4$  cells/cm<sup>2</sup> in laminin-treated culture plates for 24 h in regular culture medium (RCm). The medium was removed, and cells were incubated in cholinergic differentiation medium (*Cholinergic-N-Run* medium, hereafter Ch-N-Rm) containing DMEM/F-12 media 1:1 Nutrient Mixture (Gibco cat# 10565018; 1204 N Western St, Suite C, Amarillo, TX, USA), 10 ng/mL basic fibroblast growth factor (bFGF) recombinant human protein (Gibco Cat# 13256029), 50 µg/mL sodium heparin (Hep, Sigma-Aldrich cat# H3393; 3050 Spruce Street, St. Louis, MO 63103, USA), 0.5 µM all-trans retinoic acid, 50 ng/mL sonic hedgehog peptide (SHH, Sigma cat# SRP3156) and 1% FBS at 37 °C for 7 days. After this process of transdifferentiation, the cells were labeled as WT PSEN1 or PSEN1 E280A ChLNs. Since Ch-N-Rm contains several factors that might interfere with the experiment interpretation and measurements, WT PSEN1 and PSEN1 E280A ChLNs (obtained after 7 days in Ch-N-Rm) were left in a regular culture medium (RCm) for 4 additional days of post transdifferentiation.

### 2.2. Astrocyte-like Cells (ALCs) Differentiation

Isolation of mesenchymal stromal cells (MenSCs) derived from wild-type human menstrual blood were obtained from tissue bank code (TBC# 69308)-UdeA [29]. For astrocyte differentiation,  $1 \times 10^4$  WT MenSCs/cm<sup>2</sup> were seeded in 25 cm<sup>2</sup> culture flasks in regular culture medium (RCm, DMEM low glucose Sigma cat# D6046 media supplemented with 10% FBS) until reach 40% of confluence. Then, the medium was replaced, and cells were incubated either in DMEM low glucose media supplemented with 2% FBS (minimal culture medium, thereafter MCm) or Astrocyte medium<sup>®</sup> (GIBCO<sup>®</sup>, cat#A1261301, 1204 N Western St., Suite C, Amarillo, TX, USA) for 7 days.

### 2.3. Assay Protocol

The methodology for both WT and PSEN1 E280A ChLNs cell culture assays was the same. Initial EGCG screening was performed at least twice in triplicate between 5 µM–50 µM. Subsequently, EGCG (50 µM) was established as an optimal concentration for further experiments. ChLNs were divided into two groups: (i) untreated; (ii) treated with EGCG (50 µM).

### 2.4. Immunofluorescence Analysis

The analysis of Alzheimer's disease-, oxidative stress- and cell death-related markers, was exactly performed as described elsewhere [15]. Briefly, the cells treated under different conditions were fixed with 4% paraformaldehyde for 20 min, followed by Triton X-100 (0.1%) permeabilization and 10% bovine serum albumin (BSA) blockage. Cells were incubated overnight with primary antibodies against APP751 and/or protein amyloid β1-42 (1:500; clone 6E10 cat# 803014, Biolegend, 9727 Pacific Heights Blvd, San Diego, CA 92121, USA), total TAU (1: 500; t-Tau; cat# T6402, Sigma-Aldrich, 3050 Spruce Street, St. Louis, MO 63103, USA), and phospho-TAU (p-Tau, 1:500, Ser202/Thr205, cat# MN1020 (AT8), Thermo Fisher Scientific, 168 Third Avenue. Waltham, MA, USA); and primary antibodies against oxidized DJ-1 (1:500; ox(Cys106)DJ-1; spanning residue C106 of human PARK7/DJ1; oxidized to produce cysteine sulfonic (SO<sub>3</sub>) acid; cat # ab169520, Abcam, Discovery Drive Cambridge Biomedical Campus Cambridge CB2 0AX, UK). To assess cell death, we used primary antibodies against p53-upregulated modulator of apoptosis (1:500; PUMA, cat# ab-9643, Abcam), p53 (1:500; cat# MA5-12453, Millipore, 3050 Spruce Street, St. Louis, Mo, 63304, USA), phospho-c-Jun (1:250; c-Jun (S63/73) cat# sc-16312, Santa Cruz Biotechnology, 2145 Delaware Avenue, Santa Cruz, CA 95060, USA), and caspase-3 (1:250; cat # AB3623, Millipore). To evaluate the reactivation of astrocytes, we used primary antibodies against NF-κB (rabbit anti-NF-κB/p65, Thermo cat# PA5-16545). After exhaustive rinsing, we incubated the cells with secondary fluorescent antibodies (DyLight 488 and 594 horse anti-rabbit, -goat and -mouse, cat DI 1094, DI 3088, and DI 2488,



respectively) at 1:500. The nuclei were stained with 1  $\mu$ M Hoechst 33,342 (Life Technologies, 5791 Van Allen Way, Carlsbad, CA 92008, USA), and images were acquired on a Floyd Cells Imaging Station microscope (catalogue 4471136, Thermo Fisher Scientific, 168 Third Avenue, Waltham, MA, USA).

## 2.5. Flow Cytometry Analysis

After each treatment, cells were detached using trypsin and centrifuged for 10 min at 2000 rpm. Then, cells were washed with PBS and permeabilized with 0.2% Triton X-100 plus 1.5% bovine serum albumin (BSA) for 30 min. After, cells were incubated with primary antibodies against APP751 and/or protein amyloid  $\beta$ 1-42 (clone 6E10, 1:200), phospho-TAU (AT8; 1:200), oxidized DJ-1 (1:200), PUMA (1:200), p53 (1:200), phospho-c-Jun (1:50; c-Jun (S63/73), and caspase-3 (1:200). After exhaustive rinsing, we incubated the cells with secondary fluorescent antibodies (DyLight 488 and 594 horse anti-rabbit, -goat and -mouse, cat DI 1094, DI 3088, and DI 2488, respectively) at 1:500. Fluorescence analysis was performed on a BD LSRFortessa II flow cytometer (BD Biosciences, Becton, Dickinson and Company, BD Biosciences, 2350 Qume Dr, San Jose, CA 95131-1812, USA). Cells without primary antibodies served as a negative control. For assessment, 10,000 events and quantitative data and figures were obtained using FlowJo 7.6.2 Data Analysis Software (TIBCO®Data Science, Palo Alto, Ca, USA). Events analysis was performed by determining the cell population (Forward Scatter analysis, Y axis) that exceeded the basal fluorescence (488 nm or 594 nm, X axis) of the negative control. Accordingly, contour diagrams were created from event analysis, and the cells located in the box (quadrants labeled as + or ++) represent the cell population exceeding the basal fluorescence.

## 2.6. Western Blot Analysis

To test the effect of EGCG on A $\beta$ 42 oligomerization, 1  $\mu$ g of A $\beta$ 42 (0.1  $\mu$ g/ $\mu$ L) was incubated alone or in combination with 50  $\mu$ M EGCG or 6E10 antibody (1:10). Then, samples were heated at 95 °C for 5 min in 2  $\times$  SDS and 20 $\times$  reducing agent and loaded on to 12% gels at 120 V for 90 min, bands were transferred onto nitrocellulose membranes (Hybond-ECL, Amersham Biosciences, 800 Centennial Ave, Piscataway, NJ, USA,) at 270 mA for 90 min using an electrophoretic transfer system (BIO-RAD) according to Bio-Rad protocol ([http://www.bio-rad.com/webroot/web/pdf/lsr/literature/Bulletin\\_6376](http://www.bio-rad.com/webroot/web/pdf/lsr/literature/Bulletin_6376); accessed on 20 August 2021). The membranes were incubated overnight at 4 °C with anti-APP751 primary antibody (1:5000). Secondary infrared antibody (goat anti-mouse IRDye® 800CW, cat #926-32270; LI-COR Biosciences, 4647 Superior Street, Lincoln, Ne, USA) at 1:10,000 was used for western blotting analysis, and data were acquired using Odyssey software. The assessment was repeated two times in independent experiments. To evaluate the effect of EGCG on the conformation-dependent differences among A $\beta$  assemblies, we prepared a homogenous synthetic unaggregated (i.e., monomers) and large oligomeric A $\beta$ 42 assemblies according to ref. [30]. Briefly, after solubilization of the peptide (Sigma Cat #A9810, 3050 Spruce Street, St. Louis, MO 63103, USA) in DMSO, the “unaggregated” peptide was obtained by dissolving the DMSO-solubilized peptide in water and used immediately (0 days). To obtain the “large oligomers”, 10 mM Tris was added to DMSO-solubilized peptide solution and incubated for 15 days at 4 °C. The determination of the aggregation state of A $\beta$ 42 in the presence of EGCG or antibody 6E10 A $\beta$ 42/APP was performed by Western analysis of SDS-PAGE. The assessment was repeated two times in independent experiments.

## 2.7. Evaluation of Intracellular Hydrogen Peroxide (H<sub>2</sub>O<sub>2</sub>) by Fluorescence Microscopy

To assess the levels of intracellular H<sub>2</sub>O<sub>2</sub>, we used 2',7'-dichlorofluorescein diacetate (5  $\mu$ M, DCFH2-DA; Invitrogen, 168 Third Avenue, Waltham, MA, USA) according to ref. [15]. ChLNs were left in RCm for 4 days. Then, the cells (5  $\times$  10<sup>3</sup>) were incubated with the DCFH2-DA reagent for 30 min at 37 °C in the dark. Cells were then washed, and DCF fluorescence intensity was determined by analysis of fluorescence microscopy images. The

assessment was repeated three times in independent experiments. The nuclei were stained with 0.5  $\mu$ M Hoechst 33,342 staining compound. The assessment was repeated three times in independent experiments blind to the experimenter.

## 2.8. Analysis of Mitochondrial Membrane Potential ( $\Delta\Psi_m$ ) by Fluorescence Microscopy

The ChLNs were left in a regular culture medium (RCm) for 4 days. Then, the cells ( $5 \times 10^3$ ) were incubated with the passively diffusing and active mitochondria-accumulating dye deep red MitoTracker compound (20 nM, final concentration) for 20 min at RT in the dark (Invitrogen, cat # M22426, 168 Third Avenue. Waltham, MA, USA) [15]. Cells were then washed twice with PBS. MitoTracker fluorescence intensity was determined by analysis of fluorescence microscopy images (Floyd Cells Imaging Station microscope, catalogue 4471136, Thermo Fisher Scientific, 168 Third Avenue. Waltham, MA, USA). The assessment was repeated three times in independent experiments. The nuclei were stained with 0.5  $\mu$ M Hoechst 33,342 staining compound. The assessment was repeated three times in independent experiments blind to the experimenter and flow cytometer analyst.

## 2.9. Measurement of Extracellular (e)A $\beta$ 42 Peptide in Culture Medium

The level of (e)A $\beta$ 1-42 peptide was measured according to ref. [32] with minor modifications. Briefly, WT and PSEN1 E280A ChLNs were left in RCm for 4 days. Then, 100  $\mu$ L of conditioned medium was collected, and the levels of secreted A $\beta$ 42 peptides were determined by a solid-phase sandwich ELISA (Invitrogen, Cat# KHB3544, 168 Third Avenue. Waltham, MA, USA) following the manufacturer's instructions. The assessment was repeated four times in independent experiments blind to the experimenter.

## 2.10. Intracellular Calcium Imaging

Intracellular calcium ( $\text{Ca}^{2+}$ ) concentration changes evoked by cholinergic stimulation were assessed according to refs. [33,34], with minor modifications. For the measurement, the fluorescent dye Fluo-3 (Fluo-3 AM; Thermo Fisher Scientific, cat: F1242, 168 Third Avenue. Waltham, MA, USA) was employed. The dye was dissolved in DMSO (1 mM) to form a stock solution. Before the experiments, the stock solution was diluted in neuronal buffer solution (NBS buffer in mM: 137 NaCl, 5 KCl, 2.5  $\text{CaCl}_2$ , 1  $\text{MgCl}_2$ , pH 7.3, and 22 glucose). The working concentration of the dye was 2  $\mu$ M. The WT and PSEN1 E280A ChLNs were incubated for 30 min at 37 °C with the dye containing NBS and then washed five times. Intracellular  $\text{Ca}^{2+}$  transients were evoked by acetylcholine (1 mM final concentration) at 4 days post differentiation. The measurements were carried out using the 20 $\times$  objective of the microscope. Several regions of interest (ROIs) were defined in the visual field of the camera. One of the ROIs was cell free, and the fluorescence intensity measured here was considered background fluorescence ( $F_{bg}$ ). The time dependence of the fluorescence emission was acquired, and the fluorescence intensities (hence the  $\text{Ca}^{2+}$  levels) were represented by pseudo colors. To calculate the changes of the average  $\text{Ca}^{2+}$ -related fluorescence intensities, the  $F_{bg}$  value was determined from the cell-free ROI, and then the resting fluorescence intensities ( $F_{rest}$ ) of the cell-containing ROIs were obtained as the average of the points recorded during a consecutive period of 10 s before the addition of acetylcholine. The peaks of the fluorescence transients were found by calculating the average of six consecutive points and identifying those points that gave the highest average value ( $F_{max}$ ). The amplitudes of the  $\text{Ca}^{2+}$ -related fluorescence transients were expressed relative to the resting fluorescence ( $\Delta F/F$ ) and were calculated by the following formula:  $\Delta F/F = (F_{max} - F_{rest}) / (F_{rest} - F_{bg})$ . For the calculation of the fluorescence intensities, ImageJ was used. The terms fluorescence intensity was used as an indirect indicator of intracellular  $\text{Ca}^{2+}$  concentration. The assessment was repeated three times in independent experiments blind to the experimenter.

### 2.11. Measurement of Interleukin-6 (IL-6) in Culture Medium

The WT and PSEN1 E280A ChLNs were left in MCm for 4 days. Then, the conditioned medium was collected and used to stimulate ALCs for 4 days alone or in combination with 50  $\mu$ M EGCG. Levels of secreted IL-6 were determined through the ELISA kit (Cat. No. 430504, Biolegend, CA, USA) following the manufacturer's instructions. The assessment was repeated 3 times in independent experiments blind to the experimenter. Finally, IL-6 levels were normalized to the protein concentration of cells in the culture dish.

### 2.12. Photomicrography and Image Analysis

Light microscopy photographs were taken using a Zeiss AxioStart 50 Fluorescence Microscope equipped with a Canon PowerShot G5 digital camera (Zeiss Wöhlk-Contact-Linsen, Gmb Schöckirchen, Germany), and fluorescence microscopy photographs were taken using a Zeiss AxioStart 50 Fluorescence Microscope equipped with a Zeiss AxioCam Cm1 and (Zeiss Wöhlk-Contact-Linsfluoreen, Gmb Schöckirchen, Germany) and Floyd Cells Imaging Station microscope. Fluorescence images were analyzed by ImageJ software (<http://imagej.nih.gov/ij/>, accessed on 15 September 2021). The figures were transformed into 8-bit images, and the background was subtracted. The cellular measurement regions of interest (ROIs) were drawn around the nucleus (for the case of transcription factors and apoptosis effectors) or overall cells (for cytoplasmic probes), and the fluorescence intensity was subsequently determined by applying the same threshold for cells in the control and treatment conditions. Mean fluorescence intensity (MFI) was obtained by normalizing total fluorescence to the number of nuclei.

### 2.13. Data Analysis

In this experimental design, two vials of MSCs were thawed (PSEN1-WT and -E280A), cultured and the cell suspension was pipetted at a standardized cellular density of  $2.6 \times 10^4$  cells/cm<sup>2</sup> into different wells of a 24-well plate. Cells (i.e., the biological and observational unit [35]) were randomized to wells by simple randomization (sampling without replacement method), and then wells (i.e., the experimental units) were randomized to treatments by a similar method. Experiments were conducted in triplicate wells. The data from individual replicate wells were averaged to yield a value of  $n = 1$  for that experiment and this was repeated on three occasions blind to the experimenter and/or flow cytometer analyst for a final value of  $n = 3$  [35]. Based on the assumption that the experimental unit (i.e., the well) data comply with the independence of observations, the dependent variable is normally distributed in each treatment group (Shapiro-Wilk test), and variances are homogeneous (Levene's test), the statistical significance was determined by one-way analysis of variance (ANOVA) followed by Tukey's post hoc comparison calculated with GraphPad Prism 5.0 software. Differences between groups were only deemed significant when a  $p$ -value of  $<0.05$  (\*),  $<0.001$  (\*\*) and  $<0.001$  (\*\*\*). All data are illustrated as the mean  $\pm$  S.D.

## 3. Results

### 3.1. EGCG Scavenges Reactive Oxygen Species (ROS) and Reestablishes the Mitochondrial Membrane Potential ( $\Delta\Psi_m$ ) in PSEN1 E280A ChLNs

To determine whether EGCG recovers  $\Delta\Psi_m$  and scavenges ROS, cholinergic cells were exposed to increasing concentrations of EGCG. As shown in Figure 1A–E, EGCG (5–50  $\mu$ M) neither generated ROS (Figure 1A'–E',K) nor affected  $\Delta\Psi_m$  in wild-type ChLNs (Figure 1A''–E'',L). However, the polyphenol treatments dose-dependently reduced the endogenous production of ROS (Figure 1F'–J',K), and increased the  $\Delta\Psi_m$  in PSEN1 E280A ChLNs (Figure 1F''–J'',L). We found that 25–50  $\mu$ M, but not low concentrations (5, 10  $\mu$ M), were the maximal optimal concentrations to completely blunt ROS yield and to raise  $\Delta\Psi_m$  in mutant cells (Figure 1F–L). Therefore, we selected EGCG (50  $\mu$ M) concentration for further experiments.

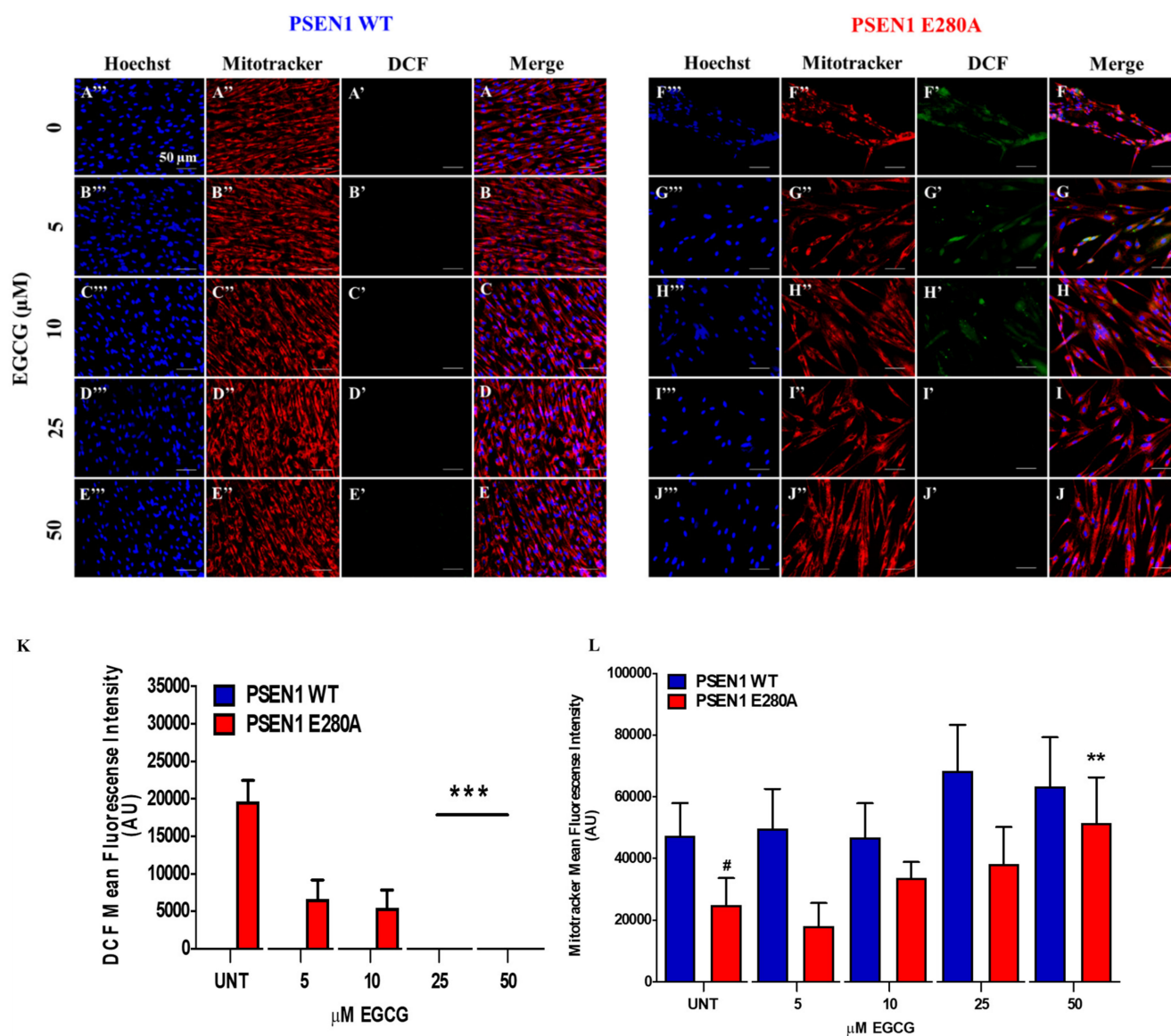


**Figure 1.** EGCG scavenges reactive oxygen species (ROS) and reestablishes the mitochondrial membrane potential ( $\Delta\Psi_m$ ) in a dependent-concentration manner in PSEN1 E280A ChLNs. After 7 days of transdifferentiation, WT PSEN1 and PSEN1 E280A ChLNs were left untreated or treated with EGCG at increasing concentrations (0, 5, 10, 25, and 50  $\mu$ M) in a regular culture medium (RCm) for 4 days. Representative DCF+ cells (A'–J'), MitoTracker (A''–J''), Hoechst (A'''–J'''), and merged (A–J) pictures of WT PSEN1 and PSEN1 E280A ChLNs treated as described. (K) Quantification of DCF fluorescence intensity. (L) Quantification of MitoTracker fluorescence intensity. Data are expressed as the mean  $\pm$  SD; #  $p < 0.05$ ; \*\*  $p < 0.01$ ; \*\*\*  $p < 0.001$ . #, \*\* represents differences compared to UNT PSEN1 E280A cells. The histograms and figures represent 1 out of 3 independent experiments.

### 3.2. EGCG Partially Reduces Intracellular sAPP $\beta$ f Aggregation but Completely Inhibits Oxidized DJ-1 in PSEN1 E280A ChLNs

Next, we assessed whether EGCG inhibits the intracellular aggregation of sAPP $\beta$ f and avoids oxidation of the stress sensor protein DJ-1. To this aim, WT and mutant ChLNs were left untreated or exposed to EGCG. Flow cytometry (FC) analysis reveals that EGCG significantly reduced the aggregation of (i)sAPP $\beta$ f (Figure 2A,B) and almost completely blunted the oxidation of DJ-1 in mutant ChLNs. Neither (i)sAPP $\beta$ f nor oxidized DJ-1 were detected in those WT ChLNs (Figure 2A,C). These results were confirmed by fluorescent microscopy (FM, Figure 2D–I).



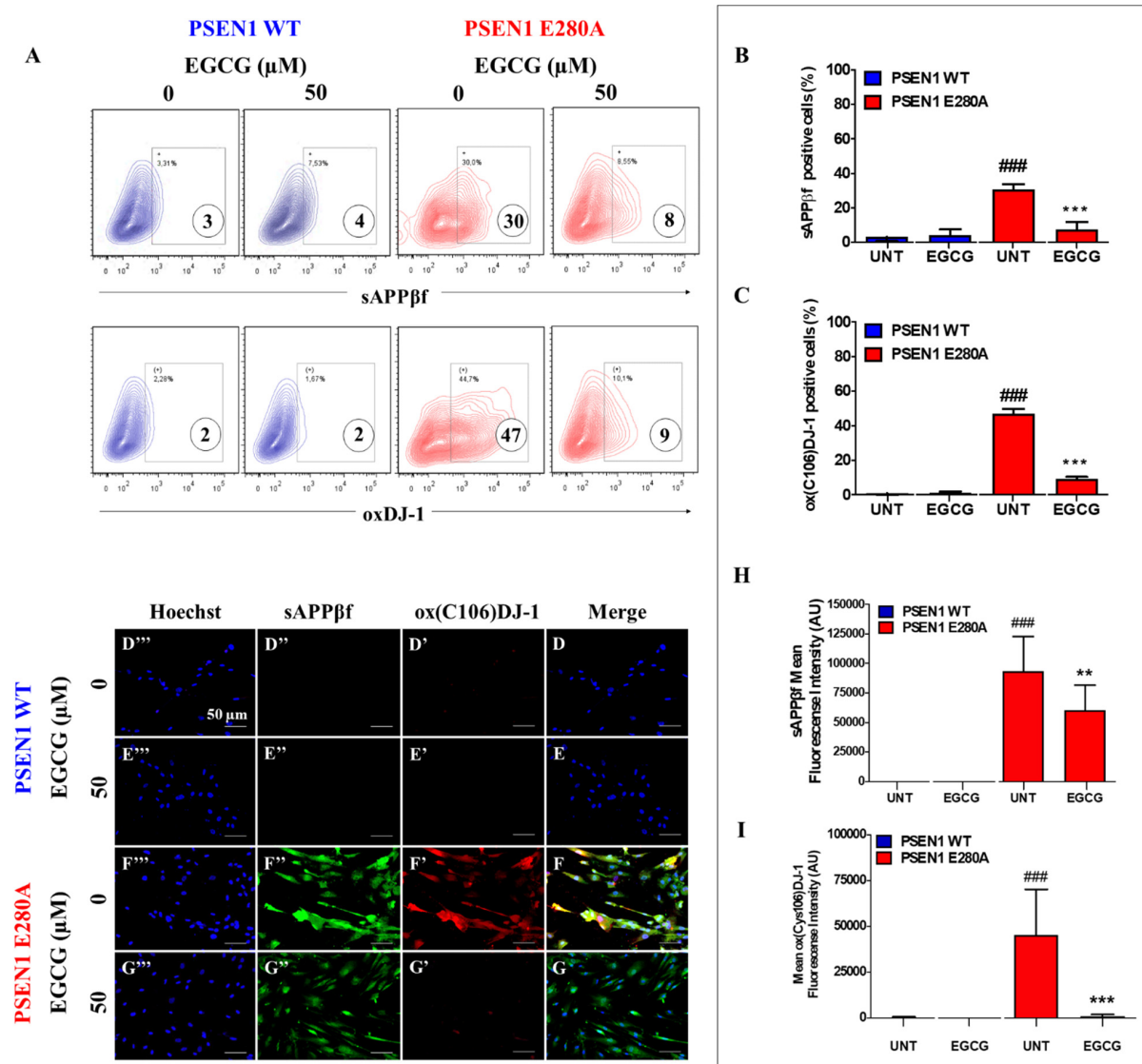


**Figure 2.** EGCG partially reduces the intracellular sAPPβf aggregation but completely inhibits oxidized DJ-1 in PSEN1 E280A ChLNs. After 7 days of transdifferentiation, WT PSEN1 and PSEN1 E280A ChLNs were left untreated or treated with EGCG in RCm for 4 days. Then, the cells were labeled with primary antibodies against Aβ42 and oxDJ-1Cys106, and fluorescent secondary antibodies. The fluorescent contour plot shown in (A) was quantified (B,C). Additionally, cells were double-stained as indicated in the figure (D–G) with primary antibodies against oxDJ-1Cys106 (red; D'–G') and APP751/Aβ42 (green; D''–G''). The nuclei were stained with Hoechst 33,342 (blue; D'''–G'''). (H) Quantification of Aβ42 fluorescence intensity. (I) Quantification of oxDJ-1Cys106 fluorescence intensity. Data are expressed as the mean ± SD; \*\*  $p < 0.01$ ; ###, \*\*\*  $p < 0.001$ . ### represents differences compared to UNT PSEN1 WT cells; \*\*\* represents differences compared to UNT PSEN1 E280A cells. The figures represent 1 out of 3 independent experiments.

### 3.3. EGCG Blocks Apoptosis Signaling in PSEN1 E280A ChLNs

Apoptosis is an important feature in mutant ChLNs [15]. To investigate whether EGCG regulates apoptosis in mutant cells, we used the activation of the transcription factors P53 and c-JUN, pro-apoptotic BH3-only protein PUMA, and protease CASPASE-3 as cell death markers. Flow cytometry (FC) analysis reveals that PSEN1 E280A ChLNs displayed high levels of protein c-JUN (Figure 3A,B), P53 (Figure 3A,C), PUMA (Figure 3A,D) and CASP-3 (Figure 3A,E), but not in WT ChLNs (Figure 3A–E). However, EGCG significantly reduced c-JUN (Figure 3A,B), P53 (Figure 3A,C), PUMA (Figure 3A,D), and CASP-3 (Figure 3A,E) in PSEN1 E280A neurons compared to treated WT ChLNs cells. These observations were confirmed by fluorescent microscopy (Figure 3F–Q).



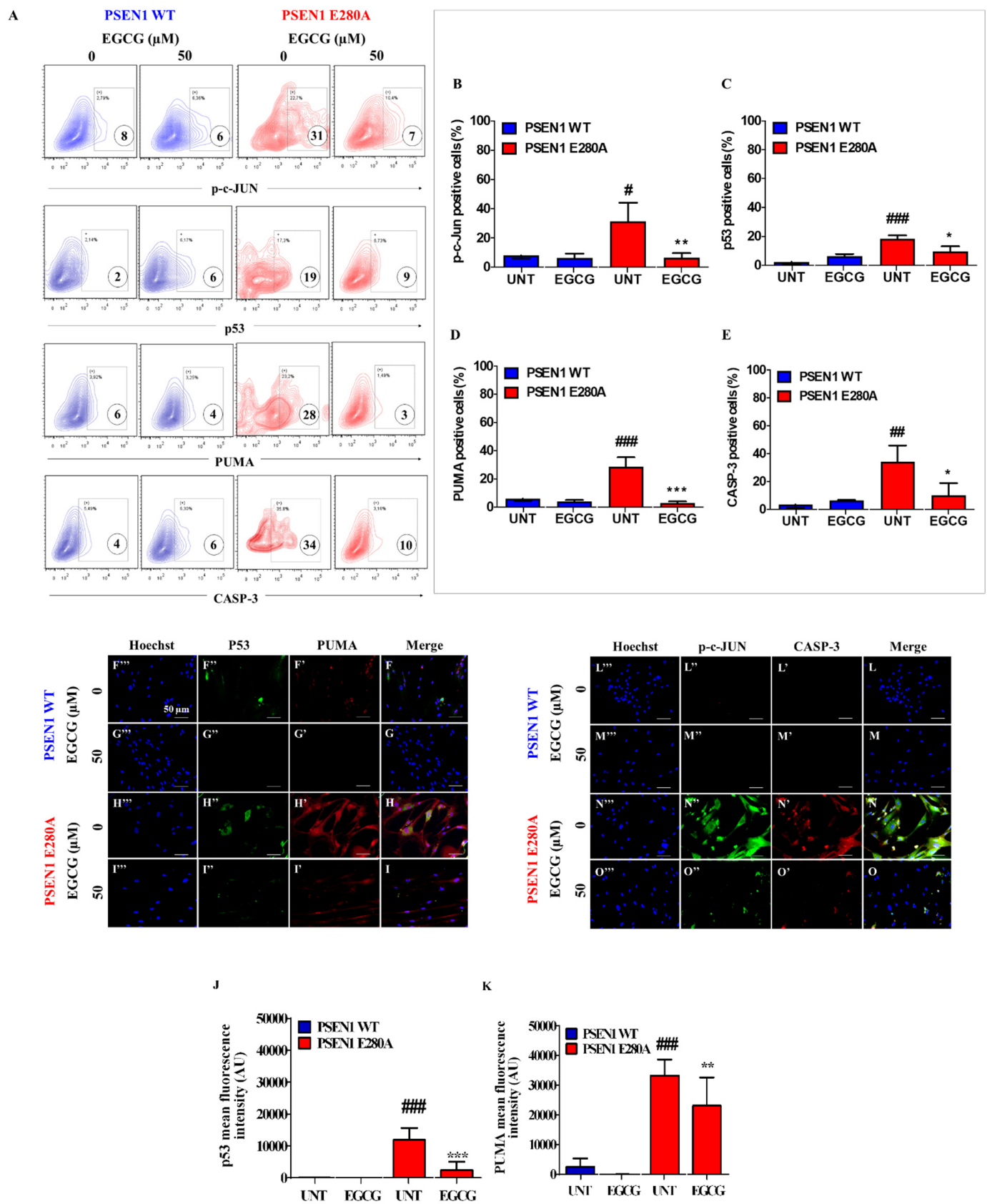
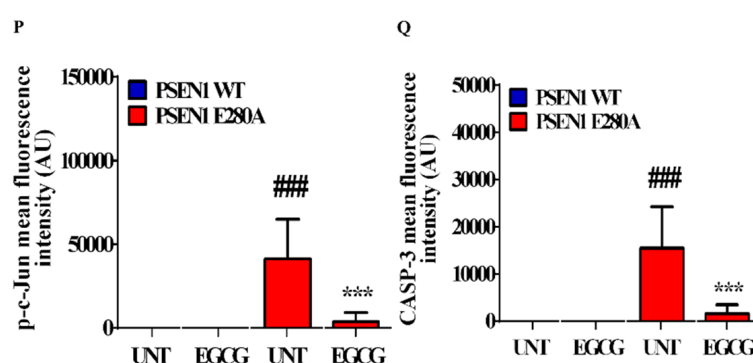


Figure 3. Cont.



**Figure 3.** EGCG reduced the activation of P53, PUMA, c-JUN, and CASPASE-3 in PSEN1 E280A ChLNs. After 7 days of transdifferentiation, WT PSEN1 and PSEN1 E280A ChLNs were left untreated or treated with EGCG in a regular culture medium for 4 days. Then, cells were labeled with primary antibodies against c-JUN/total c-JUN, P53, PUMA, CASPASE-3 (CASP-3), and fluorescent secondary antibodies. The fluorescent contour plot shown in (A) were quantified (B–E). Additionally, cells were double-stained as indicated in the figure (F–O) with primary antibodies against P53 (green; F'–I'), PUMA (red; F'–I'), c-JUN (green; L'–O'), and CASP-3 (red; N'–O'). The nuclei were stained with Hoechst 33,342 (blue; F'–O'). (J,K,P,Q) Quantification of P53 (J), PUMA (K), c-JUN (P), and CASP-3 (Q) fluorescence intensity. Data are expressed as the mean  $\pm$  SD; #, \*  $p < 0.05$ ; ##, \*\*  $p < 0.01$ ; ###, \*\*\*  $p < 0.001$ ; ### represents differences compared to UNT PSEN1 WT cells; \*\*, \*\*\* represents differences compared to UNT PSEN1 E280A cells. The figures represent 1 out of 3 independent experiments. Image magnification, 200 $\times$ .

### 3.4. EGCG Inhibits TAU Phosphorylation in PSEN1 E280A ChLNs

Previously, it was shown that (i)sAPP $\beta$ f induces the phosphorylation of TAU [15]. To investigate whether EGCG inhibits TAU phosphorylation, WT and PSEN1 E280A ChLNs were left untreated or treated with the polyphenol. As shown in Figure 4, while the level of TAU phosphorylation was detected to a similar extent in WT ChLNs under EGCG exposure (Figure 4A,B), EGCG dramatically reduced phosphorylation of protein TAU in mutant ChLNs (Figure 4A,B) compared to untreated or treated WT neurons. These observations were confirmed by fluorescent microscopy (Figure 4C–G).

### 3.5. EGCG Does Not Reduce the Levels of Extracellular A $\beta$ 42 (eA $\beta$ 42) Protein Fragment in PSEN1 E280A ChLNs

We further evaluated whether EGCG affects the amounts of secreted A $\beta$ 42 by nerve cells [15]. As shown in Figure 5, EGCG did not reduce the amounts of (e)A $\beta$ 42 secreted by mutant cells ( $870 \pm 234$  pg eA $\beta$ 42/mg protein) compared to untreated mutant neurons ( $635 \pm 46$  pg eA $\beta$ 42/mg protein) according to the ELISA technique (Figure 5A). Similar amounts of secreted eA $\beta$ 42 were detected in untreated ( $225 \pm 55$  pg eA $\beta$ 42/mg protein) as well as EGCG treated ( $274 \pm 80$  pg eA $\beta$ 42/mg protein) WT ChLNs ( $p < 0.01$ , Figure 5A). This observation prompted us to inquire further on the interactions of EGCG and (e)A $\beta$ 42. Thus, synthetic A $\beta$ 42 fragment was either incubated with DMSO or in a minimal culture medium (mCM) in the presence of antibody A $\beta$ 42 6E10 or EGCG for 24 h. As shown in Figure 5B, Western blot (WB) analysis reveals that A $\beta$ 42 in DMSO forms aggregates of circa 8–25 kDa, whereas in mCM A $\beta$ 42 forms mostly aggregate of approximately 8 kDa (probably A $\beta$ 42 dimers). Interestingly, A $\beta$ 42 incubated with antibody A $\beta$ 42 6E10 or EGCG in mCM not only showed oligomerization of A $\beta$ 42 (e.g., 8 kDa) but also high molecular weight A $\beta$ 42 fragments (circa 50–200 kDa).

### 3.6. EGCG Recovers Ca<sup>2+</sup> Dysregulation in PSEN1 E280A ChLNs

We then test whether EGCG ameliorates the physiological response of mutant ChLNs to ACh neurotransmitter stimuli. As illustrated in Figure 6, ACh induces a transient elevation of intracellular Ca<sup>2+</sup> in WT ChLNs (control, the average maximum fluorescence change ( $\Delta F/F$ ) was  $43 \pm 13$  at 40s ( $n = 20$  ChLN cells imaged,  $N = 3$  dishes were used as a standard condition in this and following experiments)) according to cytoplasmic Ca<sup>2+</sup> responses to

Fluo-3-mediated imaging (Figure 6A,E). In contrast, under similar experimental conditions, PSEN1 E280A ChLNs were almost unresponsive to ACh stimuli ( $\Delta F/F = -0.5 \pm -0.5$  at 40s, Figure 6C,E). However, when WT and mutant neurons were exposed to ACh and EGCG, both WT and mutant ChLNs increased intracellular  $Ca^{2+}$ , albeit with dissimilar strength. Indeed, while WT ChLNs increases almost 22-fold  $Ca^{2+}$  influx (Figure 6B,E,  $\Delta F/F = 62.1 \pm 13.4$  at 10 s) compared to untreated WT (Figure 6B,E,  $\Delta F/F = 2.8 \pm 0.2$ ), mutant ChLNs increases almost 100-fold  $Ca^{2+}$  influx (Figure 6D,E,  $\Delta F/F = 20.1 \pm 7.0$  at 10 s) compared to untreated mutant neurons (Figure 6C,E,  $\Delta F/F = 0.20 \pm 0.10$  at 10 s). Interestingly, EGCG increases almost 3-fold the intracellular  $Ca^{2+}$  influx in WT ChLNs compared to mutant neurons treated at 10 s.

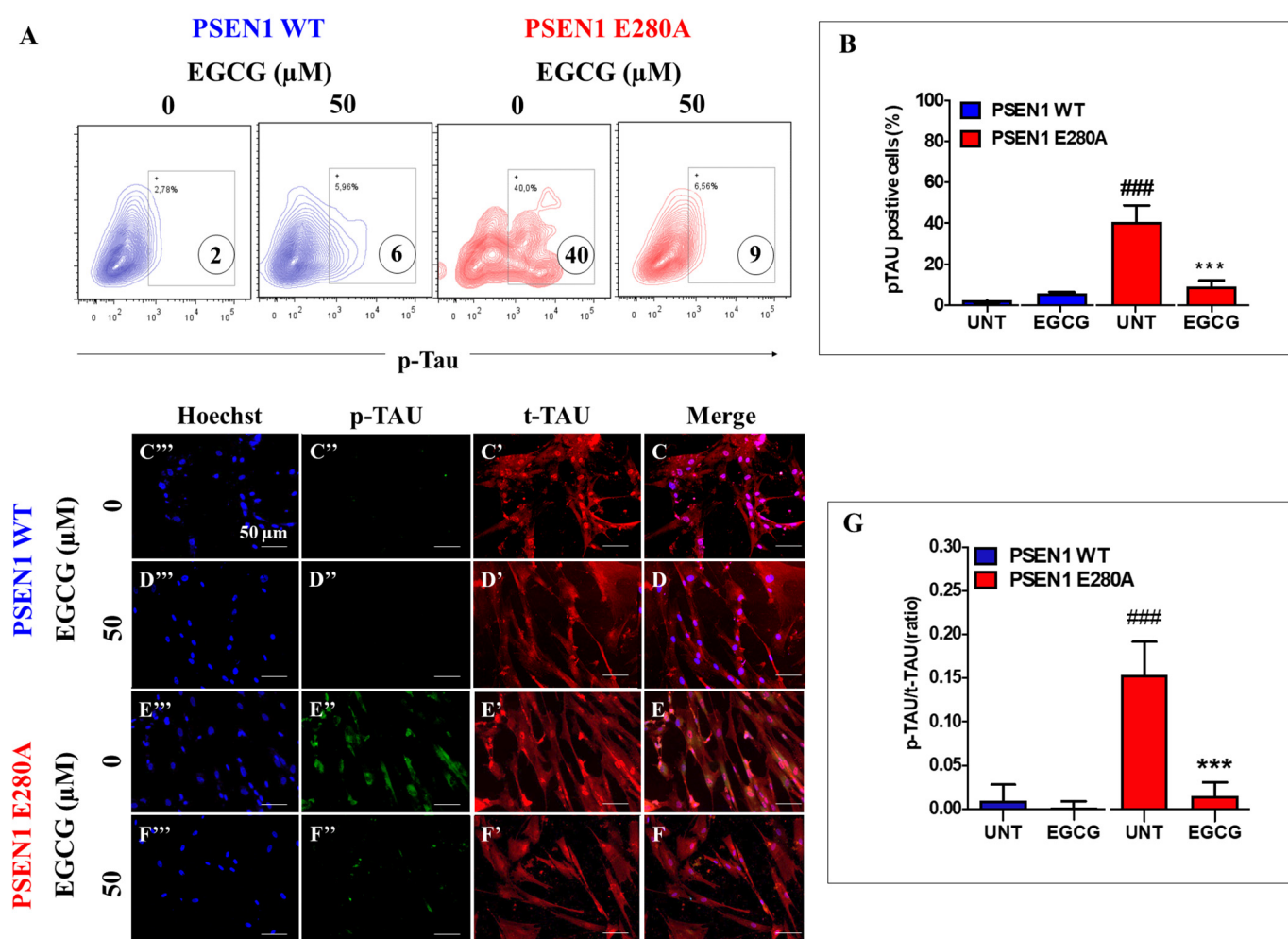


**Figure 4.** EGCG reduces the phosphorylation of TAU protein in PSEN1 E280A ChLNs. After 7 days of transdifferentiation, WT PSEN1 and PSEN1 E280A ChLNs were left untreated or treated with EGCG in a regular culture medium for 4 days. Then, the cells were labeled with primary antibodies against phosphorylated TAU (p-TAU), and fluorescent secondary antibodies. The fluorescent contour plot shown in (A) were quantified (B). Additionally, cells were double-stained as indicated in the figure (C–F) with primary antibodies against p-TAU (green; C'–F') and t-TAU (red; C''–F''). The nuclei were stained with Hoechst 33,342 (blue; C'''–F'''). (G) Quantification of the p-TAU/t-TAU fluorescence ratio. Data are expressed as the mean  $\pm$  SD; ###, \*\*\*  $p < 0.001$ ; ### represents differences compared to UNT PSEN1 WT cells; \*\*\* represents differences compared to UNT PSEN1 E280A cells. The figures represent 1 out of 3 independent experiments.

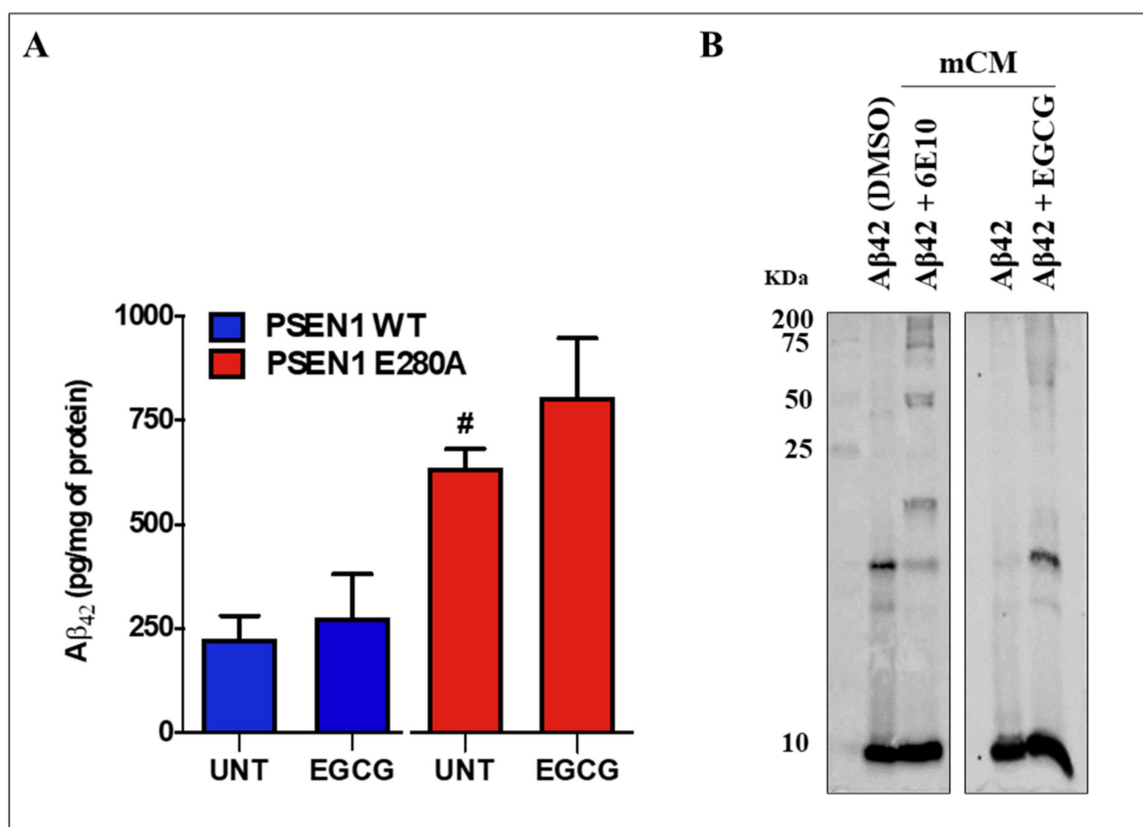


**Figure 5.** EGCG does not reduce the levels of extracellular Aβ<sub>42</sub> peptides in PSEN1 E280A ChLNs. After 7 days of transdifferentiation, WT PSEN1 and PSEN1 E280A ChLNs were left untreated or treated with EGCG in RCm for 4 days. (A) ELISA quantification of extracellular Aβ<sub>42</sub> peptides in supernatants. (B) Western blot showing the Aβ<sub>42</sub> migration profile alone or after incubation with EGCG or 6E10 antibody. Data are presented as means ± SD. <sup>#</sup> *p* < 0.05, <sup>#</sup> represents differences compared to UNT PSEN1 WT cells. The histograms represent 1 out of 4 independent experiments, and blot represents 1 out of 2 independent experiments.

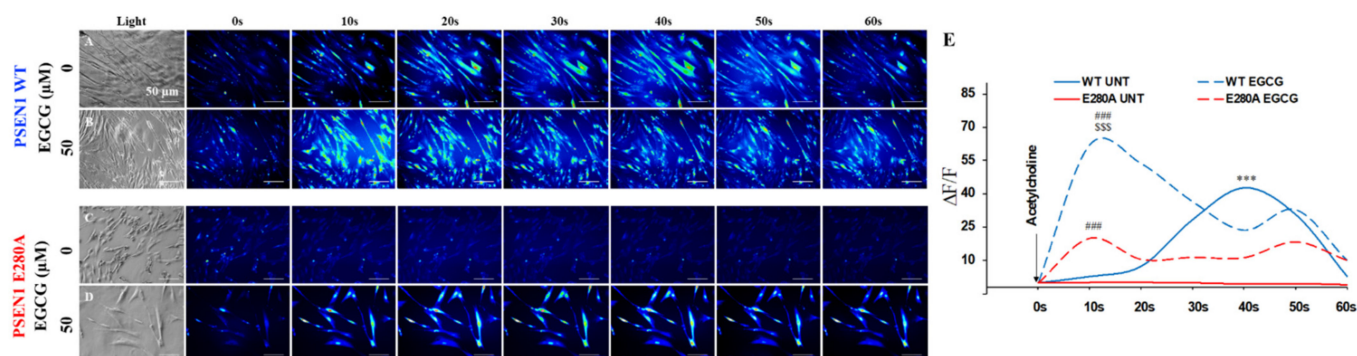


**Figure 6.** EGCG recovers Ca<sup>2+</sup> dysregulation in PSEN1 E280A ChLNs. After 7 days of transdifferentiation, WT PSEN1 and PSEN1 E280A ChLNs were left untreated or treated with EGCG in a regular culture medium for 4 days. (A–D) Time-lapse images (0, 10, 20, 30, 40, 50, and 60 s) of Ca<sup>2+</sup> fluorescence in WT PSEN1 and PSEN1 E280A ChLNs on day 4 in response to ACh treatment. ACh was puffed into the culture at 0 s (arrow). Then, the Ca<sup>2+</sup> fluorescence of the cells was monitored at the indicated times. Color contrast indicates fluorescence intensity: dark blue < light blue < green < yellow < red. (E) Normalized mean fluorescence signal (ΔF/F) over time from the cells indicating temporal cytoplasmic Ca<sup>2+</sup> elevation in response to ACh treatment. Data are presented as the mean ± SD. <sup>\*\*\*</sup>, <sup>###</sup>, <sup>\$\$\$</sup> *p* < 0.001; <sup>\*\*\*</sup> represents differences compared to UNT PSEN1 E280A cells; <sup>###</sup> represents differences compared to UNT PSEN1 WT or E280A cells; <sup>\$\$\$</sup> represents differences compared to EGCG-treated PSEN1 E280A cells. The figures represent 1 out of 3 independent experiments.



### 3.7. EGCG Dramatically Reduces Reactive Astrocyte-like Cells Derived from Menstrual Stromal Cells (MenSCs) Exposed to ChLNs' Supernatant Culture Medium

Lastly, we evaluated the anti-inflammatory effect of EGCG on astrocyte-like cells (ALCs) [27]. ALCs were incubated for 4 days with the supernatant culture medium from (7 days) cultured WT and PSEN1 E280A ChLNs (which contains significantly high amounts of A $\beta$ 42 (Figure 5A)) in the absence or presence of EGCG. Since IL-6 is a pleiotropic pro-inflammatory cytokine important for the transition from the acute phase to the chronic phase of inflammation in AD [26], we selected IL-6 as a model cytokine in our in vitro neuroinflammation test. Therefore, the amounts of secreted pro-inflammatory cytokine IL-6 by ALCs were evaluated by ELISA technique, and activation of NF- $\kappa$ B (p65), which is a critical transcription factor in immunomodulation, was assessed by immunofluorescent microscopy (IMF), an indicator of neuroinflammation and reactive astrogliosis, respectively [36]. As shown in Figure 7, both mCM and supernatant WT induced neither secretion of pro-inflammatory molecule IL-6 (Figure 7A) nor activation of NF- $\kappa$ B in WT ALCs in presence or absence of EGCG (Figure 7B–D,G). When ALCs were incubated with the PSEN1 E280A ChLNs supernatant only, the amounts of IL-6 significantly increased (Figure 7A) compared to untreated or treated ALCs with WT supernatant. Likewise, PSEN1 E280A ChLNs supernatant induced the activation of NF- $\kappa$ B in ALCs (Figure 7D,G) compared to untreated ALCs (Figure 7C,G). However, EGCG significantly diminished the secretion of IL-6 (Figure 7A) and inactivated NF- $\kappa$ B in ALCs cultured in PSEN1 E280A ChLNs supernatant (Figure 7E,G) to a similar extent as ALCs incubated with EGCG only (Figure 7E,G).

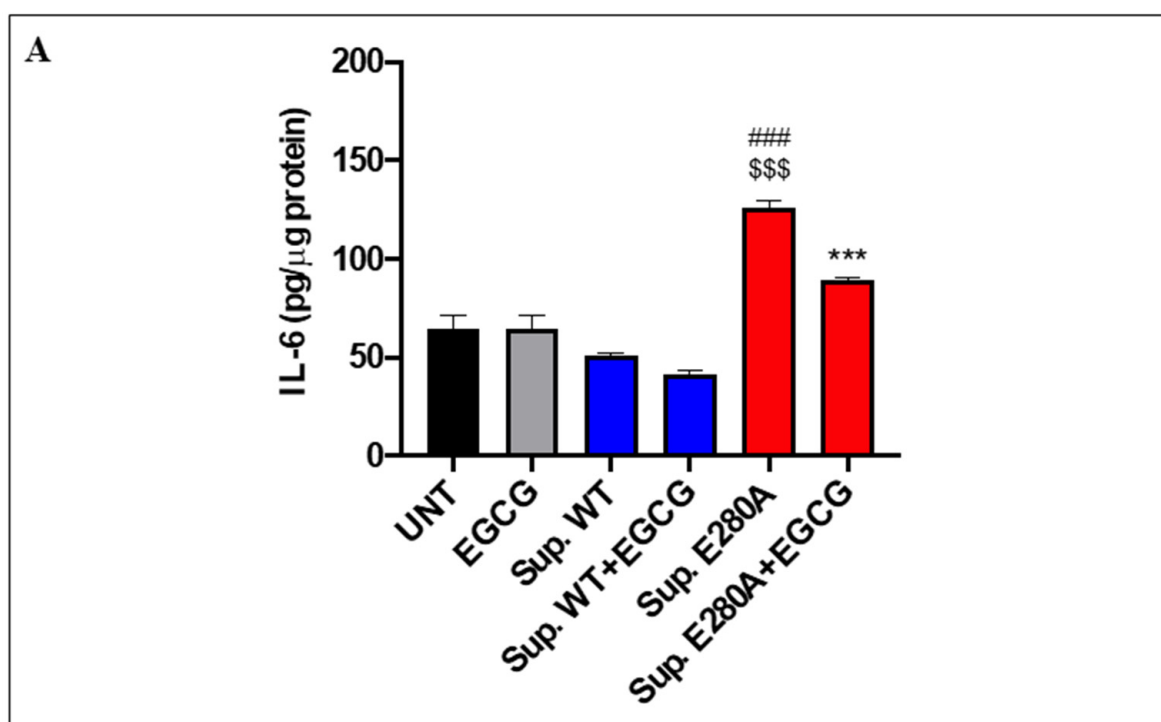
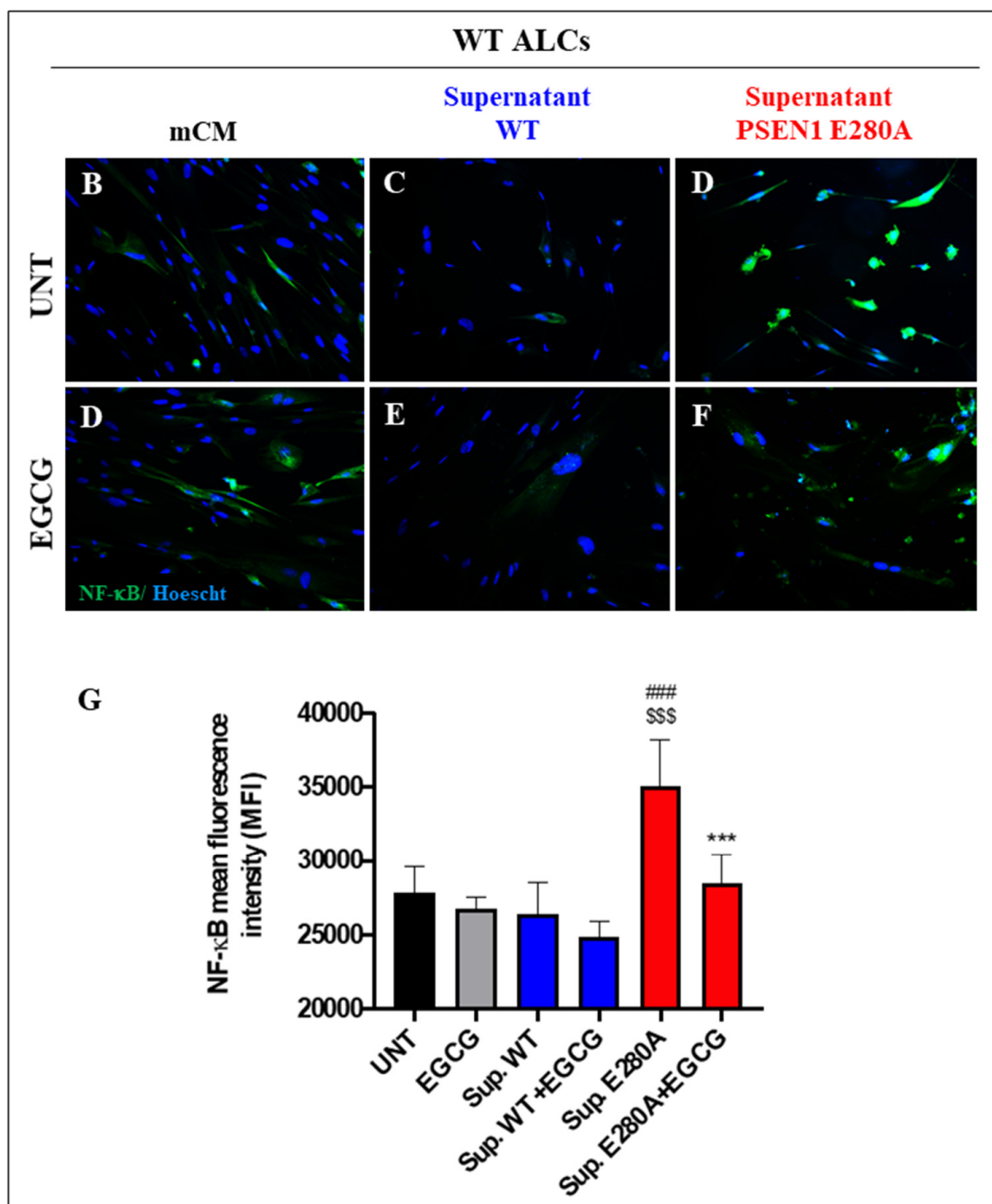


Figure 7. Cont.





**Figure 7.** The PSEN1 E280A culture supernatant induces secretion of a proinflammatory molecule (IL-6), and activation of NF-κB in astrocyte-like cells (ALCs). (A) After 7 days of transdifferentiation of MenSCs, ALCs were exposed to either mCM, WT supernatant, or PSEN1 E280A culture supernatant for 4 days in the absence (untreated, UNT) or presence of EGCG. Then, supernatants were collected and used to determine IL-6 levels according to the described method. The levels of IL-6 were normalized to the cell protein concentration. (B) After 7 days of transdifferentiation of MenSCs, ALCs were exposed to either mCM, WT supernatant, or PSEN1 E280A culture supernatant for 4 days in the absence (untreated, UNT) or presence of EGCG. Then, cells were labeled with primary antibodies against NF-κB, and fluorescent secondary antibodies. The nuclei were stained with Hoechst 33342. Representative merged images of ALCs exposed to mCM (B,D), WT supernatant (C,E), and PSEN1 E280A culture supernatant (D,E) without (B–D) or with EGCG (D–F). (G) Quantification of NF-κB fluorescence intensity. Data are expressed as the mean  $\pm$  SD; ###, \*\*\*, \$\$\$  $p < 0.001$ ; \*\*\* represents differences compared to Sup. E280A; ### represents differences compared to UNT ALCs; \$\$\$ represents differences compared to Sup. WT. The histogram and figures represent 1 out of 3 independent experiments. Image magnification, 200 $\times$ .

#### 4. Discussion

We report for the first time that the catechin EGCG protects PSEN 1 E280A ChLNs against (i)sAPP $\beta$ f and eA $\beta$ 42-induced cytotoxic effects. Indeed, EGCG inhibited the aggregation of (i)sAPP $\beta$ f, blocked p-TAU, increased  $\Delta\Psi_m$ , decreased oxidation of DJ-1 Cys106-SH residue, and inhibited the activation of transcription factor c-JUN and P53, blocked BH3-only protein PUMA, and executor protein CASPASE-3. Furthermore, it reversed Ca<sup>2+</sup> influx dysregulation as a response to ACh stimuli in mutant ChLNs, inhibited pro-inflammatory IL-6, and turned down NF- $\kappa$ B in WT ALCs exposed to mutant ChLNs culture supernatant. Taken together these results suggest that EGCG is a multitarget compound working as an anti-amyloidogenic, anti-apoptosis, anti-phospho-TAU, anti-oxidant agent,  $\Delta\Psi_m$  enhancer, transient intracellular Ca<sup>2+</sup> influx regulator in PSEN 1 E280A ChLNs, and anti-neuroinflammatory agent in ALCs.

We found for the first time that EGCG inhibited aggregation of (i)sAPP $\beta$ f (e.g., APP714, APP733, APP751, APP752), thereby reducing its toxicity in mutant ChLNs [15]. Although no information is yet available to explain its mechanism of action on (i)sAPP $\beta$ f, several data suggest that EGCG reduced the toxicity of amyloidogenic polypeptides by directly binding with unfolded protein and inhibiting the formation of  $\beta$ -sheet structure, an early event of amyloid formation cascade. At the molecular level, auto-oxidized EGCG reacts with free primary amine groups of proteins, forms a Schiff base, and induces fibril remodeling [37,38]. Interestingly, this mechanism not only might be operative with A $\beta$  and TAU [39] in AD but also to other neurodegenerative disorders such as  $\alpha$ -synuclein (in Parkinson's disease), Huntingtin protein (in Huntington's disease), and islet amyloid polypeptide (IAPP, amylin) in the pancreas most probably through a common mechanism, in which EGCG binds to cross-beta sheets amyloid aggregation intermediates remodeling the oligomeric amyloid or pre-formed amyloid fibrils into non-amyloidogenic species [21,40]. According to this view, we found that EGCG significantly reduces (i)sAPP $\beta$ f aggregates in PSEN 1 E280A ChLNs demonstrated by FM staining, and FC analysis. However, further investigation is needed to confirm this assumption. Specifically, mounting evidence has shown that EGCG inhibits the oligomerization of A $\beta$ 42 [41–43]. Consistent with previous work [21], we found that EGCG induces highly stable aggregates of synthetic A $\beta$ 42. Interestingly, previous studies have reported that EGCG attenuated A $\beta$  generation by suppressing the transcription and translation of BACE1 [41,44]. However, the present study found that EGCG did not affect the amount of secreted (e)A $\beta$ 42. This observation implies that EGCG does not interfere with or regulate the metabolism of PPA in mutant ChLNs. Taken together, these observations suggest that EGCG shifts/stabilizes the conformational structure of (i)sAPP $\beta$ f and inhibits the cytotoxicity of secreted (e)A $\beta$ 42 into non-toxic beta fragments but does not alter intracellular APP metabolism in PSEN 1 E280A ChLNs. Remarkably, PSEN1 E280A displayed hyperphosphorylation of protein TAU [15]. In agreement with Gu  roux and co-workers [45], we found that EGCG prevented TAU phosphorylation. Therefore, it is concluded that EGCG can effectively reverse the typical neuropathological toxic amyloidogenic polypeptides (i.e., A $\beta$ , TAU [39]) into non-toxic and non-amyloidogenic species in PSEN1 E280A ChLNs.

Previously, it has been shown that the earliest sign of OS in PSEN1 E280A ChLNs was the generation of ROS, and the oxidation of stress sensor protein DJ-1 Cys106-SH into DJ-1 Cys106-SO3 by H2O2 [15]. In agreement with He and co-workers [46], who observed that EGCG treatment effectively protected the mouse hippocampal neuronal cell line HT22 against H2O2-induced cell viability by decreasing and attenuating ROS generation, we found that this polyphenol completely removed ROS production and avoided the oxidation of protein DJ-1 in mutant ChLNs. Structure–function studies of EGCG concerning its molecular mechanisms of action have suggested that either its galloyl D-ring [46,47] or the B-ring of EGCG [48] might be the primary site for the free radical scavenging activity of antioxidant reactions. Since EGCG has been shown to inhibit catalase [49], our observations suggest that EGCG might operate as a free radical quencher rather than a catalase-like catalysator in PSEN1 E280A ChLNs.

Mitochondria are critical organelles in cellular life and death decisions, being both processes susceptible to be modulated by the polyphenol EGCG [50]. Indeed, it has been shown that EGCG protected human lens epithelial HLEB-3 cells [51] and pheochromocytoma PC12 cells [52,53] against H<sub>2</sub>O<sub>2</sub>-induced apoptosis mainly through inhibition of CASP-3. In line with these observations, we found that EGCG not only reestablished the  $\Delta\Psi_m$  but also dramatically decreased the activity of CASP-3, both features affected/activated in PSEN1 E280A ChLNs [15]. Furthermore, we report for the first time that EGCG blocks the activation of the pro-apoptotic proteins c-JUN, P53, and PUMA [54]; all indirect/direct players in the mitochondria depolarization, and subsequent releasing of apoptogenic proteins (e.g., cytochrome c) which ended up in the activation of CASP-3 in mutant neurons. Taken together, these observations suggest that EGCG protects PSEN1 E280A against endogenously generated OS-induced intrinsic apoptosis [55].

A previous study has shown that PSEN1 E280A ChLNs displayed reduced functional response to ACh [15]. Here, we confirm that mutant ChLNs were unresponsive to ACh. Therefore, PSEN1 E280A ChLNs essentially present a dysfunctional intracellular Ca<sup>2+</sup> influx in response to ACh compared to WT ChLNs most probably by the specific interaction between (e)A $\beta$ 42 and nAChRs [56]. Accordingly, we found that PSEN1 E280A ChLNs secreted high amounts of (e)A $\beta$ 42 (e.g., ~2.6-f.i.) compared to WT PSEN1 ChLNs. However, EGCG moderately recovered the response of PSEN1 E280A to ACh. Based on the observation that EGCG stabilized and redirected the toxic oligomers of synthetic A $\beta$ 42 into non-toxic ones (Figure 5B), we speculate that EGCG either blocks (e)A $\beta$ 42-nAChRs or EGCG stabilize (e)A $\beta$ 42 to a non-amyloidogenic peptide. Our observations favor the former assumption. However, further investigation is needed to clarify this issue. Whatever the mechanism, we demonstrate for the first time that EGCG recovers Ca<sup>2+</sup> influx in PSEN1 E280A ChLNs in a short window of time (e.g., 10 s) after being puffed ACh. Outstandingly, EGCG was much more effective in recovering mutant ChLNs (100-fold increase Ca<sup>2+</sup> influx) than enhancing the response of WT ChLNs (22-fold increase Ca<sup>2+</sup> influx) to ACh. Nonetheless, EGCG increased almost 3-fold the intracellular Ca<sup>2+</sup> influx in WT compared to mutant neurons. Taken together our observations suggest that EGCG protects PSEN1 E280A against (e)A $\beta$ 42-induced dysfunctional Ca<sup>2+</sup> influx with no involvement in the APP metabolism. EGCG did not alter the secretion of A $\beta$ 42 in untreated or treated mutant ChLNs. Therefore, EGCG might be an effective agent to protect neuronal and/or synaptic function.

Using ALCs as a cellular model of human brain astrocytes [29], we demonstrate for the first time that the supernatant culture medium from PSEN1 E280A ChLNs, but not the supernatant culture medium from WT ChLNs, induces the activation of NF- $\kappa$ B—a proinflammatory transcription factor [57] and the secretion of pro-inflammatory cytokine IL-6 [26] in WT MenSCs-derived astrocyte cells. Here, we also report for the first time that EGCG—a well-established anti-inflammatory molecule (e.g., [22]) dramatically reduced the activation of NF- $\kappa$ B and the secretion of pro-inflammatory cytokine in ALCs. Our observations comply with the notion that EGCG attenuates (e)A $\beta$ 42-induced neuroinflammation and neurotoxicity in PSEN1 E280A ChLNs.

## 5. Conclusions

In this investigation we have reproduced not only the neuropathological hallmarks of FAD (Figure 8A), but have also shown that EGCG protects ChLNs PSEN1 E280A—a cellular model of FAD by blocking, at least, seven pathological targets: (i)sAPP $\beta$ f, eA $\beta$ 42, oxDJ-1, p-TAU, down  $\Delta\Psi_m$ , Ca<sup>2+</sup> dysregulation, and reactive ALCs (Figure 8B). Remarkably, all these beneficial effects of EGCG have been extensively reported in vivo models (e.g., [58]). Therefore, our in vitro test is a valid subrogate cellular model for searching potential anti-FAD drugs. Interestingly, toxicological and human safety data for tea preparations ingested as a solid bolus dose has shown a safe intake level of 338 mg EGCG/day for adults based on human adverse event (AE) data, and observed safe level (OSL) of 704 mg EGCG/day might be considered for tea preparations in beverages [59]. A key question then arises: can

EGCG be translated to the clinic in FAD PSEN1 E280A patients [60]? Our present results and previous experimental approaches with EGCG loaded in nanoparticles (e.g., [61–63]) encourage its use in the treatment of FAD patients. Although the EGCG dose levels and administration route remain to be established, the EGCG nonetheless might be a promising therapeutic candidate for FAD.

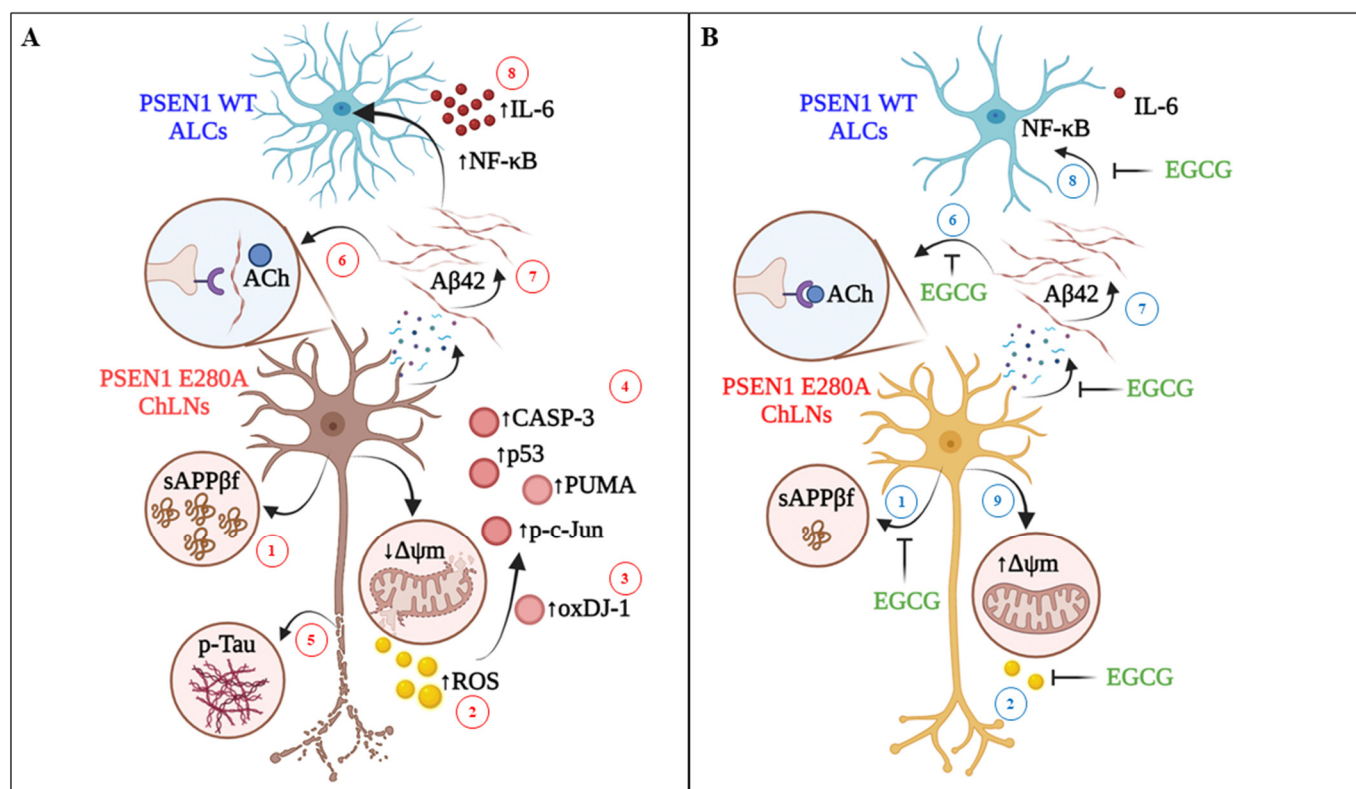


**Figure 8.** Schematic representation of the protective effect of EGCG on PSEN1 E280A ChLNs. **(A)** Intracellularly accumulation of sAPPβf (step 1) generates H<sub>2</sub>O<sub>2</sub> (s2), which in turn oxidizes the OS sensor protein DJ-1 at Cys106-SH residue into DJ-1Cys106-SO<sub>3</sub> (s3) and activates a domino-like, pro-death signaling mechanism (s4) by triggering the activation of transcription factor P53 and c-JUN, BH-3-only protein PUMA and CASP-3. Interestingly, (i)sAPPβf induces the phosphorylation of protein TAU (p-TAU, s5). Besides, PSEN1 E280A ChLNs do not respond to ACh stimuli i.e., intracellular transient Ca<sup>2+</sup> increase is missing due to extracellular interaction between (e)Aβ42 and nicotinic (n)ACh receptors (s6). Therefore, the (i) sAPPβf/Aβ42-induced signaling process (s1–s6) leads ChLNs to structural alterations, cell death (apoptosis), as well as intracellular Ca<sup>2+</sup> dysfunction. To aggravate matters, the (e)Aβ42 (s7) induces ALCs to secrete pro-inflammatory cytokine IL-6 through activation of transcription factor NF-κB (s8). **(B)** Upon exposure to EGCG, mutant ChLNs show normal features such as no oxidized protein DJ-1 (s3), unaltered ΔΨm (s9), and intact nuclei morphology. Moreover, EGCG partially inhibits the aggregation of (i)sAPPβf (s1) and blocks the generation of H<sub>2</sub>O<sub>2</sub> (s2). As a result, there is no further activation of pro-death proteins (s4), and phosphorylation of protein TAU (s5). Furthermore, EGCG reestablishes the PSEN1 E280A ChLNs response to ACh (s6–s7) and protects ALCs against (e)Aβ42-induced pro-inflammation stimuli (s8).

**Author Contributions:** Conceptualization, C.V.-P. and M.J.-D.-R.; methodology, V.S.-M. and M.M.-P.; formal analysis, V.S.-M. and M.M.-P.; investigation, C.V.-P. and M.J.-D.-R.; resources, M.J.-D.-R.; data curation, V.S.-M. and M.M.-P.; writing—original draft preparation, C.V.-P. and M.J.-D.-R.; writing—review and editing, V.S.-M., M.M.-P.; C.V.-P. and M.J.-D.-R.; supervision, M.M.-P.; project administration, C.V.-P. and M.J.-D.-R.; funding acquisition, C.V.-P. All authors have read and agreed to the published version of the manuscript.

**Funding:** This research was funded by MinCiencias, grant number 1115-844-67062, contract #2019-32092 to CV-P & MJ-Del-Rio, and the article publication charge (APC) was funded by MinCiencias. VS-M is a doctoral student of the Basic Biomedical Sciences Academic Corporation program at the



Universidad de Antioquia (UdeA) funded by the “2019 Bicentennial Doctoral Excellence Scholarship”, MinCiencias-Colombia.

**Institutional Review Board Statement:** Not applicable.

**Informed Consent Statement:** Not applicable.

**Conflicts of Interest:** The authors declare no conflict of interest. The funders had no role in the design of the study; in the collection, analyses, or interpretation of data; in the writing of the manuscript, or in the decision to publish the results.

## References

- Knopman, D.S.; Amieva, H.; Petersen, R.C.; Chételat, G.; Holtzman, D.M.; Hyman, B.T.; Nixon, R.A.; Jones, D.T. Alzheimer disease. *Nat. Rev. Dis. Primers* **2021**, *7*, 33. [\[CrossRef\]](#) [\[PubMed\]](#)
- DeTure, M.A.; Dickson, D.W. The neuropathological diagnosis of Alzheimer’s disease. *Mol. Neurodegener.* **2019**, *14*, 32. [\[CrossRef\]](#)
- Bekdash, R.A. The Cholinergic System, the Adrenergic System and the Neuropathology of Alzheimer’s Disease. *Int. J. Mol. Sci.* **2021**, *22*, 1273. [\[CrossRef\]](#) [\[PubMed\]](#)
- Leng, F.; Edison, P. Neuroinflammation and microglial activation in Alzheimer disease: Where do we go from here? *Nat. Rev. Neurol.* **2021**, *17*, 157–172. [\[CrossRef\]](#)
- Tan, J.Z.A.; Gleeson, P.A. The role of membrane trafficking in the processing of amyloid precursor protein and production of amyloid peptides in Alzheimer’s disease. *Biochim. Biophys. Acta Biomembr.* **2019**, *1861*, 697–712. [\[CrossRef\]](#) [\[PubMed\]](#)
- Wolfe, M.S. Structure and Function of the  $\gamma$ -Secretase Complex. *Biochemistry* **2019**, *58*, 2953–2966. [\[CrossRef\]](#)
- Sun, L.; Zhou, R.; Yang, G.; Shi, Y. Analysis of 138 pathogenic mutations in presenilin-1 on the in vitro production of A $\beta$ 42 and A $\beta$ 40 peptides by gamma-secretase. *Proc. Natl. Acad. Sci. USA* **2017**, *114*, E476–E485. [\[CrossRef\]](#)
- Lopera, F. Clinical Features of Early-Onset Alzheimer Disease in a Large Kindred With an E280A Presenilin-1 Mutation. *JAMA* **1997**, *277*, 793. [\[CrossRef\]](#)
- Lalli, M.A.; Cox, H.C.; Arcila, M.L.; Cadavid, L.; Moreno, S.; Garcia, G.; Madrigal, L.; Reiman, E.M.; Arcos-Burgos, M.; Bedoya, G.; et al. Origin of the PSEN1 E280A mutation causing early-onset Alzheimer’s disease. *Alzheimers Dement.* **2014**, *10* (Suppl. S5), S277–S283. [\[CrossRef\]](#)
- Fuller, J.; Cronin-Golomb, A.; Gatchel, J.R.; Norton, D.J.; Guzmán-Vélez, E.; Jacobs, H.; Hanseeuw, B.; Pardilla-Delgado, E.; Artola, A.; Baena, A.; et al. Biological And Cognitive Markers Of Presenilin1 E280a Autosomal Dominant Alzheimer’s Disease: A Comprehensive Review Of The Colombian Kindred. *J. Prev. Alzheimers Dis.* **2019**, *6*, 112–120. [\[CrossRef\]](#)
- Tariot, P.N.; Lopera, F.; Langbaum, J.B.; Thomas, R.G.; Hendrix, S.; Schneider, L.S.; Rios-Romenets, S.; Giraldo, M.; Acosta, N.; Tobon, C.; et al. The Alzheimer’s Prevention Initiative Autosomal-Dominant Alzheimer’s Disease Trial: A study of crenezumab versus placebo in preclinical PSEN1 E280A mutation carriers to evaluate efficacy and safety in the treatment of autosomal-dominant Alzheimer’s disease, including a placebo-treated noncarrier cohort. *Alzheimers Dement.* **2018**, *4*, 150–160.
- Rios-Romenets, S.; Lopera, F.; Sink, K.M.; Hu, N.; Lian, Q.; Guthrie, H.; Smith, J.; Cho, W.; Mackey, H.; Langbaum, J.B.; et al. Baseline demographic, clinical, and cognitive characteristics of the Alzheimer’s Prevention Initiative (API) Autosomal-Dominant Alzheimer’s Disease Colombia Trial. *Alzheimers Dement.* **2020**, *16*, 1023–1030. [\[CrossRef\]](#) [\[PubMed\]](#)
- Quiroz, Y.T.; Sperling, R.A.; Norton, D.J.; Baena, A.; Arboleda-Velasquez, J.F.; Cosio, D.; Schultz, A.; LaPoint, M.; Guzman-Velez, E.; Miller, J.B.; et al. Association Between Amyloid and Tau Accumulation in Young Adults With Autosomal Dominant Alzheimer Disease. *JAMA Neurol.* **2018**, *75*, 548–556. [\[CrossRef\]](#)
- Sanchez, J.S.; Hanseeuw, B.J.; Lopera, F.; Sperling, R.A.; Baena, A.; Bocanegra, Y.; Aguillon, D.; Guzmán-Vélez, E.; Pardilla-Delgado, E.; Ramirez-Gomez, L.; et al. Longitudinal amyloid and tau accumulation in autosomal dominant Alzheimer’s disease: Findings from the Colombia-Boston (COLBOS) biomarker study. *Alzheimers Res. Ther.* **2021**, *13*, 27. [\[CrossRef\]](#)
- Soto-Mercado, V.; Mendivil-Perez, M.; Velez-Pardo, C.; Lopera, F.; Jimenez-Del-Rio, M. Cholinergic-like neurons carrying PSEN1 E280A mutation from familial Alzheimer’s disease reveal in-traneuronal sAPP $\beta$  fragments accumulation, hyperphosphorylation of TAU, oxidative stress, apoptosis and Ca<sup>2+</sup> dysregulation: Therapeutic implications. *PLoS ONE* **2020**, *15*, e0221669. [\[CrossRef\]](#)
- Cummings, J.; Lee, G.; Ritter, A.; Sabbagh, M.; Zhong, K. Alzheimer’s disease drug development pipeline. *Alzheimers Dement.* **2020**, *6*, e12050.
- Soto-Mercado, V.; Mendivil-Perez, M.; Jimenez-Del-Rio, M.; Velez-Pardo, C. Multi-Target Effects of the Cannabinoid CP55940 on Familial Alzheimer’s Disease PSEN1 E280A Cholinergic-Like Neurons: Role of CB1 Receptor. *J. Alzheimers Dis.* **2021**, *82*, S359–S378. [\[CrossRef\]](#) [\[PubMed\]](#)
- Behl, T.; Kaur, I.; Fratila, O.; Brata, R.; Bungau, S. Exploring the Potential of Therapeutic Agents Targeted towards Mitigating the Events Associated with Amyloid- $\beta$  Cascade in Alzheimer’s Disease. *Int. J. Mol. Sci.* **2020**, *21*, 7443. [\[CrossRef\]](#)
- Lakey-Beitia, J.; Burillo, A.M.; La Penna, G.; Hegde, M.L.; Rao, K. Polyphenols as Potential Metal Chelation Compounds Against Alzheimer’s Disease. *J. Alzheimer’s Dis.* **2021**, *82*, S335–S357. [\[CrossRef\]](#) [\[PubMed\]](#)
- Lee, J.-H.; Ahn, N.-H.; Choi, S.-B.; Kwon, Y.; Yang, S.-H. Natural Products Targeting Amyloid Beta in Alzheimer’s Disease. *Int. J. Mol. Sci.* **2021**, *22*, 2341. [\[CrossRef\]](#)



21. Andrich, K.; Bieschke, J. The Effect of (–)-Epigallo-catechin-(3)-gallate on Amyloidogenic Proteins Suggests a Common Mechanism. *Adv. Exp. Med. Biol.* **2015**, *863*, 139–161. [\[CrossRef\]](#)
22. Wu, Y.R.; Choi, H.J.; Kang, Y.G.; Kim, J.K.; Shin, J.-W. In vitro study on anti-inflammatory effects of epigallocatechin-3-gallate-loaded nano- and microscale particles. *Int. J. Nanomed.* **2017**, *12*, 7007–7013. [\[CrossRef\]](#)
23. Pagano, K.; Tomaselli, S.; Molinari, H.; Ragona, L. Natural Compounds as Inhibitors of A $\beta$  Peptide Aggregation: Chemical Requirements and Molecular Mechanisms. *Front. Neurosci.* **2020**, *14*, 619667. [\[CrossRef\]](#)
24. Fernandes, L.; Cardim-Pires, T.R.; Foguel, D.; Palhano, F.L. Green Tea Polyphenol Epigallocatechin-Gallate in Amyloid Aggregation and Neurodegenerative Diseases. *Front. Neurosci.* **2021**, *15*, 718188. [\[CrossRef\]](#) [\[PubMed\]](#)
25. Yan, C.; Zhang, N.; Guan, P.; Chen, P.; Ding, S.; Hou, T.; Hu, X.; Wang, J.; Wang, C. Drug-based magnetic imprinted nanoparticles: Enhanced lysozyme amyloid fibrils cleansing and anti-amyloid fibrils toxicity. *Int. J. Biol. Macromol.* **2020**, *153*, 723–735. [\[CrossRef\]](#) [\[PubMed\]](#)
26. Kaur, S.; Bansal, Y.; Kumar, R.; Bansal, G. A panoramic review of IL-6: Structure, pathophysiological roles and inhibitors. *Bioorganic Med. Chem.* **2020**, *28*, 115327. [\[CrossRef\]](#)
27. González-Reyes, R.E.; Nava-Mesa, M.O.; Vargas-Sánchez, K.; Ariza-Salamanca, D.; Mora-Muñoz, L. Involvement of Astrocytes in Alzheimer's Disease from a Neuroinflammatory and Oxidative Stress Perspective. *Front. Mol. Neurosci.* **2017**, *10*, 427. [\[CrossRef\]](#) [\[PubMed\]](#)
28. Perez-Nieves, B.G.; Serrano-Pozo, A. Deciphering the Astrocyte Reaction in Alzheimer's Disease. *Front. Aging Neurosci.* **2018**, *10*, 114. [\[CrossRef\]](#) [\[PubMed\]](#)
29. Quintero-Espinosa, D.; Soto-Mercado, V.; Quintero-Quinchia, C.; Mendivil-Perez, M.; Velez-Pardo, C.; Jimenez-Del-Rio, M. Latent Tri-lineage Potential of Human Menstrual Blood-Derived Mesenchymal Stromal Cells Revealed by Specific In Vitro Culture Conditions. *Mol. Neurobiol.* **2021**, *58*, 5194–5209. [\[CrossRef\]](#)
30. Carrero, I.; Gonzalo, M.R.; Martin, B.; Sanz-Anquela, J.M.; Arevalo-Serrano, J.; Gonzalo-Ruiz, A. Oligomers of  $\beta$ -amyloid protein (A $\beta$ 1–42) induce the activation of cyclooxygenase-2 in astrocytes via an interaction with interleukin-1 $\beta$ , tumour necrosis factor- $\alpha$ , and a nuclear factor  $\kappa$ -B mechanism in the rat brain. *Exp. Neurol.* **2012**, *236*, 215–227. [\[CrossRef\]](#)
31. Mendivil-Perez, M.; Velez-Pardo, C.; Jimenez-Del-Rio, M. Direct transdifferentiation of human Wharton's jelly mesenchymal stromal cells into cholinergic-like neurons. *J. Neurosci. Methods* **2018**, *312*, 126–138. [\[CrossRef\]](#) [\[PubMed\]](#)
32. Armijo, E.; Gonzalez, C.; Shah Nawaz, M.; Flores, A.; Davis, B.; Soto, C. Increased susceptibility to A $\beta$  toxicity in neuronal cultures derived from familial Alzheimer's disease (PSEN1-A246E) induced pluripotent stem cells. *Neurosci. Lett.* **2017**, *639*, 74–81. [\[CrossRef\]](#)
33. Pap, P.; Kőszeghy, A.; Szűcs, G.; Rusznák, Z. Cytoplasmic Ca<sup>2+</sup> concentration changes evoked by cholinergic stimulation in primary astrocyte cultures prepared from the rat cochlear nucleus. *Hear. Res.* **2009**, *255*, 73–83. [\[CrossRef\]](#) [\[PubMed\]](#)
34. Sekiguchi-Tonosaki, M.; Obata, M.; Haruki, A.; Himi, T.; Kosaka, J. Acetylcholine induces Ca<sup>2+</sup> signaling in chicken retinal pigmented epithelial cells during dedifferentiation. *Am. J. Physiol. Cell Physiol.* **2009**, *296*, C1195–C1206. [\[CrossRef\]](#)
35. Lazic, S.E.; Clarke-Williams, C.J.; Munafo, M.R. What exactly is 'N' in cell culture and animal experiments? *PLoS Biol.* **2018**, *16*, e2005282. [\[CrossRef\]](#)
36. Colombo, E.; Farina, C. Astrocytes: Key Regulators of Neuroinflammation. *Trends Immunol.* **2016**, *37*, 608–620. [\[CrossRef\]](#)
37. Palhano, F.L.; Lee, J.; Grimster, N.P.; Kelly, J.W. Toward the Molecular Mechanism(s) by Which EGCG Treatment Remodels Mature Amyloid Fibrils. *J. Am. Chem. Soc.* **2013**, *135*, 7503–7510. [\[CrossRef\]](#)
38. Fernandes, L.; Messias, B.; Pereira-Neves, A.; Azevedo, E.P.; Araújo, J.; Foguel, D.; Palhano, F.L. Green Tea Polyphenol Microparticles Based on the Oxidative Coupling of EGCG Inhibit Amyloid Aggregation/Cytotoxicity and Serve as a Platform for Drug Delivery. *ACS Biomater. Sci. Eng.* **2020**, *6*, 4414–4423. [\[CrossRef\]](#) [\[PubMed\]](#)
39. Sonawane, S.K.; Chidambaram, H.; Boral, D.; Gorantla, N.V.; Balmik, A.A.; Dangi, A.; Ramasamy, S.; Marelli, U.K.; Chinnathambi, S. EGCG impedes human Tau aggregation and interacts with Tau. *Sci. Rep.* **2020**, *10*, 12579. [\[CrossRef\]](#)
40. Andrich, K.; Hegenbart, U.; Kimmich, C.; Kedia, N.; Bergen, H.R.; Schönland, S.; Wanker, E.; Bieschke, J. Aggregation of Full-length Immunoglobulin Light Chains from Systemic Light Chain Amyloidosis (AL) Patients Is Remodeled by Epigallocatechin-3-gallate. *J. Biol. Chem.* **2017**, *292*, 2328–2344. [\[CrossRef\]](#)
41. Zhang, T.; Zhang, J.; Derreumaux, P.; Mu, Y. Molecular mechanism of the inhibition of EGCG on the Alzheimer A $\beta$ (1–42) dimer. *J. Phys. Chem. B* **2013**, *117*, 3993–4002. [\[CrossRef\]](#) [\[PubMed\]](#)
42. Ngo, S.T.; Truong, D.T.; Tam, N.M.; Nguyen, M.T. EGCG inhibits the oligomerization of amyloid beta (16–22) hexamer: Theoretical studies. *J. Mol. Graph. Model.* **2017**, *76*, 1–10. [\[CrossRef\]](#) [\[PubMed\]](#)
43. Acharya, A.; Stockmann, J.; Beyer, L.; Rudack, T.; Nabers, A.; Gumbart, J.C.; Gerwert, K.; Batista, V.S. The Effect of (–)-Epigallocatechin-3-Gallate on the Amyloid- $\beta$  Secondary Structure. *Biophys. J.* **2020**, *119*, 349–359. [\[CrossRef\]](#) [\[PubMed\]](#)
44. Shimmyo, Y.; Kihara, T.; Akaike, A.; Niidome, T.; Sugimoto, H. Epigallocatechin-3-gallate and curcumin suppress amyloid beta-induced beta-site APP cleaving enzyme-1 upregulation. *Neuroreport* **2008**, *19*, 1329–1333. [\[CrossRef\]](#) [\[PubMed\]](#)
45. Guéroux, M.; Fleau, C.; Slozeck, M.; Laguerre, M.; Pianet, I. Epigallocatechin 3-Gallate as an Inhibitor of Tau Phosphorylation and Aggregation: A Molecular and Structural Insight. *J. Prev. Alzheimers Dis.* **2017**, *4*, 218–225.
46. He, J.; Xu, L.; Yang, L.; Wang, X. Epigallocatechin Gallate Is the Most Effective Catechin against Antioxidant Stress via Hydrogen Peroxide and Radical Scavenging Activity. *Med. Sci. Monit.* **2018**, *24*, 8198–8206. [\[CrossRef\]](#)

47. Guo, Q.; Zhao, B.; Shen, S.; Hou, J.; Hu, J.; Xin, W. ESR study on the structure–antioxidant activity relationship of tea catechins and their epimers. *Biochim. Biophys. Acta (BBA) Gen. Subj.* **1999**, *1427*, 13–23. [[CrossRef](#)]
48. Valcic, S.; Muders, A.; Jacobsen, N.E.; Liebler, D.C.; Timmermann, B.N. Antioxidant chemistry of green tea catechins. Identification of products of the reaction of (–)-epigallocatechin gallate with peroxy radicals. *Chem. Res. Toxicol.* **1999**, *12*, 382–386. [[CrossRef](#)]
49. Pal, S.; Dey, S.K.; Saha, C. Inhibition of Catalase by Tea Catechins in Free and Cellular State: A Biophysical Approach. *PLoS ONE* **2014**, *9*, e102460. [[CrossRef](#)]
50. de Oliveira, M.R.; Nabavi, S.F.; Daglia, M.; Rastrelli, L.; Nabavi, S.M. Epigallocatechin gallate and mitochondria—A story of life and death. *Pharmacol. Res.* **2016**, *104*, 70–85. [[CrossRef](#)]
51. Yao, K.; Ye, P.; Zhang, L.; Tan, J.; Tang, X.; Zhang, Y. Epigallocatechin gallate protects against oxidative stress-induced mitochondria-dependent apoptosis in human lens epithelial cells. *Mol. Vis.* **2008**, *14*, 217–223. [[PubMed](#)]
52. Srividhya, R.; Kalaiselvi, P. Neuroprotective potential of epigallocatechin-3-gallate in PC-12 cells. *Neurochem. Res.* **2012**, *38*, 486–493. [[CrossRef](#)]
53. Koh, S.-H.; Kim, S.H.; Kwon, H.; Park, Y.; Kim, K.S.; Song, C.W.; Kim, J.; Kim, M.-H.; Yu, H.-J.; Henkel, J.S.; et al. Epigallocatechin gallate protects nerve growth factor differentiated PC12 cells from oxidative-radical-stress-induced apoptosis through its effect on phosphoinositide 3-kinase/Akt and glycogen synthase kinase-3. *Mol. Brain Res.* **2003**, *118*, 72–81. [[CrossRef](#)]
54. Jimenez-Del-Rio, M.; Velez-Pardo, C. Alzheimer’s Disease, *Drosophila melanogaster* and Polyphenols. *Adv. Exp. Med. Biol.* **2015**, *863*, 21–53. [[CrossRef](#)]
55. Galluzzi, L.; Vitale, I.; Aaronson, S.A.; Abrams, J.M.; Adam, D.; Agostinis, P.; Alnemri, E.S.; Altucci, L.; Amelio, I.; Andrews, D.W.; et al. Molecular mechanisms of cell death: Recommendations of the Nomenclature Committee on Cell Death. *Cell Death Differ.* **2018**, *25*, 486–541. [[CrossRef](#)]
56. Ju, Y.; Asahi, T.; Sawamura, N. Arctic mutant Aβ40 aggregates on α7 nicotinic acetylcholine receptors and inhibits their functions. *J. Neurochem.* **2014**, *131*, 667–674. [[CrossRef](#)] [[PubMed](#)]
57. Liu, T.; Zhang, L.; Joo, D.; Sun, S.C. NF-κB signaling in inflammation. *Signal Transduct. Target. Ther.* **2017**, *2*, 17023. [[CrossRef](#)] [[PubMed](#)]
58. Zhang, S.; Zhu, Q.; Chen, J.Y.; OuYang, D.; Lu, J.H. The pharmacological activity of epigallocatechin-3-gallate (EGCG) on Alzheimer’s disease animal model: A systematic review. *Phytomedicine* **2020**, *79*, 153316. [[CrossRef](#)]
59. Hu, J.; Webster, D.; Cao, J.; Shao, A. The safety of green tea and green tea extract consumption in adults—Results of a systematic review. *Regul. Toxicol. Pharmacol.* **2018**, *95*, 412–433. [[CrossRef](#)] [[PubMed](#)]
60. Cascella, M.; Bimonte, S.; Muzio, M.R.; Schiavone, V.; Cuomo, A. The efficacy of Epigallocatechin-3-gallate (green tea) in the treatment of Alzheimer’s disease: An overview of pre-clinical studies and translational perspectives in clinical practice. *Infect. Agents Cancer* **2017**, *12*, 36. [[CrossRef](#)]
61. Hoyos-Ceballos, G.P.; Sánchez-Giraldo, V.; Mendivil-Perez, M.; Jimenez-Del-Rio, M.; Sierra-Garcia, L.; Vélez-Pardo, C.; López-Osorio, B.L. Design of epigallocatechin gallate loaded PLGA/PF127 nanoparticles and their effect upon an oxidative stress model. *J. Drug Deliv. Sci. Technol.* **2018**, *48*, 152–160. [[CrossRef](#)]
62. Sánchez-Giraldo, V.; Monsalve, Y.; Palacio, J.; Mendivil-Perez, M.; Sierra, L.; Velez-Pardo, C.; López, B.L.; Jiménez-Del-Rio, M. Role of a novel (–)-epigallocatechin-3-gallate delivery system on the prevention against oxidative stress damage in vitro and in vivo model of Parkinson’s disease. *J. Drug Deliv. Sci. Technol.* **2020**, *55*, 101466. [[CrossRef](#)]
63. Ding, S.; Khan, A.I.; Cai, X.; Song, Y.; Lyu, Z.; Du, D.; Dutta, P.; Lin, Y. Overcoming blood–brain barrier transport: Advances in nanoparticle-based drug delivery strategies. *Mater. Today* **2020**, *37*, 112–125. [[CrossRef](#)] [[PubMed](#)]

# Neuroprotective Effect of Combined Treatment with Epigallocatechin 3-Gallate and Melatonin on Familial Alzheimer's Disease *PSEN1 E280A* Cerebral Spheroids Derived from Menstrual Mesenchymal Stromal Cells

Viviana Soto-Mercado, Miguel Mendivil-Perez, Carlos Velez-Pardo\* and Marlene Jimenez-Del-Rio\*  
*Neuroscience Research Group, Medical Research Institute, Faculty of Medicine, University of Antioquia, SIU Medellin, Colombia*

Accepted 18 January 2023  
Pre-press 24 February 2023

## Abstract.

**Background:** Familial Alzheimer's disease (FAD) is caused by mutations in one or more of 3 genes known as *AβPP*, *PSEN1*, and *PSEN2*. There are currently no effective therapies for FAD. Hence, novel therapeutics are needed.

**Objective:** To analyze the effect of treatment with a combination of epigallocatechin-3-gallate (EGCG) and Melatonin (N-acetyl-5-methoxytryptamine, aMT) in a cerebral spheroid (CS) 3D *in vitro* model of *PSEN1 E280A* FAD.

**Methods:** We developed a CS *in vitro* model based on menstrual stromal cells derived from wild-type (WT) and mutant *PSEN1 E280A* menstrual blood cultured in *Fast-N-Spheres V2* medium.

**Results:** Beta-tubulin III, choline acetyltransferase, and GFAP in both WT and mutant CSs spontaneously expressed neuronal and astroglia markers when grown in *Fast-N-Spheres V2* medium for 4 or 11 days. Mutant *PSEN1* CSs had significantly increased levels of intracellular AβPP fragment peptides and concomitant appearance of oxidized DJ-1 as early as 4 days, and phosphorylated tau, decreased  $\Delta\Psi_m$ , and increased caspase-3 activity were observed on Day 11. Moreover, mutant CSs were unresponsive to acetylcholine. Treatment with a combination of EGCG and aMT decreased the levels of all typical pathological markers of FAD more efficiently than did EGCG or aMT alone, but aMT failed to restore  $Ca^{2+}$  influx in mutant CSs and decreased the beneficial effect of EGCG on  $Ca^{2+}$  influx in mutant CSs.

**Conclusion:** Treatment with a combination of EGCG and aMT can be of high therapeutic value due to the high antioxidant capacity and anti-amyloidogenic effect of both compounds.

**Keywords:** Alzheimer's disease, cerebral spheroids, E280A, (-) epigallocatechin 3-gallate, melatonin, menstrual mesenchymal stromal cell, mutation, presenilin

\*Correspondence to: Marlene Jimenez-Del-Rio and Carlos Velez-Pardo, Neuroscience Research Group, Medical Research Institute, Faculty of Medicine, University of Antioquia (UdeA), Calle 70 No. 52-21, and Calle 62 #52-59, Building 1,

Room 412; SIU Medellin, Colombia. E-mails: marlene.jimenez@udea.edu.co, and calberto.velez@udea.edu.co; ORCID: 0000-0003-3477-2386, 0000-0002-0557-0411.

## INTRODUCTION

Familial Alzheimer's disease (FAD) is caused by mutations in one or more of at least three genes known as amyloid- $\beta$  protein precursor (*A $\beta$ PP*), presenilin 1 (*PSEN1*), and presenilin 2 (*PSEN2*) (<https://www.alzforum.org/mutations>). A $\beta$ PP, a transmembrane protein, is cleaved to form amyloidogenic A $\beta$  peptides (mostly A $\beta_{42}$ ), and presenilin, a subunit of  $\gamma$ -secretase, is the aspartyl protease responsible for A $\beta_{42}$  generation [1]. To date, 350 different *PSEN1* mutations have been reported to cause FAD (<https://www.alzforum.org/mutations/psen-1>). A missense mutation at position 73664808 on chromosome 14, A>C (codon change: GAA to GCA, exon 8), results in a change in *PSEN1* Glu280Ala (p. E280A) [2]. This mutation has been shown to cause familial early onset Alzheimer's disease (EOAD) in a large family in Colombia [3]. The *PSEN1* E280A mutation results in the production of extracellular plaques consisting of A $\beta_{42}$  [4, 5], loss of hippocampal neurons [6], and accumulation and hyperphosphorylation of tau protein (p-tau) [7, 8] and also induces cerebellar A $\beta$  plaque deposition [9]. Of note, the "paisa" E280A mutation provokes accumulation of A $\beta$  plaque in cognitively unaffected carriers of the *PSEN1* E280A mutation ten years before autosomal dominant FAD is clinically detectable [10]. Unfortunately, although clinical trials of investigational disease-modifying drugs that target A $\beta$  have been conducted (ClinicalTrials.gov, NCT01998841) [11], no effective therapies against FAD have become available. Hence, innovative therapeutic approaches are currently needed.

Mesenchymal stromal cells (MSCs) are multipotent cells that have the potential to differentiate into mesodermal, endodermal, or ectodermal cell lineages [12, 13]. Therefore, MSCs are not only important for modeling FAD [14] but are also useful in the assessment of potential therapeutic methodologies (e.g., [15]). Given that MSCs can be obtained from menstrual blood (MensB) without bioethical constraints and/or increasing the likelihood of tumor formation [16], these cells have surfaced as a source for 3D *in vitro* modeling [17, 18] and a potential source for AD treatment [19]. Accordingly, we used menstrual stromal cells (MenSCs) from MensB to obtain cerebral spheroids (CSs), i.e., free-floating spherical conglomerates, within 4 days [20] by growth of the cells in *Fast-N-Spheres* medium [21]. However, there is no further information at present regarding whether MenSCs that carry the *PSEN1* E280A muta-

tion can generate CSs or regarding whether they are able to reproduce the classical neuropathological features of FAD, i.e., accumulation of intracellular A $\beta$ PP fragments (iA $\beta$ PPf), oxidative stress (OS), and tau phosphorylation (p-tau), as has been demonstrated in a 2D *in vitro* model [22].

We recently showed that epigallocatechin-3-gallate (EGCG) represses the accumulation of iA $\beta$ PPf, blocks tau phosphorylation, enhances mitochondrial membrane potential ( $\Delta\Psi_m$ ), decreases oxidation of the stress sensor protein DJ-1 (oxDJ-1), and inhibits the expression of cell death markers (e.g., c-JUN, TP53, PUMA, and CASP3) in *PSEN1* E280A cholinergic-like neurons (ChLNs) compared to wild-type (WT) cells in 2D *in vitro*. Although EGCG did not significantly reduce extracellular (e)A $\beta_{42}$  (although it decreased aggregation of eA $\beta_{42}$ ), it significantly inhibited Ca<sup>2+</sup> influx impairment in response to acetylcholine (ACh) in *PSEN1* E280A ChLNs [23]. Melatonin (N-acetyl-5-methoxytryptamine, aMT), a hormone that possesses antioxidant activity [24], has been found to alleviate OS [25], A $\beta$  accumulation [26, 27], tau pathology [28], and decreased mitochondrial dysfunction [29] by acting as a neuroprotectant [30]. However, it is unknown whether aMT protects *PSEN1* E280A CSs from endogenously generated iA $\beta$ PPf, tau phosphorylation, OS, apoptosis, or Ca<sup>2+</sup> influx dysfunctionality. We hypothesize that single or combined treatment with EGCG and confers neuroprotection against A $\beta$ -induced pathology in a 3D *in vitro* model of FAD.

Here, we wanted to examine whether *PSEN1* E280A MenSCs differentiate into CSs when cultured in *Fast-N-Spheres* V2 medium, a novel medium that was originally developed and named in our laboratory, and to determine whether treatment with EGCG and/or aMT alone or in combination decreases the levels of pathological markers in *PSEN1* E280A CSs. Similar to 2D cultured cells, mutant MenSCs can be converted into *PSEN1* E280A CSs by growth in *Fast-N-Spheres* V2 medium for 4 or 11 days. The *PSEN1* E280A CSs, but not WT *PSEN1* CSs, showed signs of increased accumulation of iA $\beta$ PPf (detected using antibody E610) and increased phosphorylation of tau at Ser<sup>202</sup>/Thr<sup>205</sup> (detected using antibody AT8). Mutant CSs, but not WT CSs, molecularly mimic FAD. *PSEN1* E280A CSs displayed signs of OS as early as 4 days, as demonstrated by the appearance of DJ-1Cys<sup>106</sup>-SO<sub>3</sub> and of apoptotic markers such as caspase 3 (CASP3), and concomitant loss of  $\Delta\Psi_m$ ; however, CSs contained p-tau at Day 11. Mutant

CSs also showed  $\text{Ca}^{2+}$  flux dysregulation compared to control (WT) CSs. Interestingly, exposure of the cells to EGCG and aMT alone or in combination decreased OS and the expression of apoptotic markers, increased  $\Delta\Psi_m$ , and blocked p-tau in *PSEN1 E280A* CSs. However, EGCG was much more efficient at reversing  $\text{Ca}^{2+}$  influx dysregulation in *PSEN1 E280A* CSs than was aMT alone or the combination of EGCG/aMT. Our findings demonstrate that EGCG is by far the most efficient neuroprotective agent against endogenously generated pathological iA $\beta$ PPf, OS, and p-tau in *PSEN1*-derived CSs. Combined treatment with EGCG and aMT can be of high therapeutic value in alleviating endogenously generated oxidative stress elicited by iA $\beta$ PPf in mutant neurons.

## MATERIALS AND METHODS

### *Isolation and characterization of MenSCs derived from human MensB*

The MensB samples were collected from one healthy female and one female carrier of the mutation *PSEN1 E280A* aged 30 years (Tissue Bank Code, TBC # 69308) and 25 years (TBC # 04335), respectively. Donors signed an informed consent accepted by the Ethics Committee of the Sede de Investigación Universitaria -SIU-, University of Antioquia, Medellín, Colombia. The specimens (MensB) were collected, purified, and maintained as previously described in [20]. The isolated MenSCs were used for the generation of cerebral spheroids [20].

Ethical Approval Menstrual specimen donors provided a signed informed consent approved by the ethics committee of the Sede de Investigación Universitaria (SIU), University of Antioquia, Medellín, Colombia (Act 2020-10854).

### *Generation of cerebral spheroids derived from MensB-MenSCs and induced to cholinergic-like neuronal cell lineage*

CSs were obtained by differentiation of WT or *PSEN1 E280A* MenSCs as previously described in [20]. Briefly, WT and mutant MenSCs were cultured in a brand-new medium called *Fast-N-Spheres V2* composed of serum-free culture medium containing reagents as described in [20] plus Matrigel® and 1% fetal bovine serum. Cultures were constantly shaken for 4 and 11 days. The MenSCs-derived CSs were

examined for the expression of neuronal and astrocyte markers according to [20].

### *Immunofluorescence and fluorescence microscopy analysis*

The WT or *PSEN1 E280A* CSs cultured with *Fast-N-Spheres V2* medium for 4 and 11 days without or with EGCG (25  $\mu\text{M}$ ) and/or melatonin (50  $\mu\text{M}$ ) were stained with primary antibodies against the glial fibrillary acidic protein (GFAP, cat. no. sc6170, Santa Cruz),  $\beta$ -tubulin III ( $\beta$ -TUB III cat. no. G712A, Promega), choline acetyltransferase (ChAT, cat. no. AB144P, Millipore) primary antibodies (1:500); primary antibodies against APP751 and/or protein amyloid  $\beta$ 1–42 (1:500; clone 6E10 cat# 803014, Biogen), oxidized DJ-1 (1:500; ox(Cys<sup>106</sup>)DJ-1; spanning residue Cys<sup>106</sup> of human PARK7/DJ1; oxidized to produce cysteine sulfonic ( $\text{SO}_3$ ) acid; cat # ab169520, Abcam), and total tau (1:500; t-Tau; cat# T6402, Sigma), and phospho-tau (p-tau, 1:500, Ser<sup>202</sup>/Thr<sup>205</sup>, cat# MN1020 (AT8), Thermo Fisher Scientific) antibodies. Incubation with secondary fluorescent antibodies and nuclei staining were performed according to [20]. Fluorescent Thioflavin-T derivative BTA-1 staining was performed by incubating CSs slides with a BTA-1 (Sigma) solution (500 nM) for 30 min. Nuclei were identified by incubating CSs with propidium iodide (1  $\mu\text{M}$ ). Postmortem temporal cortical slices from an Alzheimer's disease patient (case #3396) and a healthy individual (case #3648) were used as a positive and negative control, respectively [31]. Imaging processing data was performed according to an online guidance program (<https://imagej.nih.gov/ij/>).

### *Live fluorescence analysis*

The WT or *PSEN1 E280A* CSs cultured with *Fast-N-Spheres V2* medium for 11 days without or with EGCG (25  $\mu\text{M}$ ) and/or melatonin (50  $\mu\text{M}$ ) were incubated with (20 nM) MitoTracker™ Red FM (cat. no. M22425, Invitrogen) and 1X Vybrant TM FLICA (Thermo Fisher Scientific, cat: V35118) according to [20]. Fluorescence microscopy photographs were taken using a Zeiss AxioStart 50 Fluorescence Microscope equipped with a Zeiss AxioCam Cm1 (Zeiss Wöhlk-Contact-Linsfluoreen, Gmb Schöckirchen, Germany), and imaging processing data was performed according to an online guidance program (<http://imagej.nih.gov/ij/>).



### Flow cytometry analysis

Flow cytometry analysis was performed according to [32] with minor modifications. Briefly, the WT or *PSEN1 E280A* CSs cultured with *Fast-N-Spheres* V2 medium for 11 days without or with EGCG (25  $\mu$ M) and/or melatonin (50  $\mu$ M) were detached with Accutase Cell Detachment Solution (Beckton Dickinson) and washed in PBS. Cells ( $10 \times 10^5$ ) were resuspended in PBS and fixated with cold ethanol overnight and used for further flow cytometry analysis. Cell markers were analyzed by incubating cells with primary antibodies against caspase-3 (1:250; cat # AB3623, Millipore), APP751 and/or protein amyloid- $\beta$ 1-42 (1:500; clone 6E10 cat# 803014, Biolegend), oxidized DJ-1 (1:500; ox(Cys<sup>106</sup>)DJ-1; spanning residue Cys<sup>106</sup> of human PARK7/DJ1; oxidized to produce cysteine sulfonic (SO<sub>3</sub>) acid; cat # ab169520, Abcam), and total tau (1:500; t-Tau; cat# T6402, Sigma), and phospho-tau (p-tau, 1:500, Ser<sup>202</sup>/Thr<sup>205</sup>, cat# MN1020 (AT8), Thermo Fisher Scientific) antibodies, followed incubation with secondary fluorescent antibodies according to [23]. Resuspended cells were analyzed using BD LSR Fortessa II flow cytometer (BD Biosciences). Ten thousand events were acquired, and the acquisition analysis was performed using FlowJo 7.6.2 Data Analysis Software.

### Cytochemical detection of DNA fragmentation

DNA fragmentation was determined in fixed untreated or treated CSs to polylysine coated slides by the terminal deoxynucleotidyl transferase dUTP nick end labeling (TUNEL) technique according to the manufacturer's protocol (Promega catalog #G7130). Briefly, CSs samples were treated for 10 min with 25  $\mu$ g/ml protease K and fixed in 4% methanol in PBS for 5 min. CSs slides were pre-incubated with equilibration buffer (EB) (50  $\mu$ l, 200 mM potassium cacodylate, pH 6.5; 25 mM Tris-HCl pH 6.6; 0.2 mM DTT; 0.25 mg/ml BSA; 2.5 mM cobalt chloride) for 15 min. Then, slides were incubated at 37°C for 60 min with 25  $\mu$ l TdT incubation buffer (23  $\mu$ l EB; 2  $\mu$ l nucleotide mix; 0.5  $\mu$ l TdT enzyme). After the appropriate incubation time, tailing reaction was terminated by immersing the slides in 2X SSC for 15 min and rinsing twice with PBS. Then after, slides were incubated with streptavidin HRP (diluted 1:500 in PBS) for 30 min at room temperature. Finally, slides were incubated with DAB solution (prepared immediately prior to use by adding 100  $\mu$ l DAB 10X

Chromogen to 900  $\mu$ l DAB Substrate 1X Buffer). Slides were stained with safranin for 10 s at room temperature and washed twice in deionized water. Immediately, slides were coverslipped using aqueous mounting media.

### Oxygen radical absorbance capacity (ORAC) assay

The hydrophilic ORAC assay was performed as described in [33]. The AAPH (2,2'-Azobis(2-amidinopropane) dihydrochloride) was used as a peroxy radical generator, Trolox was used as a standard, and fluorescein was used as the fluorescent probe. Briefly, fluorescein, AAPH, and the samples were prepared in a phosphate buffer (75 mM, pH 7.4). First, 25  $\mu$ L of sample solution or Trolox standard was mixed with 150  $\mu$ L of fluorescein (1 mM) and pre-incubated at 37°C for 30 min before the addition of 25  $\mu$ L of AAPH solution (200 mM). The fluorescence at an excitation wavelength of 485 nm and an emission wavelength of 520 nm was measured every 2 min for 120 min using a Synergy HT Multi-Mode Microplate Reader (BioTek Instruments, Inc.; Winooski, USA). The relative ORAC values were calculated using the differences of areas under the decay curves and were expressed as  $\mu$ mol Trolox equivalents (TE)/g of solution.

### Intracellular calcium imaging

The cytoplasmic Ca<sup>2+</sup> concentration ([Ca<sup>2+</sup>]<sub>i</sub>) was measured according to Pap et al. [34]. Fluorescence microscopy photographs were taken using a Zeiss AxioStart 50 Fluorescence Microscope equipped with a Zeiss AxioCam Cm1 (Zeiss Wöhlk-Contact-Linsfluoreen, Gmb Schöckirchen, Germany), and imaging processing data was performed according to online guidance program (<http://imagej.nih.gov/ij/>) [35].

### Data analysis

This experimental design was performed as previously reported in [20] and based on the statistics considerations described in [36]. Provided that the experimental unit (i.e., the well) data fulfill the independence of observations, the dependent variable is normally distributed in each treatment group (Shapiro-Wilk test), and variances are homogeneous (Levene's test), the statistical significance was deter-

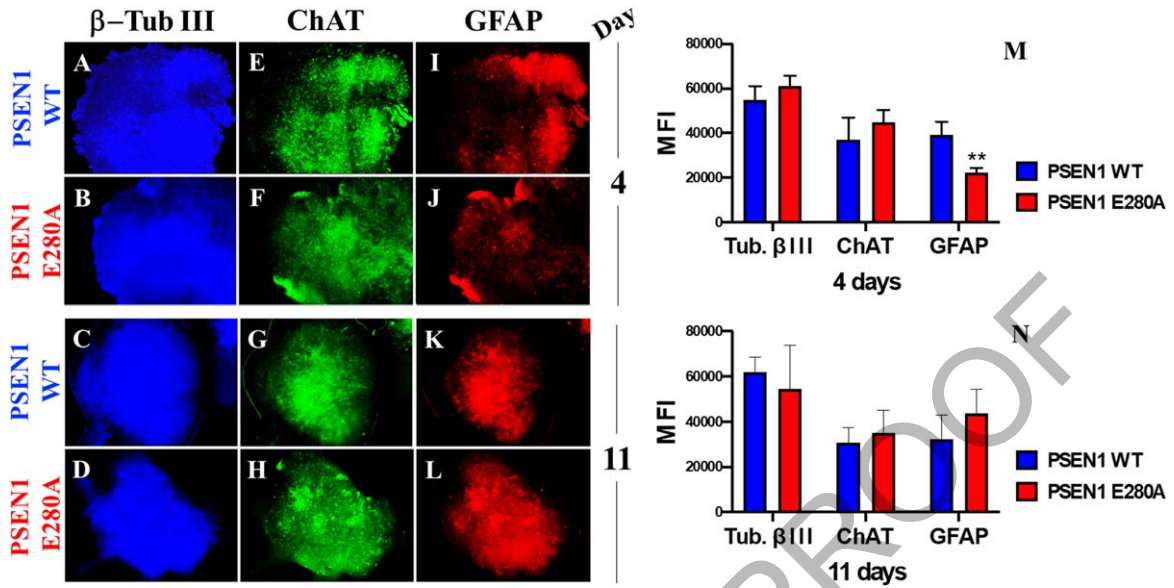


Fig. 1. MenSCs-derived CSs show cholinergic and astrocytic marker. After 4 and 11 days, WT *PSEN1* and *PSEN1* E280A CSs were triple-stained as indicated in the figure with primary antibodies against  $\beta$ -TUB III (blue; A–D), ChAT (green; E–H), and GFAP (red; I–L). M) Mean fluorescence intensity (MFI) quantification of images obtained by immunofluorescence analysis on day 4. N) MFI quantification of images obtained by immunofluorescence analysis on day 11. Images represent one out of three independent experiments. Statistical significance was determined by one-way ANOVA with a Tukey *post hoc* test; \*\* $p < 0.01$ . Image magnification 10x.

mined by Student's *t*-test, one-way, or two-way ANOVA followed by Bonferroni's or Tukey's *post hoc* comparison calculated with GraphPad Prism 5.0 software. Differences between groups were only deemed significant when a *p*-value of  $<0.05$  (\*),  $<0.001$  (\*\*), and  $<0.001$  (\*\*\*). All data are illustrated as the mean  $\pm$  S.D.

## RESULTS

### *PSEN1* E280A CSs spontaneously express cholinergic and astrocytic markers

Previous work has shown that WT CSs derived from MensB spontaneously express neuronal markers such as  $\beta$ -TUB III and ChAT, as well as the astrocyte marker GFAP, when cultured in *Fast-N-Spheres* medium for 3 days [20]. Likewise, WT and *PSEN1* E280A CSs showed similar expression of neuronal ( $\beta$ -TUB III, Fig. 1A–D), cholinergic (ChAT, Fig. 1E–H), and astrocytic (GFAP, Fig. 1I–L) lineage cell markers when grown in *Fast-N-Spheres* V2 medium for 4 (Fig. 1M) or 11 days (Fig. 1N).

### *PSEN1* E280A CSs show an early increase in iA $\beta$ PPf and OS

Next, we wanted to determine whether CSs express the typical neuropathological features of AD, such as A $\beta$  and OS. Figure 2 shows that WT NS displayed neither iA $\beta$ PPf accumulation (Fig. 2A, C) nor OS markers (Fig. 2E, G), as reflected by the absence of iA $\beta$ PPf (Fig. 2M, N), oxidized protein DJ-1 (Fig. 2M, N) and nuclear-positive cells (Fig. 2I–L). In contrast, *PSEN1* E280A CSs displayed enhanced iA $\beta$ PPf (Fig. 2B, D, M, N) and oxidation of protein DJ-1 (Fig. 2F, H, M, N) as early as 4 days in culture (Fig. 2M, N).

### *PSEN1* E280A CSs present hyperphosphorylation of tau protein

It is well established that phosphorylation of tau occurs downstream of A $\beta$  pathology in AD [37, 38]. Therefore, we assessed whether tau is phosphorylated in a time-dependent manner in mutant CSs. As shown in Fig. 3, no p-tau was observed in WT CSs (Fig. 3A, C) on Days 4 or 11, whereas p-tau was detected in *PSEN1* E280A CSs only on Day 11 (Fig. 3B versus

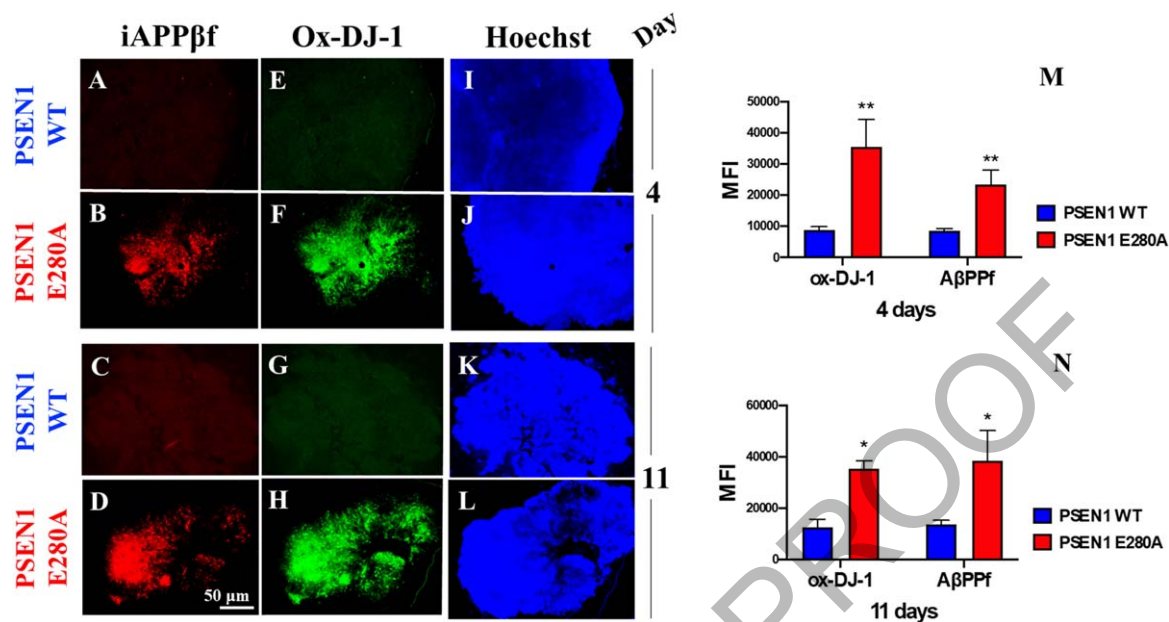


Fig. 2. *PSEN1 E280A* cerebral spheroids (CSs) accumulate intracellular AβPP fragments (iAβPPf) and oxidized (Cys<sup>106</sup>) DJ-1 protein (Ox-DJ-1). After 4 and 11 days, WT *PSEN1* and *PSEN1 E280A* CSs were double-stained as indicated in the figure with primary antibodies against (i)AβPPf (red; A–D) and Ox-DJ-1 (green; E–H). Nuclei were stained with Hoechst (blue; I–L). M) Mean fluorescence intensity (MFI) quantification of images obtained by immunofluorescence analysis on day 4. N) MFI quantification of images obtained by immunofluorescence analysis on day 11. Images represent one out of three independent experiments. Statistical significance was determined by one-way ANOVA with a Tukey *post hoc* test; \**p* < 0.05; \*\**p* < 0.01. Image magnification 10x.

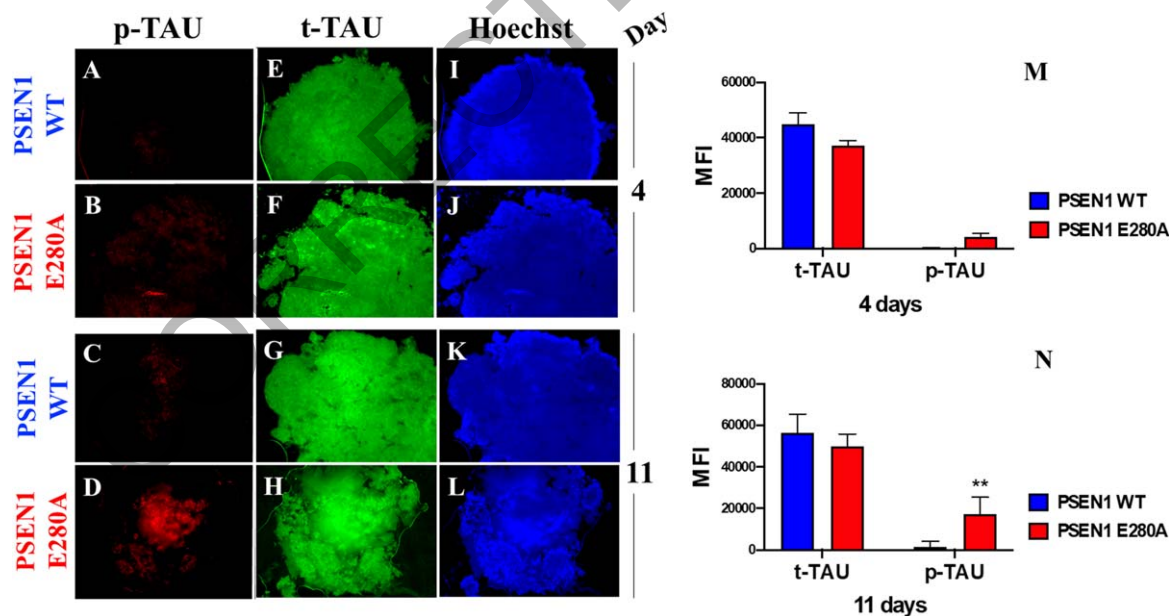


Fig. 3. *PSEN1 E280A* cerebral spheroids (CSs) show hyperphosphorylation of protein tau. After 4 and 11 days, WT *PSEN1* and *PSEN1 E280A* CSs were double-stained as indicated in the figure with primary antibodies against phosphorylated (Ser<sup>202</sup>/Thr<sup>205</sup>) Tau (p-Tau) (red; A–D) and total Tau (t-Tau) (green; E–H). Nuclei were stained with Hoechst (blue; I–L). M) Mean fluorescence intensity (MFI) quantification of images obtained by immunofluorescence analysis on day 4. N) MFI quantification of images obtained by immunofluorescence analysis on day 11. Images represent one out of three independent experiments. Statistical significance was determined by one-way ANOVA with a Tukey *post hoc* test; \*\**p* < 0.01. Image magnification 10x.

Fig. 3D and 3M versus 3N). Total tau was measured and used for protein normalization (Fig. 3E–H), and Hoechst staining was used to analyze the organoid cellularity (Fig. 3I–L).

*PSEN1 E280A CSs show diminished  $\Delta\Psi_m$ , caspase 3 activity, and fragmented nuclei*

We then wondered whether *PSEN1 E280A* CSs show endogenous alterations in  $\Delta\Psi_m$ , active CASP-3 and nuclear fragmentation similar to those demonstrated in 2D *PSEN1 E280A* human umbilical cord Wharton Jelly mesenchymal stromal cell-derived ChLNs [22]. Figure 4 shows that WT CSs displayed high  $\Delta\Psi_m$ , inactive CASP3 and intact nuclei (Fig. 4A, E). However, *PSEN1 E280A* CSs displayed typical features of apoptotic cells, including failure of  $\Delta\Psi_m$ , CASP3-positive signals, and broken nuclei (Fig. 4F, J). Similar observations were obtained by flow cytometry (Fig. 4K, L) and the TUNEL technique (Fig. 4M, Q, R, W).

*Combined treatment with EGCG and aMT increases  $\Delta\Psi_m$  and drastically reduces caspase 3 activation in *PSEN1 E280A* CSs*

Previous work has shown that EGCG diminishes amyloid-induced cytotoxic effects on 2D *PSEN1 E280A* ChLNs derived from hUC-WJ MSCs [22] and that the hormone aMT acts as a neuroprotectant [30, 39]. Therefore, we determined the effect of polyphenols and hormones on mitochondrial functionality in CSs. As shown in Fig. 4, EGCG only (Fig. 4B), aMT only (Fig. 4C), or a combination of the two (Fig. 4D) induced neither alteration in the  $\Delta\Psi_m$  nor activation of the executor protein CASP3 in WT CSs (Fig. 4E) compared to untreated CSs (Fig. 4A, E). Remarkably, treatment with EGCG only (Fig. 4G), aMT only (Fig. 4H), or a combination of the two (Fig. 4I) significantly increased  $\Delta\Psi_m$  compared to untreated *PSEN1 E280A* CSs (Fig. 4F), and these treatments were equally efficient in reducing CASP3 activation in mutant CSs (Fig. 4E versus 4J). Similar results were obtained by flow cytometry (Fig. 4K, L) and the TUNEL technique (Fig. 4N–Q, S–W).

*Combined treatment with EGCG and aMT dramatically diminishes iA $\beta$ PPf and OS levels in *PSEN1 E280A* CSs*

Based on the above observations, we were prompted to assess whether EGCG and aMT alone

or in combination can reverse the neuropathologic features of FAD in mutant CSs. To determine this, WT CSs and *PSEN1 E280A* CSs were left untreated (used as control) or incubated with EGCG at 25  $\mu$ M, a pharmacological concentration of aMT (50  $\mu$ M) or a combination of EGCG and aMT. As illustrated in Fig. 5, EGCG, aMT, and EGCG/aMT were innocuous to WT CSs (Fig. 5A versus Fig. 5B–E). However, aMT (Fig. 5H, J) was significantly more effective than EGCG alone in preventing the accumulation of iA $\beta$ PPf in *PSEN1 E280A* CSs (Fig. 5G, J), and treatment with a combination of the two reduced the level of iA $\beta$ PPf in mutant CSs (Fig. 5I, J) to nearly control values, i.e., those found in WT CSs. In contrast, EGCG was much more effective than aMT in reducing the oxidation of the sensor protein DJ-1 (Fig. 5F versus Fig. 5G and 5J). The combination of the two drugs was even more effective than EGCG alone in reducing OS in mutant CSs (Fig. 5F versus Fig. 5I and J). Flow cytometry analysis yielded comparable results (Fig. 5K–T).

To further confirm that the thwarting effect of the molecules was specifically on iA $\beta$ PP and not on extracellular A $\beta$  aggregates, we stained WT and mutant CSs with thioflavin BTA-1, a specific fluorescent thioflavin-T derivative that has high affinity for amyloid deposits and specifically labels  $\beta$ -amyloid aggregates. BTA-1 displays 50-fold higher affinity for A $\beta$  aggregates than does thioflavin-T, selectively stains A $\beta$  fibrils in postmortem brain tissue obtained from AD patients and crosses the blood-brain barrier. We also stained postmortem temporal cortical samples obtained from individuals with normal and *E280A* mutant *PSEN1* as internal negative and positive controls, respectively. As expected, the mutant *E280A* temporal postmortem sample displayed typical amyloid plaques (Fig. 5V, *arrowheads*) and A $\beta$  fibrils (Fig. 5V, *asterisks*), but such plaques were completely absent from the WT temporal postmortem sample (Fig. 5U). Interestingly, untreated or treated WT or mutant CSs showed neither BTA-1-positive staining for amyloid plaques nor A $\beta$  fibrils (Fig. 5W–AD).

Simultaneously, we wanted to determine whether the reduction in DJ-1 oxidation via H<sub>2</sub>O<sub>2</sub> activation might be due to antioxidant activity of EGCG and aMT when incubated with CSs. The ORAC assay (also known as the hydrogen atom transfer (HAT)-based assay) showed that EGCG, aMT and combined EGCG/aMT displayed high antioxidant activity, yielding values of  $37,870.75 \pm 671.43 \mu\text{mol Trolox equivalents (TE)/g}$ ,  $55,822.86 \pm 585.18 \mu\text{mol}$



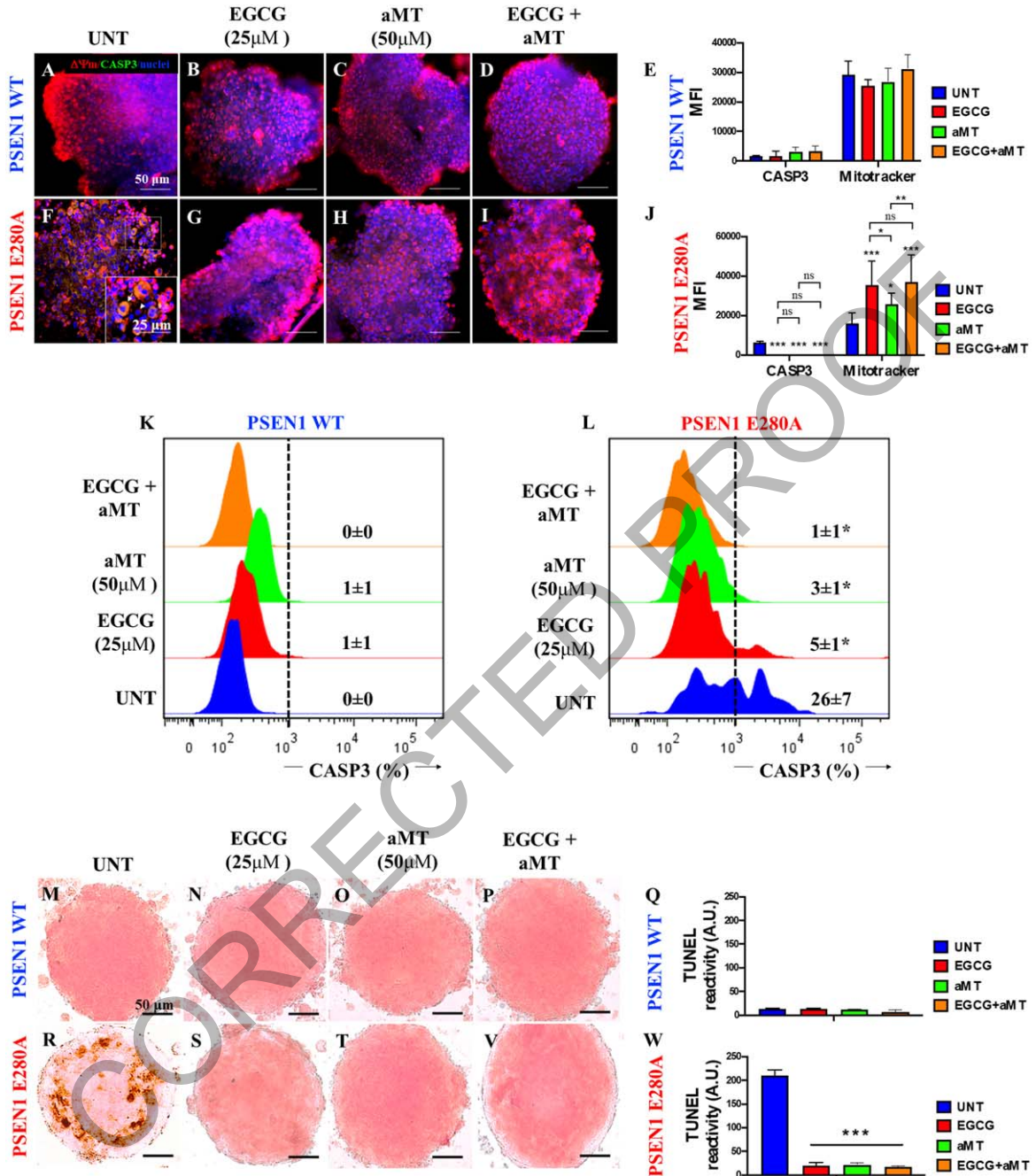


Fig. 4. Combined treatment with EGCG and aMT reestablish mitochondria membrane potential ( $\Delta\Psi_m$ ), inactivate CASPASE-3 activation, and block nuclei fragmentation in *PSEN1* E280A (CSs). The WT *PSEN1* and *PSEN1* E280A CSs were left without (UNT; A, F) or treated with 25  $\mu$ M EGCG (B, G) and 50  $\mu$ M aMT (C, H) alone or in combination (D, I) until day 11. CSs were triple stained as indicated in the figure with MitoTracker™ Red FM (red), 1X Vybrant™ TM FLICA (green), and Hoechst (blue). E) Mean fluorescence intensity (MFI) quantification of images obtained by immunofluorescence analysis of *PSEN1* WT CSs. J) MFI quantification of images obtained by immunofluorescence analysis of *PSEN1* E280A CSs. K, L) representative histograms of WT *PSEN1* (K) and *PSEN1* E280A CSs (L) treated with none (UNT) or with EGCG, aMT, and EGCG/aMT. M-P, R-V) The WT *PSEN1* and *PSEN1* E280A CSs were left without (UNT; M, R) or treated with EGCG (N, S), aMT (O, T), or in combination (P, V) for 11 days. Then, untreated or treated CS were TUNEL stained. Only untreated *PSEN1* E280A CSs (R) show TUNEL-positive cells. Q, W) TUNEL reactivity quantification of images obtained by TUNEL technique analysis after 11 days. Histograms and images represent one out of three independent experiments. Statistical significance was determined by one-way ANOVA with a Tukey *post hoc* test; \* $p < 0.05$ ; \*\*\* $p < 0.001$ . Image magnification 10x.



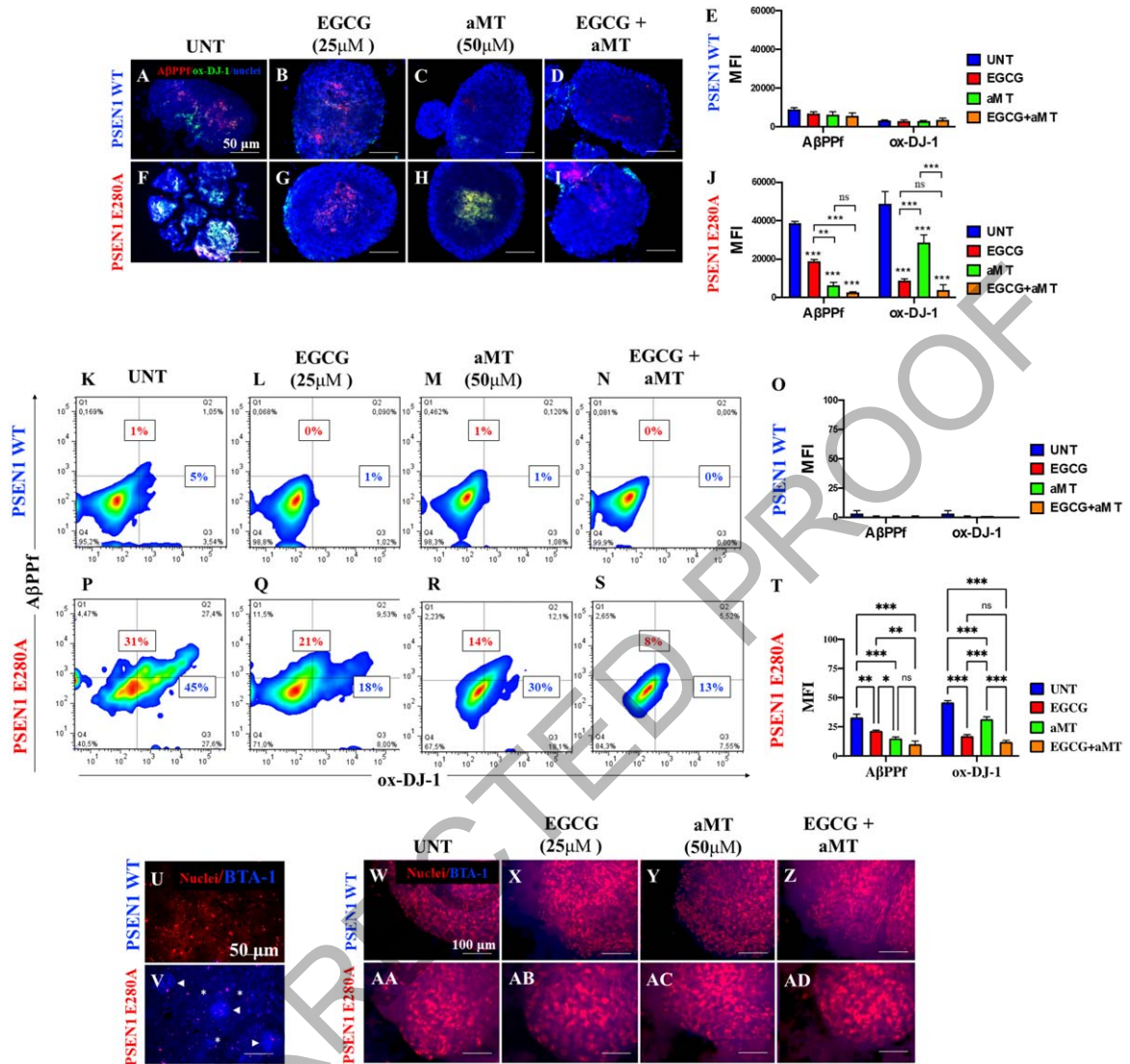


Fig. 5. Combined treatment with EGCG and aMT reduce iAβPPf and OS in *PSEN1* E280A CSs. The WT *PSEN1* and *PSEN1* E280A CSs were left without (UNT; A, F) or treated with 25 μM EGCG (B, G) and 50 μM aMT (C, H) alone or in combination (D, I) for 11 days. CSs were double-stained as indicated in the figure with antibodies against sAβPPf (red) and Ox-DJ-1 (green), and nuclei were stained with Hoechst (blue). E) Mean fluorescence intensity (MFI) quantification of images obtained by immunofluorescence analysis of *PSEN1* WT CSs. J) MFI quantification of images obtained by immunofluorescence analysis of *PSEN1* E280A CSs. K-N, P-S) Representative 2D density plot showing iAβPPf (y-axis) and ox-DJ-1 (x-axis) flow cytometry double analysis performed on untreated WT (K) and mutant CSs (P), or treated with EGCG only (L, Q), aMT only (M, R), and EGCG/ aMT (N, S). O, T) represent the quantitative analysis of the data from quadrant Q1 + Q2 for iAβPPf and Q2 + Q4 for ox-DJ-1. U-V) represent BTA-1 negative staining of a temporal cortex sample from a healthy individual (case #3648) and BTA-1 positive staining of a temporal cortex sample from a *PSEN1* E280A individual (case #3396). Arrowheads show Aβ plaques, and asterisks show Aβ fibrils. W-AD) The WT *PSEN1* and *PSEN1* E280A CSs were left without (UNT; W, AA) or treated with EGCG (X, AB) and aMT (Y, AC) alone or in combination (Z, AD) for 11 days. Then, CSs were double stained with BTA-1 and propidium iodide as indicated in the figure. BTA-1 negative staining was observed in untreated or treated CSs. Except for Fig. 5U and 5V, 2D histograms and images represent one out of three independent experiments. Statistical significance was determined by one-way ANOVA with a Tukey *post hoc* test; \*\*\**p* < 0.001. Image magnification 10x.

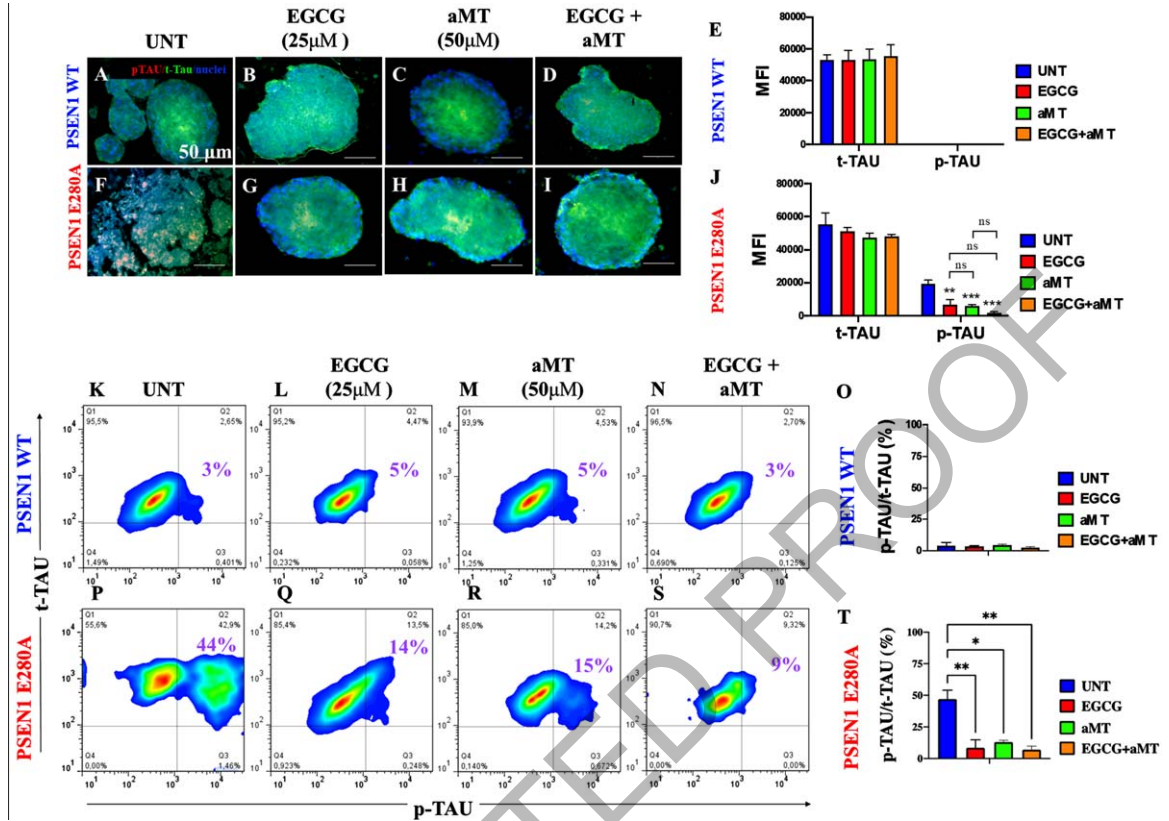


Fig. 6. Combined treatment with EGCG and aMT completely blocked the phosphorylation of protein tau. WT *PSEN1* and *PSEN1 E280A* CSs were left without (UNT; A, B) or treated with 25  $\mu$ M EGCG (C, D) and 50  $\mu$ M aMT (E, F) alone or in combination (G, H) for 11 days. CSs were double-stained as indicated in the figure with antibodies against phosphorylated (Ser<sup>202</sup>/Thr<sup>205</sup>) Tau (p-Tau; red), total Tau (t-Tau; green), and nuclei were stained with Hoechst (blue). I) Mean fluorescence intensity (MFI) quantification of images obtained by immunofluorescence analysis of *PSEN1* WT CSs. J) MFI quantification of images obtained by immunofluorescence analysis of *PSEN1 E280A* CSs. K-N, P-S) Representative 2D density plot showing t-tau (y-axis) and p-tau (x-axis) flow cytometry double analysis performed on untreated WT (K) and mutant CSs (P), or treated with EGCG only (L, Q), aMT only (M, R), or EGCG/ aMT (N, S). O, T) represent the quantitative analysis of the data from quadrant Q2. The 2D histograms and images represent one out of three independent experiments. Statistical significance was determined by one-way ANOVA with a Tukey *post hoc* test; \*\* $p < 0.01$ ; \*\*\* $p < 0.001$ . Image magnification 10x.

TE/g, and  $130,894.34 \pm 2,874.21$   $\mu$ mol TE/g, respectively. The mixture showed 3.35-fold and 2.34-fold increases in ORAC values, respectively.

#### Combined treatment with EGCG and aMT completely blocks phosphorylation of tau protein

We further evaluated whether exposure of CSs to polyphenols, hormones, or a combination of the two is able to decrease p-tau. As shown in Fig. 6, compared to untreated CSs (Fig. 6A, E), no p-tau was observed in WT CSs treated with EGCG (Fig. 6B, E), aMT (Fig. 6C, E), or EGCG/aMT (Fig. 6D, E). When mutant CSs (Fig. 6F) were exposed to these agents, both EGCG alone (Fig. 6G, J) and aMT alone (Fig. 6H, J) significantly diminished p-tau compared to the level found in untreated mutant CSs (Fig. 6J).

Interestingly, treatment with combined EGCG/aMT completely eliminated p-tau (Fig. 6I, J). Flow cytometry yielded similar results (Fig. 6K–T).

#### When applied together with EGCG, aMT limits the beneficial effect of EGCG on $Ca^{2+}$ influx in *PSEN1 E280A* CSs

Finally, we evaluated the effects of the two compounds on  $Ca^{2+}$  functionality in CSs exposed to acetylcholine (ACh). To this end, WT and mutant *PSEN1 E280A* CSs were exposed to ACh at 1 mM final concentration. As shown in Fig. 7, ACh stimulated a temporary increase in intracellular  $Ca^{2+}$  in WT CSs (Fig. 7A,  $\Delta F/F = 0.165 \pm 0.06$ , mean duration = 10 s;  $n = 9$  CSs imaged,  $N = 3$  dishes Fig. 7E).  $Ca^{2+}$  influx into WT CSs after ACh addition was

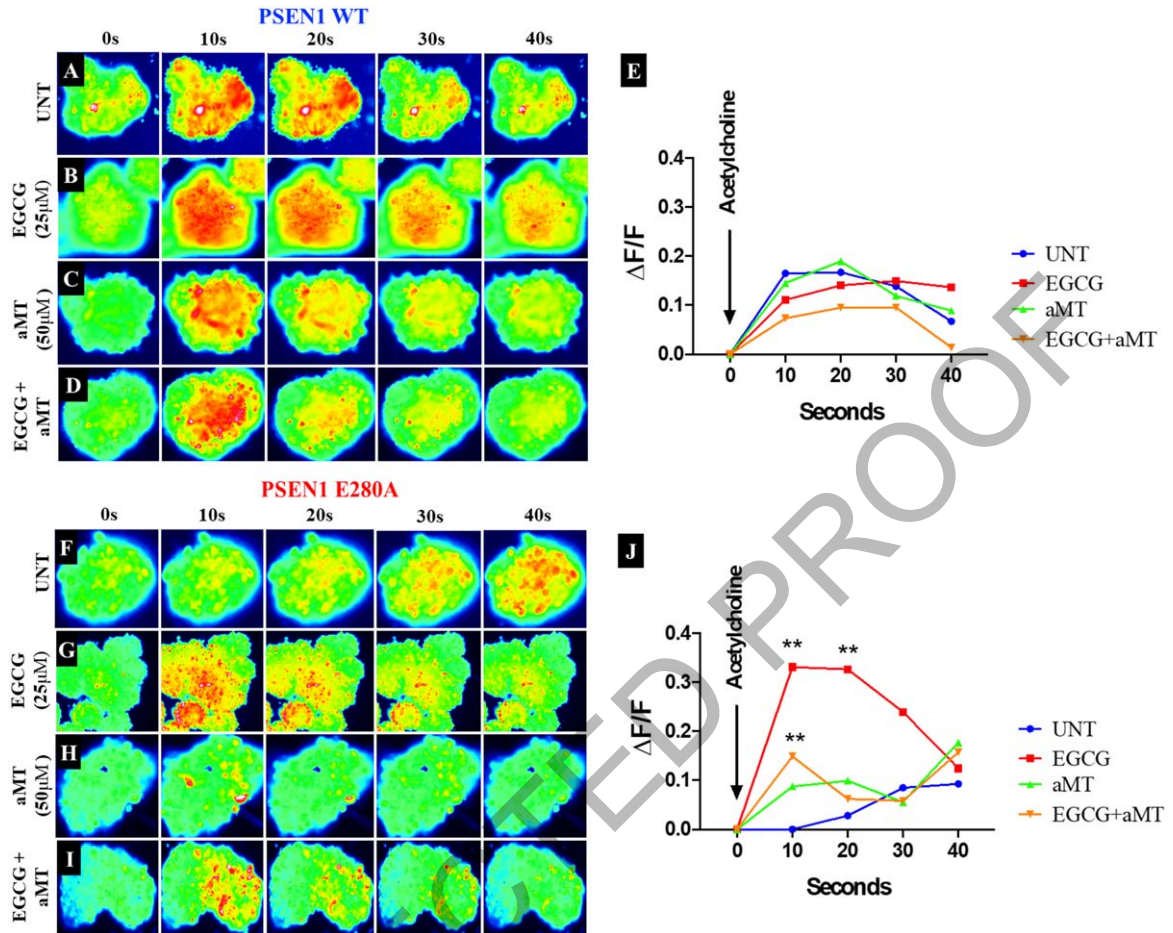


Fig. 7. aMT lessens the effect of EGCG on  $\text{Ca}^{2+}$  influx in *PSEN1 E280a* CSs. The WT *PSEN1* and *PSEN1 E280A* CSs were left without (UNT; A, F) or treated with 25  $\mu\text{M}$  EGCG (B, G) and 50  $\mu\text{M}$  aMT (C, H) alone or in combination (D, I) until day 11. Time-lapse images (0, 10, 20, 30, and 40 s) of  $\text{Ca}^{2+}$  fluorescence in CSs ( $n=9$  CSs imaged,  $N=3$  dishes) as a response to ACh treatment. ACh was puffed into the culture at 0 s (arrow). Then, the  $\text{Ca}^{2+}$  fluorescence of cells was monitored at indicated times. Color contrast indicates fluorescence intensity: dark blue < light blue < green < yellow < red. E) Normalized mean fluorescence signal ( $\Delta F/F$ ) over time, indicating temporal cytoplasmic  $\text{Ca}^{2+}$  elevation in response to ACh treatment in *PSEN1* WT CSs. J) Normalized mean fluorescence signal ( $\Delta F/F$ ) over time, indicating temporal cytoplasmic  $\text{Ca}^{2+}$  elevation in response to ACh treatment in *PSEN1 E280A* CSs. Statistical significance was determined by two-way ANOVA with a Tukey *post hoc* test; \*\* $p < 0.01$ . Image magnification 10x.

altered by EGCG (Fig. 7B), aMT (Fig. 7C), and by a combination of EGCG and aMT (Fig. 7D, E). In contrast, ACh did not affect intracellular  $\text{Ca}^{2+}$  in mutant *PSEN1* CSs (Fig. 7F,  $\Delta F/F = 0.00 \pm 0.02$ , mean duration = 10 s;  $n=9$  CSs imaged,  $N=3$  dishes, Fig. 7J). While EGCG dramatically restored  $\text{Ca}^{2+}$  influx in mutant CSs (Fig. 7G,  $\Delta F/F = 0.33 \pm 0.01$ , mean duration = 10;  $n=9$  CSs imaged,  $N=3$  dishes, Fig. 7J), aMT did not restore  $\text{Ca}^{2+}$  influx in the mutant CSs (Fig. 7H, J), in contrast to its effect on untreated mutant CSs (Fig. 7F, J). Interestingly, administration of EGCG and aMT together decreased ACh-induced  $\text{Ca}^{2+}$  influx in *PSEN1 E280A* CSs

(Fig. 7I;  $\Delta F/F = 0.15 \pm 0.02$ , mean duration = 10 s;  $n=9$  CSs imaged,  $N=3$  dishes, Fig. 7J).

## DISCUSSION

Cerebral spheroids are potential *in vitro* models for understanding neuronal dysfunction [40]. We report for the first time that cholinergic-like *PSEN1 E280A* CSs derived from MenB cells replicate the neuropathological hallmarks of FAD in 3D, mirroring previously reported findings in hUC-MSC-derived ChLNs *PSEN1 E280A* cultured in planar (2D) culture [22]. Indeed, mutant CSs, but not WT CSs,



contained high amounts of intracellular A $\beta$ PPf, OS, and hyperphosphorylated tau protein, as evidenced through immunochemistry using antibodies to E610, DJ-1-sulfonic (SO<sub>3</sub>), and AT8, flow cytometry and BTA-1 staining. Because the WT and mutant cells grow in conglomerates, i.e., in cell spheres, the pathological markers were more prominently detectable in 3D than in 2D cultures. This is indeed an advantage of 3D cultures prepared in *Fast-N-Spheres* V2 medium. Since we found no differences in the levels of iA $\beta$ PP fragments, OS markers, or p-tau after 11 days of culture, the replication of neuropathological features of FAD is easier and more cost-effective when MenSC-derived CSs are used rather than cell models based on other cell culture methods (e.g., [41]). Interestingly, a recently described A $\beta$ -GFP transgenic mouse model of AD, A $\beta$ -GFP Tg, displays increased A $\beta$  accumulation inside neurons and tau phosphorylation, among other physiological alterations [42]. Together, these observations suggest that intracellular A $\beta$ PP fragments or A $\beta$ <sub>1-42</sub>, rather than extracellular A $\beta$ <sub>42</sub> peptide deposition, might represent early-stage pathology in individuals with *PSEN1 E280A* FAD [43]. Furthermore, our observations support the view that the iA $\beta$ PP fragments identified by antibody 6E10, mass spectrometry [22] and flow cytometry (this work) trigger OS and hyperphosphorylation of intracellular tau protein in a time-dependent manner in CS-derived ChLNs, probably through a mechanism involving JNK kinase [22]. Moreover, the observation that mutant CSs, but not WT CSs, were unresponsive to ACh suggests that the mutant CSs have altered endogenous physiological Ca<sup>2+</sup> influx. In agreement with previous studies [44], our observations suggest that the accumulation of iA $\beta$ PP fragments precedes tau pathology. These findings support the idea that iA $\beta$ PP fragments and/or A $\beta$ <sub>42</sub> trigger early neurotoxicity in FAD [45, 46] and represent an early stage in the pathology of AD [43]. However, whether iA $\beta$ PP fragments and/or A $\beta$ <sub>42</sub> provoke neuronal apoptosis (represented in this work by loss of  $\Delta\Psi_m$  and CASP3-positive cells) or necrosis [43] deserves further investigation. Regardless of the mechanism, intracellular A $\beta$  is increasingly recognized as a prominent player in cholinergic neuronal demise and as a basis for new treatment approaches, e.g., bioactive polyphenols, cannabinoids, and bifunctional anti-(i)amyloid and anti-OS agents [23, 45, 47–49].

We also report here for the first time that EGCG and aMT in combination are highly effective in improving pathological (i.e., iA $\beta$ PPf and p-tau), OS (i.e., DJ-

1 Cys<sup>106</sup>-SO<sub>3</sub>), and apoptosis indicators in *PSEN1 E280A* CSs. These observations might be explained by the effect of each of the components of the mixture. Indeed, we found that both EGCG and aMT display high antioxidant capacity and that the antioxidant capacity of the combined EGCG/aMT was even higher (e.g., 3.35-fold and 2.34-fold increases in ORAC value compared to EGCG and aMT, respectively). We found that EGCG blunted the generation of H<sub>2</sub>O<sub>2</sub>, as reflected by a reduction in the level of oxDJ-1 [50], inhibition of amyloid accumulation [23, 26, 51], increased disassembly of full-length tau protein [52], blockade of the activation of the main apoptosis factors CASP3 and nuclear fragmentation, and increased  $\Delta\Psi_m$ , and thereby increased the survival of mutant CSs to a similar extent as WT CSs. Likewise, we found that aMT was also highly effective as a neuroprotective agent against intrinsic insults in *PSEN1 E280A* CSs. aMT not only efficiently scavenged H<sub>2</sub>O<sub>2</sub> by acting as an antioxidant [53] but also reduced the accretion of iA $\beta$ PPf, possibly through direct interaction with amyloid, thereby protecting CSs against iA $\beta$ PPf toxicity [54, 55]. Furthermore, aMT almost completely blocked hyperphosphorylation of tau protein ([56] and references therein), restored  $\Delta\Psi_m$  [57], and inhibited iA $\beta$ PPf-induced apoptosis in mutant CSs by inactivating CASP3 [55, 58]. These observations are consistent with the idea that both the combination of EGCG/aMT and EGCG and aMT individually act as antioxidants, antiamyloidogenic agents, inhibitors of tau aggregation, and blockers of apoptosis. In agreement with previous observations [23], EGCG altered Ca<sup>2+</sup> influx in response to ACh in *PSEN1 E280A* CSs. However, mutant CSs were almost unresponsive to ACh when exposed to a combination of aMT and EGCG. Moreover, aMT reduced the beneficial effect of EGCG on Ca<sup>2+</sup> influx in mutant CSs. How aMT affects Ca<sup>2+</sup> influx in CSs is not yet known. A possible explanation for our observations is that aMT either interacts directly with cholinergic receptors (e.g., nAChR [59]), blocking their interaction with ACh and thereby inhibiting voltage-activated calcium currents [60], or increases Ca<sup>2+</sup> efflux from CSs. Additional research is required to clarify this issue. Regardless of the mechanism, our results show that aMT does not contribute to the restoration of Ca<sup>2+</sup> influx in mutant CSs.

Several studies have shown that EGCG is not only an effective antioxidant (e.g., [61]) but that it also possesses anti-amyloidogenic properties [62].

Our current observations support this interpretation. In agreement with others [63–66], we found that EGCG displays high antioxidant activity according to the ORAC test. Furthermore, EGCG significantly reduced iA $\beta$ PP accumulation. These results suggest that early inhibition of iA $\beta$ PP and quenching of ROS, specifically H<sub>2</sub>O<sub>2</sub>, block further signaling that would otherwise lead to cell death. Interestingly, EGCG can be enzymatically modified to enhance its lipophilicity and antioxidant properties [67]. Unfortunately, no information on the antioxidant effects of such compounds on human cells is currently available. Such derivative compounds might be used to help prevent OS-induced neuronal cell death in FAD. Likewise, in agreement with others, we found that aMT displays antioxidant capacity according to the ORAC assay [68, 69]. This might explain why aMT is effective in alleviating OS induced by H<sub>2</sub>O<sub>2</sub> in PTr2 cells [70] and in mutant E280A CSs (this work). We showed here, however, for the first time that the combined action of two antioxidant agents, EGCG and aMT, is even more efficient in protecting mutant CSs. However, further experiments are necessary to establish whether the combined action of EGCG and aMT is additive or synergistic [71].

### Conclusion

Familial AD, most cases of which are caused by mutations in *PSEN1*, e.g., *PSEN1 E280A*, is a complex neurodegenerative malady in which progressive neuronal deterioration occurs, leading to loss of memory. It is now accepted that intracellular A $\beta$ , rather than extracellular A $\beta$  aggregation, is the likely cause of neuronal cell death. We have shown that early generation and accumulation of iA $\beta$ PP are responsible for initiating cellular events that lead to ROS (H<sub>2</sub>O<sub>2</sub>) production, hyperphosphorylation of tau, activation of proapoptotic proteins (e.g., CASP 3), alterations in Ca<sup>2+</sup> influx, and apoptosis in ChLNs [22] and in CSs (this work). It is, therefore, reasonable to assume that drugs designed to eliminate A $\beta$ -induced signaling cell death targets/or pathological signals may have cooperative (additive or synergistic) effects. Consistent with this view, combined use of EGCG and aMT has proven to be highly useful in almost completely reducing intracellular A $\beta$ PP, OS, p-tau, loss of  $\Delta\Psi_m$ , and apoptotic markers in *PSEN1 E280A* CSs. However, aMT and EGCG in combination were ineffective at restoring Ca<sup>2+</sup> influx in mutant CSs because of their antagonistic action. Therefore, our present observations provide a cautionary note regarding the

use of aMT to restore physiological functions associated with Ca<sup>2+</sup> influx. However, this limitation might be overcome by delivering EGCG (e.g., [72]) and aMT (e.g., [73]) nanoparticles to specific brain neurons (e.g., cholinergic or pyramidal) that can be directly loaded with the cargo (EGCG and aMT) intracellularly. Further investigation is needed to validate the effectiveness of using combined EGCG and aMT in the early treatment of FAD patients carrying the *PSEN1 E280A* mutation.

### ACKNOWLEDGMENTS

We are grateful to the Bioactive Substances Service and Research Group (SIU-UdeA) for ORAC testing.

### FUNDING

This work was funded by MinCiencias (grant. no. 1115-807-62912, contract no. 749-2018).

### CONFLICT OF INTEREST

The authors have no conflict of interest to report.

### DATA AVAILABILITY

All datasets generated for this study are included in the manuscript.

### REFERENCES

- [1] Wolfe MS, Miao Y (2022) Structure and mechanism of the  $\gamma$ -secretase intramembrane protease complex. *Curr Opin Struct Biol* **74**, 102373.
- [2] Lalli MA, Cox HC, Arcila ML, Cadavid L, Moreno S, Garcia, G, Madrigal L, Reiman EM, Arcos-Burgos M, Bedoya G, Brunkow ME, Glusman G, Roach JC, Hood L, Kosik KS, Lopera F (2014) Origin of the PSEN1 E280A mutation causing early-onset Alzheimer's disease. *Alzheimers Dement* **10**, S277-S283.e210.
- [3] Lopera F, Ardilla A, Martínez A, Madrigal L, Arango-Viana JC, Lemere CA, Arango-Lasprilla JC, Hincapié L, Arcos-Burgos M, Ossa JE, Behrens IM, Norton J, Lendon C, Goate AM, Ruiz-Linares A, Rosselli M, Kosik KS (1997) Clinical features of early-onset Alzheimer disease in a large kindred with an E280A presenilin-1 mutation. *JAMA* **277**, 793-799.
- [4] Lemere CA, Lopera F, Kosik KS, Lendon CL, Ossa J, Saido TC, Yamaguchi H, Ruiz A, Martínez A, Madrigal L, Hincapié L, Arango JC, Anthony DC, Koo EH, Goate AM, Selkoe DJ, Arango JC (1996) The E280A presenilin 1 Alzheimer mutation produces increased A beta 42 deposition and severe cerebellar pathology. *Nat Med* **2**, 1146-1150.
- [5] Duque-Castaño A, Roldán MI, Arango-Viana JC, Arcos-Burgos M, Cubillo H, Lopera F (1999) Neuropathological



- findings in early-onset Alzheimer's disease (E280a-PS1 mutation). *Rev Neurol* **29**, 1-6.
- [6] Velez-Pardo C, Arellano JI, Cardona-Gomez P, Jimenez Del Rio M, Lopera F, De Felipe J (2004) CA1 hippocampal neuronal loss in familial Alzheimer's disease presenilin-1 E280A mutation is related to epilepsy. *Epilepsia* **45**, 751-756.
- [7] Quiroz YT, Sperling RA, Norton DJ, Baena A, Arboleda-Velasquez JF, Cosio D, Schultz A, Lapoint M, Guzman-Velez E, Miller JB, Kim LA, Chen K, Tariot PN, Lopera F, Reiman EM, Johnson KA (2018) Association between amyloid and tau accumulation in young adults with autosomal dominant Alzheimer disease. *JAMA Neurol* **75**, 548-556.
- [8] Palmqvist S, Janelidze S, Quiroz YT, Zetterberg H, Lopera F, Stomrud E, Su Y, Chen Y, Serrano GE, Leuzy A, Mattsson-Carlsson N, Strandberg O, Smith R, Villegas A, Sepulveda-Falla D, Chai X, Proctor NK, Beach TG, Blennow K, Dage JL, Reiman EM, Hansson O (2020) Discriminative accuracy of plasma phospho-tau217 for Alzheimer disease vs other neurodegenerative disorders. *JAMA* **324**, 772-781.
- [9] Dinkel F, Trujillo-Rodriguez D, Villegas A, Streffer J, Mercken M, Lopera F, Glatzel M, Sepulveda-Falla D (2020) Decreased deposition of beta-amyloid 1-38 and increased deposition of beta-amyloid 1-42 in brain tissue of presenilin-1 E280A familial Alzheimer's disease patients. *Front Aging Neurosci* **12**, 220.
- [10] Ghisays V, Lopera F, Goradia DD, Protas HD, Malek-Ahmadi MH, Chen Y, Devadas V, Luo J, Lee W, Baena A, Bocanegra Y, Guzmán-Vélez E, Pardilla-Delgado E, Vila-Castelar C, Fox-Fuller JT, Hu N, Clayton D, Thomas RG, Alvarez S, Espinosa A, Acosta-Baena N, Giraldo MM, Rios-Romenets S, Langbaum JB, Chen K, Su Y, Tariot PN, Quiroz YT, Reiman EM; API ADAD Colombia Trial Group (2021) PET evidence of preclinical cerebellar amyloid plaque deposition in autosomal dominant Alzheimer's disease-causing Presenilin-1 E280A mutation carriers. *Neuroimage Clin* **31**, 102749.
- [11] Tariot PN, Lopera F, Langbaum JB, Thomas RG, Hendrix S, Schneider LS, Rios-Romenets S, Giraldo M, Acosta N, Tobon C, Ramos C, Espinosa A, Cho W, Ward M, Clayton D, Friesenhahn M, Mackey H, Honigberg L, Sanabria Bohorquez S, Chen K, Walsh T, Langlois C, Reiman EM (2018) The Alzheimer's Prevention Initiative Autosomal-Dominant Alzheimer's Disease Trial: A study of crenezumab versus placebo in preclinical PSEN1 E280A mutation carriers to evaluate efficacy and safety in the treatment of autosomal-dominant Alzheimer's disease, including a placebo-treated noncarrier cohort. *Alzheimers Dement (N Y)* **4**, 150-160.
- [12] Dominici M, Le Blanc K, Mueller I, Slaper-Cortenbach I, Marini F, Krause D, Deans R, Keating A, Prockop DJ, Horwitz E (2006) Minimal criteria for defining multipotent mesenchymal stromal cells. The International Society for Cellular Therapy position statement. *Cytotherapy* **8**, 315-317.
- [13] Viswanathan S, Shi Y, Galipeau J, Krampera M, Leblanc K, Martin I, Nolta J, Phinney DG, Sensebe L (2019) Mesenchymal stem versus stromal cells: International Society for Cell & Gene Therapy (ISCT®) Mesenchymal Stromal Cell committee position statement on nomenclature. *Cytotherapy* **21**, 1019-1024.
- [14] Shariati A, Nemati R, Sadeghipour Y, Yaghoubi Y, Baghbani R, Javidi K, Zamani M, Hassanzadeh A (2020) Mesenchymal stromal cells (MSCs) for neurodegenerative disease: A promising frontier. *Eur J Cell Biol* **99**, 151097.
- [15] Choudhary P, Gupta A, Singh S (2021) Therapeutic advancement in neuronal transdifferentiation of mesenchymal stromal cells for neurological disorders. *J Mol Neurosci* **71**, 889-901.
- [16] Lv H, Hu Y, Cui Z, Jia H (2018) Human menstrual blood: A renewable and sustainable source of stem cells for regenerative medicine. *Stem Cell Res Ther* **9**, 325.
- [17] Chen L, Qu J, Cheng T, Chen X, Xiang C (2019) Menstrual blood-derived stem cells: Toward therapeutic mechanisms, novel strategies, and future perspectives in the treatment of diseases. *Stem Cell Res Ther* **10**, 406.
- [18] Liu Y, Niu R, Yang F, Yan Y, Liang S, Sun Y, Shen P, Lin J (2018) Biological characteristics of human menstrual blood-derived endometrial stem cells. *J Cell Mol Med* **22**, 1627-1639.
- [19] Zhao Y, Chen X, Wu Y, Wang Y, Li Y, Xiang C (2018) Transplantation of human menstrual blood-derived mesenchymal stem cells alleviates Alzheimer's disease-like pathology in APP/PS1 transgenic mice. *Front Mol Neurosci* **11**, 140.
- [20] Quintero-Espinosa D, Soto-Mercado V, Quintero-Quinchia C, Mendivil-Perez M, Velez-Pardo C, Jimenez-Del-Rio M (2021) Latent tri-lineage potential of human menstrual blood-derived mesenchymal stromal cells revealed by specific *in vitro* culture conditions. *Mol Neurobiol* **58**, 5194-5209.
- [21] Bonilla-Porras AR, Velez-Pardo C, Jimenez-Del-Rio M (2017) Fast transdifferentiation of human Wharton's jelly mesenchymal stem cells into neurospheres and nerve-like cells. *J Neurosci Methods* **282**, 52-60.
- [22] Soto-Mercado V, Mendivil-Perez M, Velez-Pardo C, Lopera F, Jimenez-Del-Rio M (2020) Cholinergic-like neurons carrying PSEN1 E280A mutation from familial Alzheimer's disease reveal intraneuronal sAPP $\beta$  fragments accumulation, hyperphosphorylation of tau, oxidative stress, apoptosis and Ca<sup>2+</sup> dysregulation: Therapeutic implications. *PLoS One* **15**, e0221669.
- [23] Soto-Mercado V, Mendivil-Perez M, Velez-Pardo C, Jimenez-Del-Rio M (2021) (-)-Epigallocatechin-3-gallate diminishes intra- and extracellular amyloid-induced cytotoxic effects on cholinergic-like neurons from familial Alzheimer's disease PSEN1 E280A. *Biomolecules* **11**, 1845.
- [24] Zarezadeh M, Barzegari M, Aghapour B, Adeli S, Khademi F, Musazadeh V, Jamilian P, Jamilian P, Fakhr L, Chehregosha F, Ghoreishi Z, Ostadrahimi A (2022) Melatonin effectiveness in amelioration of oxidative stress and strengthening of antioxidant defense system: Findings from a systematic review and dose-response meta-analysis of controlled clinical trials. *Clin Nutr ESPEN* **48**, 109-120.
- [25] Feng Z, Qin C, Chang Y, Zhang JT (2006) Early melatonin supplementation alleviates oxidative stress in a transgenic mouse model of Alzheimer's disease. *Free Radic Biol Med* **40**, 101-109.
- [26] Li Y, Zhang J, Wan J, Liu A, Sun J (2020) Melatonin regulates A $\beta$  production/clearance balance and A $\beta$  neurotoxicity: A potential therapeutic molecule for Alzheimer's disease. *Biomed Pharmacother* **132**, 110887.
- [27] Dai Y, Peng L, Liu Y, Xu Y, Qiao J (2021) Melatonin binds with high affinity and specificity to beta-amyloid: LC-MS provides insight into Alzheimer's disease treatment. *FEBS Open Bio* **11**, 2800-2806.

- [28] Zhu L, Gong Y, Lju H, Sun G, Zhang Q, Qian Z (2021) Mechanisms of melatonin binding and destabilizing the protofilament and filament of tau R3-R4 domains revealed by molecular dynamics simulation. *Phys Chem Chem Phys* **23**, 20615-20626.
- [29] Wang CF, Song CY, Wang X, Huang LY, Ding M, Yang H, Wang P, Xu LL, Xie ZH, Bi JZ (2019) Protective effects of melatonin on mitochondrial biogenesis and mitochondrial structure and function in the HEK293-APPswe cell model of Alzheimer's disease. *Eur Rev Med Pharmacol Sci* **23**, 3542-3550.
- [30] Roy J, Wong KY, Aquili L, Uddin MS, Heng BC, Tipoe GL, Wong KH, Fung ML, Lim LW (2022) Role of melatonin in Alzheimer's disease: From preclinical studies to novel melatonin-based therapies. *Front Neuroendocrinol* **65**, 100986.
- [31] Velez-Pardo C, Lopera F, Jimenez Del Rio M (2000) DNA damage does not correlate with amyloid-beta-plaques and neurofibrillary tangles in familial Alzheimer's disease presenilin-1 [E280A] mutation. *J Alzheimers Dis* **2**, 47-57.
- [32] Kaminska A, Wedzinska A, Kot M, Sarnowska A (2021) Effect of long-term 3D spheroid culture on WJ-MSC. *Cells* **10**, 719.
- [33] Bravo K, Alzate F, Osorio E (2016) Fruits of selected wild and cultivated Andean plants as sources of potential compounds with antioxidant and anti-aging activity. *Ind Crops Prod* **85**, 341-352.
- [34] Pap P, Koszeghy A, Szucs G, Rusznák Z (2009) Cytoplasmic Ca(2+) concentration changes evoked by cholinergic stimulation in primary astrocyte cultures prepared from the rat cochlear nucleus. *Hear Res* **255**, 73-83.
- [35] Schindelin J, Arganda-Carreras I, Frise E, Kaynig V, Longair M, Pietzsch T, Preibisch S, Rueden C, Saalfeld S, Schmid B, Tinevez JY, White DJ, Hartenstein V, Eliceiri K, Tomancak P, Cardona A (2012) Fiji: An open-source platform for biological-image analysis. *Nat Methods* **9**, 676-682.
- [36] Lazic SE, Clarke-Williams CJ, Munafò MR (2018) What exactly is 'N' in cell culture and animal experiments? *PLoS Biol* **16**, e2005282.
- [37] Bloom GS (2014) Amyloid-beta and tau: The trigger and bullet in Alzheimer disease pathogenesis. *JAMA Neurol* **71**, 505-508.
- [38] Wu HY, Kuo PC, Wang YT, Lin HT, Roe AD, Wang BY, Han CL, Hyman BT, Chen YJ, Tai HC (2018)  $\beta$ -amyloid induces pathology-related patterns of tau hyperphosphorylation at synaptic terminals. *J Neuropathol Exp Neurol* **77**, 814-826.
- [39] Mendivil-Perez M, Soto-Mercado V, Guerra-Librero A, Fernandez-Gil BI, Florido J, Shen YQ, Tejeda MA, Capilla-Gonzalez V, Rusanova I, Garcia-Verdugo JM, Acuña-Castroviejo D, López LC, Velez-Pardo C, Jimenez-Del-Rio M, Ferrer JM, Escames G (2017) Melatonin enhances neural stem cell differentiation and engraftment by increasing mitochondrial function. *J Pineal Res* **63**, e12415.
- [40] da Silva Siqueira L, Majolo F, da Silva APB, da Costa JC, Marinowicz DR (2021) Neurospheres: A potential *in vitro* model for the study of central nervous system disorders. *Mol Biol Rep* **48**, 3649-3663.
- [41] Ha J, Kang JS, Lee M, Baek A, Kim S, Chung SK, Lee MO, Kim J (2020) Simplified brain organoids for rapid and robust modeling of brain disease. *Front Cell Dev Biol* **8**, 594090.
- [42] Ochiishi T, Kaku M, Kiyosue K, Doi M, Urabe T, Hattori N, Shimura H, Ebihara T (2019) New Alzheimer's disease model mouse specialized for analyzing the function and toxicity of intraneuronal Amyloid  $\beta$  oligomers. *Sci Rep* **9**, 17368.
- [43] Okazawa H (2021) Intracellular amyloid hypothesis for ultra-early phase pathology of Alzheimer's disease. *Neuropathology* **41**, 93-98.
- [44] Welikovitsh LA, Do Carmo S, Maglóczy Z, Szocsics P, Löke J, Freund T, Cuello AC (2018) Evidence of intraneuronal Abeta accumulation preceding tau pathology in the entorhinal cortex. *Acta Neuropathol* **136**, 901-917.
- [45] Gallego Villarejo L, Bachmann L, Marks D, Brachthäuser M, Geidies A, Müller T (2022) Role of intracellular amyloid  $\beta$  as pathway modulator, biomarker, and therapy target. *Int J Mol Sci* **23**, 4656.
- [46] Antonino M, Marmo P, Freitas CL, Quassollo GE, Sánchez MF, Lorenzo A, Bignante EA (2022) A $\beta$  assemblies promote amyloidogenic processing of APP and intracellular accumulation of A $\beta$ 42 through Go/G $\beta$ y signaling. *Front Cell Dev Biol* **10**, 852738.
- [47] Hilt S, Altman R, Kálai T, Maezawa I, Gong Q, Wachsmann-Hogiu S, Jin LW, Voss JC (2018) A bifunctional anti-amyloid blocks oxidative stress and the accumulation of intraneuronal amyloid-beta. *Molecules* **23**, 2010.
- [48] Schubert D, Kepchia D, Liang Z, Dargusch R, Goldberg J, Maher P (2019) Efficacy of cannabinoids in a pre-clinical drug-screening platform for Alzheimer's disease. *Mol Neurobiol* **56**, 7719-7730.
- [49] Soto-Mercado V, Mendivil-Perez M, Jimenez-Del-Rio M, Velez-Pardo C (2021) Multi-target effects of the cannabinoid CP55940 on familial Alzheimer's disease PSEN1 E280A cholinergic-like neurons: Role of CB1 receptor. *J Alzheimers Dis* **82**, S359-S378.
- [50] Tang G, Xu Y, Zhang C, Wang N, Li H, Feng Y (2021) Green tea and epigallocatechin gallate (EGCG) for the management of nonalcoholic fatty liver diseases (NAFLD): Insights into the role of oxidative stress and antioxidant mechanism. *Antioxidants (Basel)* **10**, 1076.
- [51] Andrich K, Bieschke J (2015) The effect of (-)-Epigallo-catechin-(3)-gallate on amyloidogenic proteins suggests a common mechanism. *Adv Exp Med Biol* **863**, 139-161.
- [52] Sonawane SK, Chidambaram H, Boral D, Gorantla NV, Balmik AA, Dangi A, Ramasamy S, Marelli UK, Chinathambi S (2020) EGCG impedes human tau aggregation and interacts with tau. *Sci Rep* **10**, 12579.
- [53] Reiter RJ, Melchiorri D, Sewerynek E, Poeggeler B, Barlow-Walden L, Chuang J, Ortiz GG, Acuña-Castroviejo D (1995) A review of the evidence supporting melatonin's role as an antioxidant. *J Pineal Res* **18**, 1-11.
- [54] Pappolla M, Bozner P, Soto C, Shao H, Robakis NK, Zagorski M, Frangione B, Ghiso J (1998) Inhibition of Alzheimer beta-fibrillogenesis by melatonin. *J Biol Chem* **273**, 7185-7188.
- [55] Ali T, Kim MO (2015) Melatonin ameliorates amyloid beta-induced memory deficits, tau hyperphosphorylation and neurodegeneration via PI3/Akt/Gsk3 $\beta$  pathway in the mouse hippocampus. *J Pineal Res* **59**, 47-59.
- [56] Chen D, Zhang T, Lee TH (2020) Cellular mechanisms of melatonin: Insight from neurodegenerative diseases. *Biomolecules* **10**, 1158.
- [57] Reiter RJ, Rosales-Corral S, Tan DX, Jou MJ, Galano A, Xu B (2017) Melatonin as a mitochondria-targeted antioxidant: One of evolution's best ideas. *Cell Mol Life Sci* **74**, 3863-3881.

- [58] Jang MH, Jung SB, Lee MH, Kim CJ, Oh YT, Kang I, Kim J, Kim EH (2005) Melatonin attenuates amyloid beta25-35-induced apoptosis in mouse microglial BV2 cells. *Neurosci Lett* **380**, 26-31.
- [59] Su-Hyun, J, Seung-Hyun, L, Kyong-Tai K, Se-Young C (2019) Melatonin inhibits nicotinic acetylcholine receptor functions in bovine chromaffin cells. *Int J Oral Biol* **44**, 50-54.
- [60] Ayar A, Martin DJ, Ozcan M, Kelestimur H (2001) Melatonin inhibits high voltage activated calcium currents in cultured rat dorsal root ganglion neurones. *Neurosci Lett* **313**, 73-77.
- [61] Singh NA, Mandal AK, Khan ZA (2016) Potential neuro-protective properties of epigallocatechin-3-gallate (EGCG). *Nutr J* **15**, 60.
- [62] Wang Y, Wang K, Yan J, Zhou Q, Wang X (2022) Recent progress in research on mechanisms of action of natural products against Alzheimer's disease: Dietary plant polyphenols. *Int J Mol Sci* **23**, 13886.
- [63] Henning SM, Fajardo-Lira C, Lee HW, Youssefian AA, Go VL, Heber D (2003) Catechin content of 18 teas and a green tea extract supplement correlates with the antioxidant capacity. *Nutr Cancer* **45**, 226-235.
- [64] Zhong Y, Ma CM, Shahidi F (2012) Antioxidant and antiviral activities of lipophilic epigallocatechin gallate (EGCG) derivatives. *J Funct Foods* **4**, 87-93.
- [65] Zhao C, Li C, Liu S, Yang L (2014) The galloyl catechins contributing to main antioxidant capacity of tea made from *Camellia sinensis* in China. *ScientificWorldJournal* **2014**, 863984.
- [66] Badmus JA, Ekpo OE, Rautenbach F, Marnewick JL, Hussein AA, Hiss DC (2016) Isolation and antioxidant activity of flavonoids from *Holarrhena floribunda* (G.don) leaves. *Acta Biochim Pol* **63**, 353-358.
- [67] Jiang C, Wang L, Huang X, Zhu S, Ma C, Wang H (2021) Structural characterization and antioxidant property of enzymatic-transesterification derivatives of (-)-epigallocatechin-3-O-gallate and vinyl laurate. *J Food Sci* **86**, 4717-4729.
- [68] Pieri C, Marra M, Moroni F, Recchioni R, Marcheselli F (1994) Melatonin: A peroxyl radical scavenger more effective than vitamin E. *Life Sci* **55**, PL271-276.
- [69] Sofic E, Rimpapa Z, Kundurovic Z, Sapcanin A, Tahirovic I, Rustembegovic A, Cao G (2005) Antioxidant capacity of the neurohormone melatonin. *J Neural Transm (Vienna)* **112**, 349-358.
- [70] Fu Y, Chen Y, Jin Z, Gao H, Song G, Wang Q, Xu K (2022) Melatonin alleviates oxidative stress induced by H<sub>2</sub>O<sub>2</sub> in porcine trophectoderm cells. *Antioxidants (Basel)* **11**, 1047.
- [71] Roell KR, Reif DM, Motsinger-Reif AA (2017) An introduction to terminology and methodology of chemical synergy-perspectives from across disciplines. *Front Pharmacol* **8**, 158.
- [72] Safwat MA, Kandil BA, Elblbesy MA, Soliman GM, Eleraky NE (2020) Epigallocatechin-3-gallate-loaded gold nanoparticles: Preparation and evaluation of anticancer efficacy in Ehrlich tumor-bearing mice. *Pharmaceuticals (Basel)* **13**, 254.
- [73] Chuffa LGA, Seiva FRF, Novais AA, Simão VA, Martín Giménez VM, Manucha W, Zuccari DAPC, Reiter RJ (2021) Melatonin-loaded nanocarriers: New horizons for therapeutic applications. *Molecules* **26**, 3562.